Self-assembly of Rhenium(I) Metallocycles Using Pyrazole Based Ligands

A Thesis Submitted for the Degree of

DOCTOR OF PHILOSOPHY

By

UPASANA PHUKON

School of Chemistry

University Of Hyderabad

Hyderabad 500046

INDIA

JANUARY 2024

Dedicated to

Ma, Deuta and Dada

CONTENTS

STATEMENT

I hereby declare that the matter embodied in this thesis is the result of investigations carried out by me in School of Chemistry, University of Hyderabad, Hyderabad, under the supervision of **Prof. M. Sathiyendiran**.

In keeping with the general practice of reporting scientific observations, due acknowledgments have been made wherever the work described is based on the findings of other investigators.

Hyderabad
January 2024

Upasana Phukon

Upasana Phukon
(18CHPH06)

DECLARATION

I, **Upasana Phukon**, hereby declare that this thesis entitled **"Self-assembly of Rhenium(I) Metallocycles Using Pyrazole Based Ligands"** submitted by me under the guidance and supervision of **Prof. M. Sathiyendiran**, is a bonafide research work which has been prepared without resorting to plagiarism. This thesis in full or any part of it has not been submitted this university or any other university or institution for the award of any degree or diploma. I hereby agree that my thesis can be deposited in Shodhganga/INFLIBNET.

A report on plagiarism statistics from the University Librarian is enclosed.

Date:

Name: Upasana Phukon

Reg. No.: 18CHPH06

Upasana Phukon

Signature of the student

M. Sathiyendiran

Signature of the Supervisor

Dr. M.Sathiyendiran
Professor
School of Chemistry
University of Hyderabad
Hyderabad - 500 046, India.

UNIVERSITY OF HYDERABAD

Prof. M. Sathiyendiran

SCHOOL OF CHEMISTRY

HYDERABAD-500046, INDIA

Phone: +91-40-2313-4811 (Office), 2313-4911 (Lab) E-mail: msathi@uohyd.ac.in

CERTIFICATE

This is to certify that the thesis entitled "Self-assembly of Rhenium(I) Metallocycles Using Pyrazole Based Ligands" submitted by Upasana Phukon bearing registration number 18CHPH06 in partial fulfillment of the requirements for the award of the Doctor of Philosophy (Ph. D.) is a bonafide work carried out by her under my supervision and guidance in the School of Chemistry, University of Hyderabad. This thesis is free from plagiarism and has not been submitted previously in part or in full to this or any other University or Institution for the award of any degree or diploma. Further, the student has seven publications before submission of the thesis for adjudication and has produced shreds of evidence for the same in the form of reprints.

Parts of this thesis have been published as the following articles:

1. **U. Phukon,** M. Priyatharsini, M. Sathiyendiran, *J. Organomet. Chem.*, **2020**, *923*, 121460 (Chapter 4).
2. **U. Phukon**, B. Shankar, M. Sathiyendiran, *Dalton Trans.*, **2022**, *51*, 16307–16315 (Chapter 2).
3. **U. Phukon**, M. kedia, B. Shankar, M. Sathiyendiran, *ACS Omega* **2023**, *8*, 41773–41784 (Chapter 3).

She has also made presentations in the following conferences:

1. **Poster**: *CHEMFEST-2020: 17th Annual in- House Symposium*, University of Hyderabad, Telangana, India; 2020 Feb. 27-28.
2. **Oral**: *CHEMFEST-2022: 19th Annual in- House Symposium*, University of Hyderabad, Telangana, India; 2022 Apr. 22-23
3. **Poster**: *CHEMFEST-2023: 20th Annual in- House Symposium*, University of Hyderabad, Telangana, India; 2023 Mar. 03-04.
4. **Poster**: *MTIC 2023: International Conference on Modern Trends In Inorganic Chemistry-XX*, Indian Institute of Science, Bangalore, Karnataka India; 2023 Dec.14-17 **(Best Poster Award)**.

5. **Poster:** *MMM III 2023: International Conference on Main group Molecules to Materials*, Indian Institute of Technology Hyderabad & University of Hyderabad, Telangana, India; 2023 Dec.9-11 **(Best Poster Award by RSC).**

Further the student has passed the following courses towards the fulfilment of coursework requirement for Ph. D.

Sl. No.	Course No.	Title of the Course	No. of Credits	Result
1.	CY801	Research Proposal	4	B+
2.	CY805	Instrumental Methods-A	4	B+
3.	CY806	Instrumental Methods-B	4	B+

M. Sathiyendiran

Hyderabad
January 2024

Prof. M. Sathiyendiran
(Thesis Supervisor)

Dr. M.Sathiyendiran
Professor
School of Chemistry
University of Hyderabad
Hyderabad - 500 046, India.

Dean

School of Chemistry
University of Hyderabad
Hyderabad- 500046, INDIA

Dean
SCHOOL OF CHEMISTRY
University of Hyderabad
Hyderabad-500 046.

ACKNOWLEDGEMENTS

I would like to express my sincere gratitude to my Ph.D. supervisor Prof. M. Sathiyendiran for his valuable guidance and support during my Ph.D. research work.

I wish to extend my heartiest gratitude to my doctoral committee members, Prof. K. C. Kumaraswamy and Prof. R. Chandrasekar for their encouragement and support.

I thank present and former deans, School of Chemistry, University of Hyderabad, and all the faculty members of the school of chemistry for their kind help and support throughout the tenure.

My special thanks to Dr. B. Shankar, Thiagarajar Institute of Engineering for his help throughout my Ph.D tenure. I would also like to offer my heartiest thanks to Dr. A. K. Rengan, IIT-Hyd and Dr. M. K. Rana, IISER Berhampur for their help with biological experiments and molecular docking studies respectively.

I want to acknowledge University Grant Commission, Delhi (UGC NET) for fellowship and Institute of Eminence (IoE) for funding.

I want to extend my thanks to all non-teaching members of the school of chemistry, especially Mr. Abram for his help in official work (School Office), Mr. Durgesh and Mr. Mahender (NMR, School of Chemistry), Mr. Mahesh Rathod (SC-XRD, School of Chemistry), Mrs. Asia Parwez and Dr. Manasi Dalai (HRMS, School of Chemistry), and Mr. Anand (IR, School of Chemistry), for their kind help, assistance, and cooperation with instruments during my research work.

I am highly indebted to the teachers of my undergraduate and postgraduate programs who were instrumental in igniting my interest in chemistry.

I would also like to thank all my lab seniors, Dr. Bhaskaran Shankar, Dr. C. Kiran Kumar, Dr. Sruthi Bayya, Dr. Amritanjali Tiwari, Dr. R. Arumugam, Dr. Soumya K. R., Dr. Mamina Bhol, Dr. Isha Mishra and Dr. Abinaya Mayavan for their constructive comments and helpful discussions. I am indebted to Dr. Mamina Bhol and Dr. Isha Mishra for being wonderful seniors who always had an open ear for my worries, guided me throughout the tenure and helped me figure things out. I am very grateful to all my colleagues Moon, Bhuvana, Reema, Vengadeshwaran, Sujeet and Tejasri for creating a pleasant work environment and making it a memorable and enjoyable journey. I extend my thanks to all the project students who worked with me, Sabita, Shruthi and Anet.

I am grateful to Sajmina Khatun, Chandra Lekha Putta and Saroj Kumar Panda for their kind help and support in my collaborative projects.

I express my heartiest thanks to all my batch mates especially Shampita, Sridatri, Seema, Somdutta, Rani, Manasa and Swathi for their support throughout my Ph.D tenure and for providing a homely atmosphere making my stay in Hyderabad a memorable one.

I would also like to thank my friends especially Sunika*, Alpana*, Swapnali*, Suprava*, Sukanya* for always being my constant sources of support (*contributed equally). Thank you for always being patient with me and listening to my rants while guiding me through all of it.

I was sustained by the magical world of K-pop, K-dramas and my frequent visits to AMB which kept me sane during all the hard times.

Special warmest thanks to Moon for being there with me through the good, the bad, and all the in betweens. This journey would not have been possible without your love, understanding and immense support. You definitely are one of my greatest takeaways from this journey. Thank you for being a wonderful friend and for all the fun we have had in last five years.

Most importantly, I thank Deuta, Ma and Dada for the unwavering support throughout my academic research and daily life. It is only because of your love and support that I am able to stand strong and face the world. Dada thank you for always inspiring me and for giving me the courage to fly to a different state and pursue my studies. You are my role model and I look up to you in every way possible.

I offer my warm thanks to Khuri and Tikli for being the constant pillars of support and being there for me through all the thick and thin, which provided me comfort and courage during my Ph.D journey.

This dissertation is the conclusion of a memorable journey, encompassing happy and sad moments and it stands as a testament to hard work put together in any form by all the people and myself. So I would like to thank myself for never giving up, for doing the hard work and for being resilient. These years taught me the value of grit and made me stronger in the face of difficulties. Finally, I thank God Almighty for his grace and blessings.

Upasana Phukon

January 2024

List of abbreviations and symbols

SCCs	Supramolecular coordination complexes
fac	facial
Re	Rhenium
2D	Two Dimensional
3D	Three Dimensional
DMSO	Dimethyl Sulfoxide
THF	Tetrahydrofuran
DMF	N,N-Dimethylformamide
DCM	Dichloromethane
$CHCl_3$	Chloroform
$CDCl_3$	Deuterated Chloroform
DMSO-d_6	Deuterated Dimethyl Sulphoxide
UV-Vis	Ultraviolet-Visible
ATR-IR	Attenuated Total Reflectance Infrared spectroscopy
FT-IR	Fourier-transform Infrared Spectroscopy
NMR	Nuclear Magnetic Resonance
DOSY	Diffusion Ordered Spectroscopy
ESI- HR-MS	Electron Spray Ionization High Resolution Mass Spectrometry
SCXRD	Single Crystal X-Ray Diffraction
DNA	Deoxyribonucleic acid
IC_{50}	Concentration of a substance to inhibit the growth of 50% cells
Ppm	Parts per million
Å	Angstrom
hr	Hour
m/z	Mass to charge ratio
mg	Milligram

mL	Millilitre
nm	Nanometer
μM	Micro molar
δ	Chemical shift
Hz	Hertz
MHz	Megahertz
J	Coupling constant
KOH	Potassium hydroxide
NaH	Sodium hydride
NaOH	Sodium hydroxide
AcOH	Acetic acid
HBr	Hydrobromic acid
NaCl	Sodium Chloride
Na_2SO_4	Sodium Sulphate
KBr	Potassium bromide
H_2-dhbq	2,5-dihydroxy-1,4-benzoquinone
H_2-dhaq	1,4-dihydroxy-9,10-anthraquinone
H_2-dhnq	5,8-Dihydroxy-1,4-naphthoquinone
H_2-dhnd	6,11-dihydroxy-5,12-naphthacenedione
H_2-pydc	2,5-Pyrazinedicarboxylic acid
H_4-thbq	2,3,5,6-tetrahydroxy-1,4-benzoquinone
H_2-bbim	Bisbenzimidazole
H_2-RBC	Rigid bischelating ligand
H_2-pBC	1,4-bis(2-(2-hydroxyphenyl)benzimidazol-1-ylmethyl)benzene
H_2-mBC	1,3-bis(2-(2-hydroxyphenyl)benzimidazol-1-ylmethyl)2,4,6-trimethylbenzene
dppz	bis(4-((pyrazolyl) methyl)phenyl)methane

dpbim	bis(4-((benzoimidazolyl)methyl)phenyl)methane
bpz	1,2-bis((pyrazolyl)methyl)benzene
PTA	1,3,5-Triaza-7-phosphaadamantane
H-pz	Pyrazole
H-Ind	Indazole
H-Br-pz	4-Bromopyrazole
XyBim	1,2-bis((benzoimidazolyl)methyl)benzene

SYNOPSIS

The thesis entitled "Self-assembly of Rhenium(I) Metallocycles Using Pyrazole Based Ligands" consists of six chapters.

Chapter 1: Introduction

Chapter 1 contains brief literature overview on metallocyclic architectures in general and particularly rhenium(I)tricarbonyl-based supramolecular coordination complexes (SCCs) spanning from dinuclear metallocycles to multinuclear complexes. The chapter also provides a general overview on flexibile ligands containing various types of N/P=O donors and their use to prepare rhenium(I)tricarbonyl-based SCCs of various shapes and sizes.

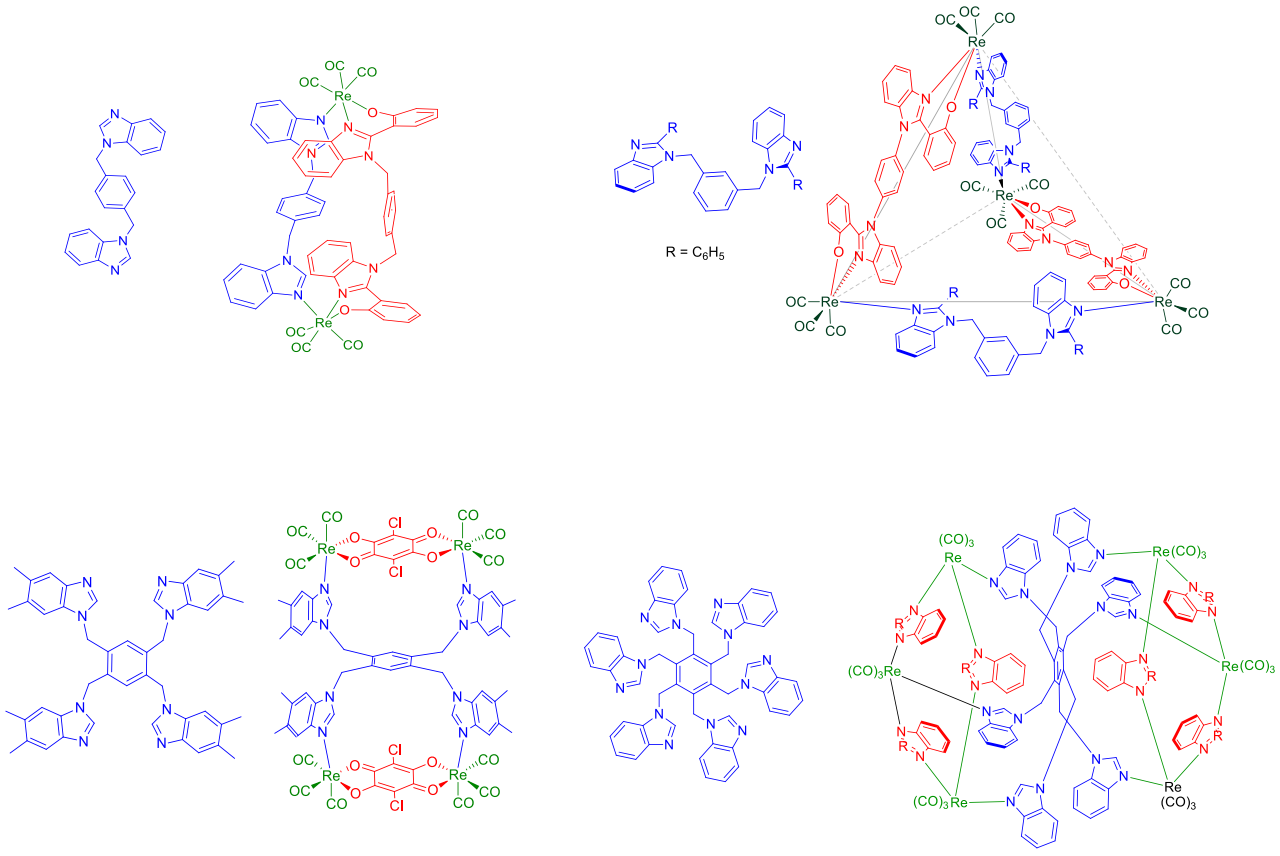

Figure 1. Various types of nitrogen donors and their corresponding rhenium-based metallocycles.

Chapter 2: Self-assembly of a new class of rhenium(I)-based double stranded dinuclear monohelicates

This chapter describes the design and synthesis of two new neutral ditopic flexible N-donor ligands (L^n = (L^1 = bis(4-((pyrazol-1-yl)methyl)phenyl)methane, L^2 = bis(4-((pyrazol-1-yl)methyl)phenyl)methanone possessing bis(4-methylphenyl)methane spacer with pyrazolyl donor unit. The chapter also describes the synthetic strategy for a new class of double stranded dinuclear monohelicates, *fac*-[{$Re(CO)_3$-(μ-L)-$Re(CO)_3$}L^n] (**1–4**) which were self-assembled from $Re_2(CO)_{10}$, a rigid bischelating donor (H_2-L: 1,4-dihydroxybenzoquinone (H_2-dhbq) for **1** and **3**; 2,5-pyrazine dicarboxylic acid (H_2-pydc) for **2** and **4**) and a flexible bis(monodentate) pyrazolyl N donor L^n (L^1 for **1** and **2**; L^2 for **3** and **4**) in mesitylene via solvothermal approach.

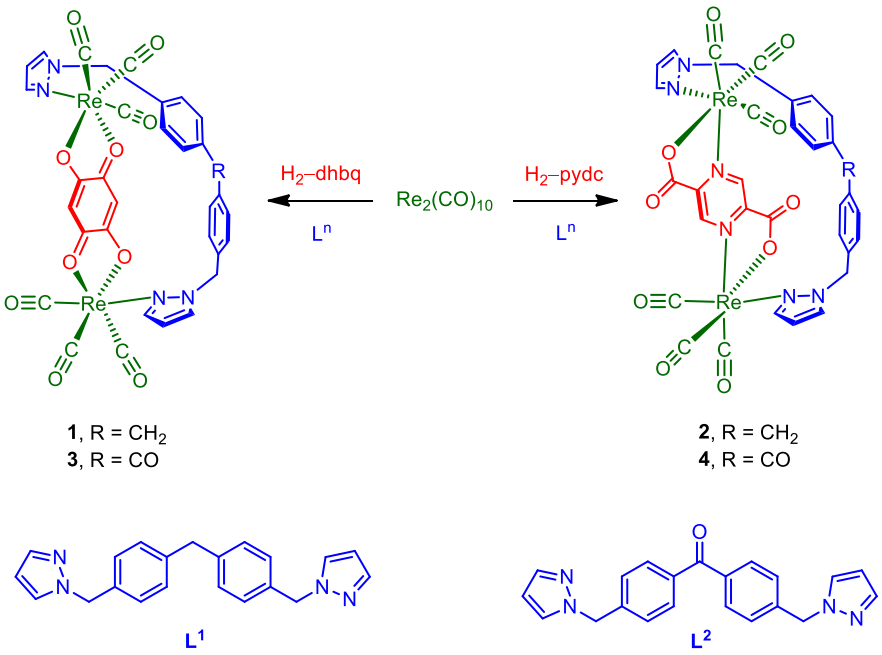

Scheme 1. Synthesis of helicates **1-4**.

The complexes were characterized using analytical and spectroscopic methods and further the molecular structure of **1** was confirmed by single crystal X-ray diffraction analysis. The XRD data reveals that **1** is helical in nature where although two organic ligand strands are present only one strand is arranged in a helical fashion, which is an unprecedented form in the helicate architecture. The molecular structures of **1–4** as helicates and mesocates were also optimized using DFT methods. The study provides a way to synthesize dinuclear monohelicates via simple one-pot method.

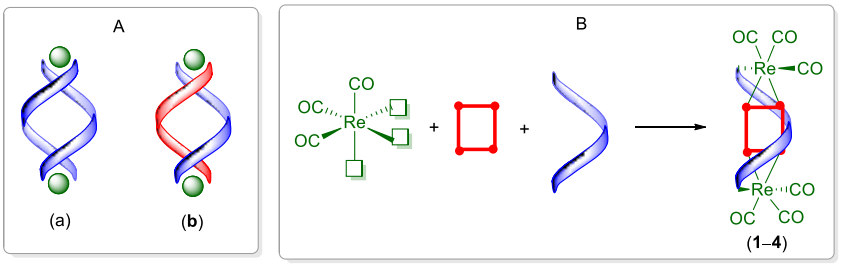

Scheme 2. (A) Commonly observed double-stranded dinuclear (a) homoleptic and (b) heteroleptic double helicates. (B) The design principle of new forms of double-stranded dinuclear monohelicates **1–4**.

Chapter 3: Self-assembly, solution dynamics and competitive ligand induced supramolecular transformations of "figure-eight" and "Z" shaped metallocycles

Chapter 3 describes the synthetic strategy, structural studies of rhenium(I)tricarbonyl core-based heteroleptic "*figure-eight*"- and *Z*-shaped metallocycles (**1a**–**4a**) of the general formula *fac*-[{Re(CO)$_3$(μ-L)Re(CO)$_3$}$_2$(dppz)$_2$] which were self-assembled from $Re_2(CO)_{10}$, H_2-L (H_2-L = 5,8-dihydroxy-1,4-naphthaquinone (H_2-dhnq) for **1a**; 1,4-dihydroxy-9,10-anthraquinone (H_2-dhaq) for **2a**; 6,11-dihydroxy-5,12-naphthacenedione (H_2-dhnd) for **3a**; 2,2′-bisbenzimidazole (H_2-bbim) for **4a**), and bis(4-((pyrazolyl)methyl)phenylmethane) (dppz) via one-pot coordination-driven synthetic approach. The molecular structures of **1a** and **4a** were unambiguously confirmed by single-crystal X-ray diffraction (SC-XRD) methods.

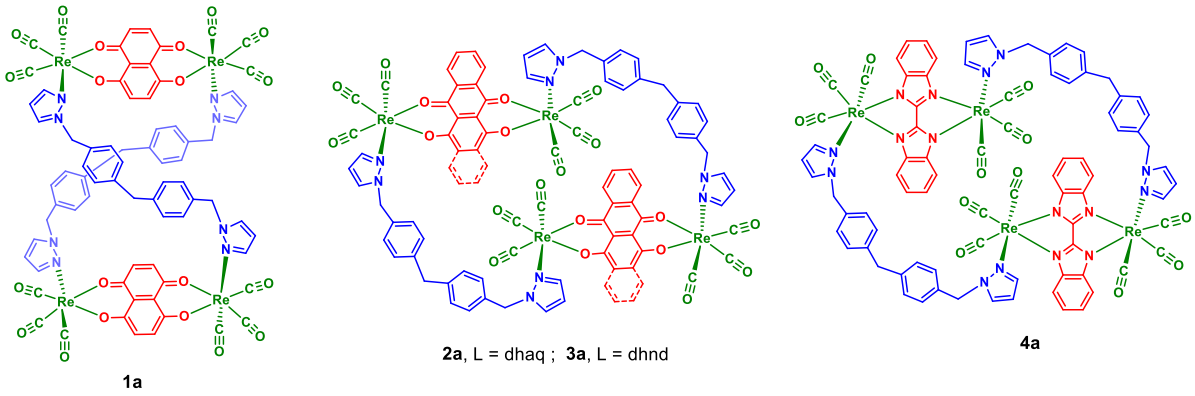

Figure 2. Metallocycles **1a–4a**.

The metallocycles in the DMSO solution exist as an acyclic dinuclear–DMSO adduct of the general formula *fac*-[{$(CO)_3$Re(μ-L)Re$(CO)_3$}$(DMSO)_2$] (**1b**, L = dhnq; **2b**, L = dhaq; **3b**, L = dhnd; **4b**, L = bbim) and dppz, which are in dynamic equilibrium. The dynamic behavior of the rhenium–pyrazolyl bond in the solution state was effectively utilized to transform metallocycles **1a**–**4a** into pyridyl/benzimidazolyl/phosphine donor-based heteroleptic metallocycles and acyclic dinuclear complexes (**4**–**13**). These include tetranuclear rectangles *fac*-[{$(CO)_3$Re(μ-L)Re$(CO)_3$}$_2$(4,4′-bpy)$_2$] (**4** and **11**, L = dhaq for **4** and bbim for **11**), dinuclear metallocycles *fac*-[{$(CO)_3$Re(μ-L)Re$(CO)_3$}(dpbim)] (**5**–**7** and **12**; L = dhnq for **5**, dhaq for **6**, dhnd for **7**, and bbim for **12**), and dinuclear acyclic complexes *fac*-[{$(CO)_3$Re(μ-L)Re$(CO)_3$}$(PTA)_2$] (**8**–**10** and **13**; L = dhnq for **8**, dhaq for **9**, dhnd for **10**, and bbim for **13**).

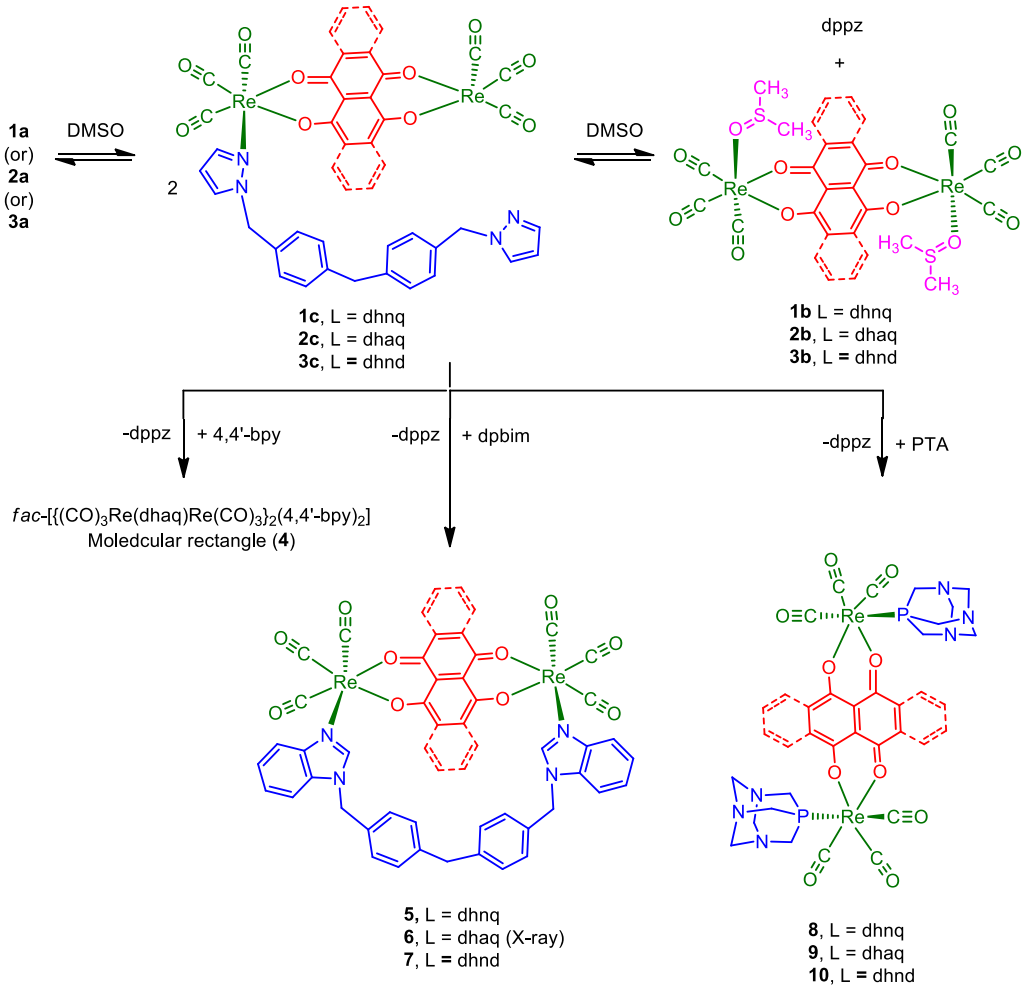

Scheme 3. Proposed dynamic nature of **1a**, (or) **2a**, (or) **3a** and component-induced supramolecular transformations into tetranuclear rectangle (**4**), dinuclear metallocycles (**5–7**), and dinuclear acyclic complexes (**8**–**10**) in DMSO.

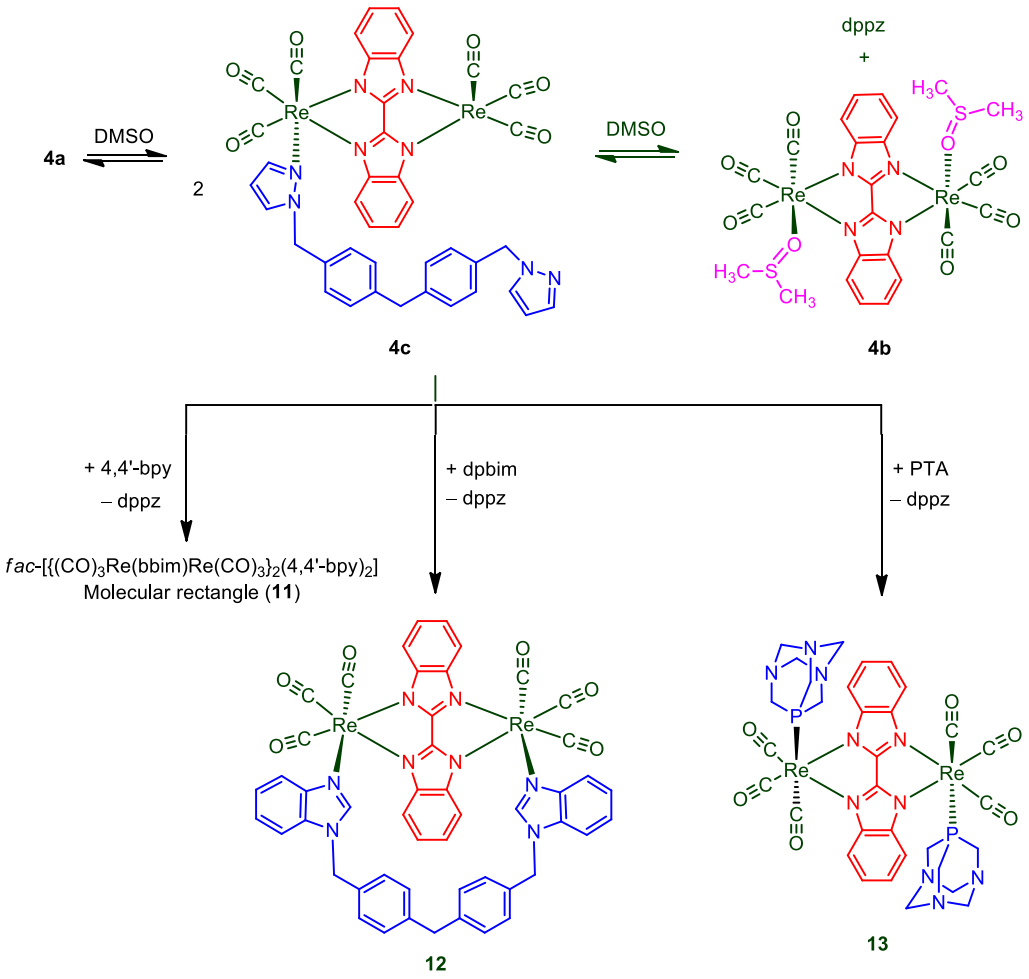

Scheme 4. Proposed dynamic nature of **4a** and component-induced supramolecular transformations into tetranuclear rectangle (**11**), dinuclear metallocycle (**12**), and dinuclear acyclic complex (**13**) in DMSO.

These transformations were achieved through component-induced supramolecular reactions while treating with competitive ligands 4,4′-bipyridine (4,4′-bpy), bis(4-((1H-benzoimidazole-1-yl)methyl)phenyl)methane (dpbim), and 1,3,5-triaza-7-phosphaadamantane (PTA). The reaction mixture in the solution was analyzed using NMR and electrospray ionization mass spectrometry (ESI-MS) analysis. Additionally, crystal structures of **4**, **6**, and **13**, which were obtained in the mixture of the solutions, were determined, providing unequivocal evidence for the occurrence of supramolecular transformation within the system.

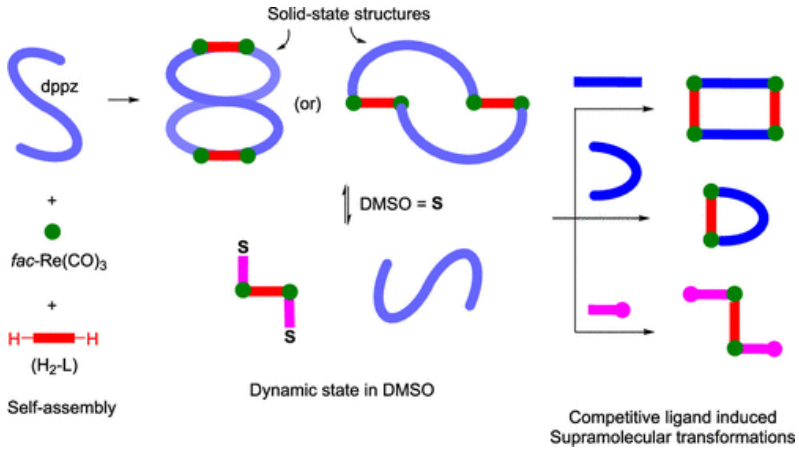

Scheme 5. Schematic representation of synthesis, dynamic nature and competitive ligand induced transformations of metallocycles.

The results reveal that the size of the chelating ligand and the pyrazolyl donor angle of the ditopic ligand play crucial roles in determining the resulting solid-state metallocyclic architecture in these synthetic combinations. The dynamic behavior of the rhenium–pyrazolyl bond in the metallocycles can be utilized to transform into other metallocycles and acyclic complexes using suitable competing ligands via ligand-induced supramolecular transformations.

Chapter 4: Design and synthesis of conjoined bicyclic rhenium(I) based metallocycles

Chapter 4 describes the synthesis of neutral conjoined bicyclic supramolecular coordination complexes (**1**-**3**) which were self-assembled using $Re_2(CO)_{10}$, anionic pyrazole donor and flexible hexatopic/tetratopic pyrazolyl donors. A new type of metal-ligand bonding combinations was seen in which two partially protected metal acceptor *fac*-$Re(CO)_3$-cores were bridged by pyrazolate motif and hydroxyl (OH^-) motif. The bicyclic metallomacrocycles were characterized using FT-IR, ESI-MS analysis and single crystal X-ray diffraction analysis.

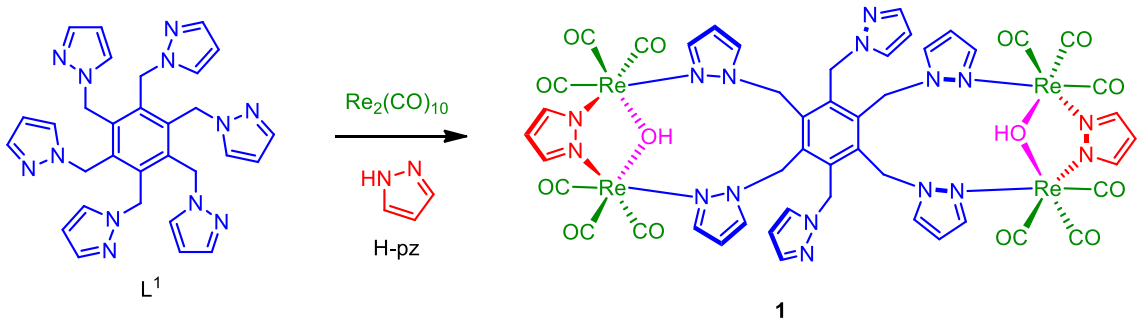

Scheme 6. Synthesis of metallocycle **1**.

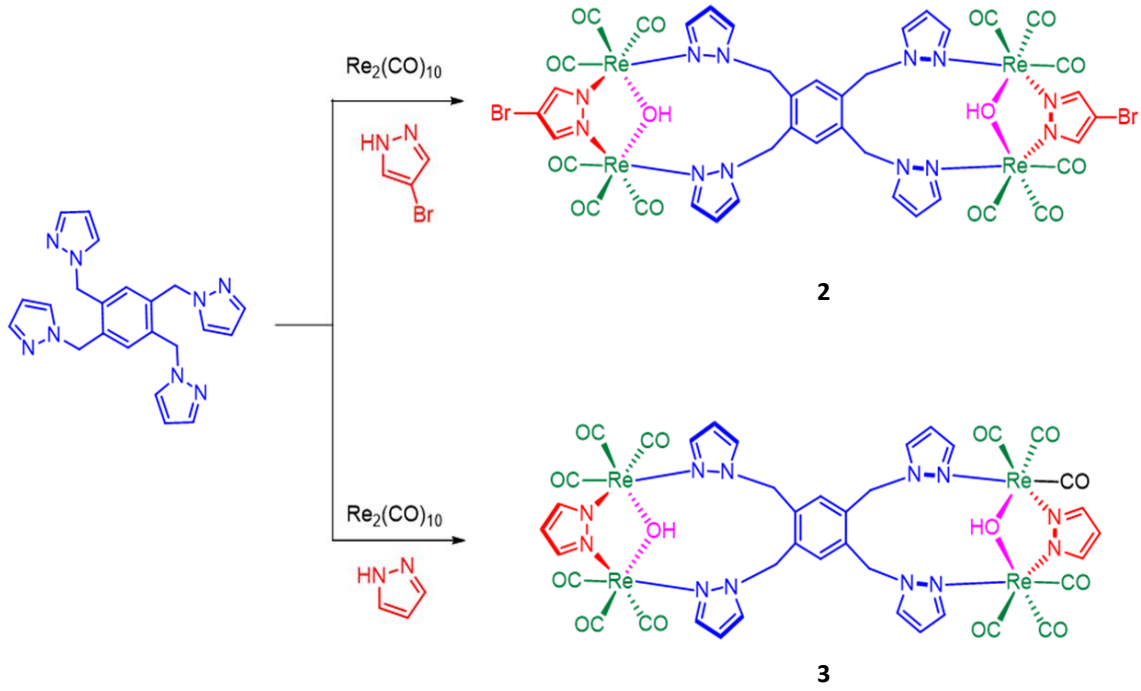

Scheme 7. Synthesis of metallocycles **2-3**.

Single crystal X−ray diffraction analysis of **1-3** reveal that the metallocycles consist of four *fac*-$Re(CO)_3$ cores, two anionic pyrazolate (for **1** and **3**)/Br-pyrazolate (for **2**) units, two hydroxyl ions, and one hexatopic pyrazolyl ligand (for **1**)/ one tetratopic pyrazolyl ligand (for **2-3**). The complexes contain two metallocyclic units that have one common phenylene framework and thus can be regarded as conjoined bicyclic supramolecular coordination complexes. The work provides a way to prepare a new type of conjoined SCC and acyclic complex via a simple one-pot approach.

Chapter 5: Self-assembly of a new class of azolato bridged rhenium(I) metallocycles as anticancer agents

Chapter 5 describes the design and synthetic approach for a new type of small multicomponent rhenium metallocycles (**1-4**) which consists of azolate, hydroxyl, α,α′-bis(pyrazol-1-yl)-o-xylene (bpz)/1,2-bis((benzoimidazol-1-yl)methyl)benzene(XyBim) nitrogen donor, and two rheniumtricarbonyl groups. The metallocycles were self-assembled using a one-pot, multi-component coordination-driven self-assembly approach and characterized using various spectroscopic and analytical techniques.

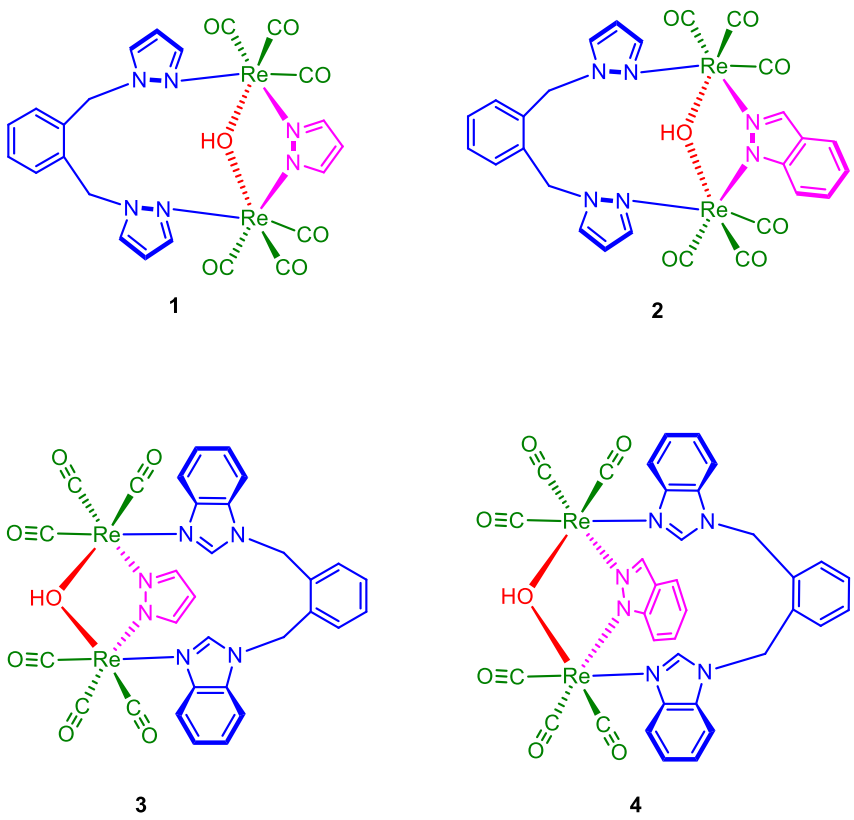

Figure 3. Synthesized metallocycles **1-4**.

The metallocycles **1-4** reported herein demonstrates effective anticancer property against triple negative breast cancer (TNBC) cells in vitro, exceeding that of cisplatin as evident from MTT assay. Molecular docking studies of **1** with B-DNA provided insights into its binding posture and nature of interactions with DNA.

Chapter 6: Conclusion and future perspective

This chapter summarizes the thesis work and gives a brief perspective of future direction of the research work. The design and synthesis of several *fac*-$Re(CO)_3$ core based architectures such as monohelicates, "*figure-eight*", "Z" shaped molecules, conjoined bicyclic metallocycles and compact dinucler metallocyles using pyrazole based ligands are discussed. The complexes were well characterized using various spectroscopic and analytical techniques. The anticancer properties of compact dinuclear metallocycles with azolato and hydroxyl cores against triple negative breast cancer cells (4T1) were studied and were found to exhibit good cytotoxic properties.

Chapter 1

Introduction

1.1. Overview

Supramolecular chemistry deals with the chemistry of non-covalent interactions between molecules to form molecular assemblies. Supramolecular chemistry is defined as "Chemistry beyond molecules" by Jean Marie Lehn which is basically self-organization of two or more discrete molecules via various intermolecular noncovalent interactions.[1-2] Supramolecular chemistry mainly covers host-guest interactions, molecular self-assembly, molecular recognition and molecular folding. Various types of weak intermolecular interactions such as H-bonding, ion-ion, π–π stacking, van der Waals, hydrophobic interactions and metal-ligand bonds form the basis of supramolecular chemistry.[1-4] Supramolecular chemistry that involves the directional metal-ligand bonds is termed as metallosupramolecular chemistry. Metallosupramolecular chemistry has garnered significant interest for design and synthesis of intricate architectures of higher complexity as well as functionality. Coordination-driven self-assembly is a method for synthesizing supramolecular coordination complexes (SCCs) where the predesigned ligands and metal precursor units self-organize themselves leading to the formation of stable discrete supramolecules.[4-5] The properties of the metal cores such as their shapes, bonding modes along with the lability of predesigned ligands and their coordinating units control the final shape of the metallomacrocycles. The availability of various metal coordination geometries along with ligand geometry unfolds numerous synthetic routes for rational design of various 2D and 3D SCCs such as metallocycles, metallocages, tetrahedrons, catenanes, rotaxanes, knots, links etc.[5-9] Significant attention is given towards synthesizing supramolecules of various architectures owing to their application prospects in the field of molecular recognition, catalysis, bioimaging, anti-cancer activities, sensors etc., and by use of proper metal cores and predesigned ligands, one can synthesize metallocycles with required functionality. [10-11] Several synthetic approaches such as directional bonding, orthogonal bonding, weak link and symmetry interactions can be utilized for the self assembly of supramolecular metallocycles.[5a]

1.2. Rhenium-based metallocycles

Rhenium tricarbonyl cores are one among the many metal cores used for synthesis of metallocycles. In literature several reports are known for metallocycles using rhenium core. For the synthesis of *fac*-rheniumtricarbonyl core based complexes often a variety of rhenium carbonyl precursors are used which includes $Re_2(CO)_{10}$, $Re(CO)_5Br$, $Re(CO)_5Cl$, $Re(CO)_5OTf$ and $[Re(CO)_3(dmso\text{-}O)_3](CF_3SO_3)$ along with predesigned known or newly synthesized organic ligand strands.[11-13] Use of the dinuclear $Re_2(CO)_{10}$ metal precursor leads to the synthesis of a variety of 2D and 3D complexes utilizing the three orthogonal vacant sites as provided in the *fac*-$Re(CO)_3$ core. A plethora of *fac*-$Re(CO)_3$ core based complexes with different architecture spanning from simple dinuclear metallocycle to complex multinuclear systems are synthesized and reported.[11-13] Much attention is given for the design and synthesis of these metallocycles because by modulating the basic coordination framework a wide range of complexes of various shapes and sizes can be synthesized.

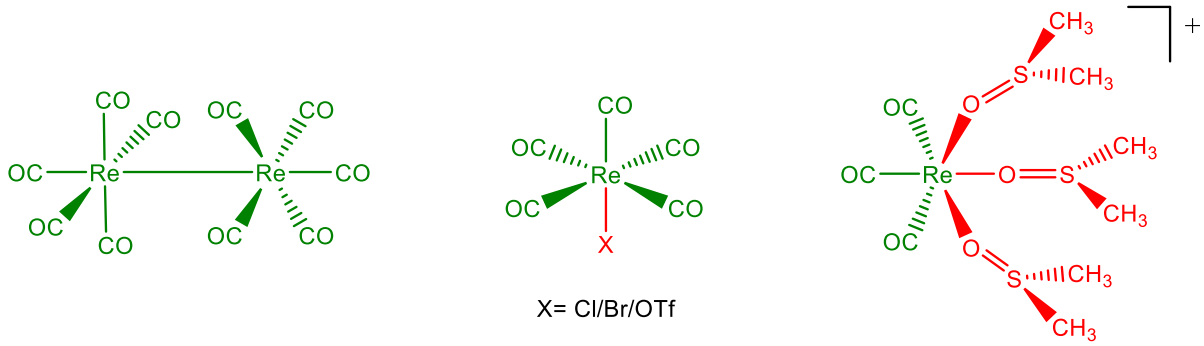

Figure 1.1. Three types of sources for the construction of *fac*-$[Re(CO)_3]$ core-based SCCs.

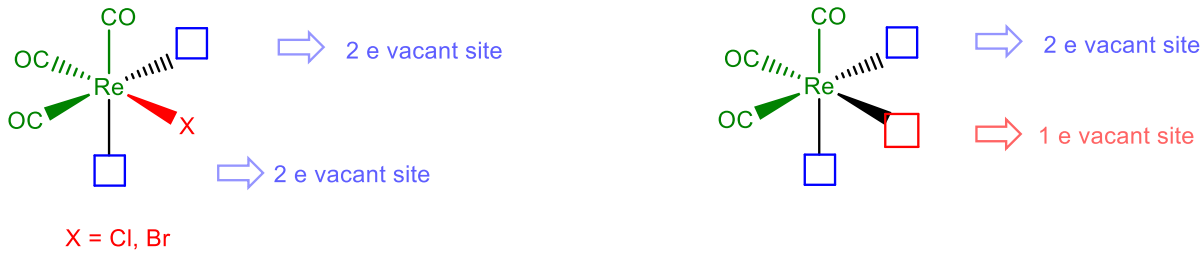

Figure 1.2. Vacant coordination sites available on *fac*–$Re(CO)_3$ core from $Re_2(CO)_{10}$.

A vast array of rhenium based architectures including dinuclear metallocycle (metallocavitands, helicates/mesocates), trinuclear (traingles, metallocages), tetranuclear (square, rectangles, tetrahedrons), hexanuclear (prism, wheel, spheroid) metallocycles are known in literature. For synthesis of these complexes usually soft donors such as N, O, P are used. Usually for rhenium metallocycles a neutral rigid or flexible ligand with two electron donor imidazolyl/benzimidazolyl/pyridyl as coordinating motifs is used along with a three electron donor bischelating anionic ligand.

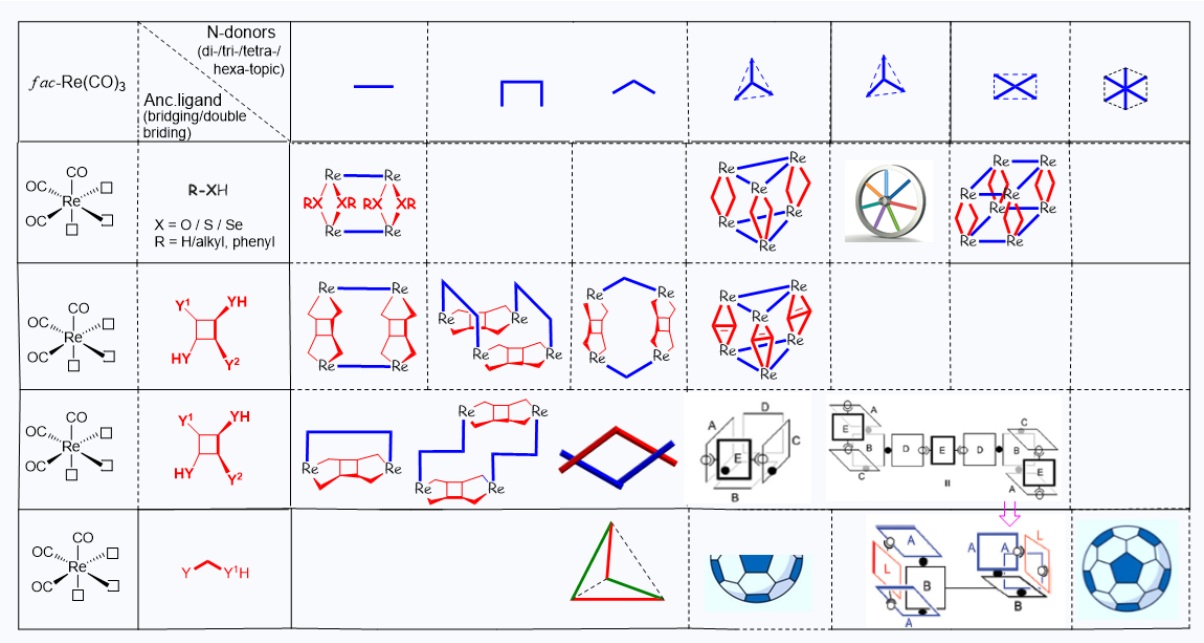

Figure 1.3. Library of rhenium complexes synthesized using various neutral N donor ligands and bischelating anionic ligands.

The bischelating anionic ligands used usually are N∩O, N∩N and O∩O donor based. The rigidity or flexibility of the bischelating ligands can be modulated by the incorporation of suitable spacer motifs in the ligand framework. For example the presence of xylene spacer in H_2-pBC, H_2-mBC renders flexibility to the ligand framework while the presence of phenyl spacer in H_2-RBC makes the ligand framework rigid.

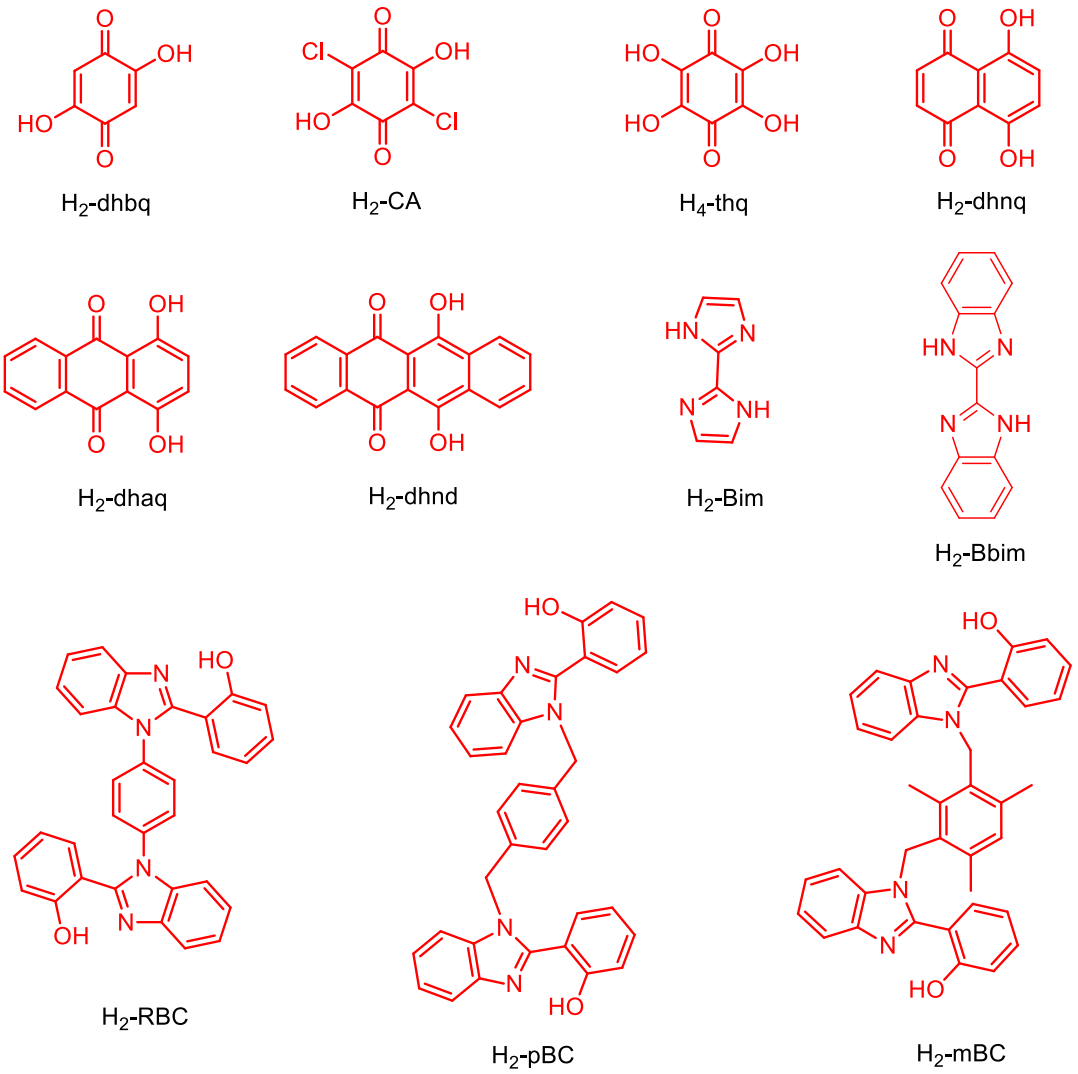

Figure 1.4. Anionic bischelating ligands used in synthesis of rhenium(I) based complexes.

1.3. Flexible Ligands

The choice of both neutral and anionic ligand plays an important role in dictating the final architecture and functional properties of the final complexes. The type of donor, binding sites as well as the geometry of their coordination sites plays an important role in the process. And hence a reasonable selection of ligands needs to be done for synthesizing the desired complexes. Flexible ligands contain at least one sp^3 hybrid atom which facilitates free rotation of the ligand and helps in adaptive coordination to metal cores.[14] Also the ligands possess multiple coordination sites that can bind to metal core. The shape, angle and flexibility of the ligand allow them to coordinate with metal cores and adopt various

topologies. The flexibility also provides the complexes with breathable properties which can adapt to different reaction conditions by minimising the steric condition through conformational changes. Flexible ligands thus provide a guiding significance for the diversity.

Functional groups can be introduced to the flexible ligands for synthesis of complexes with applicational value. The flexible ligands containing aromatic rings are well reported and they provide some rigidity to the framework leading to the formation of larger metallocycles.[15] These ligands also allow bending, rotation or stretching of the framework facilitating helical structure. The design strategy for synthesizing molecules using this kind of "soft and rigid" flexible ligands can yield several architectures with interesting properties including adaptive recognition and breathing ability.

Rigidity modulated approach is often used for directing the flexible ligands to bind with metal cores based on a rigid ancilliary ligand.[16] The rigid ligand provides the directionality needed for synthesis of required metallocycles. For example in a tetratopic flexible ligand as shown below the use of short rigid ancilliary ligand leads to formation of metallocycle through ortho selection of the flexible ligand whereas when long rigid bridger is used metallocyles are formed through meta selection.

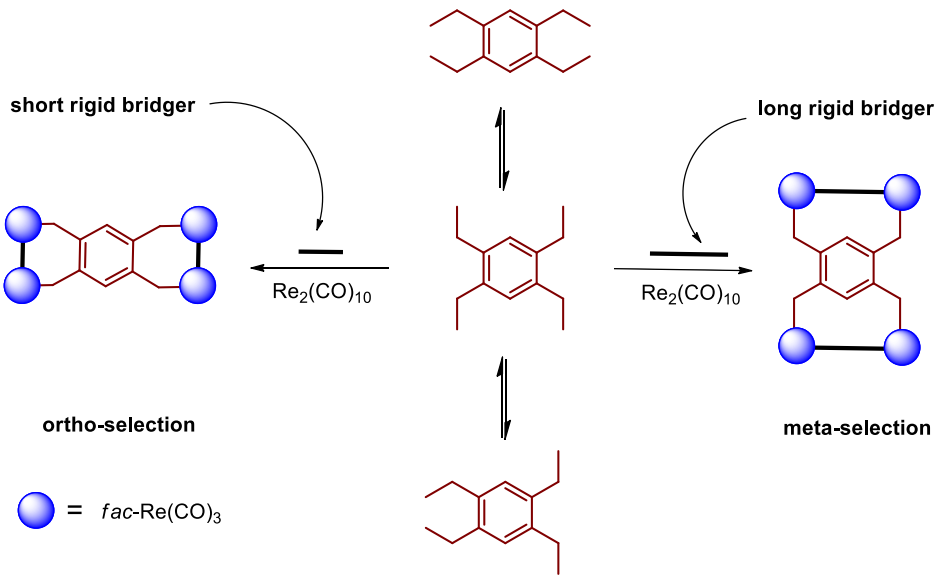

Figure 1.5. Representation of the flexibility in tetratopic ligand and their final architecture.

1.4. Neutral flexible ditopic ligands and their SCC's

Flexible neutral ditopic ligands containing alkyl or aryl spacer with imidazolyl/pyridyl/phosphine oxide (P=O) donors as coordinating units are widely used for the synthesis of rhenium(I)tricarbonyl core based coordination complexes of various shapes and sizes. Several pyridyl/imidazolyl/phosphine oxide based donor ligands are designed and synthesized for creating new metallocycles of desired architecture. Use of different spacer motifs in both neutral ditopic flexible ligands and anionic flexible ligands also plays a role for formation of different architecture.

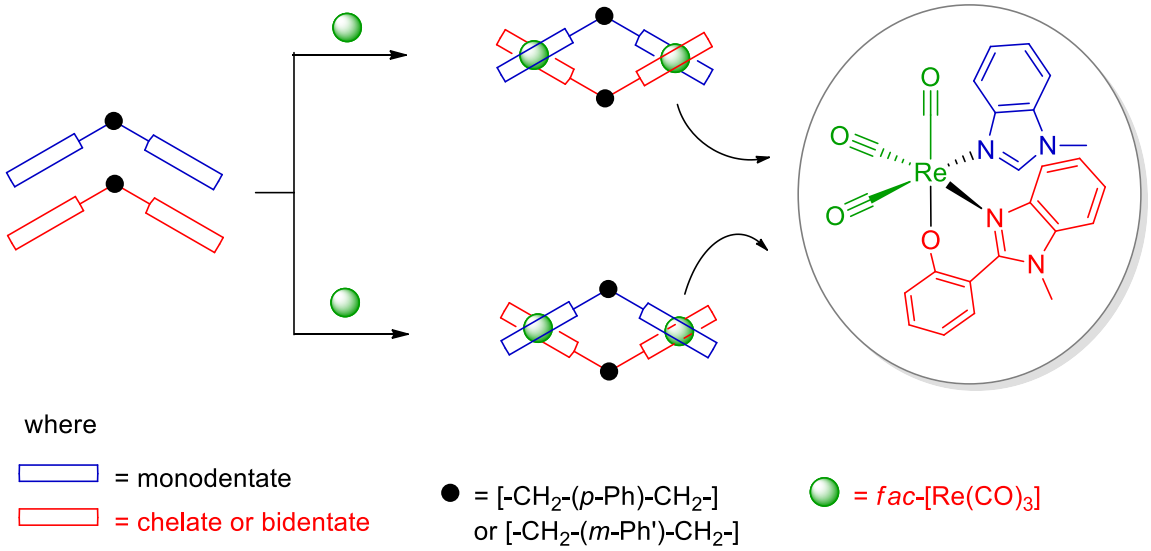

Scheme 1.1. Cartoon representation of self-assembly of *fac*-$Re(CO)_3$–based neutral unsaturated heteroleptic dinuclear double-stranded helicate and mesocate.

Use of both monodentate ditopic flexible ligands and flexible bidentate anionic ligands with $Re_2(CO)_{10}$ leads to the formation of helicates or mesocates depending on the spacer motifs used in each ligand. Ligands L^1-L^6 are few examples of neutral flexible ditopic ligands with different spacer motifs and coordinating units. L^1-L^2 are simple –CH_2-(*p*-Ph)-CH_2– spacer containing ligands with benzimidazolyl as the coordinating units. Ligand L^3 contains two mesitylene spacer motifs with benzimidazolyl as the coordinating motif. Similarly flexible ligand L^4 was designed and synthesized using bismesitylene methane spacer motifs and napthanoimidazolyl motifs as the coordinating unit. Ligand L^6 was synthesized using Troger base as the spacer unit and benzimidazolyl as the coordinating motif.

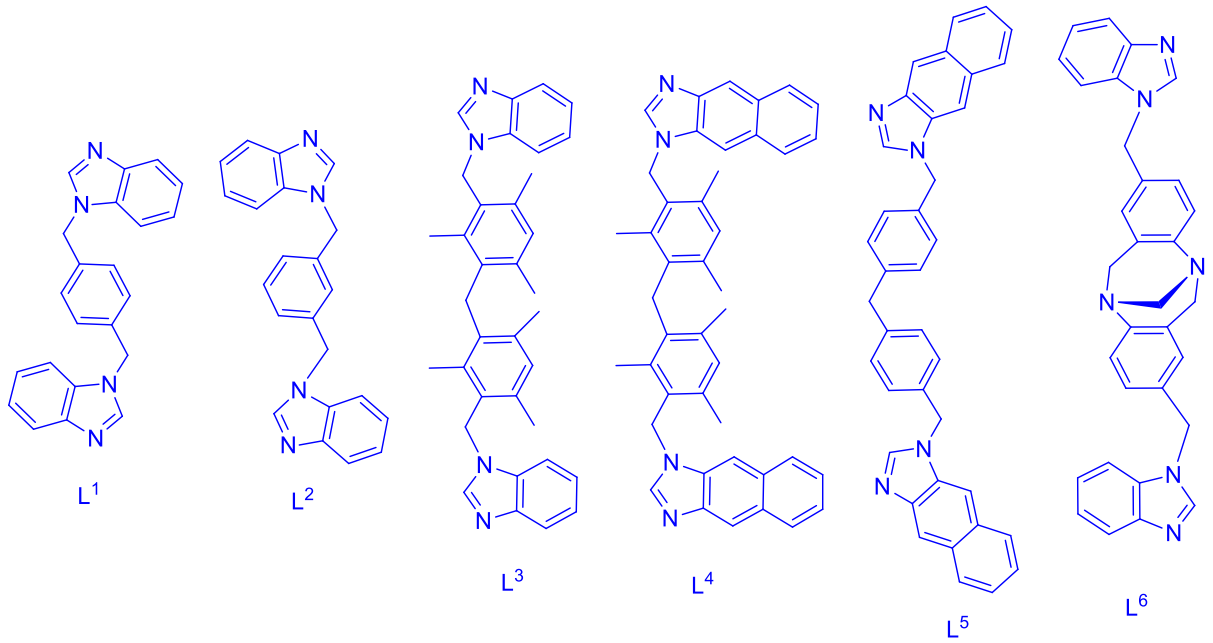

Figure 1.6. Ligands L^1-L^6 used in this work.

The use of L^1/L^2 in the presence of flexible anionic ligand 1,4-bis(2-(2-hydroxyphenyl)benzimidazol-1-ylmethyl)benzene (H_2-pBC) or 1,3-bis(2-(2-hydroxyphenyl)benzimidazol-1-ylmethyl)2,4,6-trimethylbenzene (H_2-mBC) and $Re_2(CO)_{10}$ leads to the formation of helicate **1** and mesocate **2** respectively.[17] In complex **1** both the ligands are arranged in helical manner resulting in heterostranded dinuclear double helicate. However, in complex **2** both the ligands are parallely arranged leading to the formation of mesocate architecture.

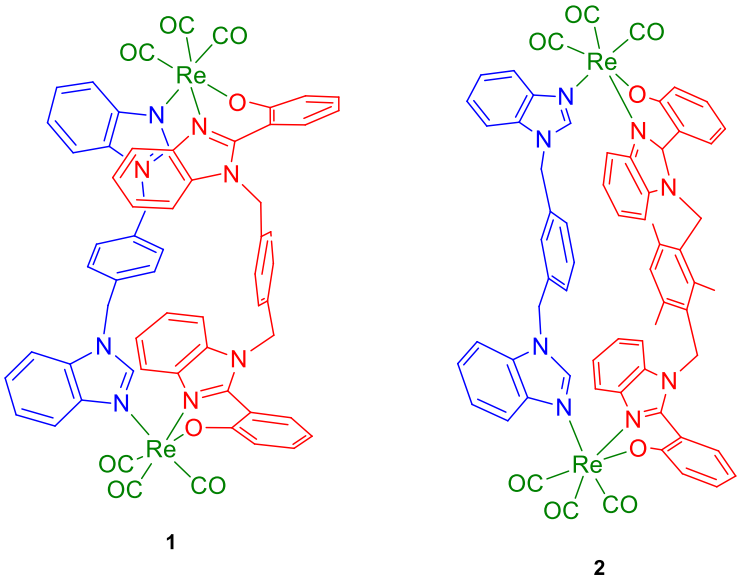

Figure 1.7. Double stranded dinuclear helicate **1** and mesocate **2**.

Flexible ligands L^1/L^2 in the presence of another flexible anionic bischelating ligand 5,5'-methylenebis(3-(tert-butyl)-2-hydroxybenzaldehyde) yielded neutral dinuclear double stranded helicates **3** and **4** respectively.[18]

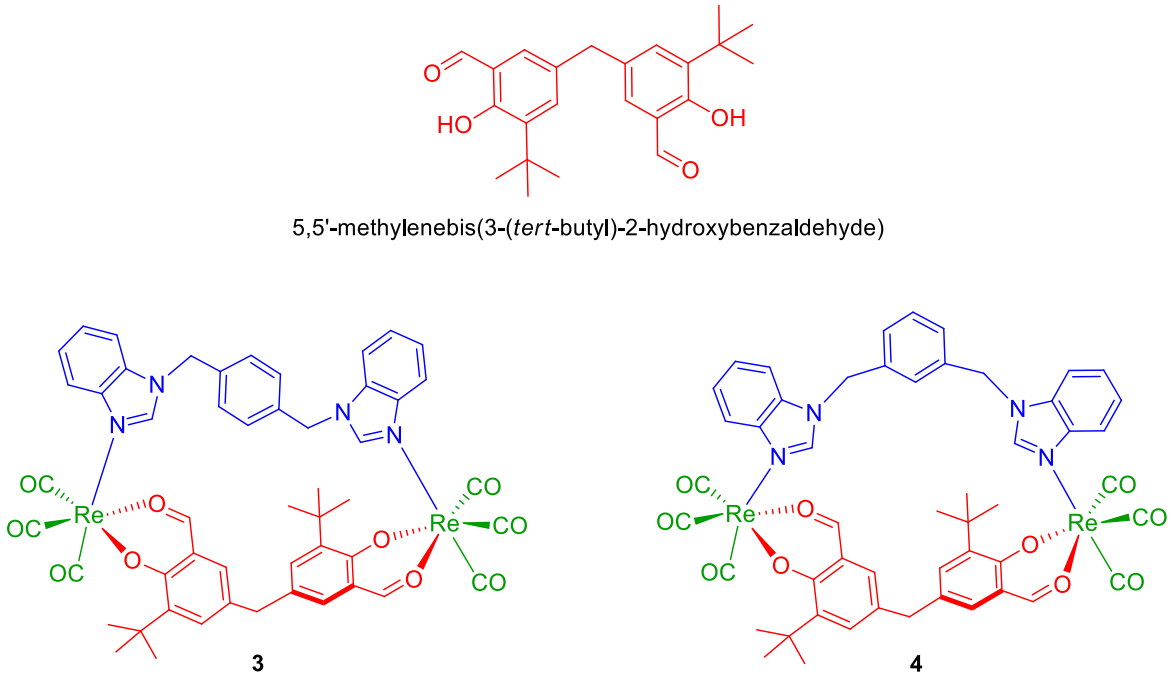

Figure 1.8. Dinuclear double stranded helicates **3** and **4**.

Similarly when flexible ligands L^3-L^4 were reacted with a rigid bischelating ligand H_2-RBC and $Re_2(CO)_{10}$ helical shaped architectures **5** and **6** were formed.[19] In the complexes both the rigid anionic ligand flexible neutral ligands are wrapped around in a helical manner. Self-assembly of ligand L^5 with H_2-RBC and $Re_2(CO)_{10}$ leads to the formation of metallocycle **7**. Metallocycle **7** adopts a mesocate structure with both the rigid and flexible ligands parallel to one another and the Re···Re axis. No helical twist was present in any of the ligand strands. The absence of methyl groups in the ligand framework of L^5 in **7** resulted in the non-helical arrangement of the metallocycle.

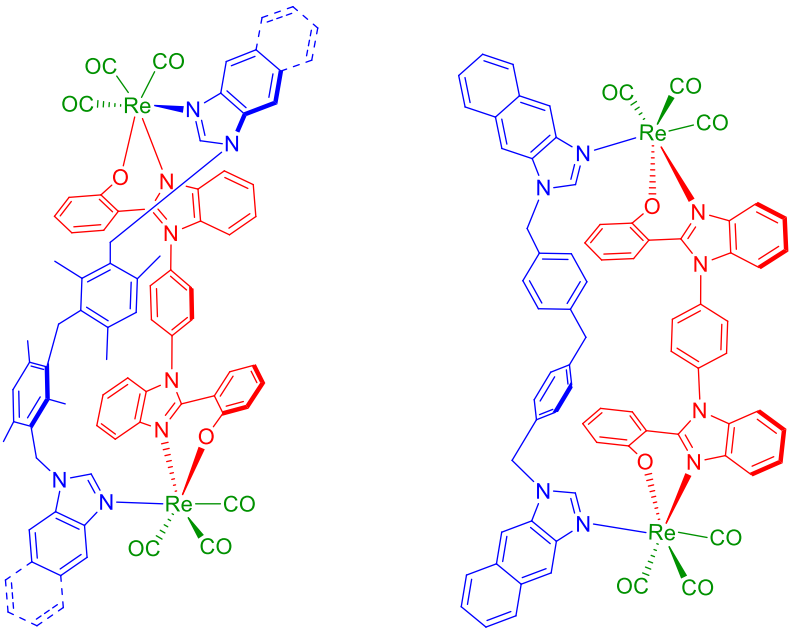

5, L^3
6, L^4

7

Figure 1.9. Dinuclear double stranded helicates **5-6** and mesocate **7**.

In a similar manner use of a Troger base spacer based ligand L^6 with benzimidazolyl motifs along with flexible bischelating anionic ligands H_2-pBC or H_2-mBC and $Re_2(CO)_{10}$ under solvothermal conditions using toluene as solvent leads to the formation of heteroleptic dinuclear helicates **8** and **9** respectively.[20]

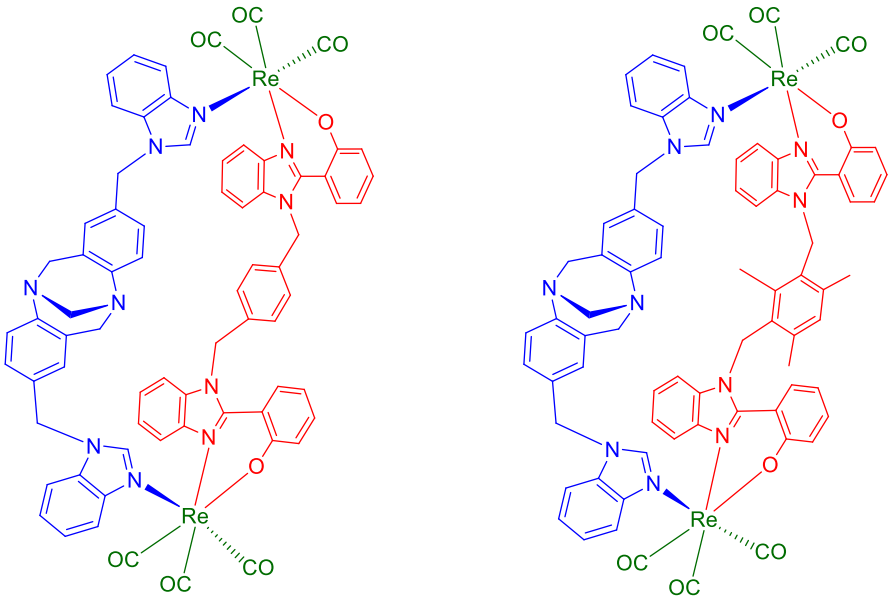

8

9

Figure 1.10. Dinuclear double strand helicates **8** and **9** using Troger base based ligand L^6.

Flexible ligands L^3/L^4 when reacted with $Re(CO)_5Cl$/$Re(CO)_5Br$ results in the formation of mononuclear metallocycles **10-11**.[21]

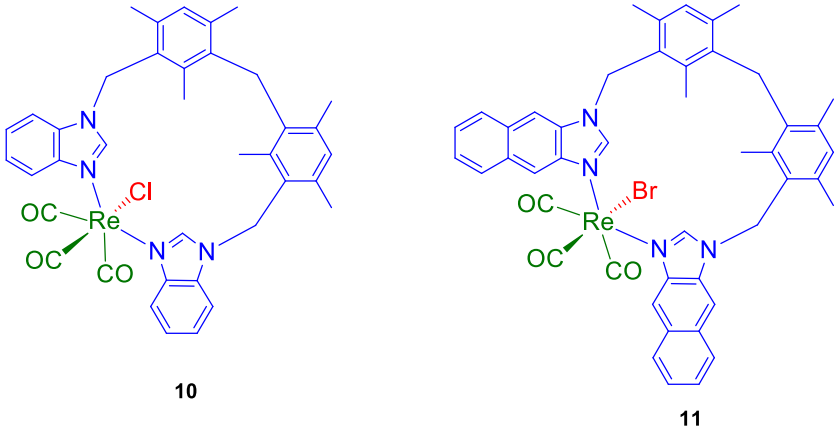

Figure 1.11. Mononuclear metallocycles **10-11** using flexible ditopic ligand L^3.

–CH_2-(*p*-Ph)-CH_2– spacer based ditopic ligands L^6-L^9 having different coordinating motif units were designed and synthesized for synthesis of metallocycles.

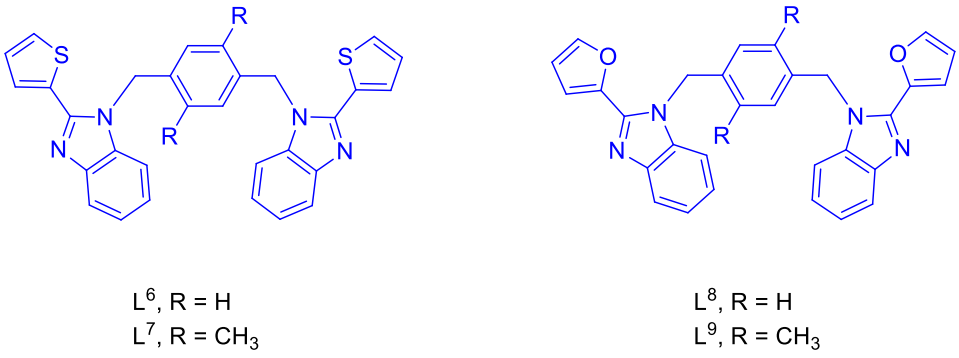

L^6, R = H
L^7, R = CH_3

L^8, R = H
L^9, R = CH_3

Figure 1.12. Phenylene spacer based flexible neutral ligands L^6-L^9.

Using these flexible ligands with rigid bischelating ligands H_2-dhbq/H_2-dhnd/H_2-CA/H_4-thbq and $Re_2(CO)_{10}$ via solvothermal approach or reflux method dinuclear metallacalix[4]arene supramolecules **12-23** were synthesized.[22] These metallocycles contains a cavity which can accommodate small guest molecules. The functionality of these cavity containing molecules can be modulated by changing the coordinating motif or the ligand framework.

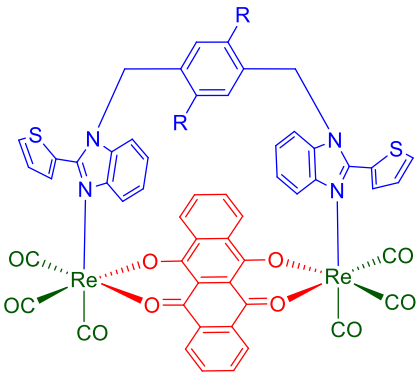

12, R = H
13, R = OCH_3

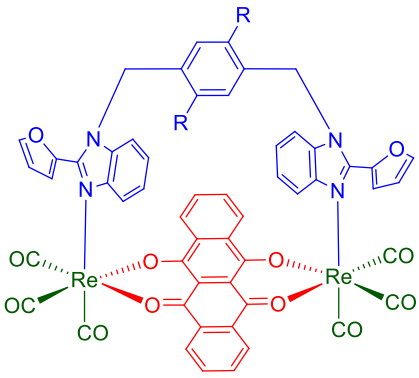

14, R = H
15, R = OCH_3

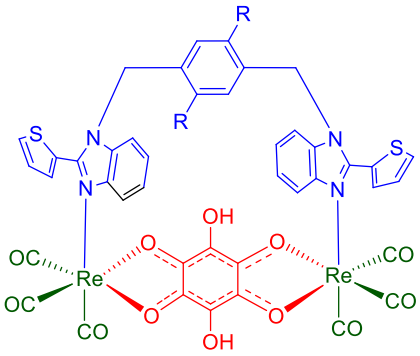

16, R = H
17, R = OCH_3

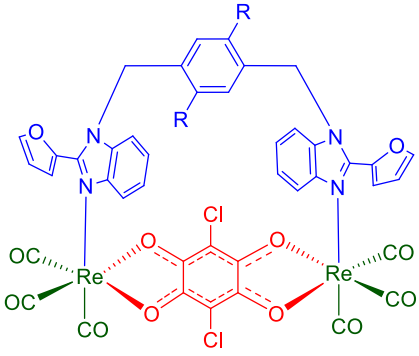

18, R = H
19, R = OCH_3

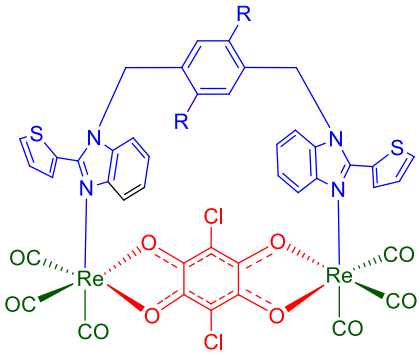

20, R = H
21, R = OCH_3

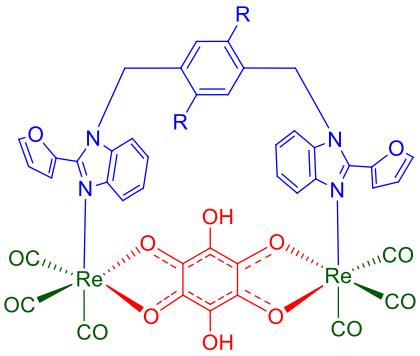

22, R = H
23, R = OCH_3

Figure 1.13. Dinuclear rhenium core based SCCs **12-23** using flexible neutral ligands and rigid anionic ligands.

Uses of alkyl spacer based ditopic flexible ligands for synthesis of metallocycles are well known. Several pyridyl coordinating motif based ditopic flexible ligands L^{10}-L^{11} containing alkyl spacer units are known. Ligands L^{10} and L^{11} when reacted with anionic rigid bischelating ligands 2-(pyridin-2-yl)-benzimidazole or bisbenzimidazole yielded dinuclear metallocycles **24-26**.[23]

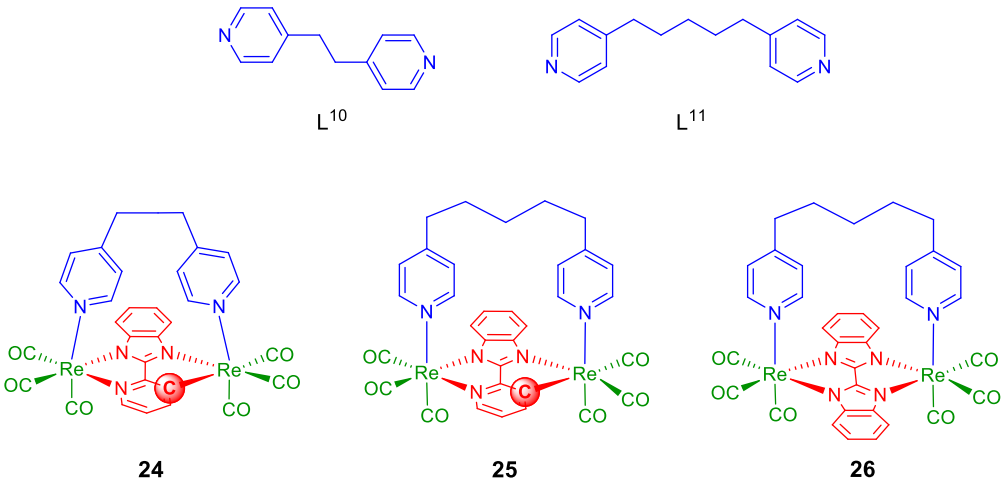

Figure 1.14. Dinuclear rhenium core based SCCs **24-26** using flexible neutral ligands and rigid/flexible anionic ligands.

Several polyether spacer containing pyridyl based flexible ditopic ligands are used for synthesis of metallocycles. Self-assembly of $Re(CO)_5Cl$ and ligand L^{12} leads to the formation of a mononuclear metallocycle **27**.[24] Ligands L^{10} and L^{11} when reacted with $Re_2(CO)_{10}$ and oxamide ligands (H_2L = N,N′-diphenyloxamide, and N,N′-dibenzyloxamide) bridging amide base donor ligands resulting in formation of dinuclear rhenium(I) metallacrown ethers **28-30**.[25]

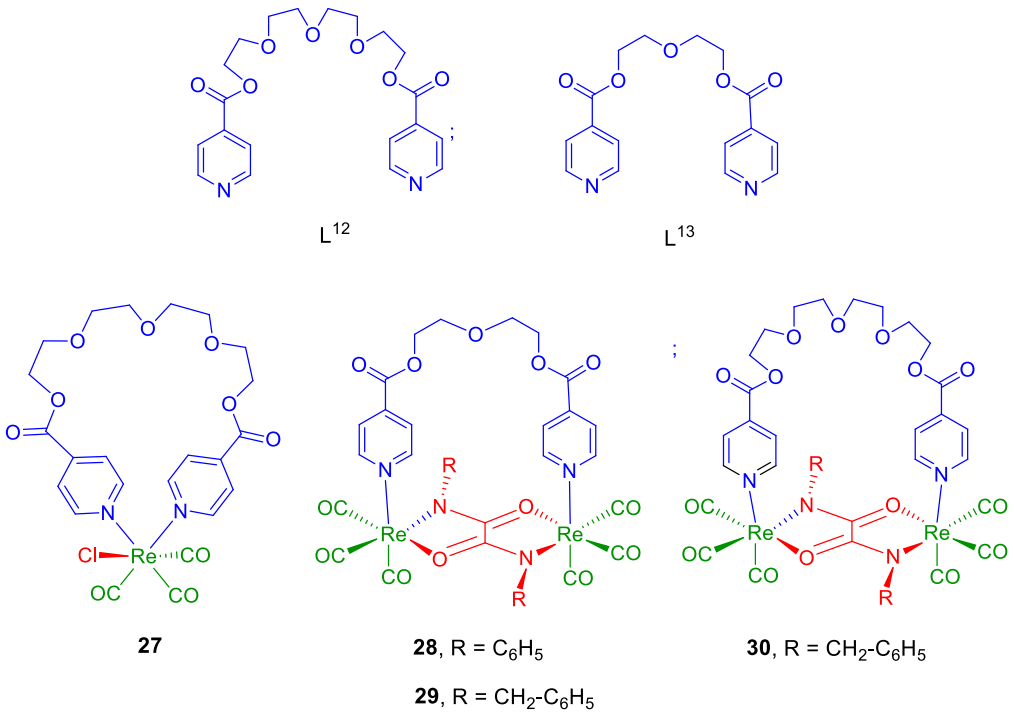

Figure 1.15. Mononuclear metallocycle **27** and dinuclear metallocycles **28-30** using flexible neutral ligands L^{12} or L^{13}.

When biphenyl methane spacer containing flexible ligands L^{14}-L^{16} are synthesized with benzimidazolyl motif as the coordinating unit and used along with rigid anionic ligands and $Re_2(CO)_{10}$, dinuclear metallocavitands **31-34** are formed.[26] These metallocavitands are found to possess a bigger cavity than their single phenylene spacer metallocycles as evident from their molecular structures.

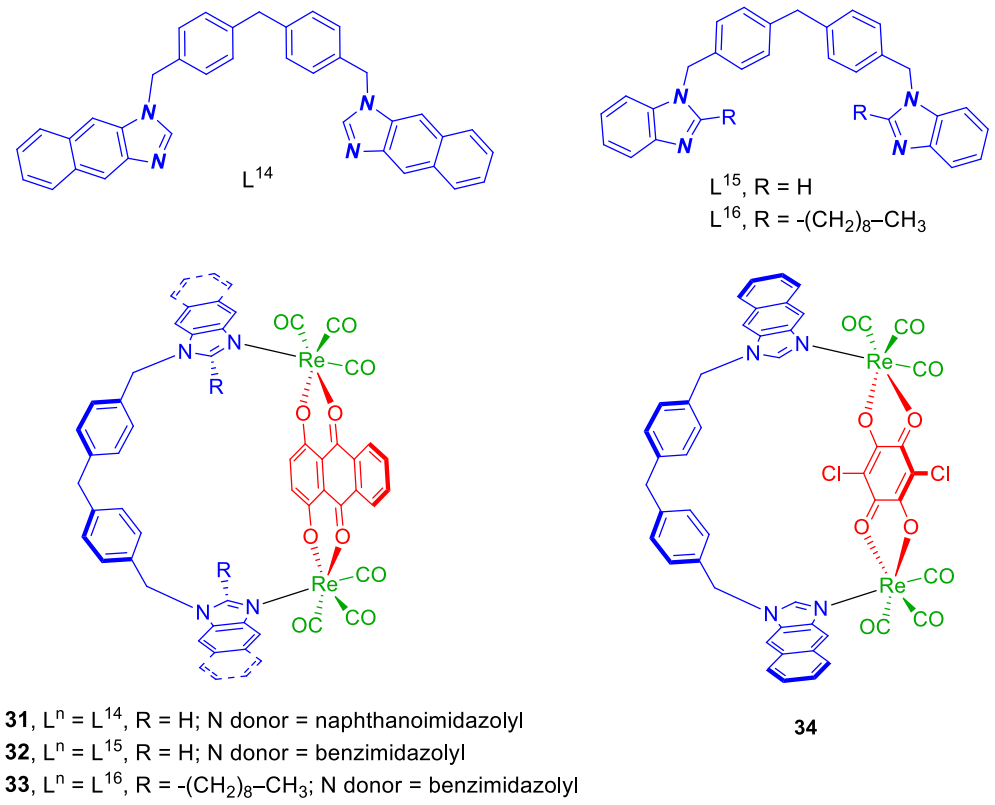

Figure 1.16. Neutral N donor ditopic ligands L^{14}-L^{16} and metallocavitands **31-34**.

A wide variety of xylene spacer based flexible ditopic ligands L^{17-22} having N donor coordinating unit are known.

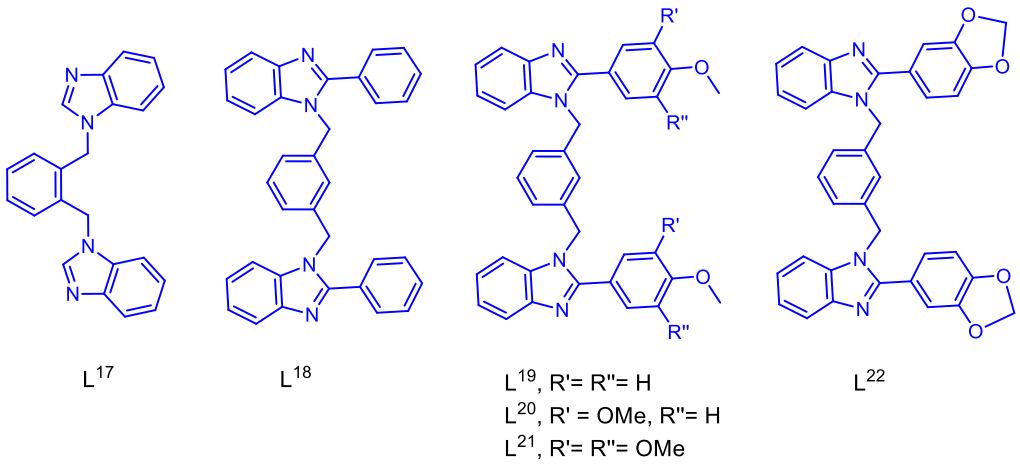

Figure 1.17. Neutral xylene spacer based flexible ligands L^{17}-L^{22}.

A xylene spacer based, benzimidazolyl donor motif containing ditopic flexible ligand L^{17} when reacted with rigid bischelating ligand H_2-dhnd lead to the formation of tetranuclear metallocycle **35**.[23a]

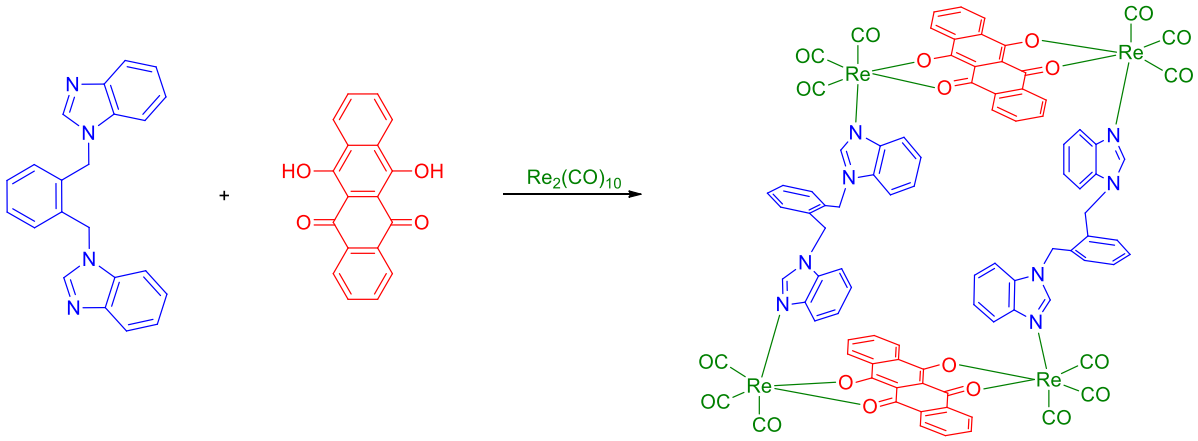

35

Scheme 1.2. Synthesis of tetranuclear metallocycle **33** using flexible ligand L^{17}.

The use of similar ligands L^{18}-L^{22}, along with rigid bischelating ligand with 2-(hydroxyphenyl)benzimidazolyl motifs and a phenylene spacer, and $Re_2(CO)_{10}$ resulted in a new type of heteroleptic tetrahedrons **36**-**40**.[27] The vertices of the tetrahedrons are occupied by rheniumtricarbonyl cores while the ligands occupy the edges.

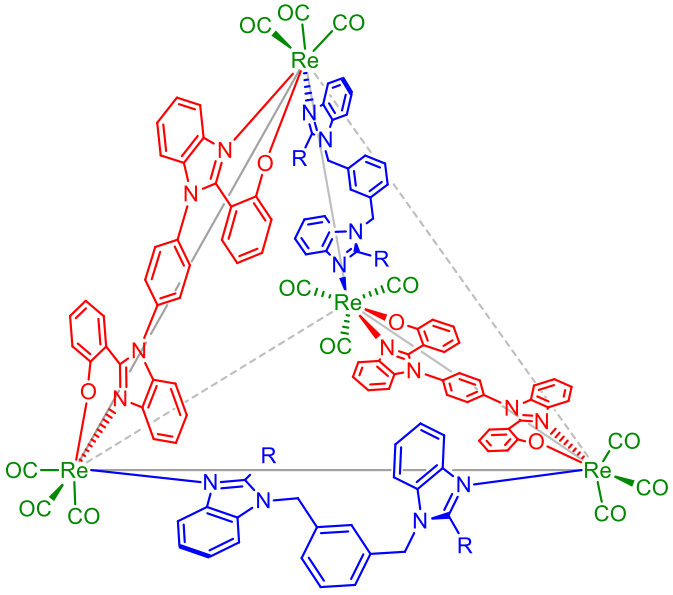

36, $L^n = L^{18}$; **37,** $L^n = L^{19}$
38, $L^n = L^{20}$, **39**, $L^n = L^{21}$
40, $L^n = L^{22}$

Figure 1.18. *fac*-$Re(CO)_3$ core base heteroleptic tetrahedrons **36**-**40**.

Uses of phosphine oxide based donor ligands in the synthesis of rhenium based metallocycles are very rare. Few reports are known for use of ditopic flexible ligands with phosphine oxide donor motif in literature. L^{23}-L^{27} are few examples of neutral ditopic phosphine based ligands containing alkyl or aryl spacer units.

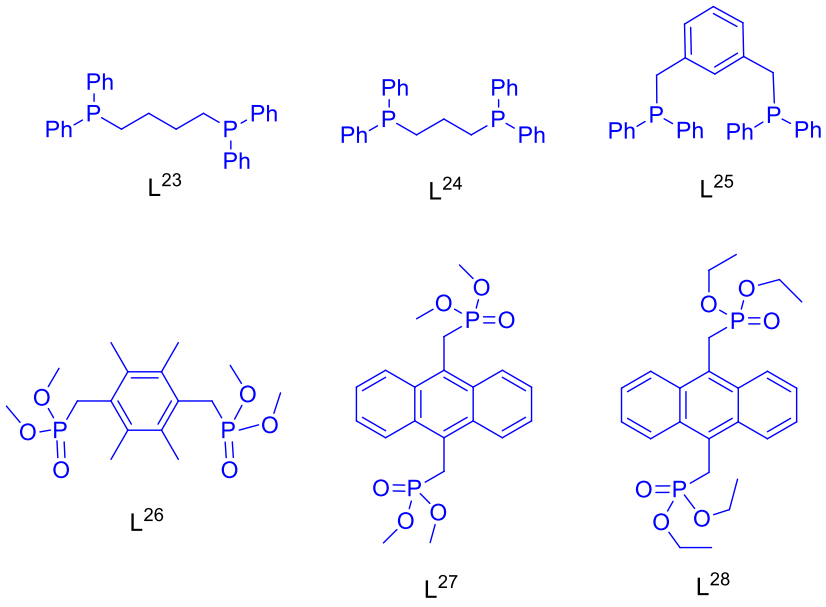

Figure 1.19. Ditopic phosphine/phosphine oxide based flexible ligands L^{23}-L^{27}.

A series of dinuclear metallocycles **41-48** were synthesized by the self-assembly of $Re_2(CO)_{10}$, ditopic phosphine/phosphine oxide donor ligands L^{23}-L^{26} and rigid bischelating ligands H_2-CA/ H_2-dhbq in solvothermal conditions.[28] Phosphine donor ligands L^{23}-L^{25} get converted into phosphine oxide in situ during the self-assembly and thereby leads to the formation of metallocycles with phosphine oxide motifs. In case of metallocycles **47-48** hard phosphine oxide based ligand L^{26} is only used.

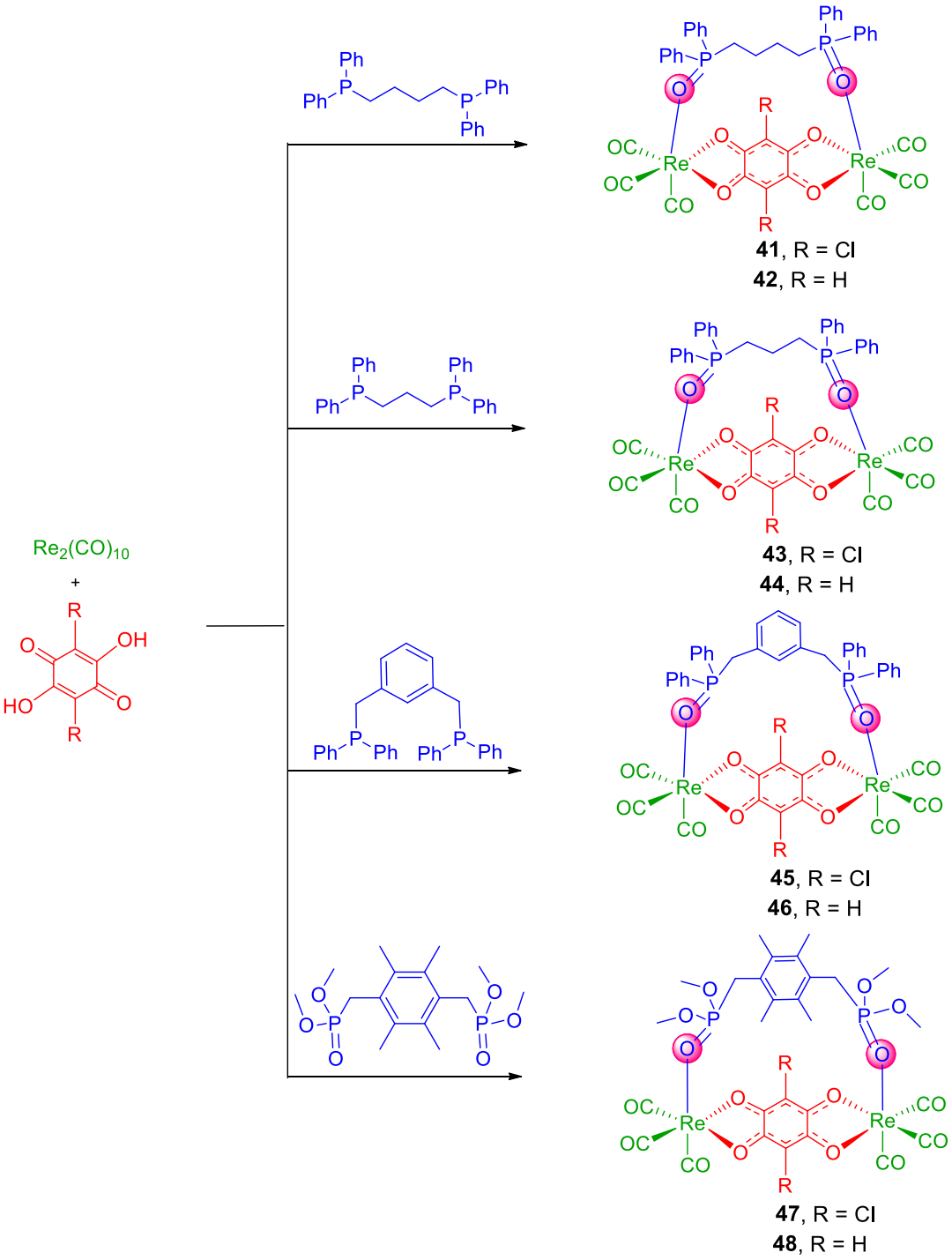

Scheme 1.3. Synthesis of dinuclear metallocycles **41-48**.

Tetranuclear complexes **49** and **50** were synthesized using phosphine donor based ligands L^{23}/L^{25} with $Re_2(CO)_{10}$ and H_4-thbq as the rigid bischelating ligand. These complexes adopt a M_4L_2L'-type conjoined bicyclic structure with two rhenium atoms in each cyclic motif clipped by a phosphine oxide based donor ligand.[28-29]

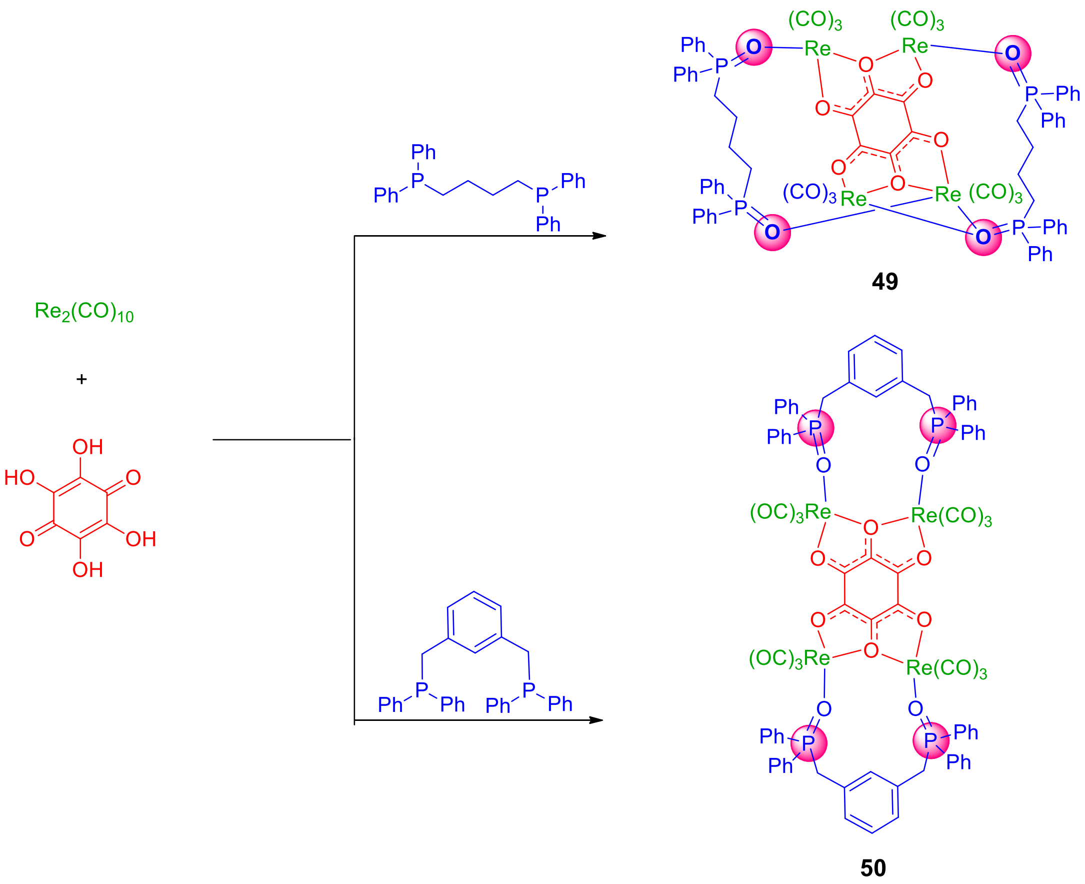

Scheme 1.4. Synthesis of tetranuclear hetroleptic metallocycles **49** and **50**.

Similarly neutral heteroleptic binuclear metallocycles **51-52** were obtained using flexible ditopic phosphine oxide donor ligands L^{27}/L^{28}, $Re_2(CO)_{10}$, and chloranilic acid (H_2-CA) as the rigid bischelating donor via one-pot solvothermal approach.[30]

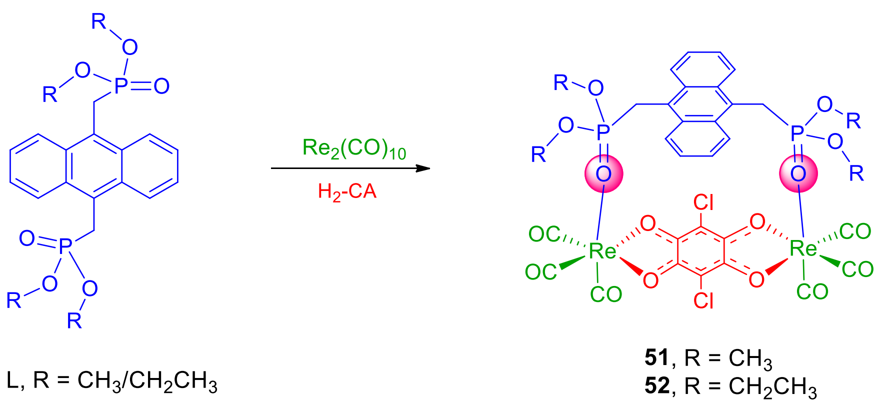

Scheme 1.5. Synthesis of dinuclear metallocycles **51-52** using phosphine oxide based ligands L^{27}-L^{28}.

1.5. Flexible tetratopic ligand and their SCC's

A wide variety of tetratopic flexible ligands having various coordinating motifs are designed and synthesized for using them in synthesizing rheniumtricarbonyl core based complexes. Usually imidazolyl, benzimidazolyl or phosphine oxide donor based flexible tetratopic ligands are synthesized. Reaction of a neutral benzimidazolyl based flexible tetratopic ligand L^{29} with $Re_2(CO)_{10}$ and H_2-CA via one pot self-assembly approach leads to the formation of metallocycle **53**.[16] The metallocycle can be considered as conjoined bicyclic metallocycle in which each cyclic motif of complex consist of two rheniumtricarbonyl cores bridged by CA^{2-} unit and coordinated to two benzimidazolyl motifs of the neutral ligand L^{29}. The two cyclic motifs are connected to each other through the phenylene ring of the tetratopic ligand.

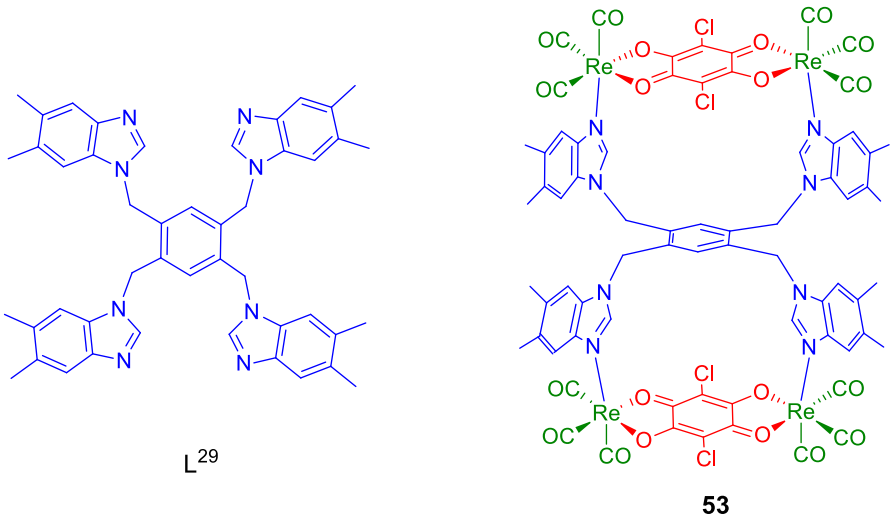

Figure 1.20. Neutral tetranuclear metallocycle **53** using benzimidazolyl based flexible ligand L^{29}.

A similar kind of bicyclic tetranuclear complexes **54-55** was synthesized by using flexible tetratopic ligand L^{30}.[31] This tetratopic flexible ligand contains bismesitylene spacer and benzimidazole as the coordinating motif. The reaction of the flexible tetratopic ligand L^{30} with $Re_2(CO)_{10}$ and H_2-dhaq/H_2-dhnd as the anionic ligand leads to the formation of conjoined bicyclic metallocycles **54-55**. One pot self assembly approach was used for synthesizing the metallocycles.

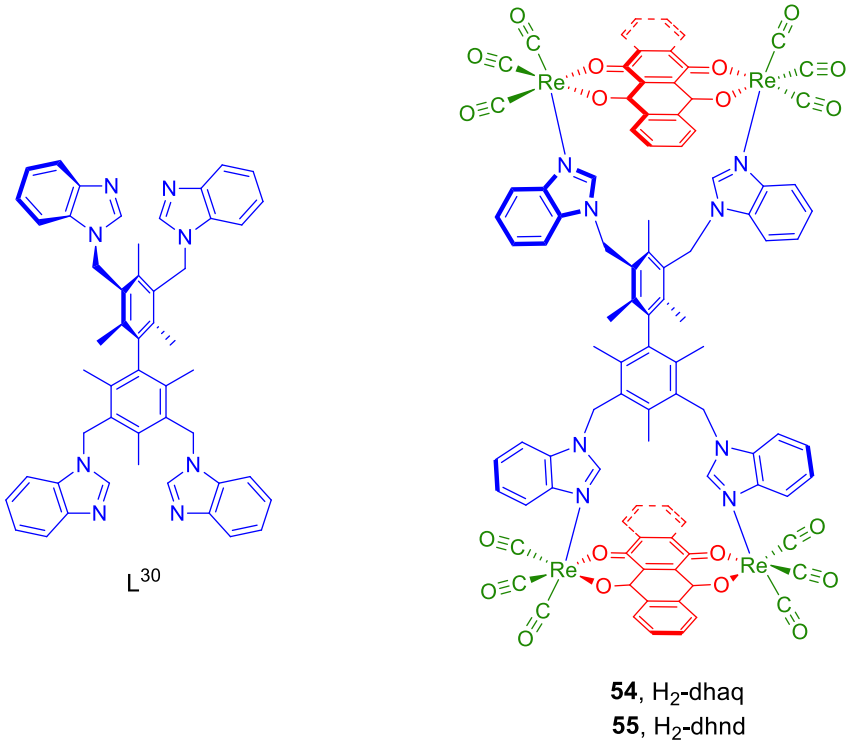

Figure 1.21. Neutral conjoined bicyclic metallocycles **54-55** using benzimidazolyl based flexible ligand L^{30}.

The design and synthesis of phosphine oxide donor ligand for synthesis of rhenium metallocycles is quite less. A phosphine oxide donor ligand L^{31} on reaction with $Re_2(CO)_{10}$ and bischelating anionic ligand H_2-dhbq/H_2-CA lead to formation of M_4L_2L'-type bicyclic structures **56-57**.[28]

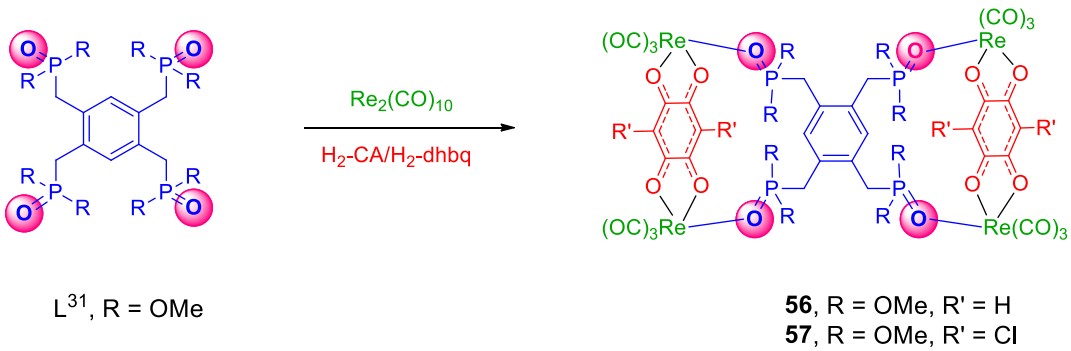

Scheme 1.6. Synthesis of tetranuclear metalloycles **56-57** from tetratopic phosphine oxide donor ligand L^{31}.

1.6. Flexible hexatopic ligand and their SCC's

In the synthesis of rhenium(I) based metallocycles, for creating a molecule with multiple receptor sites hexatopic flexible ligands L^{32}-L^{34} are used. In most of the cases imidazolyl/benzimidazolyl/napthanoimidazolyl coordinating motifs are used for synthesis of the hexatopic ligands. These ligands when treated with rigid anionic ligands such as benzimidazole/benzotriazole and $Re_2(CO)_{10}$ resulted in spheroid-shaped metallacycles **58**-**59**.[32] These synthesized metallocycles contained multiple cavities. The complexes contained two metallacalix[3]arene units and six- metallacalix[4]arene motifs. Further each cavity in the spheroid shaped metallocycles has ability to accommodate guest molecules which are occupied by solvent molecules as revealed in the X-ray structure.

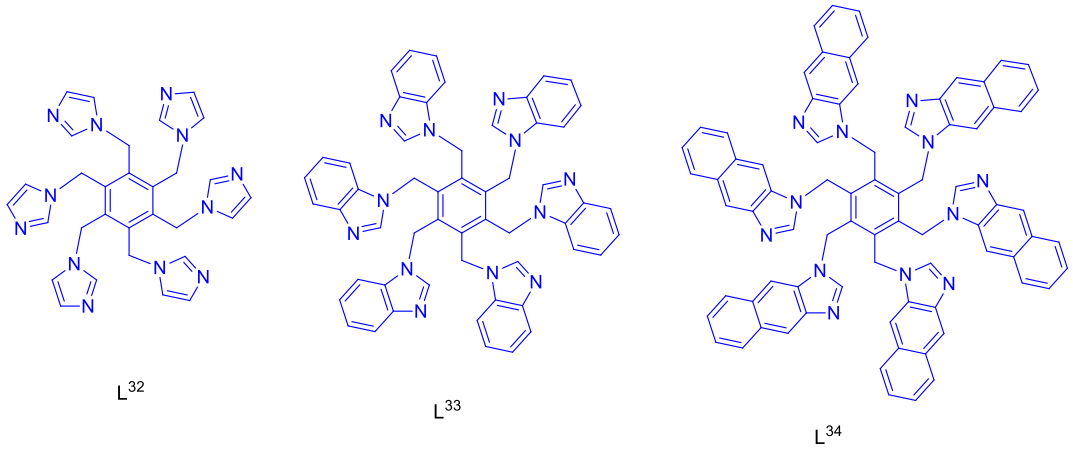

Figure 1.22. Neutral flexible hexatopic ligands L^{32}-L^{34}.

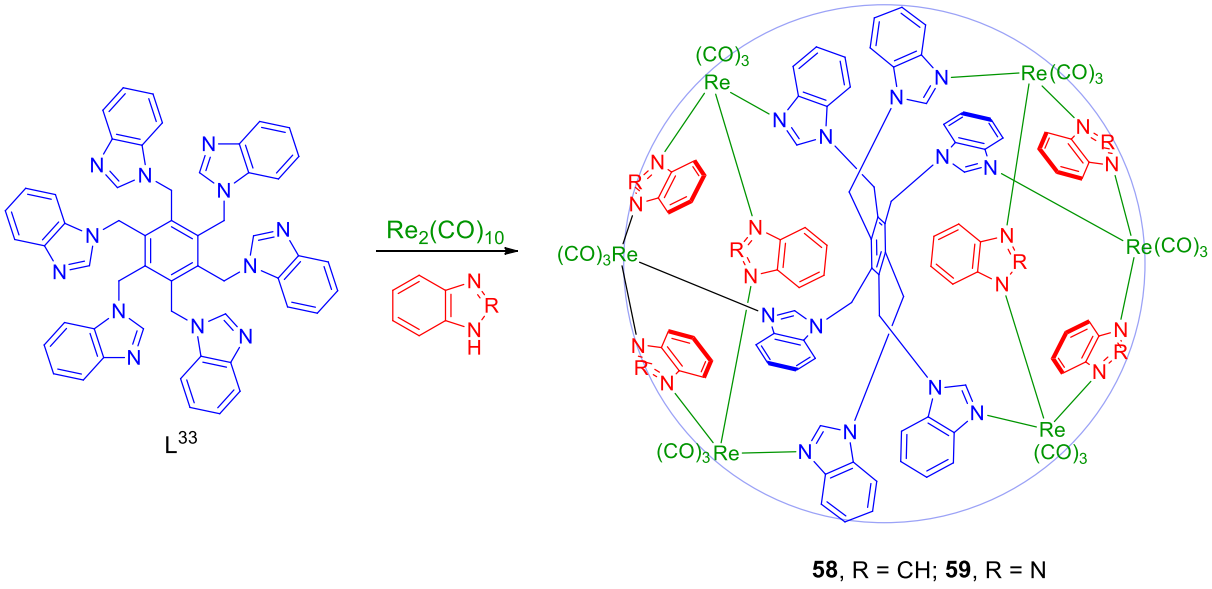

Scheme 1.7. Synthesis of spheroid shaped complexes **58**-**59**.

By changing the coordinating motif in the flexible ligands the cavity sizes can be tuned. Increase in cavity sizes was seen when the coordinating motif was changed from benzimidazolyl to napthanoimidazolyl.[33] Modulation of the anionic ligands can change the functionality of the cavities in the spheroids.

1.7. Scope of the present thesis

Rhenium-containing self-assembled coordination complexes (SCCs) show promise for various applications in materials and medicine. Small dinuclear metallocycles and hitherto unknown complex architectures such as molecular knots and various other topologies can be prepared. The earlier studies indicate that ditopic, tritopic, and polytopic ligands based on imidazolyl/benzimidazolyl donor serve as good structural frameworks for synthesizing homoleptic/heteroleptic helicates, bowls and cages. However, the use of pyrazolyl-based ligands in the self-assembly of metallocyclic architectures has only been recently initiated. While some acyclic complexes and other metallocycles featuring pyrazolyl donors are known with alternative metal cores. To the best of our knowledge, supramolecular coordination complexes based on rhenium(I) using pyrazolyl-based ligands remain unexplored. I believe that changing imidazolyl to pyrazolyl would result in hitherto unknown supramolecular coordination complexes because the coordination of the heterocyclic motif plays a crucial role in adopting the metal geometry. This significantly influences the architecture of the final complexes thus ultimately determining their properties and functions of the final supramolecular architectures.

Hence, the main objectives of the Ph.D. research work are:

· To design new pyrazolyl-based ditopic, tetratopic and hexatopic ligands.

· To explore the use of the synthesized ligands as one of the structural framework to self-assemble supramolecular coordination complexes using $Re_2(CO)_{10}$ and ancillary ligands.

· To characterize the synthesized molecules making use of spectroscopic methods and analytical techniques.

· To investigate the anticancer activities of the new supramolecular coordination complexes.

1.8. References

1. J. M. Lehn, Supramolecular Chemistry–Concepts and Perspectives, VCH, Weinheim, 1995. (b) J. M. Lehn, *Angew. Chem. Int. Ed. Engl.* 1988**, 27**, 89-112. (c) J. M. Lehn, *Proc. Nat. Acad. Sci. USA*, 2002, **99**, 4763-4768.
2. (a) J. W. Steed, J. L. Atwood and P. A. Gale, In *Definition and emergence of supramolecular chemistry*, John Wiley & Sons Ltd, 2012; pp 3-7; (b) J. W. Steed, D. R. Turner and K. J. Wallace, *Core Concepts in Supramolecular Chemistry and Nanochemistry*, John Wiley & Sons. Chichester, 2007.
3. J. M. Lehn, A. Rigault, J. Seigel, J. Harrowfield, B. Chevrier and D. Moras, *Proc. Natl. Acad. Sci. USA*, 1987, **84**, 2565-2569.
4. (a) P. J. Steel, *Chem. N. Z*. 2003, **67**, 57-60. (b) P. J. Steel, *Chem. N. Z*. 2011, **75**, 194-197. (c) I. Dance, *New J. Chem*. 2003, **27**, 1-2.
5. (a) T. R. Cook and P. J. Stang, *Chem. Rev*. 2015, **115**, 7001-7045; (b) P. J. Stang and B. Olenyuk, *Acc. Chem. Res.*, 1998, **30**, 502-518; (c) R. Chakrabarty, P. S. Mukherjee and P. J. Stang, *Chem. Rev*. 2011, **111**, 6810-6818; (d) W. -X. Gao, H. N. Zhang and G. -X. Jin, *Coord. Chem. Rev*. 2019, **386**, 69-84; (e) S. Sharma, M. Sarkar and D. K. Chand, *Chem. Commun.*, 2023,**59**,535-554.
6. (a) J. M. Lehn, A. Rigault, J. Siegel, J. Harrowfield, B. Chevrier and D. Moras, *Proc. Natl. Acad. Sci. USA*. 1987, **84**, 2565-2569; (b) M. Albrecht, *Chem. Rev*. 2001, **101**, 3457–3498; (c) A. P. Paneerselvam, S. S. Mishra and D. K. Chand, *J. Chem. Sci.*, 2018,130:96.
7. (a) D. Zhang, T. K. Ronson and J. R. Nitschke, *Acc. Chem. Res.* 2018, **5**, 2423-2436. (b) Z. Wu, K. Zhou, A. V. Ivanow, M. Yusobov and F. Verpoort, *Coord. Chem. Rev*. 2017, **353**, 180-200.
8. (a) M. Fujita, K. Umemoto, M. Yoshizawa, N. Fujita, T. Kusukawa and K. Biradha, *Chem. Commun*. 2001, 509‑518; (b) B. Therrien, *Eur. J. Inorg. Chem.* 2009, 2445-2453; (c) Y. Y. Zhang, W. X.Gao, L. Lin and G. X. Jin, *Coord. Chem. Rev*. 2017, **344**, 323-344.
9. (a) L. L. Dang, H. J. Feng, Y. J. Lin and G. X. Jin, *J. Am. Chem. Soc*. 2020, **142**, 18946–18954; (b) R. S. Forgan, J. P. Sauvage and J. F. Stoddart, *Chem. Rev*. 2011, **111**, 5434–5464; (c) Z. Ashbridge, S. D. P. Fielden, D. A. Leigh, L. Pirvu, F. Schaufelberger and L. Zhang, *Chem. Soc. Rev*. 2022, **51**, 7779–7809; (d) M. Han, D. M. Engelhard and G. H. Clever, *Chem. Soc. Rev*. 2014, **43**, 1848–1860; (e) Y. Inomata, T. Sawada and M. Fujita, *J. Am. Chem. Soc*. 2021, **143**, 16734–16739.

10. (a) A. A. Haase, E. B. Bauer, F. E. Kühn and D. C. Crans, *Coord. Chem. Rev*. 2019, **394**, 135-161. (b) E. B. Bauer, A. A. Haase, R. M. Reich, D. C. Crans and F. E. Kühn, *Coord. Chem. Rev.* 2019, **393**, 79-117. (c) D. Gupta and M. Sathiyendiran, *ChemistrySelect* 2018, **3**, 7439-7458 and references cited therein. (d) P. H. Dinolfo and J. T. Hupp, *Chem. Mater*. 2001, **13**, 3113–3125.
11. (a) J. R. Dilworth, *Coord. Chem. Rev*. 2021, **436**, 213822 ; (b) K. Schindler and F. Zobi, *Molecules* 2022, **27**, 539 ; (c) A. Sharma, N. Vaibhavi, B. Kar, U. Das and P. Paira, *RSC Adv*. 2022, **12**, 20264–20295 ; (d) P. Thanasekaran, C-C. Lee and K-L. Lu, *Acc. Chem. Res*. 2012, **45**, 1403–1418.
12. (a) M. Sathiyendiran, C. Tsai, P. Thanasekaran, T. Luo, C. Yang, G. Lee, S. Peng and K. Lu, *Chem. Eur. J*. 2011, **1**, 3343–3346 ; (b) G. Jin, T. Wang, Y. Sun, Y. Li and J. Ma, *Inorg. Chem*. 2020, **59**, 15019–15027 ; (c) C. Y. Chan, P. A. Pellegrini, I. Greguric and P. J. Barnard, *Inorg. Chem*. 2014, **53**, 10862–10873; (d) S. Sato and O. Ishitani, *Coord. Chem.Rev*. 2015, **282–283**, 50–59.
13. (a) R. Govindarajan, R. Nagarajaprakash, V. Veena, N. Sakthivel and B. Manimaran, *Polyhedron*. 2018, **139**, 229–236; (c) G. G. Huang, C. Lee, J. Yang, Z. Lu, M. Sathiyendiran, C. Huang, Y. Kao, G. Lee and K. Lu, *Sens. Actuators B*, 2018, **254**, 424–430, (c) J. Rohacova and O. Ishitani, *Dalton Trans*. 2017, **46**, 8899–8919.
14. X. Zhao, X. Miao, *Coord. Chem. Rev*. 2024, **502**, 215611 and references therein.
15. Z. Zeng, W. Wang, X. Xiong, N. Zhu, Y. Xiong, Z.Wei and J. J. Jiang, *Inorg. Chem*. 2021, **60**, 8456–8460
16. C. H. Chuang, M. Sathiyendiran, Y.-H. Tseng, J. Y. Wu, K. C. Hsu, C. H. Hung, Y. S. Wen and K. L. Lu, *Organomet*. 2010, **29**, 283–285.
17. B. Shankar, S. Sahu, N. Deibel, D. Schweinfurth, B. Sarkar, P. Elumalai, D. Gupta, F. Hussain, G. Krishnamoorthy and M. Sathiyendiran, *Inorg. Chem*. 2014, **53**, 922−930.
18. B. Shankar, P. Elumalai, P. J. Jackmil, P. Kumar, S. Singh and M. Sathiyendiran, *J. Organomet. Chem.* **2013**, *743*, 109-113.
19. M. Bhol, R. L. Borkar, B. Shankar, S. K. Panda, M. Wolff and M. Sathiyendiran, *Inorg. Chem*. 2023, **62**, 11554–11569
20. P. Saxena, B. Shankar, A. Sathyanarayana, G. Prabusankar and M. Sathiyendiran, *Chimia*. 2015, **69**, 675–677.
21. M. Bhol, G. Claude, M. R. Jungfer, U. Abram and M. Sathiyendiran, *Inorg. Chem*.2022, **61**, 5173−5177.

22. P. Rajakannu, S. M. Mobin and M. Sathiyendiran, *J. Organomet. Chem*. 2014, **771**, 68-77.
23. (a) M. Sathiyendiran, C. H. Chang, C. H. Chuang, T. T. Luo, Y. S. Wena and K. L. Lu, *Dalton Trans.*, 2007, 1872-1874; (b) Y. H. Tseng, D. Bhattacharya, S. M. Lin, P. Thanasekaran, J. Y. Wu, L. W. Lee, M. Sathiyendiran, M. L. Ho, M. W. Chung, K. C. Hsu, P. T. Chao and K. L. Lu, *Inorg. Chem.* 2010, **49**, 6805–6807.
24. C. A. Kumar, R. Nagarajaprakash, W. Victoria, V. Veena, N. Sakthivel and B. Manimaran, *Inorg. Chem. Commun.*, 2016, **64**, 39-44.
25. B. Ramakrishna, C. A. Kumar, T. J. Logesh and B. Manimaran, *J. Organomet. Chem.* 2017, **828**, 116-121
26. M. Bhol, B. Shankar and M. Sathiyendiran, *Dalton Trans*. 2018, **47**, 4494–4500.
27. R. Arumugam, B. Shankar, K. R. Soumya and M. Sathiyendiran, *Dalton Trans*. 2019, **48**, 7425–7431.
28. B. Shankar, R. Arumugam, P. Elumalai and M. Sathiyendiran, *ACS Omega* 2016, **1**, 507–517
29. B. Shankar, P. Elumalai, R. Shanmugam, V. Singh, D. T. Masram and M. Sathiyendiran, *Inorg. Chem.* 2013, **52**, 10217–10219.
30. M. Kedia, V. Singh, B. Shankar and M. Sathiyendiran, *J. Organomet. Chem.* 2024, **1004**,122937
31. P. Elumalai, R. Kanagaraj, R.Marimuthu, B. Shankar, A. C. Kalita and M. Sathiyendiran, *Dalton Trans.* 2015, **44**, 11274-11277.
32. B. Shankar, P. Elumalai, S. D. Sathiyashivan and M. Sathiyendiran, *Inorg. Chem*. 2014, **53**, 10018-10020.
33. B. Shankar, R. Marimuthu, S. D. Sathiyashivan and M. Sathiyendiran, *Inorg. Chem.* 2016, **55**, 4537−4544.

Chapter 2

Self-assembly of new class of rhenium(I)-based double stranded dinuclear monohelicates

Abstract

A new type of double stranded dinuclear monohelicates, *fac*-[{$Re(CO)_3$–(μ-L)–$Re(CO)_3$}L^n] (**1**–**4**), were self-assembled from $Re_2(CO)_{10}$, rigid bischelating donor (H_2–L: 1,4-dihydroxybenzoquinone (H_2-dhbq) for **1** and **3**; 2,5-pyrazine dicarboxylic acid (H_2-pydc) for **2** and **4**) and flexible bis(monodentate) pyrazolyl N donor L^n (L^1 = bis(4-((pyrazolyl)methyl)phenyl)methane for **1** and **2**; L^2 = bis(4-((pyrazolyl)methyl)phenyl)methanone for **3** and **4**) in mesitylene. The metallomacrocycle **1** was confirmed by single crystal X–ray crystallography. Though the helicate contains two organic ligand strands, only one strand is arranged in a helical fashion, which is an unprecedented form in the helicate architectures. The molecular structures of **1**–**4** as helicates and mesocates were optimized using DFT methods.

This work has been published in *Dalton Trans.*, **2022**, *51*, 16307–16315.

2.1. Introduction

The currently known self-assembly principles using pre-designed organic ligands, naked and partially protected metal ions provide a vast array of 2D- and 3D supramolecular coordination complexes (SCCs = metallomacrocycles) of various sizes and shapes including helicates.[1] Though it appears that limits are reached in the design principle for SCCs, new bonding combinations have been evolving continuously to create simple to complex new supramolecular architectures. The intense research focused in this area is due to the simple synthetic approach i.e., mixing of two/three compounds for the formation of simple as well as highly complex SCCs and their potential applications in material and biological fields.[2] Among the SCCs, dinuclear double-stranded double helicate is the simplest supramolecule and is known to have potential applications in the field of medicine.[3] In general, the dinuclear double helicates can be easily achieved by mixing of naked metal ions and ditopic flexible ligands.[4] However, the use of partially protected metal ions is less common in the self-assembly of dinuclear double-stranded double helicates. In particular, *fac*-[Re(CO)$_3$] core-based complexes as starting materials for assembling dinuclear double helicates are scarce[5a–c] but several dinuclear homotopic- and heterotopic- mesocates are known.[5d–g] It is worth mentioning that the *fac*-[Re(CO)$_3$] core directed self-assembly approach is well-established for making kinetically stable and biologically active SCCs.[6]

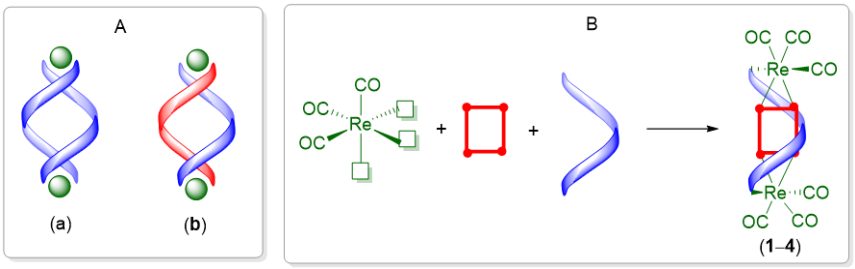

Figure 2.1. A: Commonly observed double-stranded dinuclear (a) homoleptic and (b) heteroleptic double helicates. B: The design principle of new form of double-stranded dinuclear monohelicates **1**–**4**.

Herein, we report a unique self-assembly approach for a new type of dinuclear double-stranded helicate (Figure 2.1). In these dinuclear helicates, only one ligand strand is arranged in a helical fashion. To the best of our knowledge, *fac*-[Re(CO)$_3$] core-based dinuclear heteroleptic monohelicates are unknown. The helicates **1**–**4** were assembled

using $Re_2(CO)_{10}$, rigid bis-chelating ligand and flexible ditopic nitrogen donor in one-pot approach (Scheme 2.1).

2.2. Experimental

2.2.1 Materials and Methods

General Data. $Re_2(CO)_{10}$, pyrazole (H–pz), diphenylmethane, bis(4–methylphenyl)methanone, KOH, NaOH, DMF, HBr-acetic acid (33%), paraformaldehyde, orthophosphoric acid, NBS, CCl_4, 1,4-dihydroxybenzoquinone (H_2–dhbq), 2,5-pyrazine dicarboxylic acid dihydrate (H_2-pydc·$2H_2O$), mesitylene and DMSO were purchased and used as received. Bis(4-(bromomethyl)phenyl)methane and bis(4-(bromomethyl) phenyl)methanone were prepared by following known procedures. [7] ATR-IR spectra were recorded on a Nicolet iS5 IR spectrophotometer. NMR spectra were recorded on a Bruker Avance III 500 MHz spectrometer. ESI-MS spectra were recorded on Bruker-maXis mass spectrometer.

2.2.2 X-ray crystallography

Single crystal X-ray data of **1** was collected on a Rigaku Oxford Diffractometer (λ (Mo Kα) = 0.71073Å). The structure was solved by direct methods using SHELXS–97 (Sheldrick 2008) and refined using the SHELXL–2018/3 program (within the WinGX program package). Non-H atoms were refined anisotropically.[8]

2.2.3 Computational section

The ground state geometry optimization of complexes **1**-**4** was performed in the gas phase using B3LYP method, [9] in Gaussian 09 program package,[10] The initial geometry for **1** was obtained from the coordinates of X-ray crystal structure of helicate **1**. The Stuttgart-Dresden (SDD) ECP,[11] was used for Re. The 6–311G*[12] was used for O, N, C and H atoms. Geometry optimizations were achieved without any constraints. No negative IR frequencies were observed for the optimized structures.

2.2.4 Synthesis of ligands and complexes.

Synthesis of L^1

Pyrazole (459.0 mg, 6.75 mmol), KOH (400.0 mg) and DMF (~30 mL) were taken in a round bottom flask. The reaction mixture was allowed to stir for ~3 hr at room temperature. Bis(4-(bromomethyl)phenyl)methane (1.2 g, 6.75 mmol) was added to the mixture and allowed to stir for another ~48 hr. The final solution was poured into ice-cold water (~500 mL). White precipitate obtained was filtered and air-dried. Yield: 53% (1.19 g).^{1}H NMR (500 MHz, DMSO-d_6, δ): 7.76 (d, J = 2 Hz, 2H, H^5), 7.42 (d, J = 1 Hz, 2H, H^3), 7.16 (d, J = 8 Hz, 4H, H^7), 7.11 (d, J = 8 Hz, 4H, H^8), 6.24 (t, J = 2 Hz, 2H, H^4), 5.25 (s, 4H, H^6), and 3.86 (s, 2H, H^9). HRMS–ESI (*m/z*): $[M + H]^+$ calcd for $C_{21}H_{21}N_4$, 329.1766; found, 329.1766.

Synthesis of L^2

Pyrazole (73.90 mg, 1.086 mmol), bis(4-(bromomethyl)phenyl)methanone (200 mg, 0.5430 mmol), NaOH (95.00 mg) and THF (~12 mL) were taken in an round bottom flask. The reaction mixture was then refluxed for ~20 hr. The solvent was evaporated under vacuum. Water (~100 mL) was added to the precipitate. Pale yellow precipitate obtained was filtered and air-dried. Yield: 43 % (160 mg). HRMS–ESI (*m/z*): $[M + H]^+$ calcd for $C_{21}H_{19}N_4O$, 343.1559; found, 343.1550. ^{1}H NMR (500 MHz, DMSO-d_6, δ): 7.88 (d, J = 2 Hz, 2H, H^5), 7.69 (d, J = 8 Hz, 4H, H^7), 7.50 (d, J = 1.5 Hz, 2H, H^3), 7.33 (d, J = 8.5 Hz, 4H, H^8), 6.39 (d, J = 2 Hz, 2H, H^4) and 5.45 (s, 4H, H^6).

General synthetic procedure for helicates

$Re_2(CO)_{10}$, flexible ditopic ligand (L^1 or L^2), rigid bis-chelating ligand and mesitylene were taken in a round bottom flask. The reaction mixture was refluxed for 4 hr. The obtained precipitate (helicate) was filtered off, washed with excess amount of hexane. The filtrate (mesitylene solution) was kept as such. Crystals suitable for single crystal X–ray diffraction analysis were collected from the filtrate. The same reaction can be performed in the solvothermal conditions.

Synthesis of *fac*-[{Re(CO)$_3$(dhbq)Re(CO)$_3$}(L^1)]•mesitylene (1•mesitylene)

By following the general synthetic approach **1** was obtained using $Re_2(CO)_{10}$ (50.4 mg, 0.077 mmol), H_2–dhbq (11.00 mg, 0.0785 mmol), L^1 (25.20 mg, 0.076 mmol), and mesitylene (~20 mL). Yield: 67% (40 mg of ppt. + 12 mg crystals). ATR–IR (cm^{-1}): 2012 (s) and 1875 (s) (C≡O). HRMS–ESI (*m/z*): $[M + H]^+$ calcd for $C_{33}H_{23}N_4O_{10}Re_2$, 1007.0497; found, 1007.0496. ^{1}H NMR (500 MHz, DMSO-d_6, δ): 7.76 (d, *J* = 2 Hz, 2H, H^5), 7.42 (d, *J* = 1 Hz, 2H, H3), 7.16 (d, *J* = 8 Hz, 4H, H^7), 7.11 (d, *J* = 8 Hz, 4H, H^8), 6.79 (s, mesitylene), 6.24 (t, *J* = 2 Hz, 2H, H^4), 5.79 (s, 1H, dhbq), 5.79 (s, 1H, dhbq), 5.25 (s, 4H, H^6), and 3.86 (s, 2H, H^9).

Synthesis of *fac*-[{Re(CO)$_3$(pydc)Re(CO)$_3$}(L^1)] (2)

By following the general synthetic approach, **2** was obtained using $Re_2(CO)_{10}$ (51.00 mg, 0.07800 mmol), H_2–pydc·2H_2O (15.90 mg, 0.0780 mmol), L^1 (25.20 mg, 0.0770 mmol), and mesitylene (~12 mL). Yield: 89 % (72 mg). ATR–IR (cm^{-1}): 2026 (s) and 1885 (s) (C≡O). HRMS–ESI (m/z): $[M + H]^+$ calcd for $C_{33}H_{23}N_{6O}O_{10}Re_2$, 1037.0591; found, 1037.0588. 1H NMR (500 MHz, DMSO-d_6, δ): 9.14 (s, 1H, pydc), 9.12 (s, 1H, pydc), 7.76 (d, *J* = 2 Hz, 2H, H5), 7.42 (d, *J* = 1 Hz, 2H, H3), 7.16 (d, *J* = 8 Hz, 4H, H^7), 7.11 (d, *J* = 8 Hz, 4H, H^8), 6.79 (s, mesitylene), 6.24 (t, J = 2 Hz, 2H, H^4), 5.25 (s, 4H, H^6), and 3.86 (s, 2H, H^9).

Synthesis of *fac*-[{Re(CO)$_3$(dhbq)Re(CO)$_3$}(L^2)] (3)

By following the general synthetic approach, **3** was obtained using $Re_2(CO)_{10}$ (50.00 mg, 0.0760mmol), H_2–dhbq (10.70 mg, 0.0760mmol), L^2 (26.20 mg, 0.0760mmol), and mesitylene (~20 mL). Yield: 64% (50 mg). ATR–IR (cm^{-1}):2016 (s) and 1881 (s) (C≡O). HRMS–ESI (*m/z*): $[M + H]^+$ calcd for $C_{33}H_{21}N_4O_{11}Re_2$, 1021.0294; found, 1021.0173.^{1}H NMR (500 MHz, DMSO-d_6, δ): 7.88 (d, *J* = 2 Hz, 2H, H^5), 7.69 (d, *J* = 8 Hz, 4H, H^7), 7.50 (d, *J* = 1.5 Hz, 2H, H^3), 7.33 (d, *J* = 8.5 Hz 4H, H^8), 6.39 (d, *J* = 2 Hz, 2H, H^4), 5.79 (s, 1H, dhbq), 5.79 (s, 1H, dhbq), and 5.45 (s, 4H, H^6)

Synthesis of *fac*-[{Re(CO)$_3$(pydc)Re(CO)$_3$}(L^2)] (4)

By following the general synthetic approach, **4** was obtained using $Re_2(CO)_{10}$ (50.00 mg, 0.0760 mmol), H_2–pydc.2H2O(16.00 mg, 0.0780 mmol), L^2 (26.20 mg, 0.0760 mmol), and mesitylene (~20 mL). Yield: 87% (70 mg). ATR–IR (cm^{-1}): 2030 (s) and 1889 (s) (C≡O).

HRMS–ESI (*m/z*): $[M + H]^+$ calcd for $C_{33}H_{21}N_6O_{11}Re_2$, 1051.0383; found, 1049.0131.^{1}H NMR (500 MHz, DMSO-d_6, δ): 9.14 (s, 1H, pydc), 9.12 (s, 1H, pydc), 7.88 (d, *J* = 2 Hz, 2H, H^5), 7.69 (d, *J* = 8 Hz, 4H, H^7), 7.50 (d, *J* = 1.5 Hz, 2H, H^3), 7.33 (d, *J* = 8.5 Hz 4H, H^8), 6.39 (d, *J* = 2 Hz, 2H, H^4), and 5.45 (s, 4H, H^6).

2.3. Results and discussion

2.3.1 Synthesis and characterization of ligands L^1- L^2.

Two new flexible bidentate ligands (L^1 and L^2) were synthesized by treating pyrazole (H–pz) with bis(4-(bromomethyl)phenyl)methane or bis(4-(bromomethyl)phenyl)methanone in presence of KOH/NaOH in DMF/THF (Scheme 2.1).[13] The ^{1}H NMR spectrum of L^1 in DMSO–d_6 displays a single set of well-separated sharp signals for the protons of pz, two p-phenylene motifs, and three methylene groups. A similar pattern was observed for L^2. The formation of the ligands are further supported by mass spectra which exhibit molecular ion peaks as *m/z* 329.1766 for $[L^1 + H]^+$ and *m/z* 343.1550 for $[L^2 + H]^+$ (Figure 2.2-2.8).

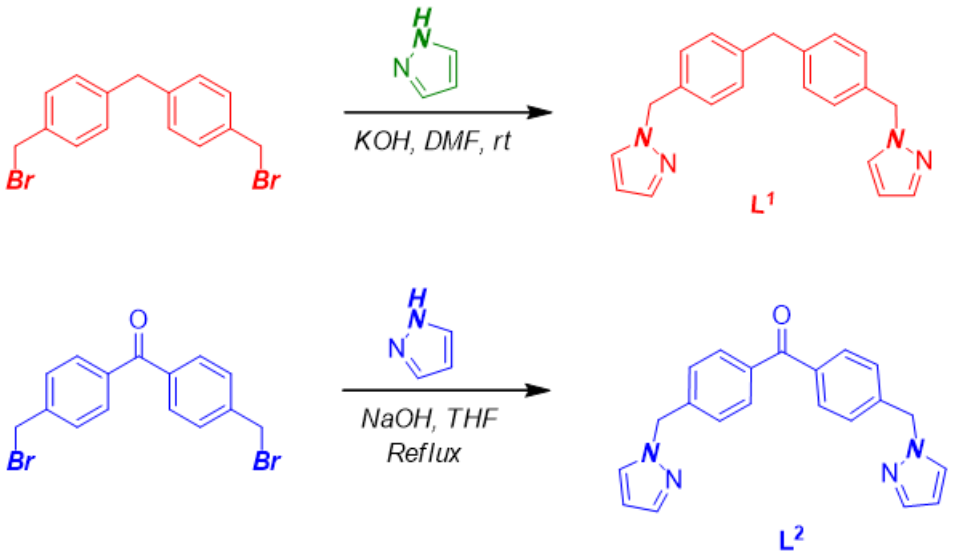

Scheme 2.1 Synthesis of ligands L^1-L^2.

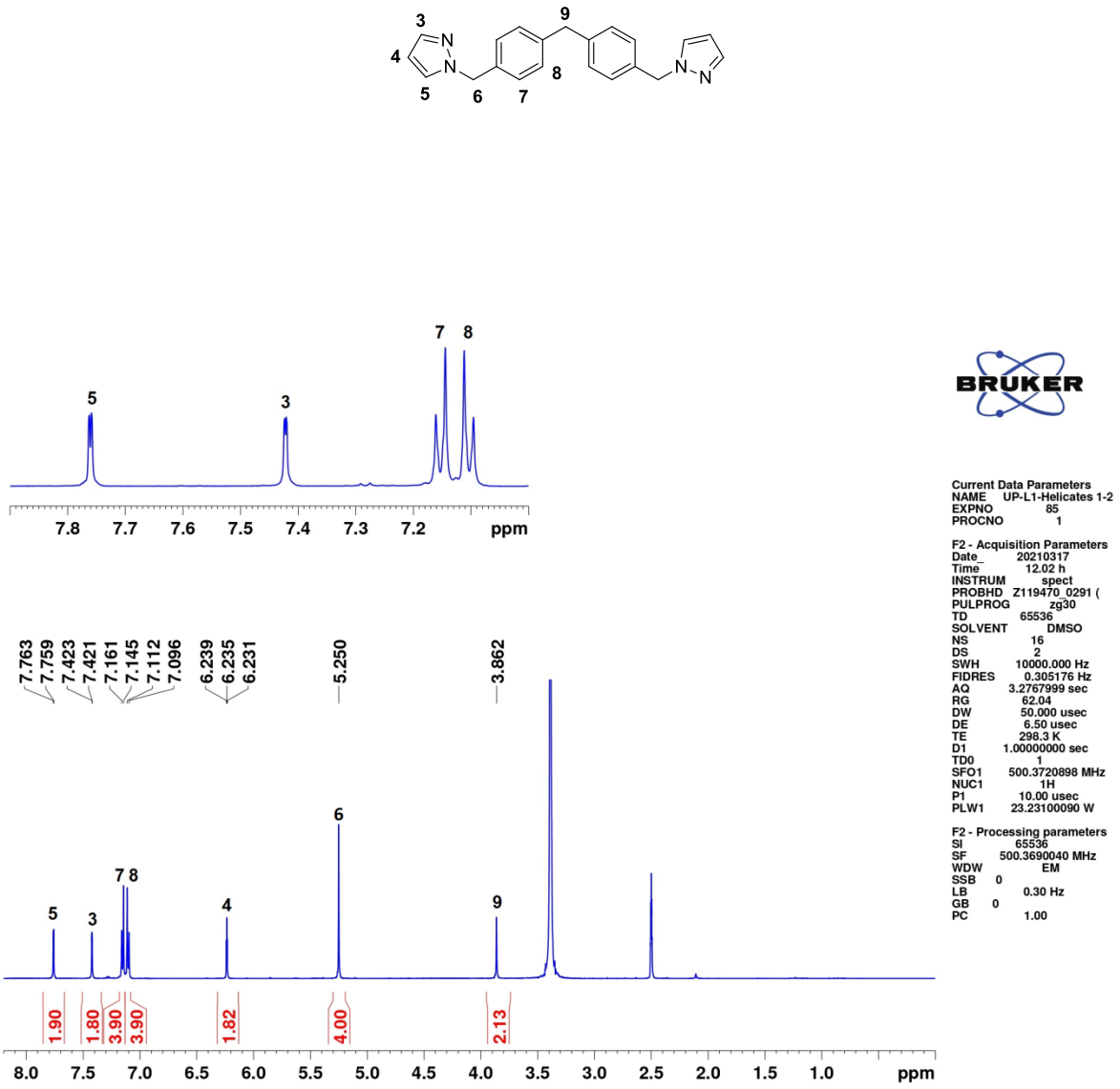

Figure 2.2. ^{1}H NMR spectrum of L^{1} in DMSO- d_6 (* is solvent).

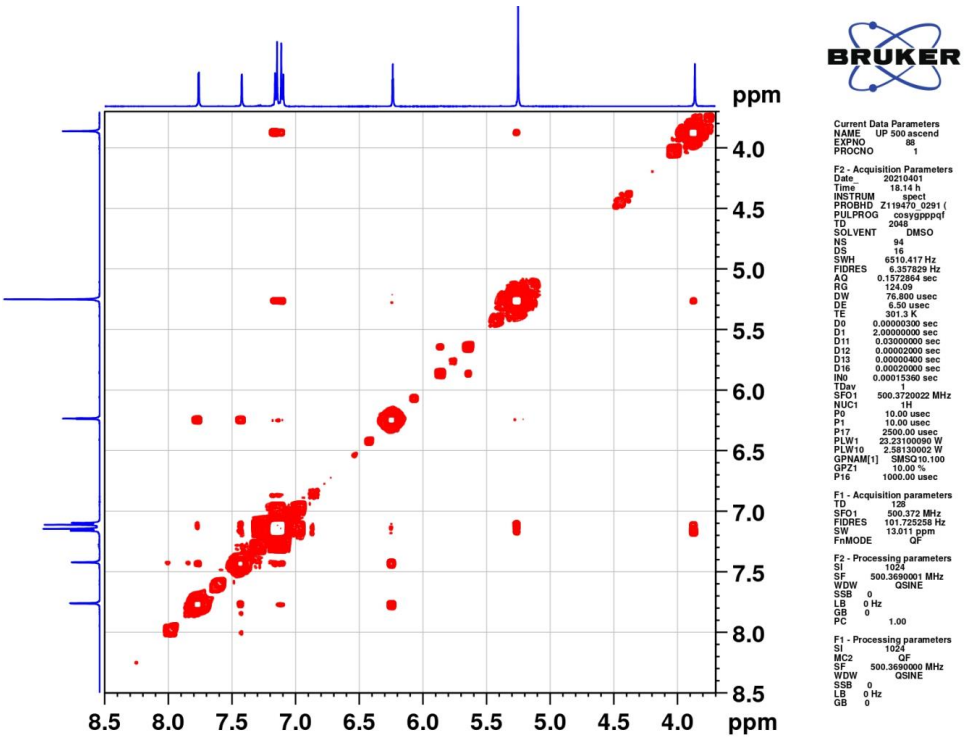

Figure 2.3. ^{1}H–^{1}H COSY NMR spectrum of L^{1} in DMSO–d_6.

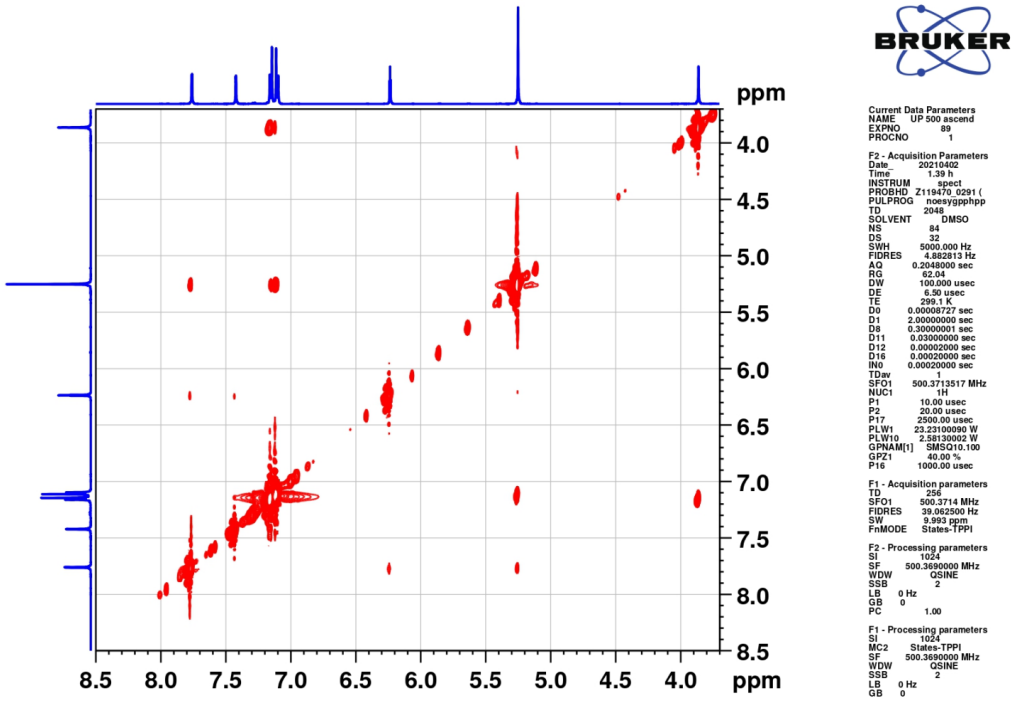

Figure 2.4. ^{1}H–^{1}H NOESY NMR spectrum of L^{1} in DMSO–d_6.

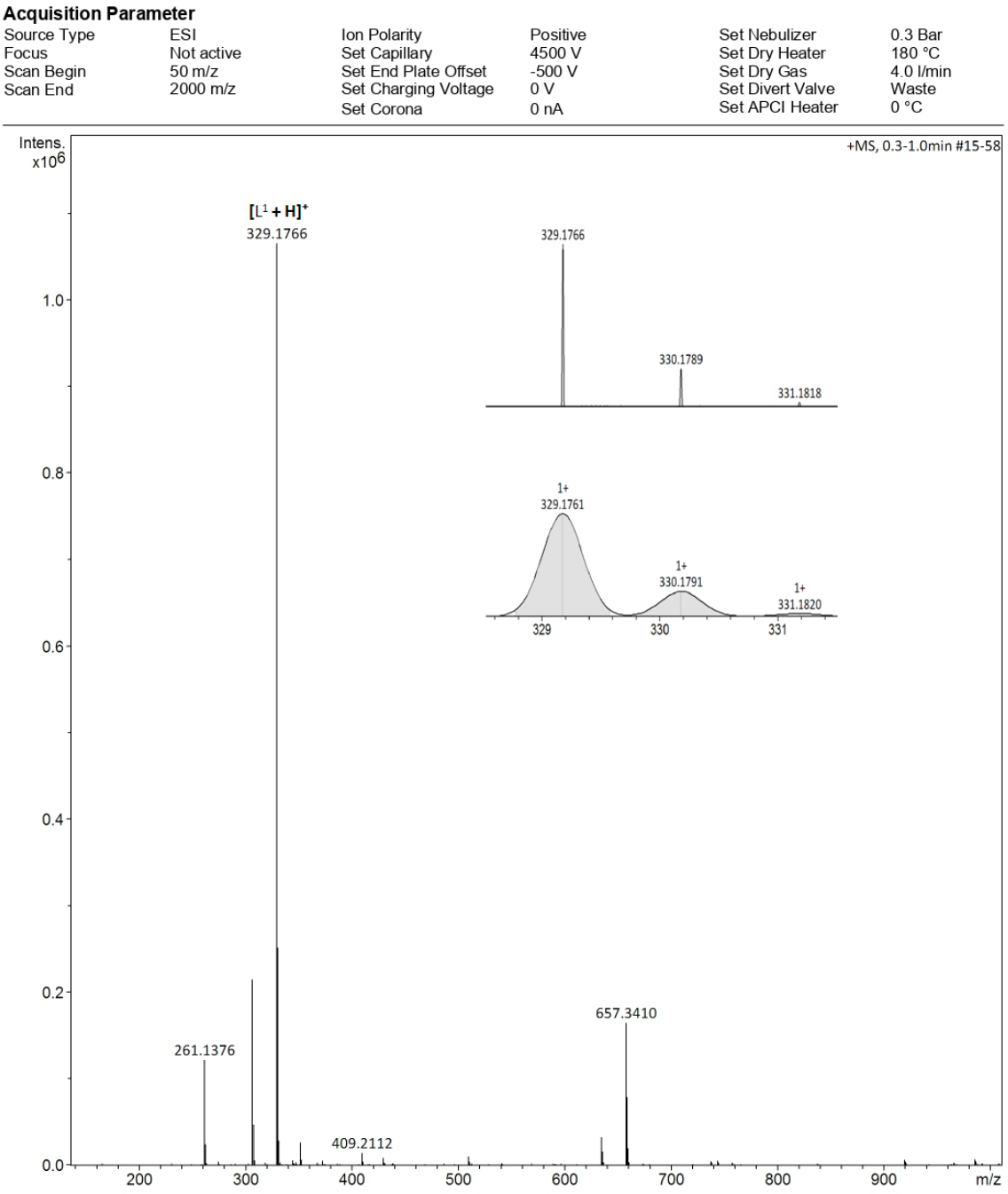

Figure 2.5. ESI mass spectrum of L^1 in positive ion mode (simulated pattern in inset).

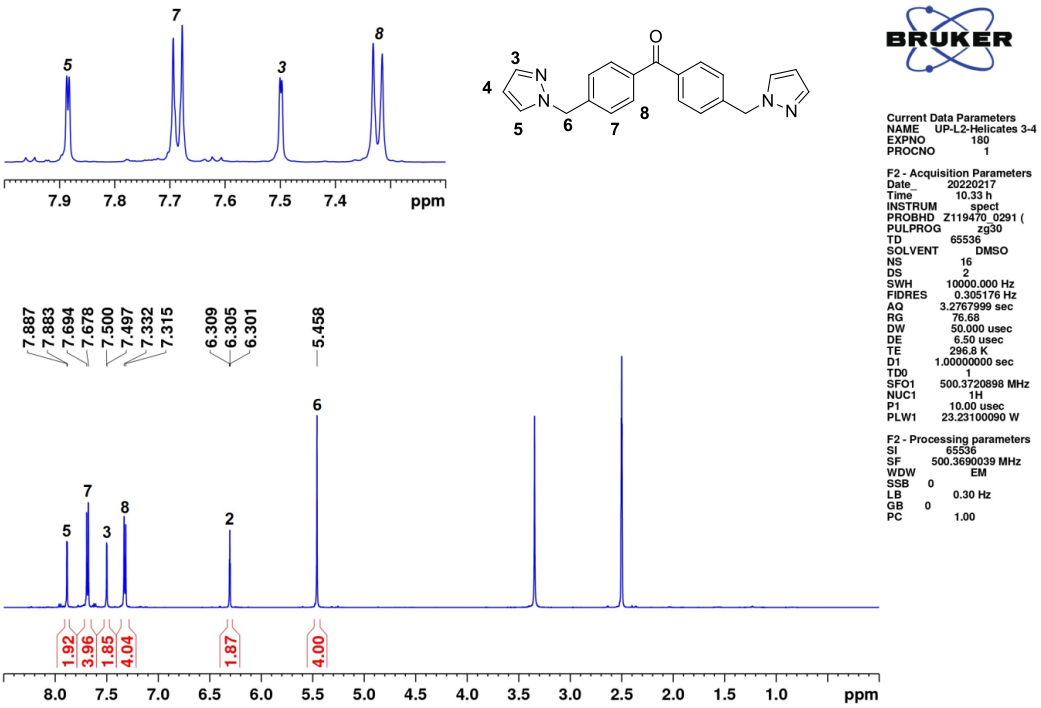

Figure 2.6. ^{1}H NMR spectrum of L^{2} in DMSO–d_6.

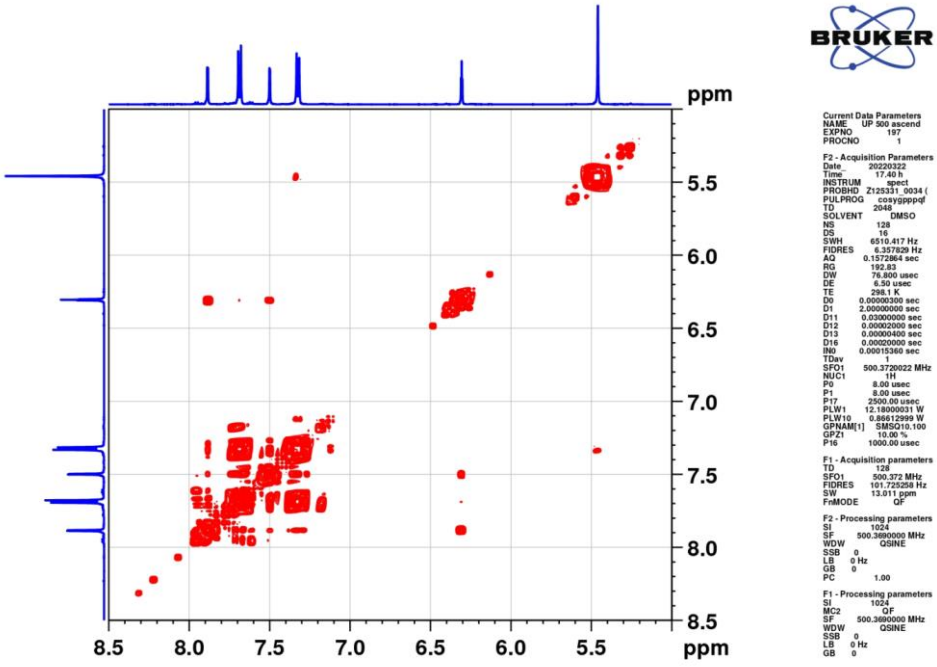

Figure 2.7. ^{1}H–^{1}H COSY NMR spectrum of L^{2} in DMSO–d_6.

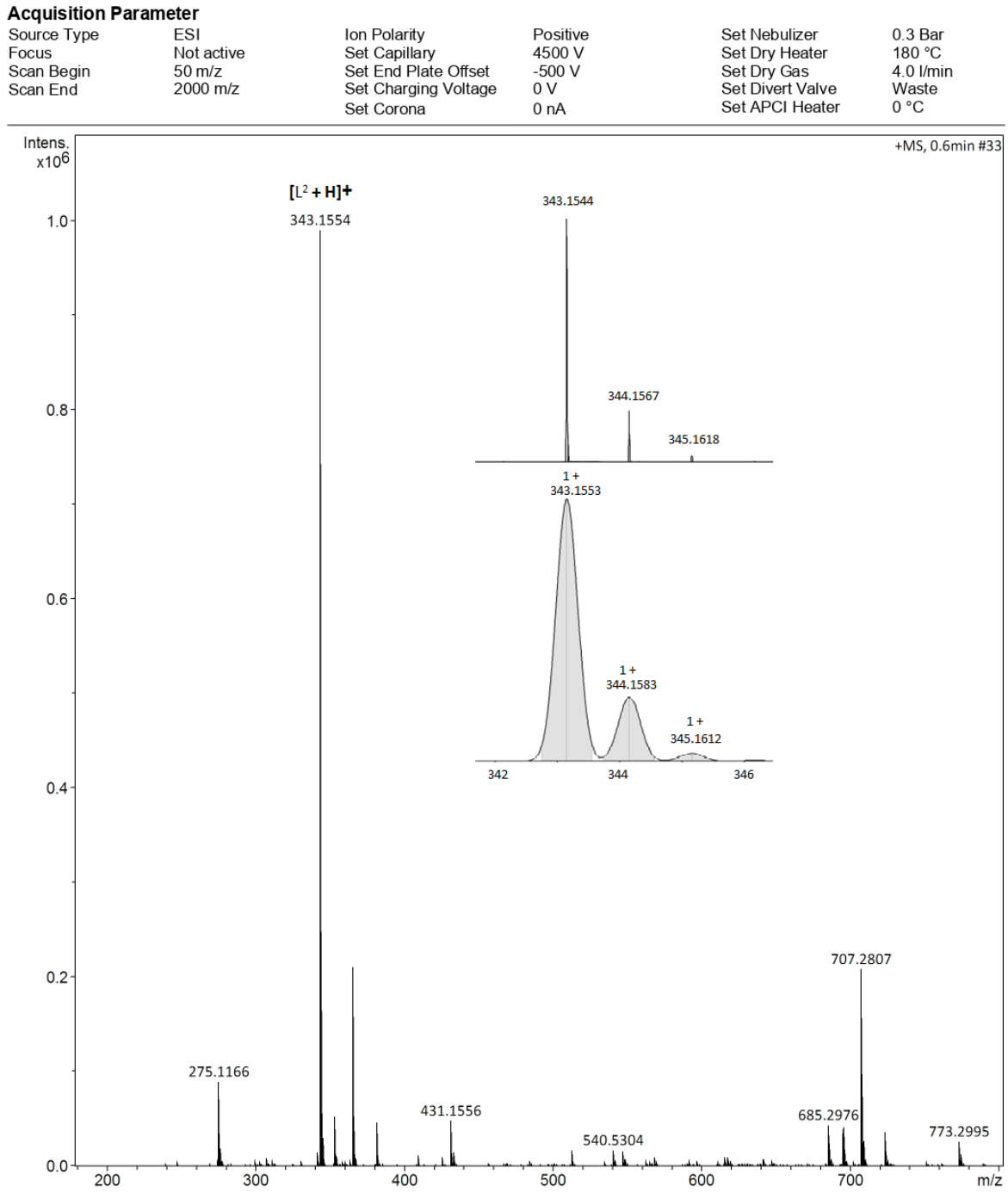

Figure 2.8. ESI mass spectrum of L^2 in positive ion mode (simulated pattern in inset).

2.3.2 Synthesis and characterization of SCCs (1-4)

Metallomacrocycles **1**–**4** were obtained by treating $Re_2(CO)_{10}$, H_2–dhbq or H_2–pydc, and L^n in refluxing mesitylene (Scheme 1). The products are air and moisture stable and are completely soluble in hot DMSO. Complexes **1**–**4** display two strong C≡O stretching bands in 2030–1875 cm^{-1} region, characteristic of *fac*-[$Re(CO)_3$] motif in an asymmetric environment. HR–MS spectra of the macrocycles show molecular ion peaks (*m*/*z* 1007.0497 for [**1**+ H]$^+$, *m*/*z* 1037.0591 for [**2**+ H]$^+$, *m*/*z* 1021.0173 for [**3**+ H]$^+$ and *m*/*z* 1049.0131 for [**4**+ H]$^+$), that match with the theoretical values. The ^{1}H NMR spectra of **1**–**4** display a pattern similar to those of the free ligands (L^1/L^2). Two more additional peaks that appear as a single sharp peak for **1**, **3** and closely spaced pairs for **2**, **4**, corresponding to the protons of $dhbq^{2-}$/$pydc^{2-}$ motif were found. These two signals are slightly upfield shifted compared to that of the free ligand (H_2–dhbq or H_2–pydc). This suggests that $dhbq^{2-}$/$pydc^{2-}$ is bis-chelated to rhenium ions and its two protons experience ring current effect slightly from the neighboring arene core in the metallomacrocycle. Further, the solution contains slightly unequal amount of two conformers. (Figure 2.9-2.22)

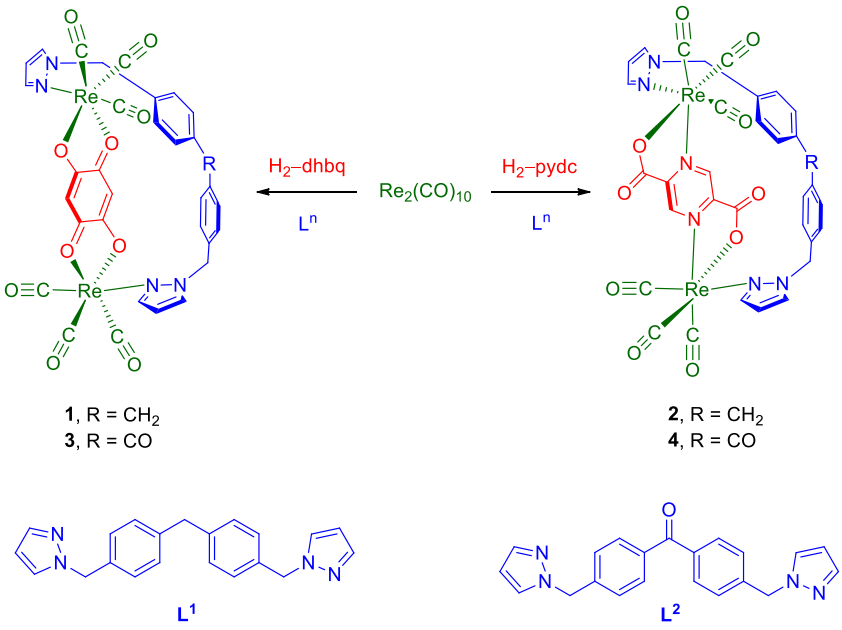

Scheme 2.2. Self-assembly of helicates **1**–**4**.

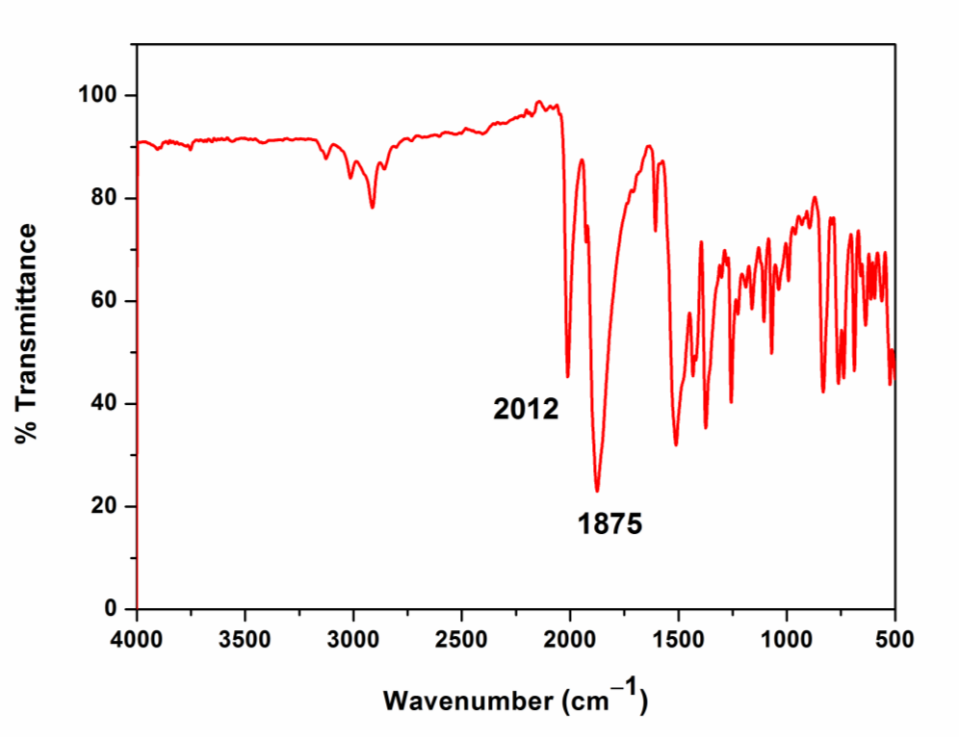

Figure 2.9. ATR–IR spectrum of **1**.

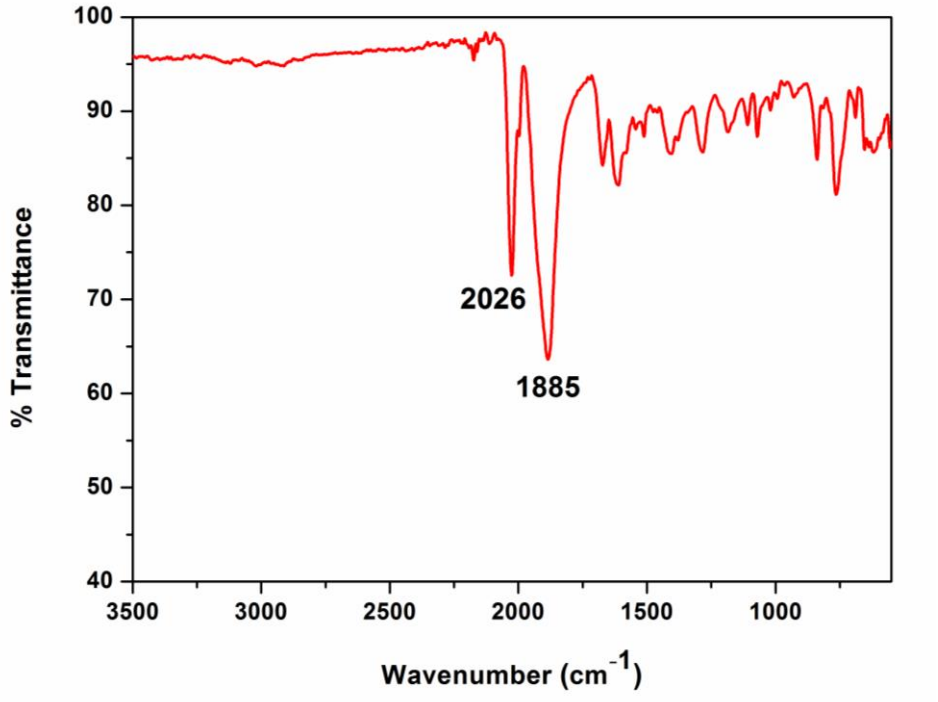

Figure 2.10. ATR–IR spectrum of **2**.

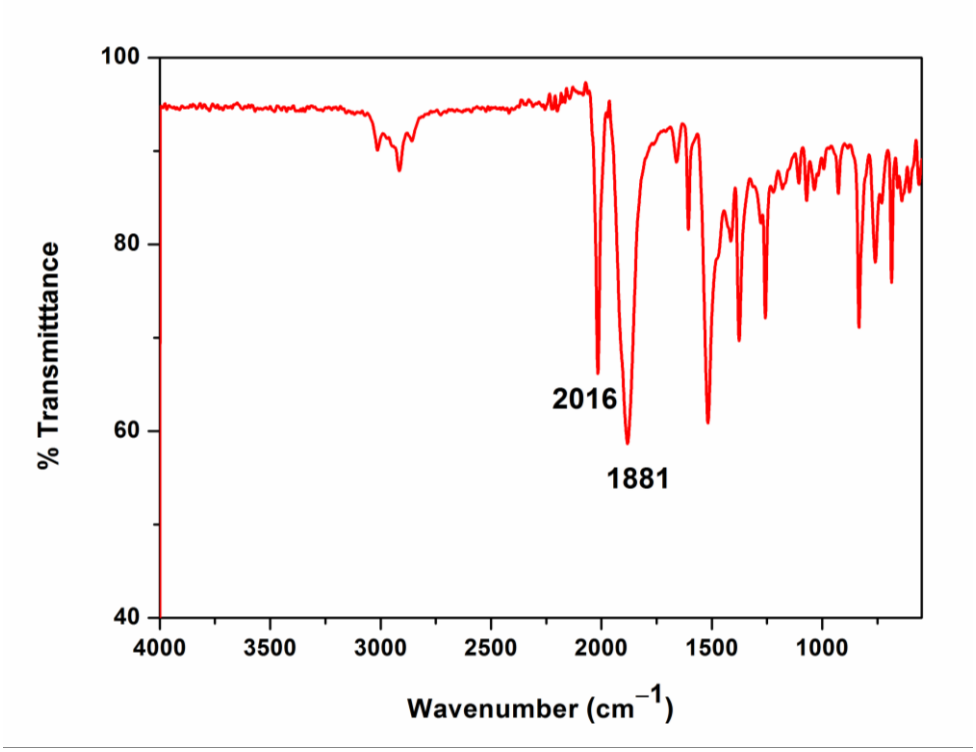

Figure 2.11. ATR–IR spectrum of **3**.

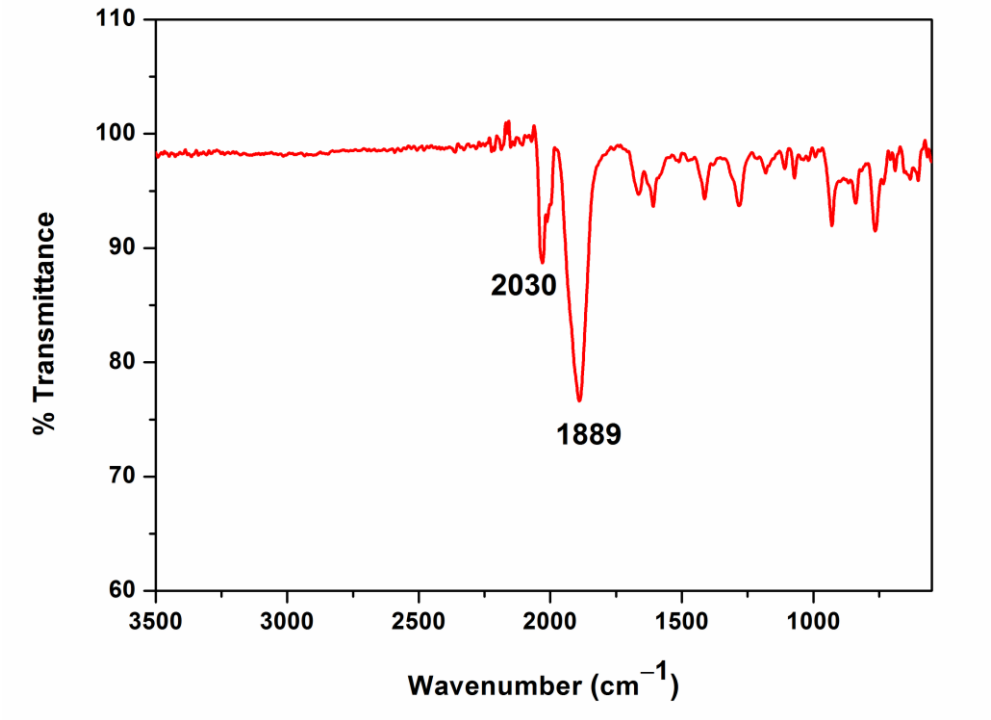

Figure 2.12. AT–IR spectrum of **4**.

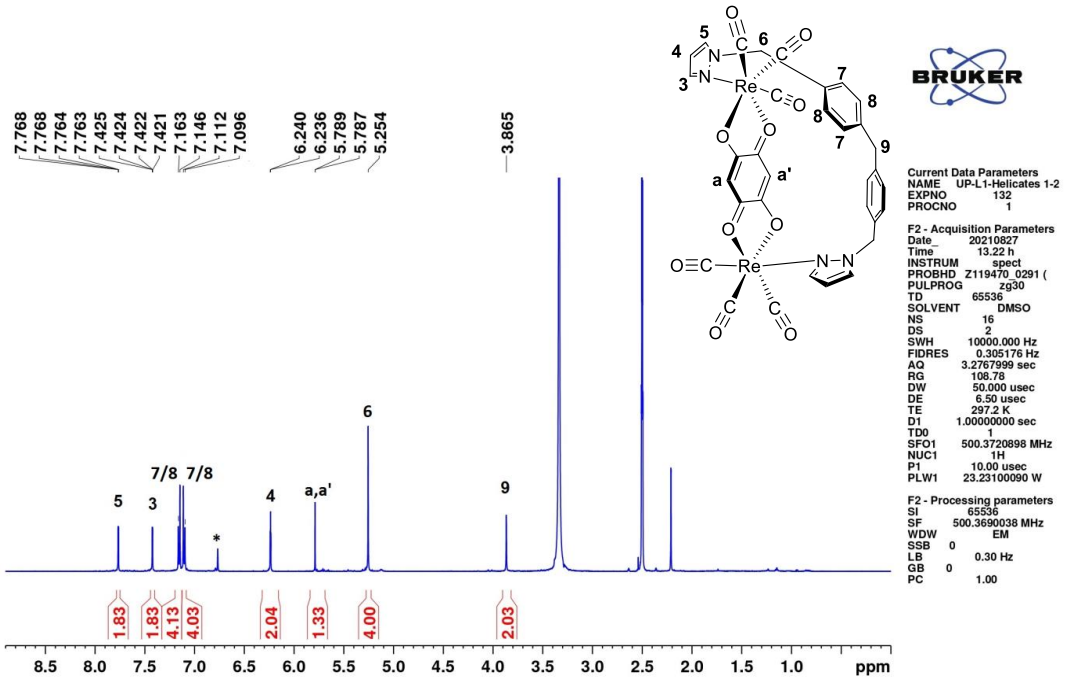

Figure 2.13. ^{1}H NMR spectrum of **1** in DMSO–d_6 (* = Mesitylene).

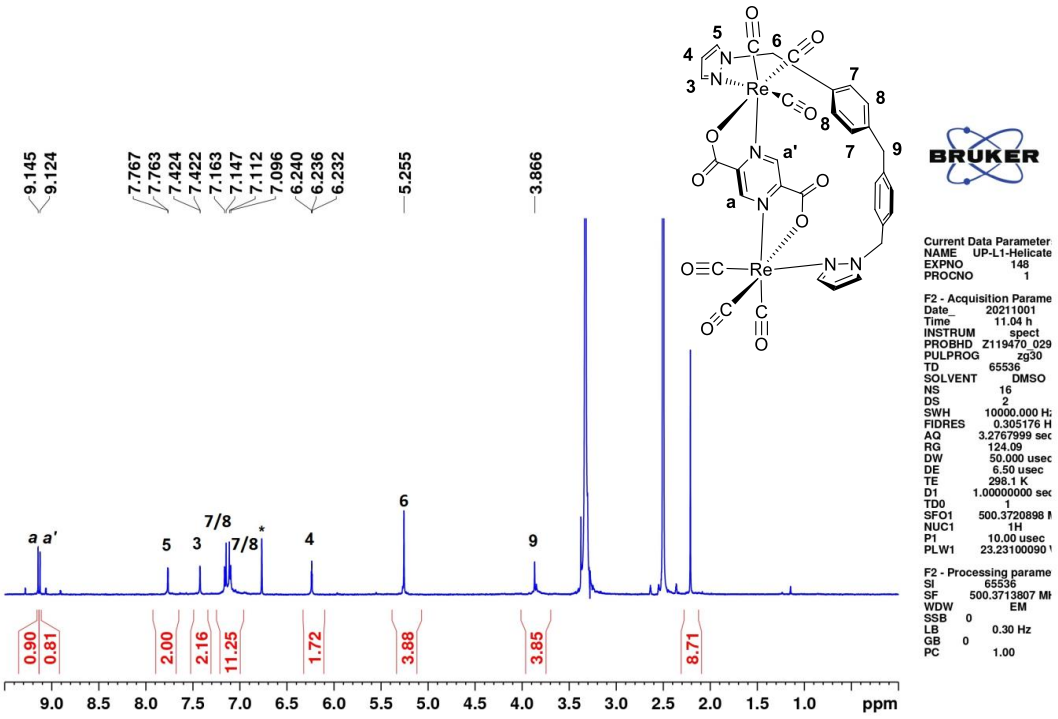

Figure 2.14 ^{1}H NMR spectrum of **2** in DMSO–d_6 (* = Mesitylene).

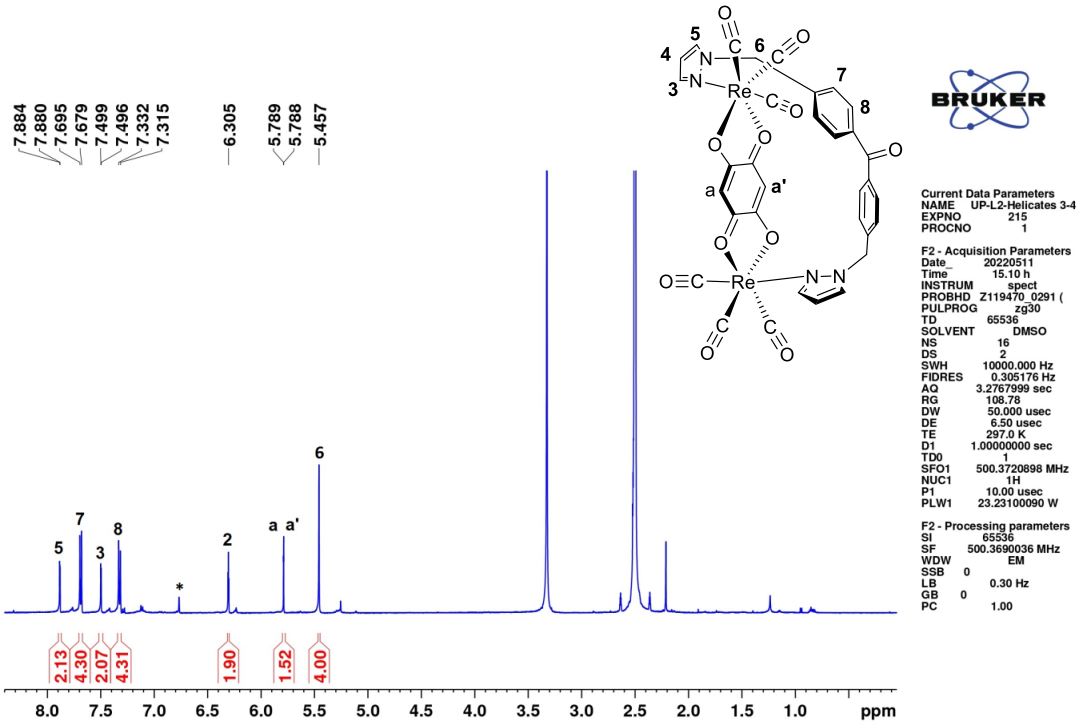

Figure 2.15. ^{1}H NMR spectrum of **3** in DMSO–d_6 (* = Mesitylene).

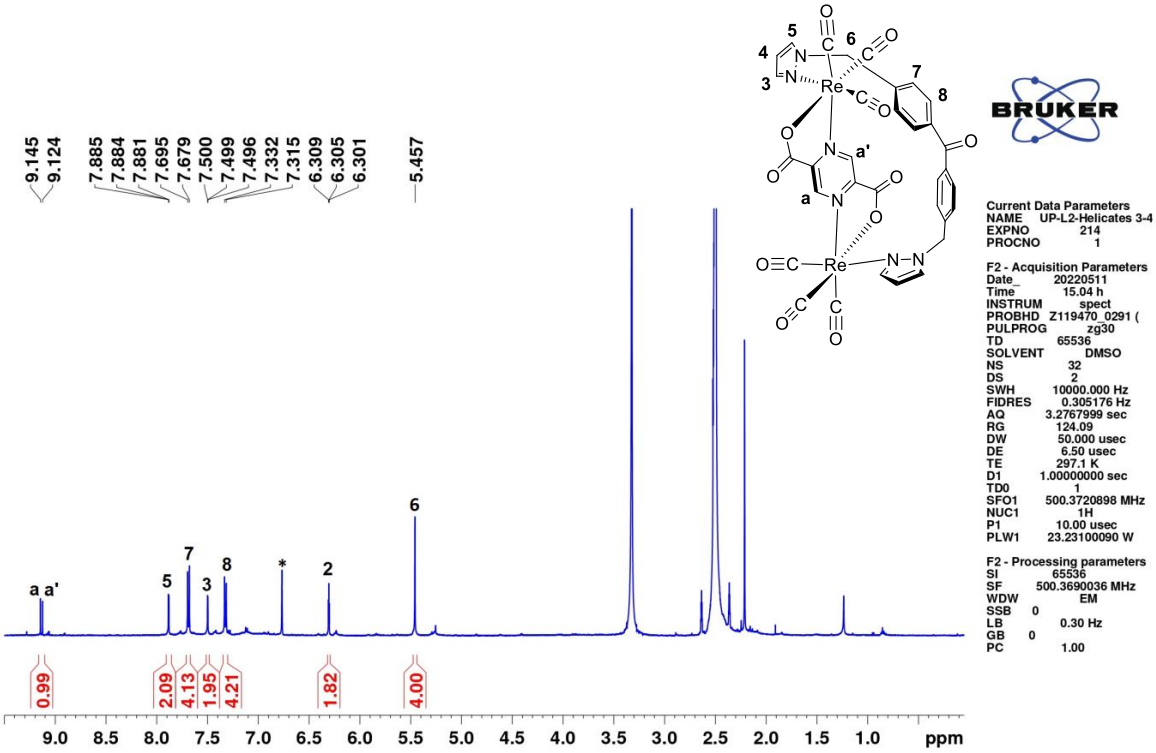

Figure 2.16. ^{1}H NMR spectrum of **4** in DMSO–d_6 (* = Mesitylene).

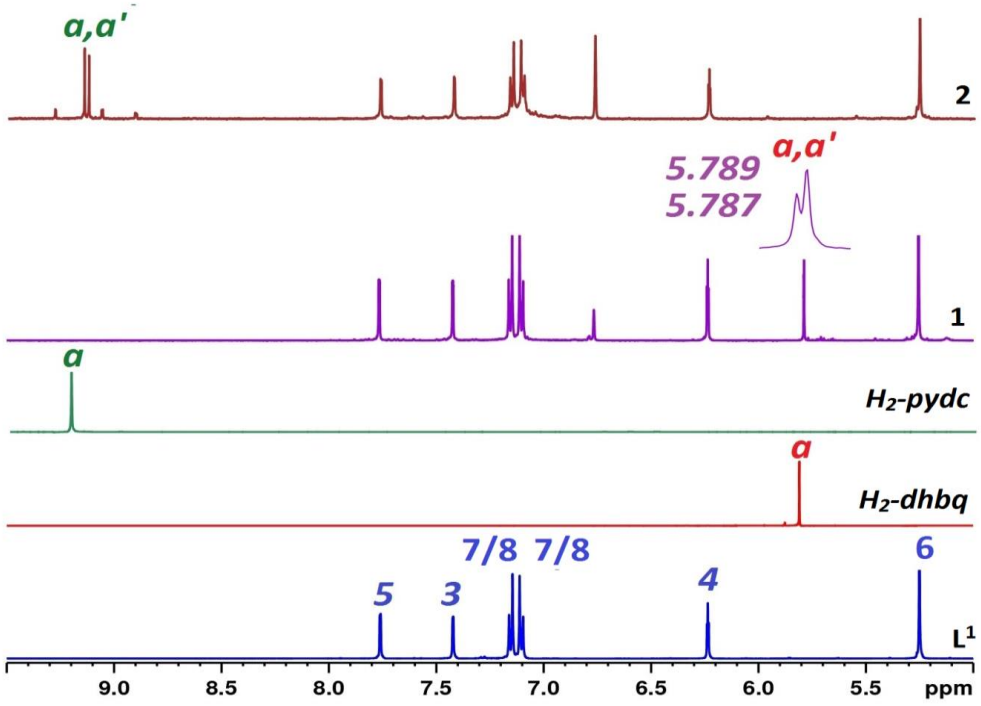

Figure 2.17. Partial ^{1}H NMR spectra of ligands and complexes **1** and **2** in DMSO–d_6.

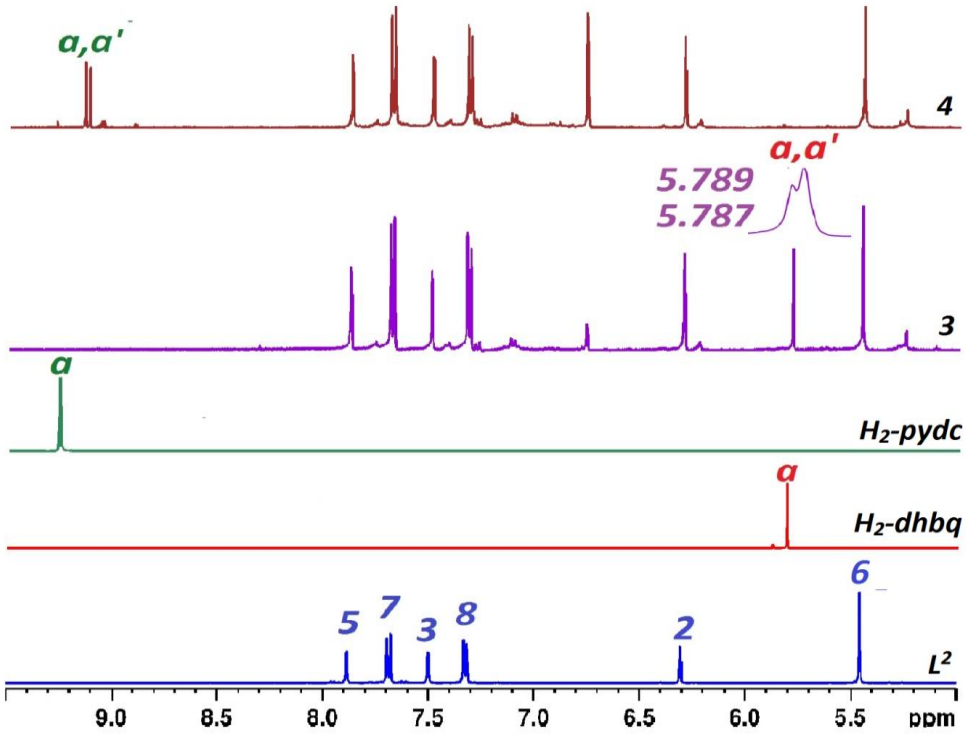

Figure 2.18. Partial ^{1}H NMR spectra of ligands and complexes **3** and **4** in DMSO–d_6.

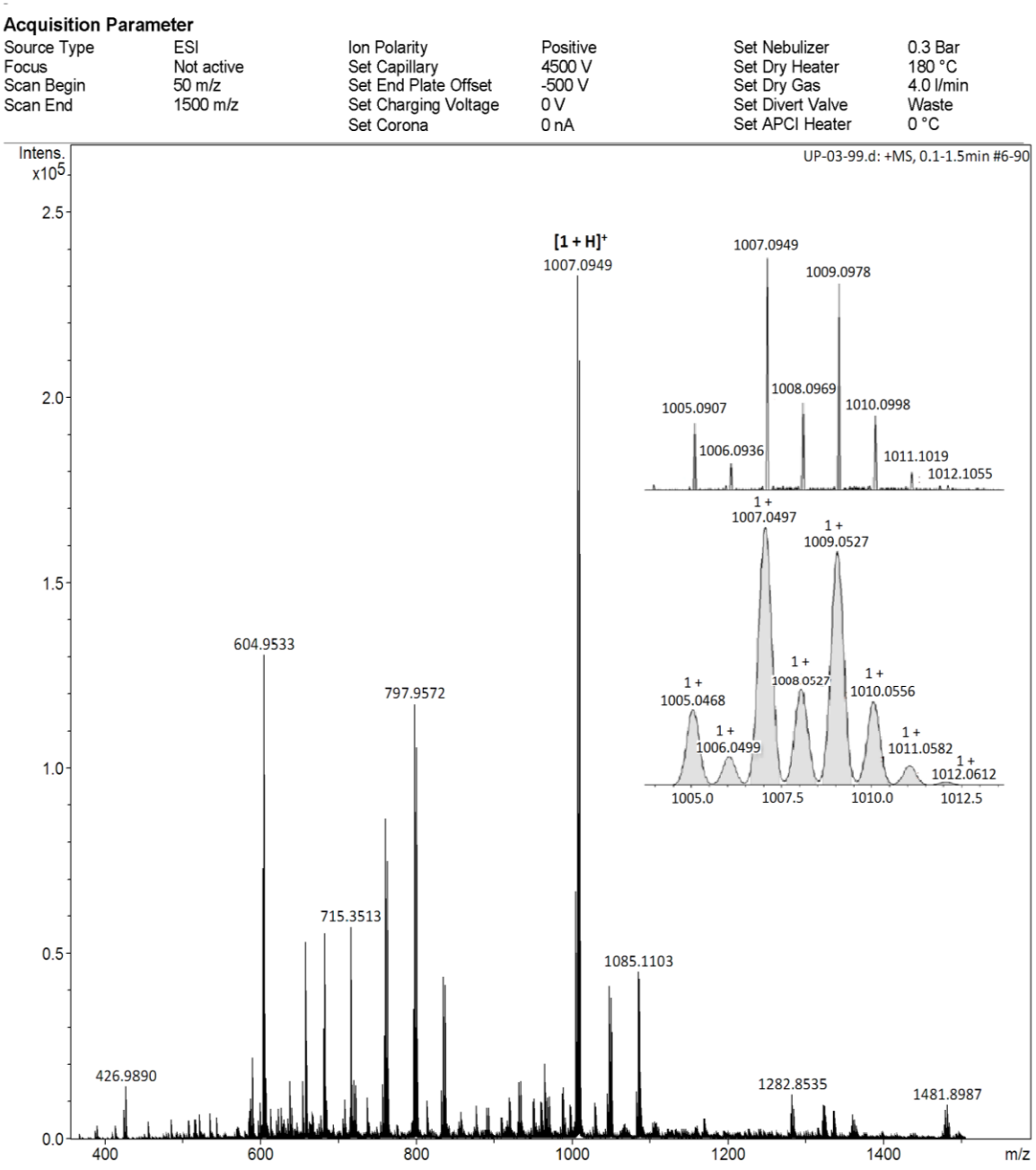

Figure 2.19. ESI mass spectrum of **1** in positive ion mode (simulated pattern in inset).

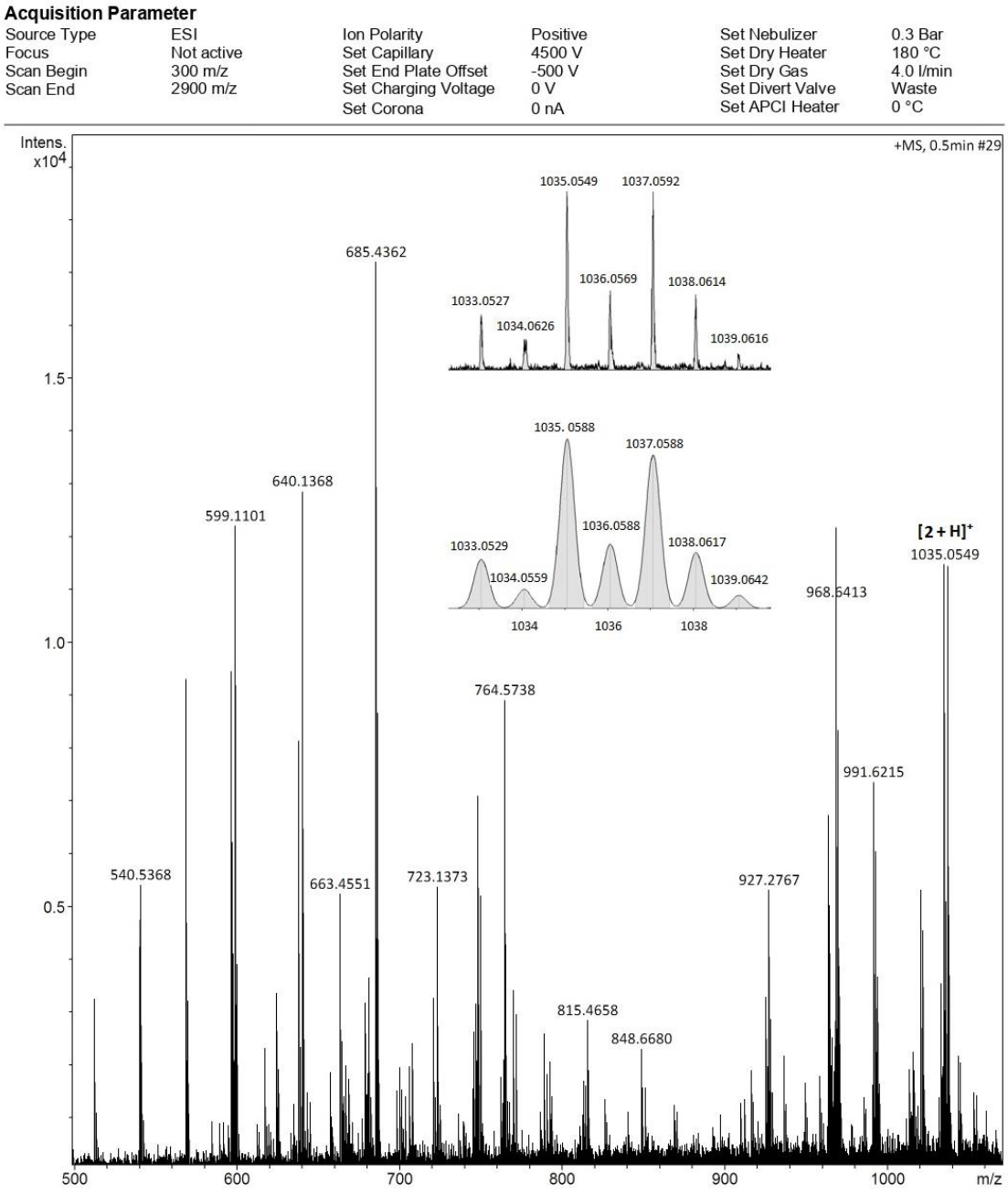

Figure 2.20. ESI mass spectrum of **2** in positive ion mode (simulated pattern in inset).

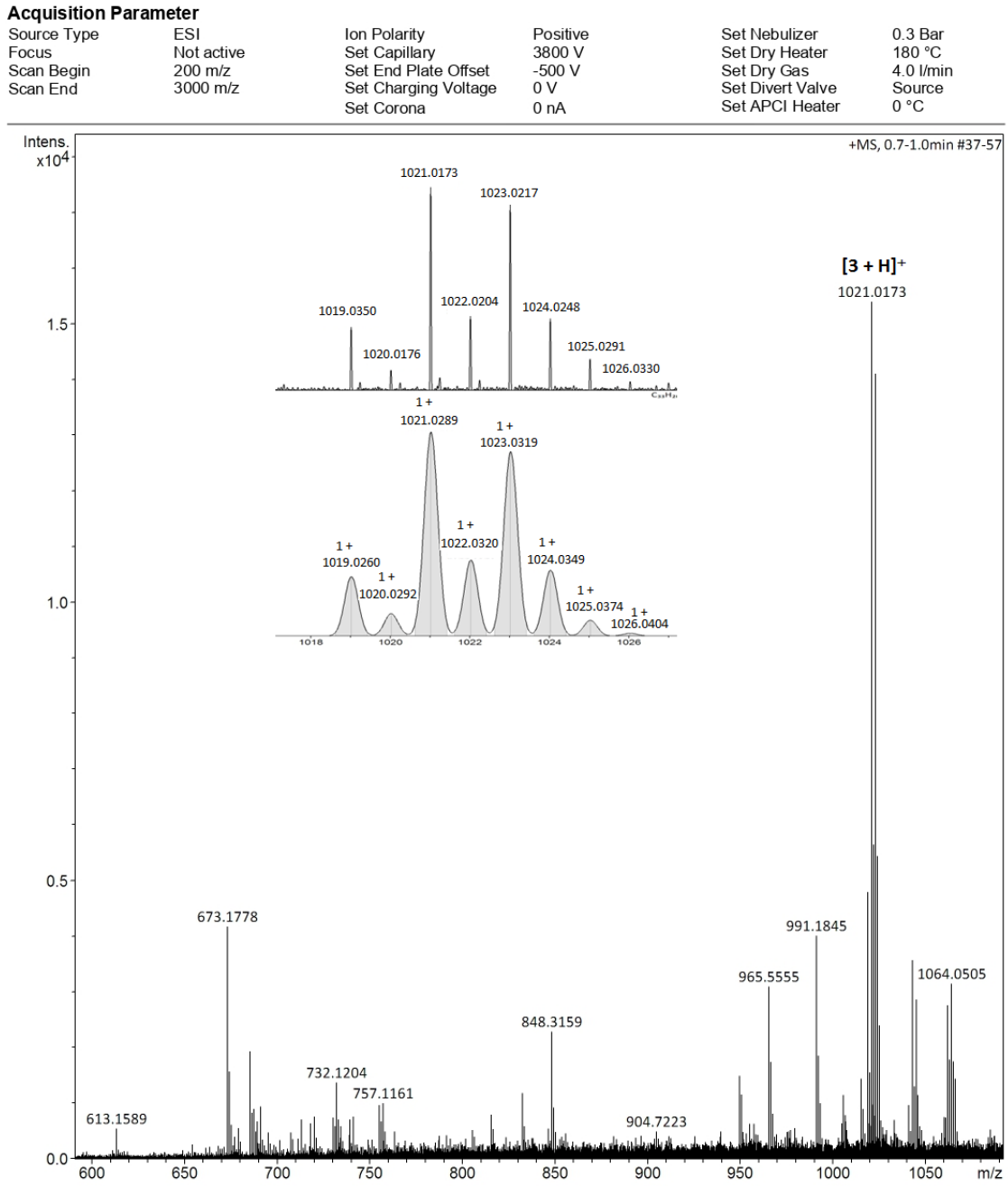

Figure 2.21. ESI mass spectrum of **3** in positive ion mode (simulated pattern in inset).

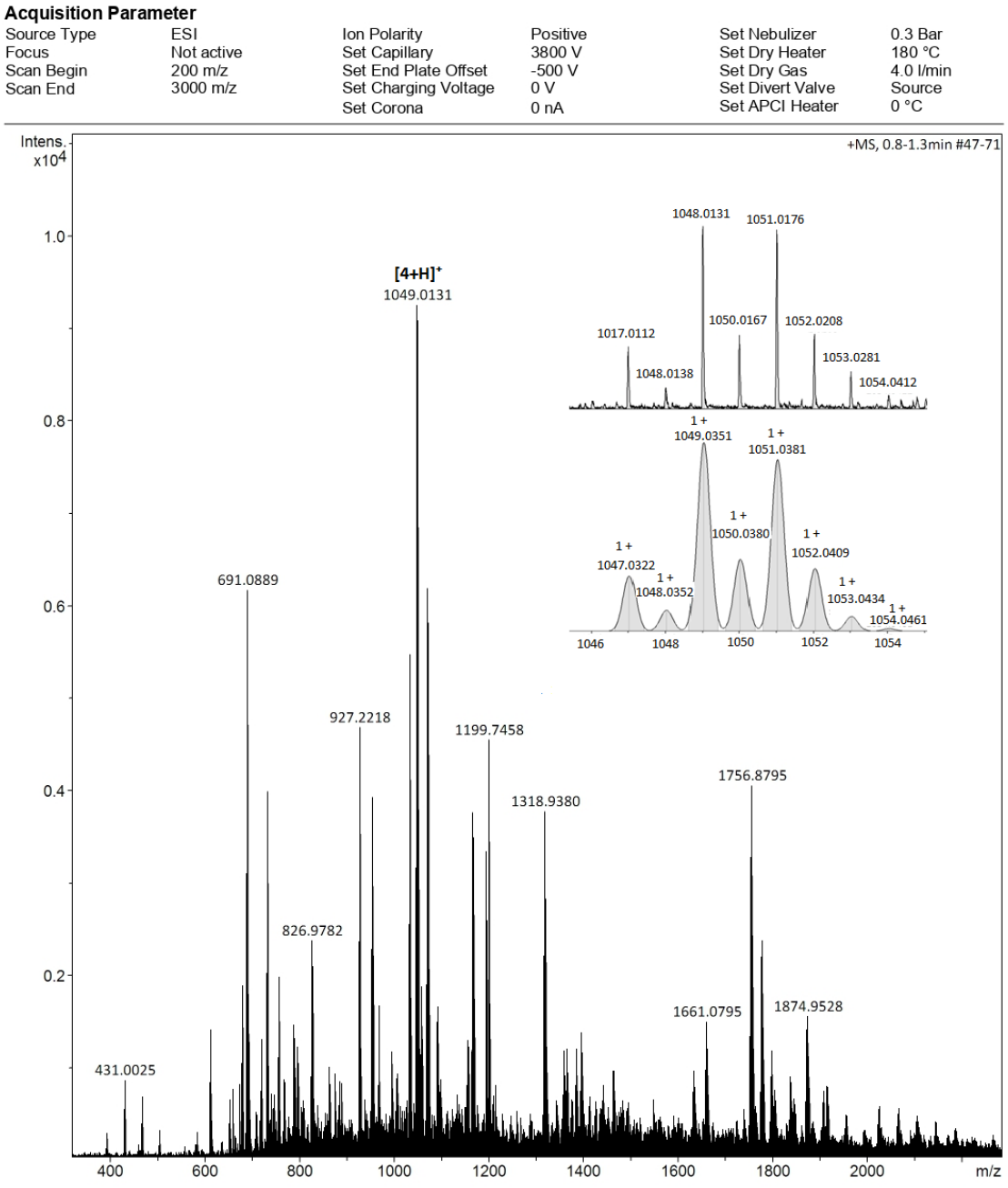

Figure 2.22. ESI mass spectrum of **4** in positive ion mode (simulated pattern in inset).

2.3.3 Molecular structure of metallocycle 1

Crystals of **1** with mesitylene solvent for X–ray diffraction analysis were obtained by slow evaporation of mother liquor. Molecular structure of **1** shows that it adopts a helical architecture (Figure 2.23). The $dhbq^{2-}$ ligand strand partitions into two separate chelating sites and each coordinate a different rhenium ion. The two rhenium atoms and dhbq ligand are in the same axis without any twisting resulting in [Re–dhbq–Re] rigid dinuclear strand. The flexible L^1 strand acts as bis(monodenate) N donor and coordinates two rhenium ions of [Re–dhbq–Re] in **1**. In particular, the flexible ligand strand wraps around the dinuclear strand in a helical manner. Two types of equal amount of helicates are present in the crystal. Among these helicates, one molecule adopts right handed helical structure, whereas the other molecule takes left-handed helical structure. The $dhbq^{2-}$ unit is perpendicular to the biphenyl methane unit of L^1 in **1**. As a result one of the hydrogen atoms of $dhbq^{2-}$ unit lies close to the two phenyl units of L^1 and contacts each other via non-covalent C–H···π interactions (C30···C17 = 3.548 Å, ∠C30–H···C17 = 139° and C30···C6 = 3.512 Å, ∠C30–H···C6 = 134°) in one helicate. A similar arrangement was found for another hydrogen atom of the $dhbq^{2-}$ in the other helicate.

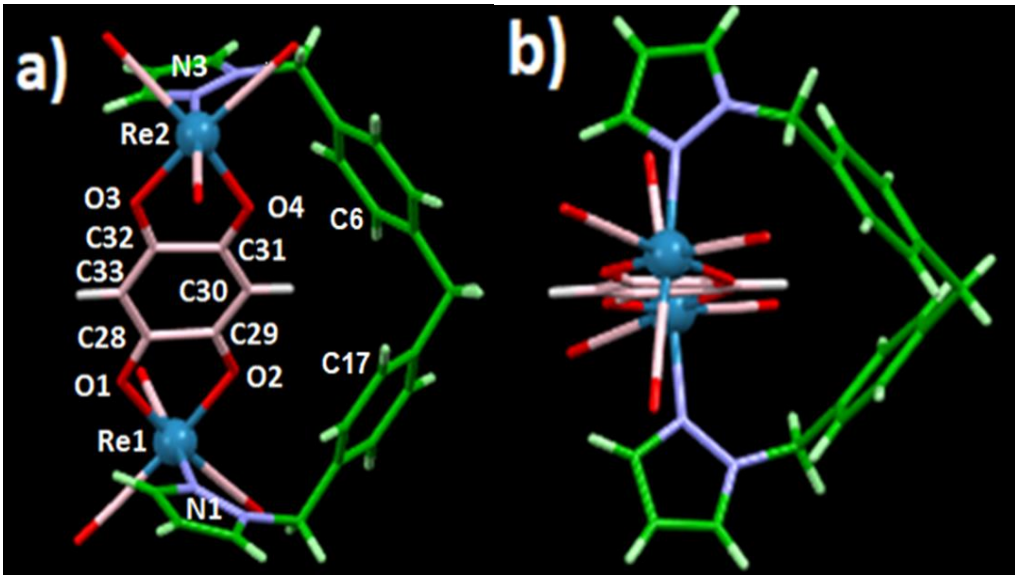

Figure 2.23 (a-b) Side- and top-views of helicate **1**. Color code: C = green for L^1 & pink for dhbq and CO; H = light green for L^1 & pink for dhbq; O = red, N = blue, Re = azure blue.

The length of the helix, as defined by the intramolecular Re•••Re distance, is ~8.05 Å. The overall arrangement of metallomacrocycle **1** is structurally unique as only one-strand in the double-stranded dinuclear unit adopts a helical arrangement. Therefore, complex **1** can be best regarded as dinuclear heterostranded monohelicate. The rhenium ions are in distorted octahedral geometry. The Re–O, Re–N, and Re–C bond lengths in **1** are in the expected range.[14]

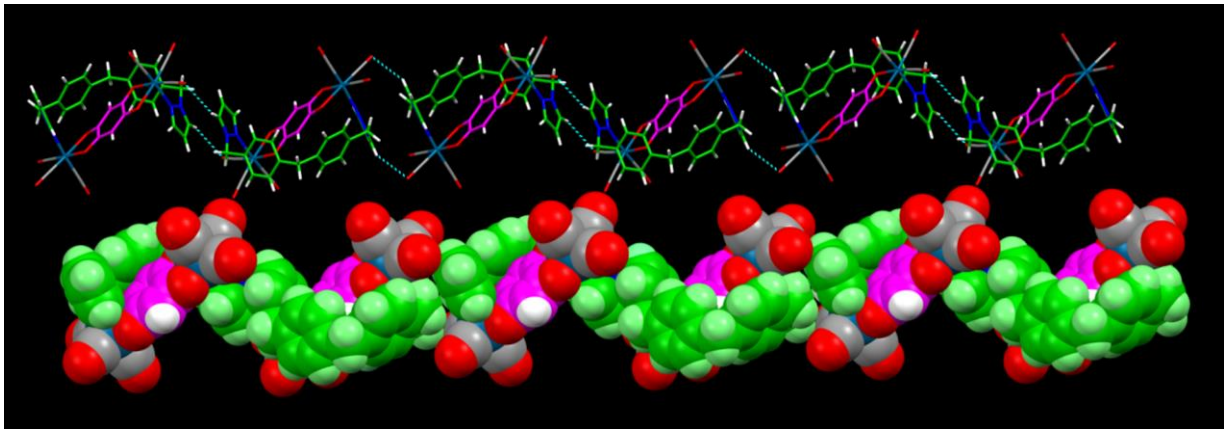

Figure 2.24. Partial packing diagram of **1** showing two 1D-supramolecular helical chains (stick and space-filling view) consisting of alternatively arranged right- and left-handed helicates. Solvent mesitylene molecules are removed for clarity.

Table 1. Selected bond lengths (Å) in 1

Re(1)–O(1)	2.147(5)	O(2)–C(29)	1.269(8)
Re(1)–O(2)	2.135(5)	O(3)–C(32)	1.270(8)
Re(2)–O(3)	2.143(5)	O(4)–C(31)	1.269(8)
Re(2)–O(4)	2.133(5)	C(28)–C(33)	1.365(8)
Re(1)–N(1)	2.210(6)	C(33)–C(32)	1.382(10)
Re(2)–N(3)	2.229(6)	C(31)–C(32)	1.520(10)
O(1)–C(28)	1.265(8)	C(31)–C(30)	1.375(8)
		C(29)–C(30)	1.383(9)
		C(29)–C(28)	1.523(10)

In the crystal structure of **1**, alternatively arranged right and left-handed helicates along the *c*-axis contact each other via intermolecular hydrogen bonds, occurring between hydrogen of pyrazolyl unit of helical strand L^1 to oxygen of carbonyl group (C3···O6 = 3.33 Å, ∠C3–H···O6 = 125°; C19···O8 = 3.54 Å, ∠C19–H···O8 = 151°). Each helicate has two such complementary interactions between the two neighbouring molecules, one at each end. This interaction propagates along the "*c*" axis resulting in

right-handed helical chains with the helical pitch of ~19.2 Å i.e. two L^1 motifs make one helical turn. The super-structure is similar to a single creeper helically wrapping around a rigid trunk (Figure 2.24).[15]

2.3.4 Structure optimization studies

Several attempts for growing single crystals of **2**–**4** from either slow evaporation of the mother liquor or direct solvothermal approaches in mesitylene/toluene were fruitless. Molecular structures of **2**–**4** as helicates and mesocates were calculated using DFT methods (Figure 2.25). The energy minimized structure of **1** matches with the X–ray structure except slight variation in the ligands, presumably due to the packing interactions in the crystal. No noticeable difference was found in the bonding parameters among these two structures. Therefore, the optimized methods for the remaining complexes can be considered as reliable data.

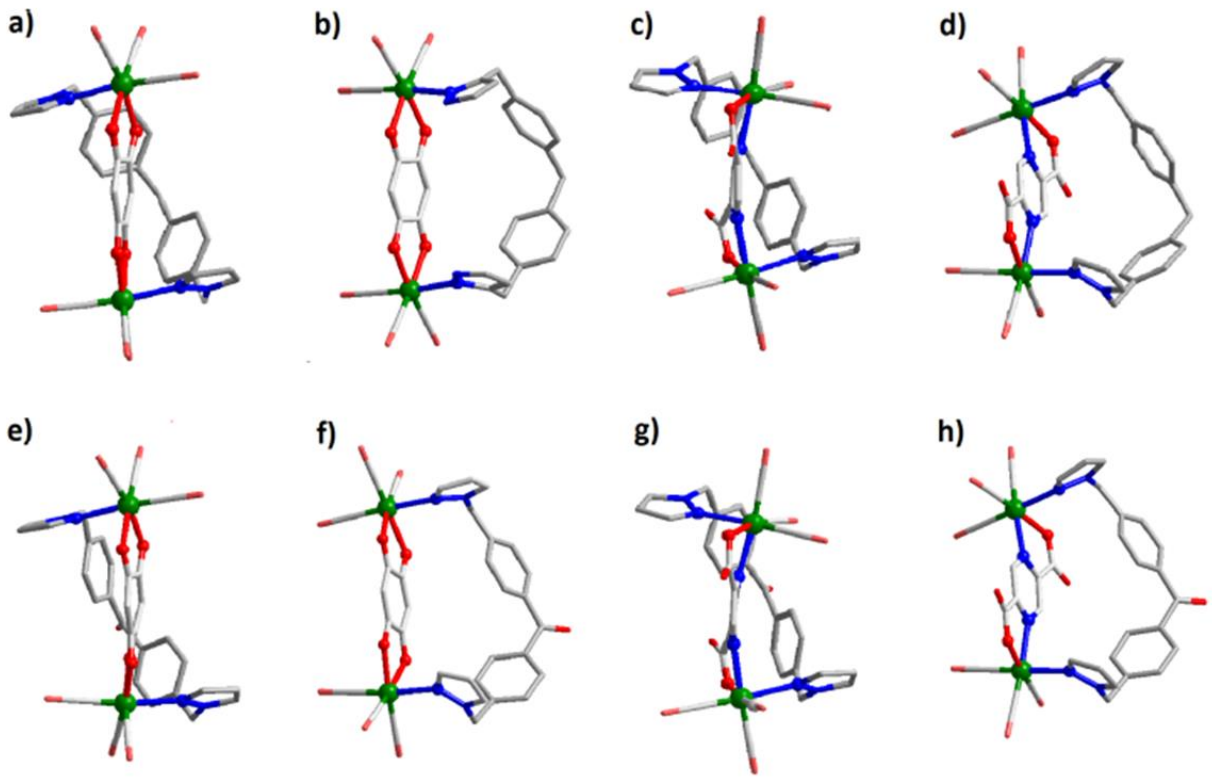

Figure 2.25. Optimized structures of helicates (a = **1,** c = **2,** e = **3** and g = **4**) and mesocates (b = **1**, d = **2**, f = **3** and h = **4**). H atoms are removed for clarity, Color code: C = gray, N = blue, O = red and Re = green.

In the helicates, $dhbq^{2-}/pydc^{2-}$ adopts little strain whereas L^n adopts strain free environment. On the other hand in the mesocate structures, both pyrazolyl motifs are slightly deviated along the coordinated axis and there is not much twisting of $dhbq^{2-}/pydc^{2-}$. The calculated energy difference between the helicates and mesocates is 0.455 kcal/mol for **1** and 5.019 kcal/mol for **3**, suggesting that the equilibrium between helicate and mesocate is favourable without any energy barrier. The mesocate geometry is more stable than the helicate for **2** by 4.056 kcal/mol and **4** by 3.802 kcal/mol.

2.4 Conclusion

In conclusion, a new class of dinuclear heteroleptic monohelicates (**1**–**4**) were self-assembled by using $Re_2(CO)_{10}$, rigid bis-chelating ligand strand and newly designed flexible bis(monodentate) pyrazolyl N–donor in mesitylene. Though these helicates contain two organic ligand strands, only one strand is arranged in a helical fashion. X-ray structure of **1** reveals that both right- and left-handed helicates are present which interact with each other via non-covalent interactions resulting in one dimensional right-handed superhelical architecture. All the metallosupramolecules are optimized as helicates and mesocates via DFT methods which reveal that the energy difference between the structures is less.

2.5 References

1. (a) J. M. Lehn, *Angew. Chem. Int., Ed*. 2013, **52**, 2836–2850; (b) M. D. Ward, *Chem. Commun*., 2009, 4487–4499; (c) R., P. S. Mukherjee and P. J. Stang, *Chem. Rev.,* 2011, **111**, 6810–6918. (d) M. M. J. Smulders, I. A. Riddell, C. Browne and J. R. Nitschke, *Chem. Soc. Rev.,* 2013, **42**, 1728–1754; (e) T. R. Cook and P. J. Stang, *Chem. Rev.,* 2015, **115**, 7001–7045; (f) J. M. Lehn, A. Rigault, J. Siegel, J. Harrowfield, B. Chevrier and D. Moras, *Proc. Natl. Acad. Sci. USA.,* 1987, **84**, 2565–2569; (g) M. Albrecht, *Chem. Rev.,* 2001, **101**, 3457–3497; (h) J. F. Ayme, J. M. Lehn, C. Bailly and L. Karmazin, *J. Am. Chem. Soc.,* 2020, **142**, 5819–5824.
2. (a) A. Casini, B. Woods and M. Wenzel, *Inorg. Chem*., 2017, **56**, 14715–14729; (b) M. J. Hannon and L. Childs, *J. Supramol. Chem.,* 2004, **16**, 7–22; (c) W-X.Gao, H. N. Zhang and G-X. Jin, *Coord. Chem. Rev*., 2019, 386, 69–84.

3. (a) C. Piguet, G. Bernardinelli and G. Hopfgartner, *Chem. Rev*., 1997, **97**, 2005−2062; (b) M. J. Hannon, C. L. Painting and N. W. Alcock, *Chem. Commun.*, 1999, 2023–2024; (c) C. M. Naranthatta, S. Bandi, R. Jagan and K. D. Chand, *Cryst. Growth Des.*, 2016, **16**, 6722−6728; (d) A. P. Paneerselvan, S. S. Mishra and D. K.Chand, *J. Chem. Sci.*, 2018, **130**, 1–18; (e) X. Li, Z. Shi, J. Wu, J. Wu, C. He, X. Hao and C. Duan, *Chem. Commun.*, 2020, **56**, 7537−7548; (f) E. Yashima, N. Ousaka, D. Taura, K. Shimomura, T. Ikai and K. Maeda, *Chem. Rev*., 2016, **116**, 13752−13990.
4. (a) J.Sahoo, R. Arunachalam, P. S. Subramanian, E. Suresh, A. Valkonen, K. Rissanen and M. Albrecht, *Angew. Chem. Int. Ed.*, 2016, **55**, 9625–9629; (b) S. J. Allison, D. Cooke, F. S. Davidson, P. I .P. Elliott, R. A. Faulkner, H. B. S. Griffiths, O. J. Harper, O. Hussain, P. J. Owen-Lynch, R. M. Phillips, C. R. Rice, S. L. Shepherd and R. T. Wheelhouse, *Angew. Chem. Int. Ed.*, 2018, **57**, 9799–9804; (c) A. Stephenson and M. D. Ward, *Chem. Commun.*, 2012, **48**, 3605–3607.
5. (a) B. Shankar, S. Sahu, N. Deibel, D. Schweinfurth, B. Sarkar, P. Elumalai, D. Gupta, F. Hussain, G. Krishnamoorthy and M. Sathiyendiran, *Inorg. Chem*., 2014, **53**, 922–930; (b) P. Saxena, B. Shankar, A. Sathyanarayana, G. Prabusankar and M. Sathiyendiran, *Chimia*., 2015, **69**, 675–677; (c) K. R. Soumya, R. Arumugam, B. Shankar and M. Sathiyendiran, *Inorg. Chem*., 2018, **57**, 10718–10725; (d) M. Karthikeyan, R. Govindarajan, E. Duraisamy, V. Veena, N. Sakthivel and B. Manimaran, *ChemistrySelect*, 2017, **2**, 3362–3368; (e) B. Ramakrishna, R. Nagarajaprakash, V. Veena, N. Sakthivel and B. Manimaran, *Dalton Trans.*, 2015, **44**, 17629–17638; (f) C. A. Kumar, S. Karthikeyan, B.Varghese , V. Veena, N. Sakthivel and B. Manimaran, *J. Organomet. Chem*., 2014, **766**, 86–94; (g) C. A. Kumar, D. Divya, R. Nagarajaprakash, V. Veena, P. Vidhyapriya , N. Sakthivel and Bala. Manimaran, *J. Organomet. Chem*., 2017, **846**, 152–160.
6. (a) S. Sato and O. Ishitani, *Coord. Chem.Rev*., 2015, 282–283, 50–59; (b) R. Govindarajan, R. Nagarajaprakash, V. Veena, N. Sakthivel and B. Manimaran, *Polyhedron*., 2018, **139**, 229–236; (c) G. G. Huang, C. Leeb, J. Yang, Z. Luc, M. Sathiyendiran, C. Huang, Y. Kao, G. Lee and K-L. Lu, *Sensors and Actuators B*., 2018, **254**, 424–430; (d) D. Gupta and M. Sathiyendiran, *ChemistrySelect*., 2018, **3**, 7439–7458; (e) A. M. Cancelliere, F. Puntoriero, S. Serroni, C. Campagna, Y. Tamaki, D. Saito and O. Ishitani, *Chem. Sci*., 2020, **11**, 1556–1563; (f) P. Thanasekaran, C-C.

Lee and K-L.Lu, *Acc. Chem. Res.*, 2012, **45**, 1403–1418; (g) D. Sinha, S. P. Paruaand and K. K. Rajak, *J. Organomet. Chem*., 2019, **889**, 62–69. (h) J. R. Dilworth, *Coord. Chem. Rev.*, 2021, **436**, 213822–213858; (i) E. B. Bauer, A. A. Haase, R. M. Reich, D. C. Crans and F. E. Kuhn, *Coord. Chem. Rev.*, 2019, **393**, 79–117.

7. (a) R. L. Halterman, X. Pan, D. E. Martyn, J. L. Moore and A. T. Long, *J. Org. Chem*., 2007, **72**, 6454–6458; (b) S. Woo, Y. G. Kim, B. Lim, J. Oh, Y. Lee, H. Gwon and K. Nahm, *RSC Adv.*, 2018, **8**, 2157–2160.
8. (a) G. M. Sheldrick, SHELXS-97: Program for Crystal Structure Solution; University of Göttingen: Göttingen, Germany, 1997. (b) G. M. Sheldrick, *Acta Crystallogr., Sect. A: Found. Crystallogr*. 2008, **64**, 112−122; (c) G. M. Sheldrick, *Acta Crystallogr., Sect. C: Struct. Chem.* 2015, **71**, 3−8; (d) A. L. Spek, *J. Appl. Crystallogr.*, 2003, **36**, 7−13.
9. (a) A. D. Becke, *J. Chem. Phys.* 1993, **98**, 5648–5652; (b) C. Lee, W. Yang, R.G. Parr, *Phys. Rev. B* 1988, **37**, 785–789; (c) S. H. Vosko, L. Wilk, M. Nusair, *Can. J. Phys.* 1980, **58** 1200–1211.
10. M. J. Frisch, G. W. Trucks, H. B. Schlegel, G. E. Scuseria, M. A. Robb, J. R. Cheeseman, G. Scalmani, V. Barone, B. Mennucci, G. A. Petersson, H. Nakatsuji, M. Caricato, X. Li, H. P. Hratchian, A. F. Izmaylov, J. Bloino, G. Zheng, J. L. Sonnenberg, M. Hada, M. Ehara, K. Toyota, R. Fukuda, J. Hasegawa, M. Ishida, T. Nakajima, Y. Honda, O. Kitao, H. Nakai, T. Vreven, J. A. Montgomery Jr, J. E. Peralta, F. Ogliaro, M. Bearpark, J. J. Heyd, E. Brothers, K. N. Kudin, V. N. Staroverov, R. Kobayashi, J. Normand, K. Raghavachari, A. Rendell, J. C. Burant, S. S. Iyengar, J. Tomasi, M. Cossi, N. Rega, J. M. Millam, M. Klene, J. E. Knox, J. B. Cross, V. Bakken, C. Adamo, J. Jaramillo, R. Gomperts, R. E. Stratmann, O. Yazyev, A. J. Austin, R. Cammi, C. Pomelli, J. W. Ochterski, R. L. Martin, K. Morokuma, V. G. Zakrzewski, G. A. Voth, P. Salvador, J. J. Dannenberg, S. Dapprich, A. D. Daniels, O. Farkas, J. B. Foresman, J. V. Ortiz, J. Cioslowski, D. J. Fox, Gaussian 09, Gaussian, Inc., Wallingford, CT, 2010.
11. (a) A. D. McLean, G. S. Chandler, *J. Chem. Phys.* 1980, **72**, 5639–5648; (b) R. Krishnan, J. S. Binkley, R. Seeger, J. A. Pople, *J. Chem. Phys*. 1980, **72**, 650–654.
12. (a) R. E. Stratmann, G. E. Scuseria, M. J. Frisch, *J. Chem. Phys.* 1998, **109**, 8218–8224; (b) R. Bauernschmitt, R. Ahlrichs, *Chem. Phys. Lett.* 1996, **256**, 454–464; (c) M. E. Casida, C. Jamorski, K. C. Casida, D. R. J. Salahub, *Chem. Phys.* 1998, **108**, 4439–4449.

13. M. Bhol, B. Shankar and M. Sathiyendiran, *Dalton Trans.*, 2018, **47**, 4494–4500.
14. (a) U. Phukon, M. Priyatharsini and M. Sathiyendiran, *J. Organomet. Chem*., 2020, **923**, 121460–121463; (b) J. R. Gardinier, J. S. Hewage, B. Bennett, D. Wang and S. V. Lindeman, *Organometallics*., **2018**, **37**, 989–1000; (c) P. Govindaswamy, B. Therrien, G. Suss-Fink, P. Stepnicka and J. Ludvık, *J. Organomet. Chem.*, 2007, **692**, 1661–1667; (d) A. Yadav, A. K. Gupta, A. Steiner and R. Boomishankar, *Chem. Eur. J.*, 2017, **23**, 18296–18302.
15. S. T. Schneebeli, M. Frasconi, Z. Liu, Y. Wu, D. M. Gardner, N. L. Strutt, C. Cheng, R. Carmieli, M. R. Wasielewski and F. Stoddart, *Angew. Chem. Int. Ed.*, 2013, **52**, 13100–13104.

Chapter 3

Self-assembly, dynamic properties in solution and competitive ligand induced supramolecular transformations of rhenium-pyrazolyl based figure-eight- and *Z*-shaped metallocycles

Abstract

Rhenium(I)tricarbonyl core-based heteroleptic figure-eight- and *Z*-shaped metallocycle (**1a**-**4a**) of the general formula *fac*-[{$(CO)_3$Re(μ-L)Re$(CO)_3$}$_2$(dppz)$_2$] were self-assembled from $Re_2(CO)_{10}$, H_2-L (H_2-L = 5,8-dihydroxy-1,4-naphthaquinone (H_2-dhnq) for **1a**; 1,4-dihydroxy-9,10-anthraquinone (H_2-dhaq) for **2a**; 6,11-dihydroxy-5,12-naphthacenedione (H_2-dhnd) for **3a**; 2,2′-bisbenzimidazole (H_2-bbim) for **4a**) and bis(4-((pyrazolyl)methyl)phenylmethane) (dppz) via one-pot coordination-driven synthetic approach. The molecular structures of **1a** and **4a** were unambigously confirmed by single crystal X-ray diffraction (SCXRD) methods. The metallocycles in DMSO solution exist as acyclic dinuclear DMSO adduct of the general formula *fac*-[{$(CO)_3$Re(μ-L)Re$(CO)_3$}$(DMSO)_2$] (**1b**, L = dhnq; **2b**, L = dhaq; **3b**, L = dhnd; **4b**, L = bbim) and dppz which are in dynamic equilibrium. The dynamic behavior of rhenium-pyrazolyl bond in the solution state was effectively utilized to transform metallocycles **1a**–**4a** into pyridyl/benzimidazolyl/phosphine donor-based heteroleptic metallocycles and acyclic dinuclear complexes (**4**-**13**). These include tetranuclear rectangles *fac*-[{$(CO)_3$Re(μ-L)Re$(CO)_3$}$_2$(4,4′-bpy)$_2$] (**4** and **11**, L = dhaq for **4** and bbim for **11**), dinuclear metallocycles *fac*-[{$(CO)_3$Re(μ-L)Re$(CO)_3$}(dpbim)] (**5**-**7** and **12**; L = dhnq for **5**, dhaq for **6**, dhnd for **7**, and bbim for **12**), and dinuclear acyclic complexes *fac*-[{$(CO)_3$Re(μ-L)Re$(CO)_3$}$(PTA)_2$] (**8**–**10** and **13**; L = dhnq for **8**, dhaq for **9**, dhnd for **10**, and bbim for **13**). These transformations were achieved through component-induced supramolecular reactions while treating with competitive ligands 4,4′-bipyridine (4,4′-bpy), bis(4-((^{1}H-benzoimidazole-1-yl)methyl)phenyl)methane (dpbim) and 1,3,5-triaza-7-phosphaadamantane (PTA). The reaction mixture in the solution was analyzed using NMR and ESI-MS analysis. Additionally, crystal structures of **4**, **6** and **13**, which were obtained in the mixture of the solutions, were

determined, providing unequivocal evidence for the occurrence of supramolecular transformation within the system. The results reveal that the size of the chelating ligand and the pyrazolyl donor angle of the ditopic ligand play crucial roles in determining the resulting solid-state metallocyclic architecture in these synthetic combinations. The dynamic behavior of the rhenium-pyrazolyl bond in the metallocycles can be utilized to transform into other metallocycles and acyclic complexes using suitable competing ligands via ligand-induced supramolecular transformations

---

This work has been published in *ACS Omega* 2023, **8**, 41773–41784.

3.1. Introduction

The design and synthesis of metallocycles such as cages, helicates and simple-to-complex topological architectures via coordination-driven self-assembly have been gaining still significant attention owing to their potential applications in materials and medicinal fields.[1-9] Further, new aesthetically appealing molecular architectures including intricate topological metallocyclic architectures such as metallo-links (a series of interlocked metallocyclic rings where atleast one ring has to be broken to separate them) and metallo-knots similar to those found in nature can be prepared using the self-assembly.[10-18] Among the various topologies, figure-eight architecture is one of the elegant self-assembled structures which is found in natural systems such as Lissoclinamide 7, recombinant structure of circular DNA and marine alkaloid.[19-20] However, very few examples of figure-eight-shaped metallocycles are known till now.[21-26]

The design and synthesis of figure-eight-shaped metallocycles and other metallocyclic architectures using various metal precursors and organic building units are important in the development of the field, which might yield molecules having various potential applications in the near future. Among the few metal ions based coordination-driven approaches, *fac*-[$Re(CO)_3$] core-based self-assembly method is one of the methods to construct neutral homoleptic and heteroleptic metallocycles which have potential applications in the field of host−guest encapsulation, catalysis, selective reactivity, sensing, and as bioactive agents.[27-57] Though considerable number of synthetic principles for the preparation of various sizes and shapes of *fac*-[$Re(CO)_3$] core-based metallocycles are currently available, synthetic approach for preparing figure-eight topology, complex-knots and complex-links-shaped metallocycles are scarce. In addition to the metal core, the nature of ligand is crucial to obtain the complex topological architectures.

To the best of our knowledge, pyridyl and imidazolyl/benzimidazolyl and their structural analogous-based ditopic-/tritopic- and multitopic ligands are frequently used to construct *fac*-[$Re(CO)_3$] core-based metallocycles. These rhenium(I)-based metallacycles are generally kinetically inert and robust in solution including coordinating DMSO solvent. On the other hand, only a countable number of pyrazolyl donor-based ligands are used in constructing *fac*-[$Re(CO)_3$] metallacycles.[46,58] It is well-known that metal-pyrazolyl bond are labile in the donor solvents. It is expected that rhenium-pyrazolyl bond in the metallocycles can also be dynamic in the donor solvent. This dynamic nature of metal-donor bonds in the metallocycles

can be utilized potentially both in supramolecular transformations and active agent for the biological systems. However, the design and synthesis and structural transformation of rhenium-pyrazolyl motif containing metallacycles are unknown.

We have used flexible ditopic pyrazolyl donor (dppz) consisting of biphenylmethane (-CH_2-Ph-CH_2-Ph-CH_2-) as spacer and utilized it in constructing new type of helicates with bis-chelating ligand and $Re_2(CO)_{10}$.[46] In this approach, both the rigid ligand (H-L) and the coordination angle of pyrazolyl donor play an important role in dictating the helical structure because the flexible ditopic ligand containing the same spacer with benzimidazolyl donor yields metallocavitand.[47] Therefore, we envision that modulating the width and the length of the rigid bis-chelating ligands (H-L) in the self-assembly combinations of $Re_2(CO)_{10}$, H-L, and dppz would result in hitherto unknown metallocycles including figure-eight architecture, metallo-links or metallo-knots. Hence, rigid bis-chelating ligands 5,8-dihydroxyl-1,4-naphthaquinone (H_2-dhnq), 1,4-dihydroxy-9,10-anthraquinone (H_2-dhaq), 6,11-dihydroxy-5,12-naphthacenedione (H_2-dhnd), and 2,2′-bisbenzimidazole (H_2-bbim) having different width and length were chosen along with dppz in the present study. These rigid bis-chelating ligands are widely used in the construction of supramolecular coordination complexes including Ir/Rh based metallo-links/metallo-knots and considerable number of Re molecular rectangles, which have potential applications in the medicinal and material field.[16,56-57]

Herein, we combine the self-assembly of pyrazolyl motif-based *fac*-[$Re(CO)_3$] core metallocycles, studies their dynamic behavior in DMSO solution, and utilizing the dynamic nature of rhenium-pyrazolyl bond in creating potential new metallacycles and acyclic complexes via ligand induced supramolecular transformation. Herein, we report on a neutral heteroleptic "figure-eight"- and "Z"-shaped metallocycle (**1a**–**4a**) which were self-assembled using $Re_2(CO)_{10}$, rigid bis-chelating ligands and dppz in a one-pot approach. The solid-state structures of **1a** and **4a** were determined by single crystal X-ray diffraction analysis. The metallocycles are in dynamic equilibrium with disassembled dinuclear-DMSO complexes (**1b**–**4b**) and dppz in the solution state. The dynamic nature of Re-pyrazolyl bond of the metallocycles were fruitfully utilized further to transform these metallocycles into other nitrogen donor based tetranuclear- and dinuclear-metallocycles and phosphine donor-based dinuclear acyclic complexes (**4-13**) via ligand exchange process which were studied using NMR, ESI-MS analysis, and single crystal X-ray analysis.

3.2. Experimental

3.2.1. Materials and methods

$Re_2(CO)_{10}$, pyrazole (H−pz), diphenylmethane, H_2-dhnq, H_2-dhaq, H_2-dhnd, KOH, DMF, HBr-acetic acid (33%), paraformaldehyde, o-phenylene diamine, hexachloroacetone, orthophosphoric acid, NBS, CCl_4, toluene, mesitylene, hexane and ethylene glycol were purchased and used as received. H_2-bbim and dppz were prepared by following known procedures.[47] ATR-IR spectra were recorded on a Nicolet iS5 IR spectrophotometer. ^{1}H NMR spectra were recorded on a Bruker Avance III 500 MHz spectrometer. HR-ESI-MS spectra were recorded on Bruker-maXis mass spectrometer.

3.2.2. Crystallography

Single crystal X-ray data of **1a**, **4a**, **6**, and **13** were collected on a Rigaku Oxford Diffractometer (λ(Mo Kα) = 0.71073 Å). The molecular structures were solved by direct methods using SHELXS−97 (Sheldrick 2008) and refined using the SHELXL−2018/3 program (within the WinGX program package).[60-61] Non-H atoms were refined anisotropically.

3.2.3. Synthesis of metallocycles

Synthesis of *fac*-[{(CO)$_3$Re(μ-dhnq)Re(CO)$_3$}$_2$(dppz)$_2$] (1a)

A mixture of $Re_2(CO)_{10}$ (50.0 mg, 0.076 mmol), H_2-dhnq (14.6 mg, 0.076 mmol), dppz (25.1 mg, 0.076 mmol), and mesitylene (20 ml) was refluxed for 5 h and cooled to 30 °C. Dark green precipitate obtained was filtered, washed with hexane and air-dried. Yield: 35 % (115 mg). Green crystals suitable for single crystal X-ray diffraction analysis were obtained from the filtrate. The ^{1}H NMR spectra of precipitate and crystals are same. AT-IR (cm^{-1}): 2010 (s) and 1882 (s) (C≡O). HR-ESI-MS (*m/z*): $[M + H]^+$ calcd for $C_{74}H_{49}N_8O_{20}Re_4$, 2115.1269; found, 2115.1687. ^{1}H NMR (500 MHz, DMSO−d_6, ppm): 7.76 (d, *J* = 1.5 Hz, 4H, H^c), 7.42 (d, *J* = 1.5 Hz, 4H, H^a), 7.26 (d, *J* = 2.5 Hz, 4H, H^A), 7.16 (d, *J* = 5 Hz, 8H, H$^{e/f}$), 7.11 (d, *J* = 5 Hz, 8H, H$^{e/f}$), 6.24 (t, *J* = 1 Hz, 4H, H^b), 5.25 (s, 8H, H^d), and 3.86 (s, 4H, H^g).

Synthesis of *fac*-[{(CO)$_3$Re(μ-dhaq)Re(CO)$_3$}$_2$(dppz)$_2$] (2a)

A mixture of $Re_2(CO)_{10}$ (200.0 mg, 0.3065 mmol), H_2-dhaq (74.0 mg, 0.3065 mmol), dppz (101.6 mg, 0.3065 mmol), and mesitylene (30 ml) was refluxed for 5 h and cooled to 30 °C. Compound **2a** was obtained as dark green powder. The product was filtered, washed with hexane and air-dried. Yield: 41 % (150 mg). AT-IR (cm^{-1}): 2008 (s) and 1886 (s) (C≡O). HRMS-ESI (*m/z*): $[M + H]^+$ calcd for $C_{82}H_{53}N_8O_{20}Re_4$, 2215.1583; found, 2215.1185. ^{1}H NMR (500 MHz, d_6-DMSO, δ): 8.36-8.43 (m, 8H, H^C), 7.94-7.92 (m, 8H, H^B), 7.76 (d, J = 1.5 Hz, 4H, H^c), 7.42 (d, J = 1.5 Hz, 4H, H^a), 7.29 (d, J = 4 Hz, H^A), 7.16 (d, J = 5 Hz, 8H, $H^{e/f}$), 7.11 (d, J = 5 Hz, 8H, $H^{e/f}$), 6.24 (t, J = 1 Hz, 4H, H^b), 5.25 (s, 8H, H^d), and 3.86 (s, 4H, H^g).

Synthesis of *fac*-[{(CO)$_3$Re(μ-dhnd)Re(CO)$_3$}$_2$(dppz)$_2$] (3a)

A mixture of $Re_2(CO)_{10}$ (100.1 mg, 0.1532 mmol), H_2-dhnd (45.2 mg, 0.153 mmol), dppz (50.4 mg, 0.153 mmol), and toluene (10 ml) was kept in an oven maintained at 160 °C for 48 h and cooled to 30 °C. Compound 3a was obtained as dark purple powder. The product was filtered, washed with hexane and air-dried. Yield: 27 % (48 mg). AT-IR (cm^{-1}): 2011 (s) and 1872 (s) (C≡O). HRMS-ESI (*m/z*): $[M + H]^+$ calcd for $C_{90}H_{57}N_8O_{20}Re_4$, 2315.1898; found, 2315.1704. ^{1}H NMR (500 MHz, DMSO–d_6, ppm): 8.42-8.39 (m, 8H, H^A), 7.94-7.92 (m, 8H, H^B), 7.76 (d, J = 1.5 Hz, 4H, H^c), 7.42 (d, J = 1.5 Hz, 4H, H^a), 7.16 (d, J = 5 Hz, 8H, $H^{e/f}$), 7.11 (d, J = 5 Hz, 8H, $H^{e/f}$), 6.24 (t, J = 1 Hz, 4H, H^b), 5.25 (s, 8H, H^d), and 3.86 (s, 4H, H^g).

Synthesis of *fac*-[{(CO)$_3$Re(μ-bbim)Re(CO)$_3$}$_2$(dppz)$_2$] (4a)

A mixture of $Re_2(CO)_{10}$ (100 mg, 0.153 mmol), H_2-bbim (36.0 mg, 0.156 mmol), dppz (50.5 mg, 0.157 mmol), and mesitylene:hexane (10:2 mL) in a Teflon flask was placed in a steel bomb. The bomb was kept in an oven maintained at 175 °C for 72 h and cooled to 30 °C. Compound **4a** was obtained as light yellow crystals. The product was filtered, washed with hexane and air-dried. Yield: 50% (84 mg crystals). ATR–IR (cm^{-1}): 2017 (s) and 1882 (s) (C≡O). HRMS–ESI (*m/z*): $[M + H]^+$ calcd for $C_{82}H_{57}N_{16}O_{12}Re_4$, 2203.2548; found, 2203.2252. ^{1}H NMR (500 MHz, DMSO–d_6, ppm): 7.76 (d, J = 1.5 Hz, 4H, H^c), 7.65-7.61 (m, 8H, H^A), 7.42 (d, J = 1.5 Hz, 4H, H^a), 7.39-7.37 (m, 8H, H^B), 7.16 (d, J = 5 Hz, 8H, $H^{e/f}$), 7.11 (d, J = 5 Hz, 8H, $H^{e/f}$), 6.24 (t, J = 1 Hz, 4H, H^b), 5.25 (s, 8H, H^d), and 3.86 (s, 4H, H^g).

3.3. Results and discussion

3.3.1. Synthesis and characterization of metallocycles 1a-4a

Compounds **1a**–**4a** were synthesized by treating $Re_2(CO)_{10}$, rigid bis-chelating ligand (H_2−dhnq for **1a**; H_2−dhaq for **2a**) and dppz in mesitylene using one-pot reflux approach. Compounds **3a**–**4a** were synthesized by treating $Re_2(CO)_{10}$, rigid bis-chelating ligand (H_2−dhnd for **3a**; H_2−bbim for **4a**) and dppz in toluene for **3a** and in mesitylene:hexane for **4a** under one-pot solvothermal approach (Scheme 3.1). The products are air and moisture stable. All the complexes displayed two strong C≡O stretching bands in the region of 2008–1886 cm^{-1}, (2010 and 1882 cm^{-1} for **1a**; 2008 and 1886 cm^{-1} for **2a**; 2011 and 1872 $cm^{-1}$for **3a**; 2017 and 1882 $cm^{-1}$for **4a**), characteristic of *fac*-[$Re(CO)_3$] motif in an asymmetric environment (Figure 3.1-3.4). The formation of tetranuclear structures in solution was further confirmed by ESI mass analysis which show molecular ion peaks (*m/z*: 2115.1687 for [**1a** + H]$^+$; 2215.1185 for [**2a** + H]$^+$; *m/z*: 2315.1704 for [**3a** + H]$^{+;}$ *m/z*: 2203.2252 for [**4a** + H]$^+$) that matches with the theoretical values (Figure 3.5-3.10).

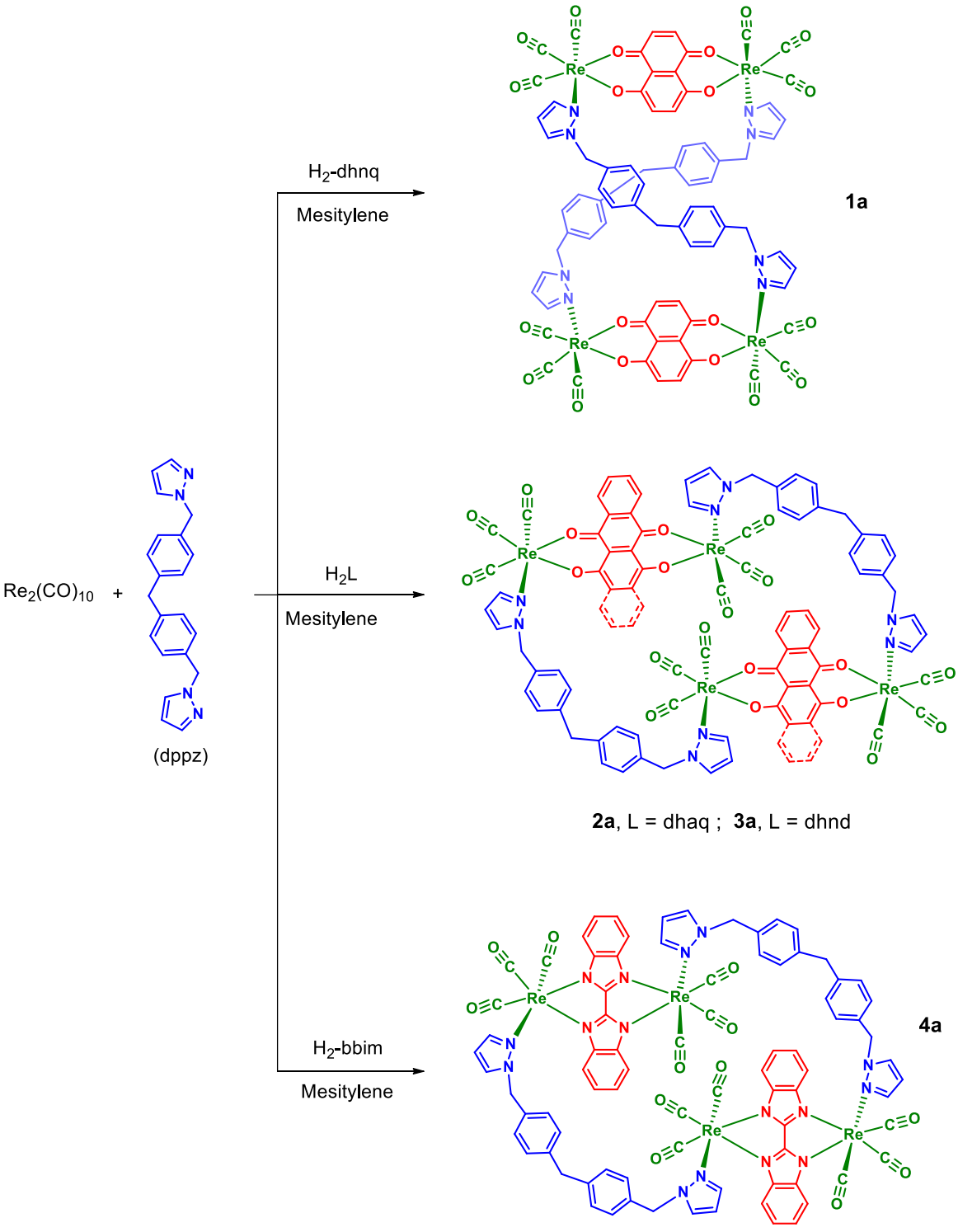

Scheme 3.1. Self-Assembly of Metallocycles **1a-4a**.

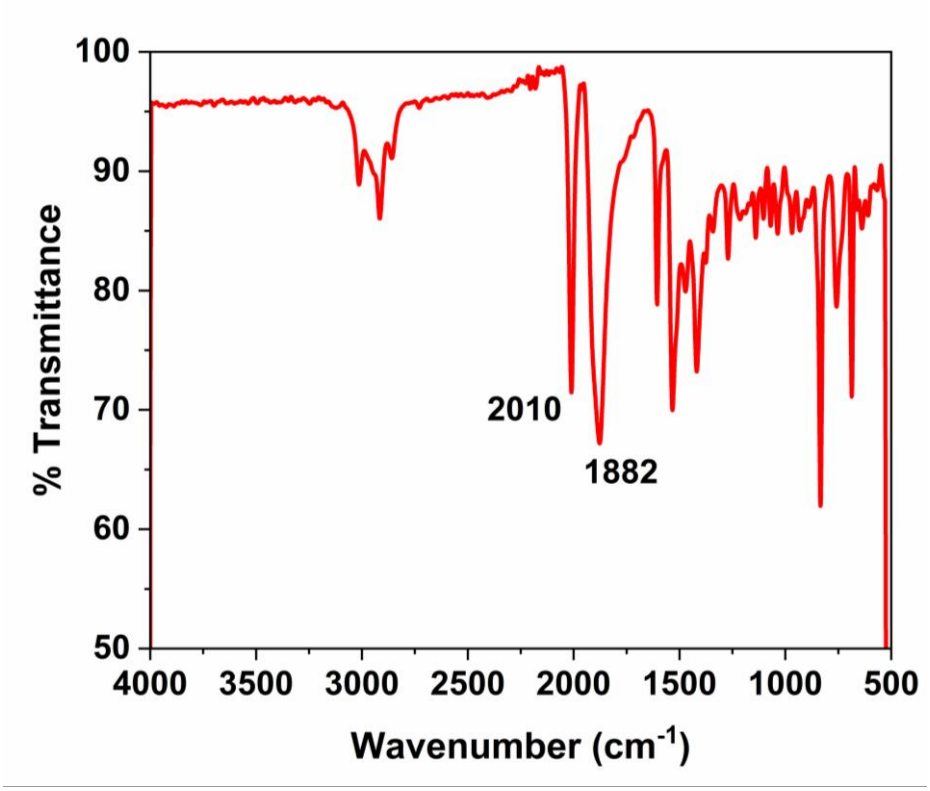

Figure 3.1. ATR-IR spectrum of **1a**.

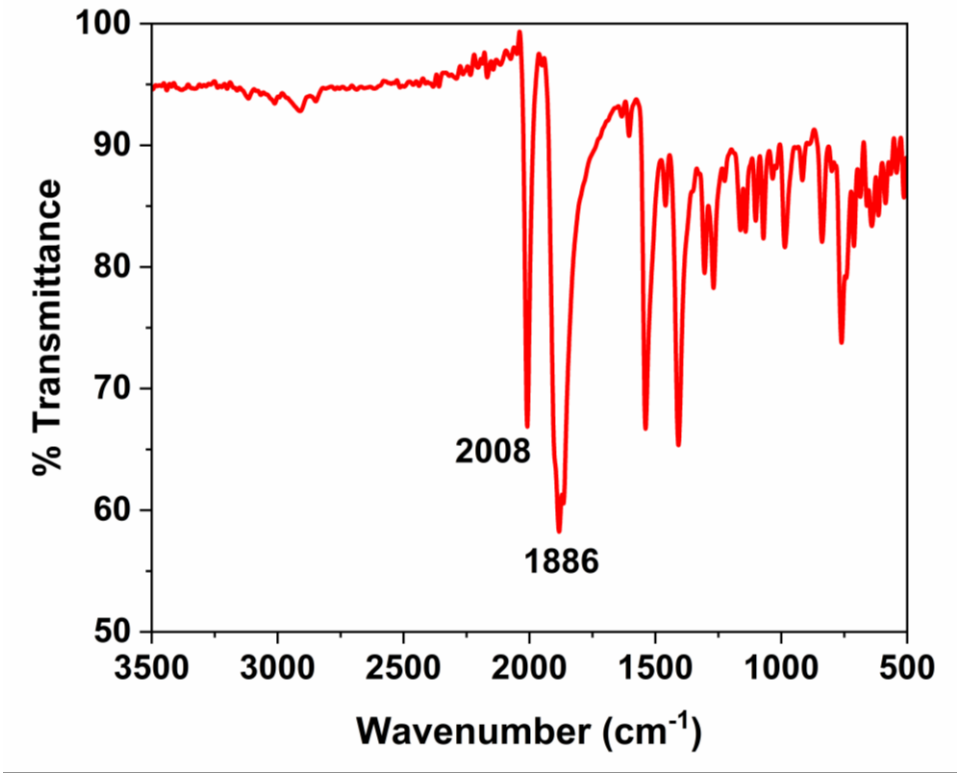

Figure 3.2. ATR-IR spectrum of **2a**.

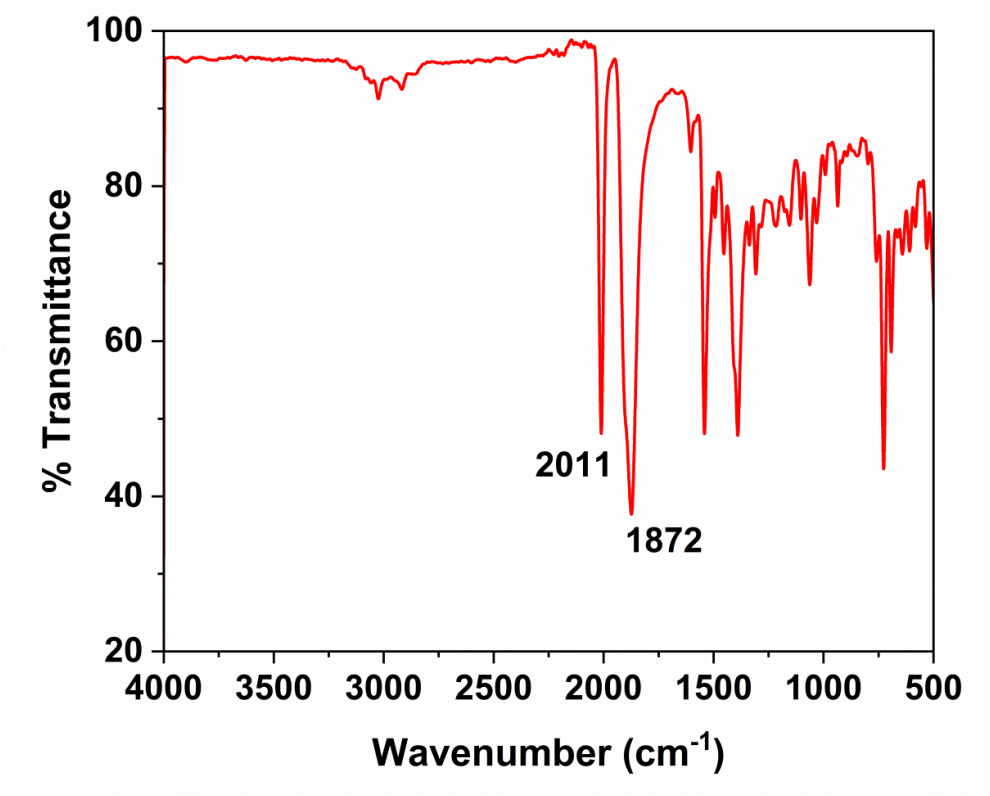

Figure 3.3. ATR-IR spectrum of **3a**

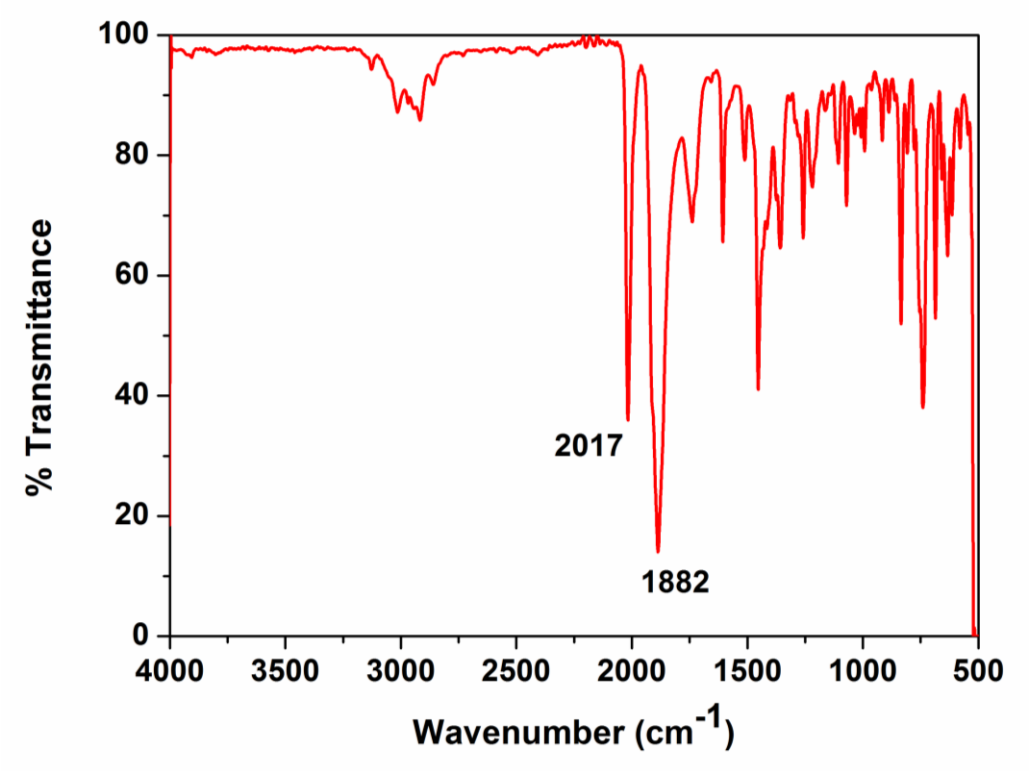

Figure 3.4. ATR-IR spectrum of **4a**.

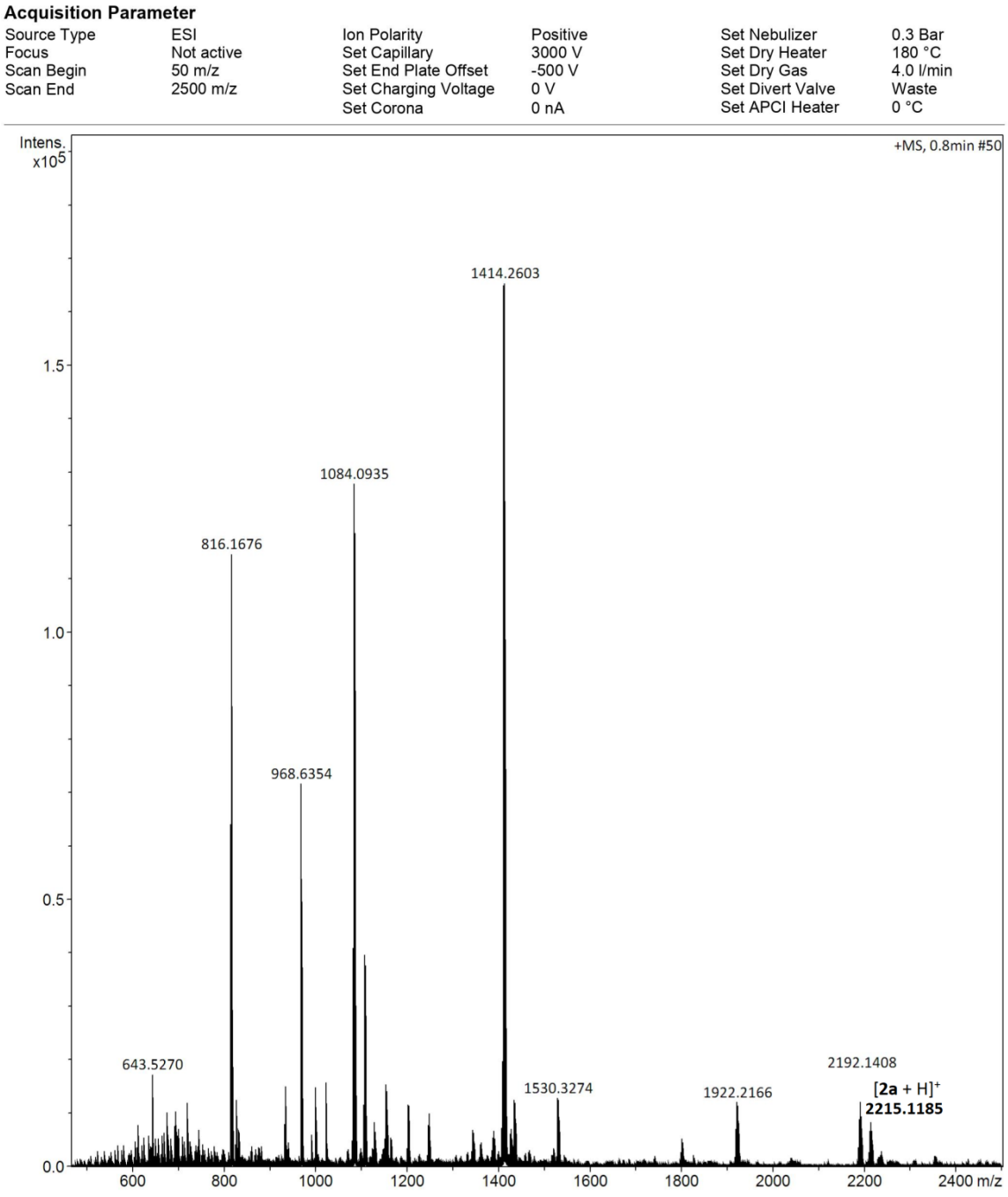

Figure 3.5. HR-MS spectrum of **2a** in positive ion mode.

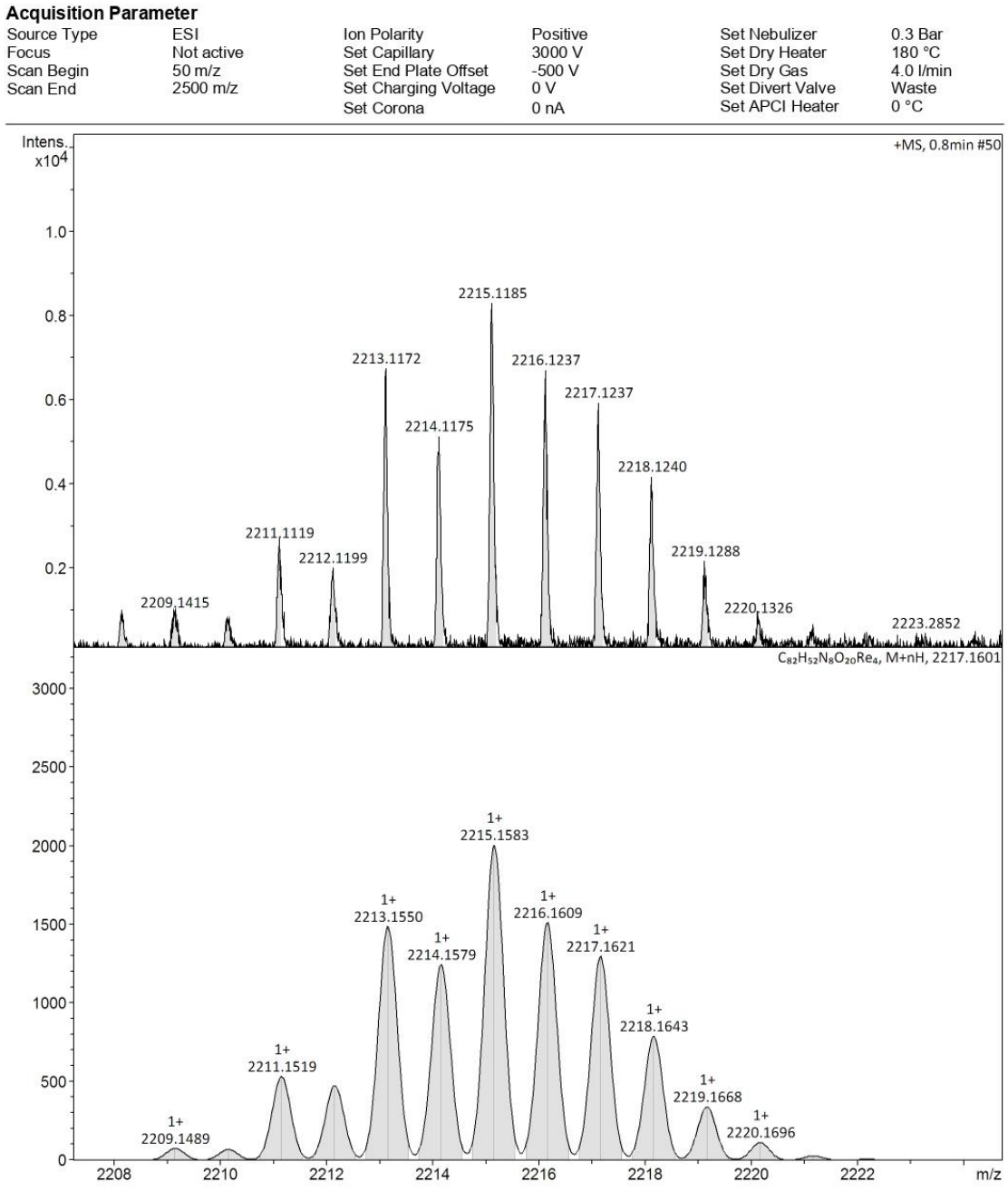

Figure 3.6. Experimental and calculated ESI mass spectra of **2a** in positive ion mode.

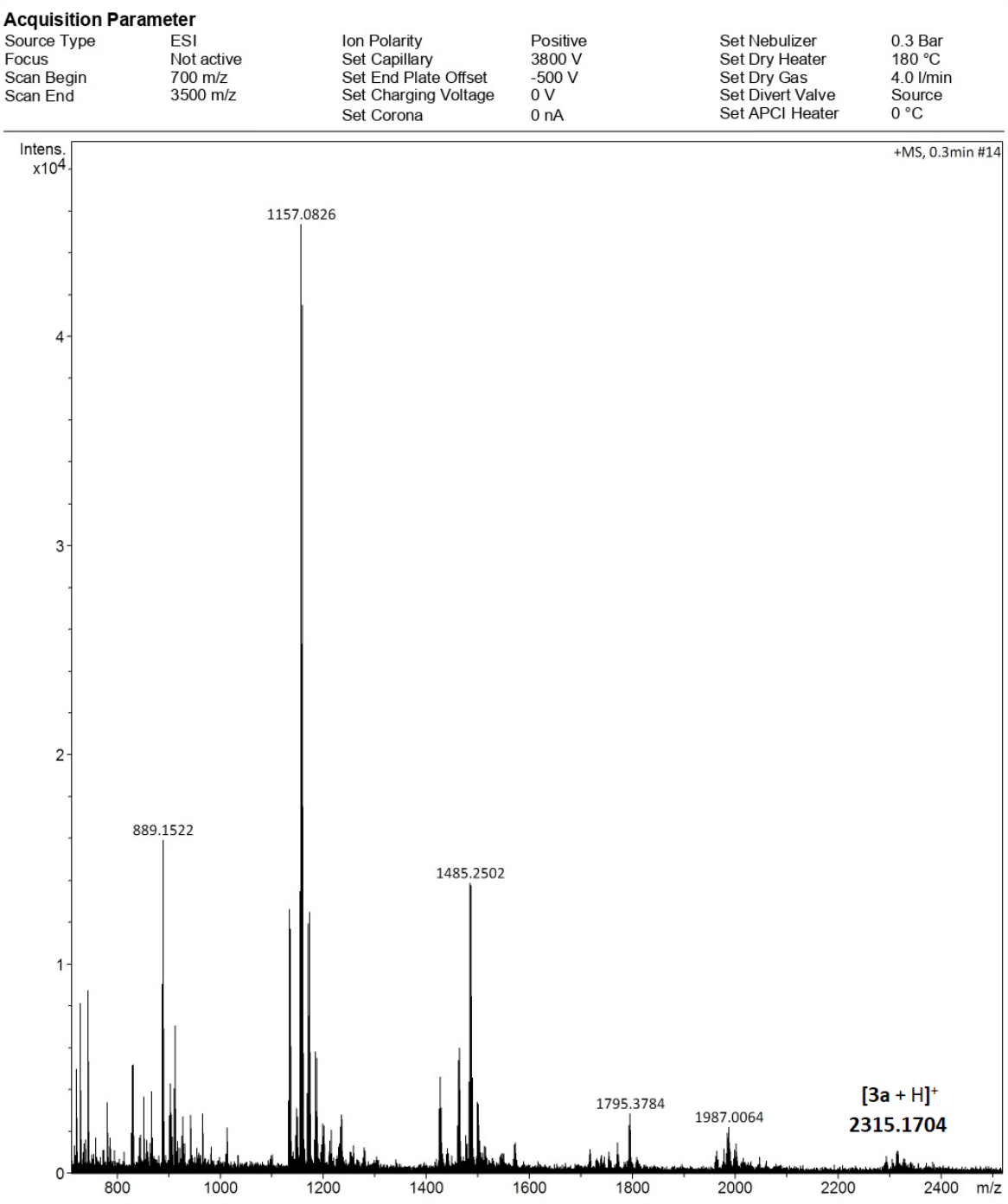

Figure 3.7. ESI mass spectrum of **3a** in positive ion mode.

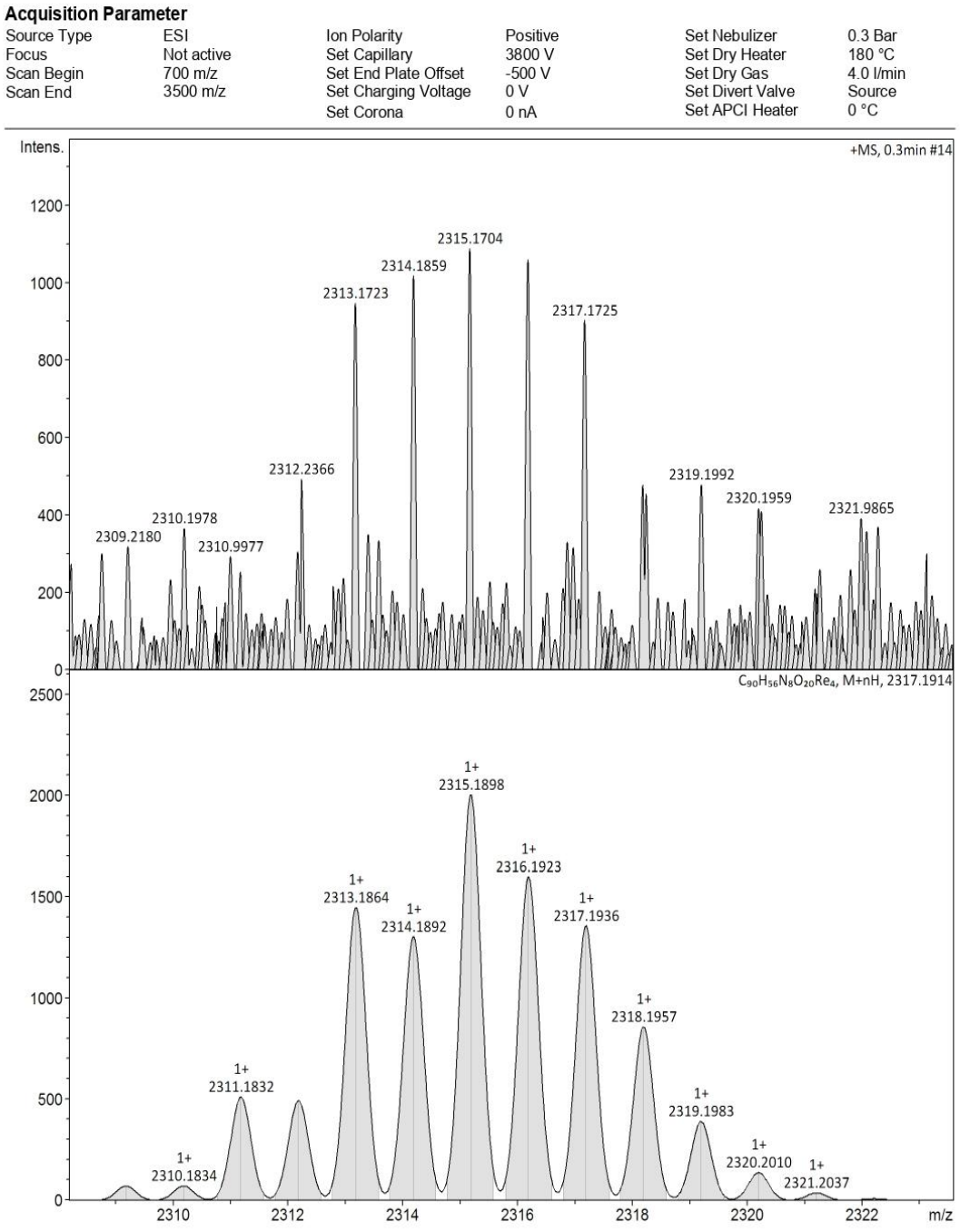

Figure 3.8. Experimental and calculated ESI mass spectra of **3a** in positive ion mode.

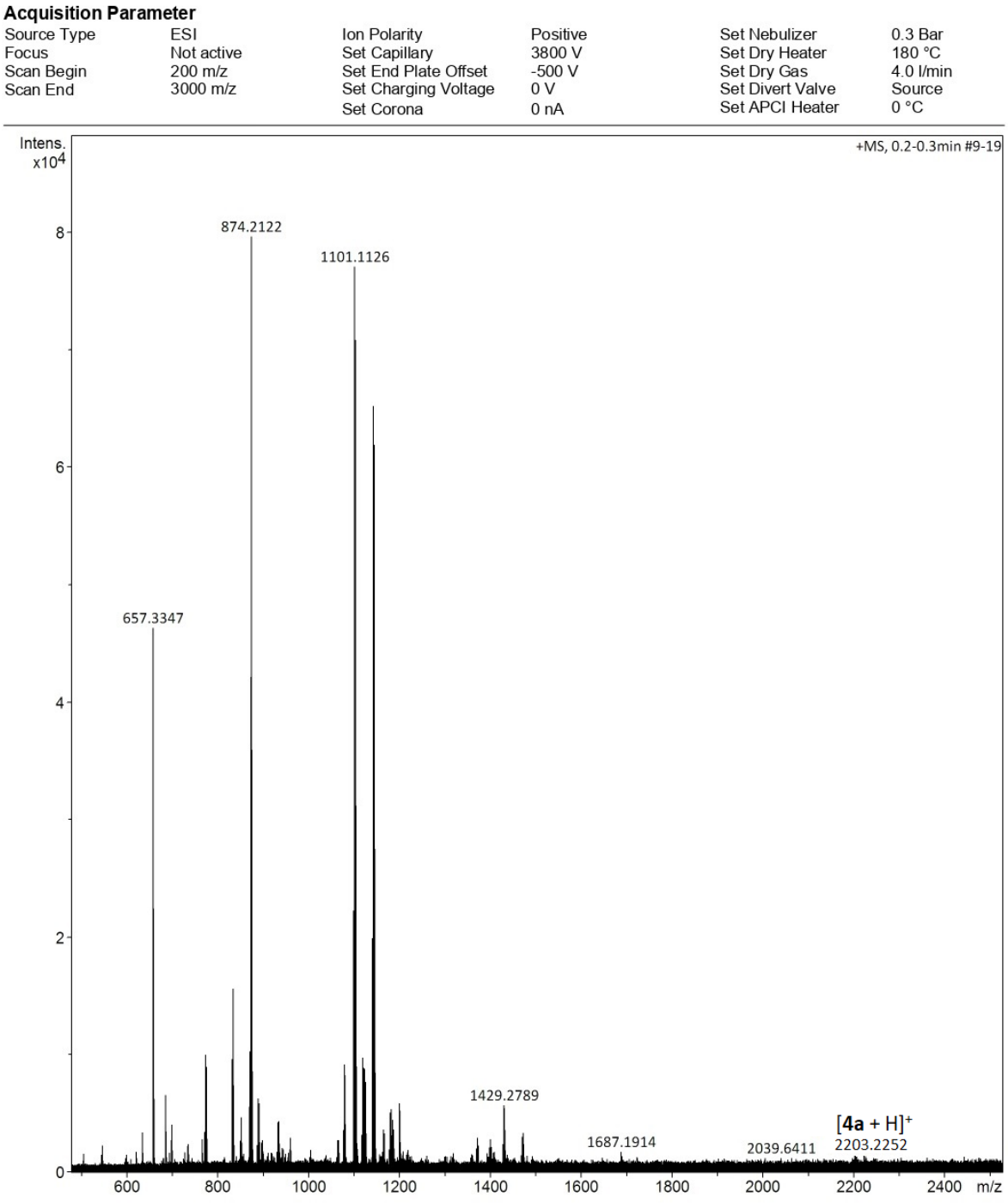

Figure 3.9. ESI mass spectrum of **4a** in positive ion mode.

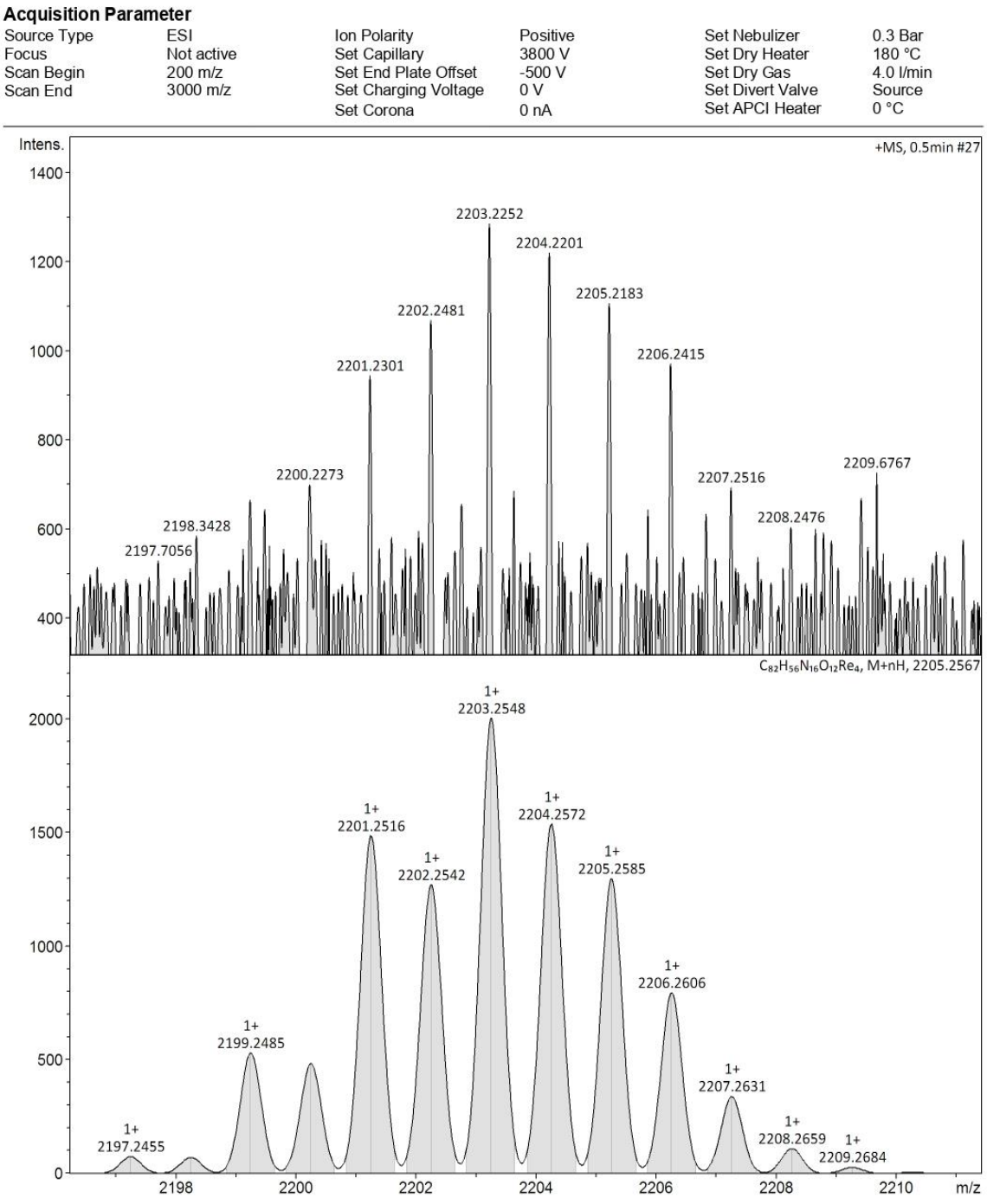

Figure 3.10.. Experimental and calculated ESI mass spectra of **4a** in positive ion mode.

3.3.2. Molecular Structures of Metallocycles 1a and 4a.

The molecular structures of **1a** and **4a** were confirmed by single crystal X-ray diffraction analysis. Both the complexes adopt M_4L_2L'-type supramolecular metallomacrocyclic structure and consist of four *fac*-[$Re(CO)_3$] cores, two dianionic bis-chelating dhnq/bbim motifs, and two dppz ligands (Figure 3.11). The asymmetric unit of complex **1a** consists of one metallocycle and five mesitylene solvent molecules. The overall shape of complex **1a** can be best described as "*figure-eight*" topology. This can be viewed as the dinuclear *fac*-[{$Re(CO)_3$}(dhnq){$Re(CO)_3$}] motif as one node and dppz motif as "*S*"-shaped helical framework unit. Two dppz motifs helically coordinated to two dinuclear nodes resulting in the figure-eight metallomacrocyclic architecture.

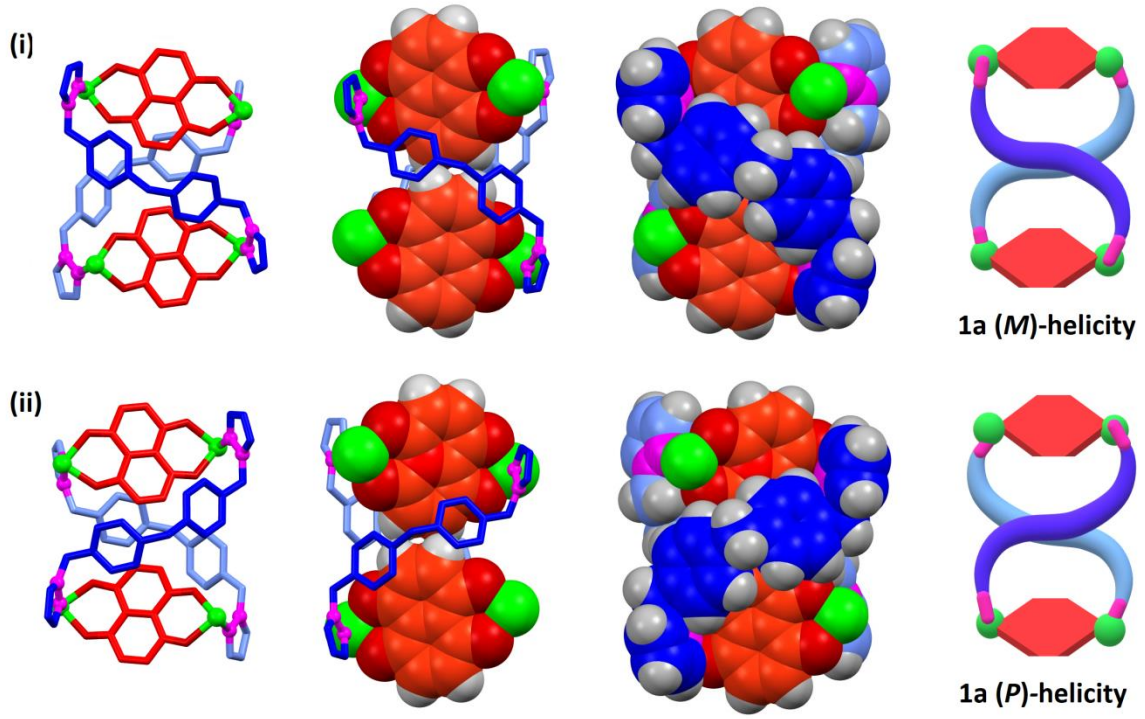

Figure 3.11. Various views of "*Figure-Eight*"-shaped metallocycle **1a** showing both (M)-helicity and (P)-helicity. Carbonyl groups are removed for clarity. Color code: Re = green, red = $dhnq^{2-}$, blue/pale blue with pink = dppz with N, and H = gray.

Unit cell of **1a** contains two metallomacrocycles and ten mesitylene solvent molecules. One metallomacrocycle adopts (M)-helicity (50%) whereas the other metallocycle adopts (P)-helicity (50%). The two dhnq units in **1a** are positioned one over the other where the edge of the one dhnq faces the edge of another dhnq (dihedral angle = ~31°) i.e., no face-to-face

stacking of the two dhnq units. The closest H•••H contacts between two dhnq units are 2.348 and 2.652 Å, indicating weak non-covalent dispersion contacts present between these units. The two dhnq units almost act as one central twisted rigid strand, restricting any direct intramolecular non-covalent contacts between the aromatic units of the two dppz motifs. However, intramolecular noncovalent contacts are present between dhnq motif and phenyl unit of dppz motif. The dppz ligand adopts a *syn-anti* cofacial arrangement i.e., two phenyl units are V-shaped and two pyrazolyl units are arranged *anti*-cofacially. The N···N distance of dppz in 1a is 12.16 Å/12.33 Å (N1···N5/N7···N3). The pyrazolyl unit is co-ordinated to rhenium core and is *trans* to carbonyl unit. The plane of the pyrazolyl ring is not overlying on the plane of the dhnq unit. The biphenyl spacer is arranged as V-shape with the dihedral angle of 117/111°. Among the biphenyl units, the one adjacent to coordinated pyrazolyl unit overlie the dhnq unit in a face tilted manner.

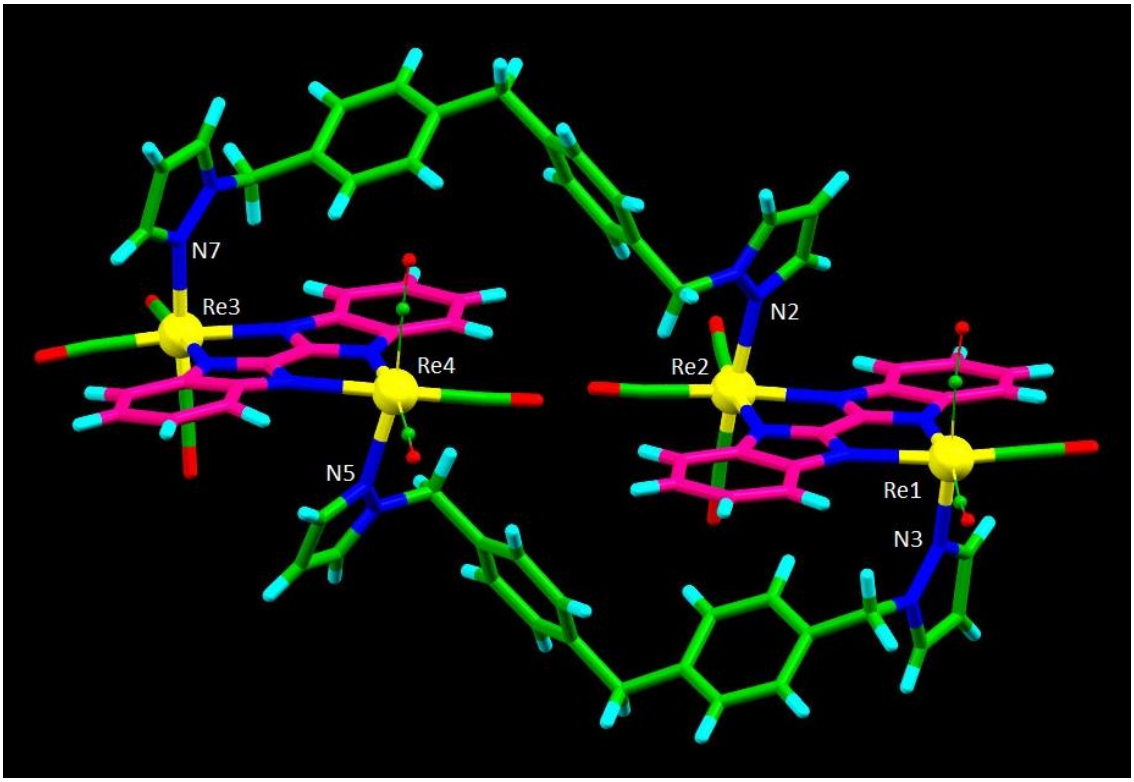

Figure 3.12. Molecular structure of metallocycle **4a**. Four carbonyl groups are shown as thin ball and stick model for clarity. Color code: C = Green/purple, N = Blue, O = Red, and H = Aqua.

The molecular structure of **4a** consists of four *fac*-[$Re(CO)_3$] cores, two bis-benzimidazolate motifs and two dppz motifs (Figure 3.12). The complex adopts "*Z*"-shaped tetranuclear

metallocyclic architecture. The overall sizes of metallocycle are 22.4 Å (length, terminal O···O along the Re···Re axis), 13.5 Å width and 11.2 Å (height, length of bbim). Rhenium core is surrounded by three carbonyl groups that are arranged in a facial manner, one chelating motif from bbim and one pyrazolyl motif. Rhenium(I) adopts an octahedral geometry. Among the four rhenium tricarbonyl groups, two are arranged by directing their carbonyl groups outward and another two *fac*-$Re(CO)_3$ are arranged at the center by directing two of their carbonyl inward. Dianionic bbim ligand bischelates two Re cores symmetrically with Re···Re distances of 5.71 (Re1···Re2) and 5.72 Å (Re3···Re4). The bond distances of two-chelating ring and C–C distance (which connects two bim unit) is 1.42(3) Å and 1.43(3) Å, revealing that the electronic delocalization of the π- system occurs in the bridging site, i.e imidazolate unit. The Re–N bond distances are 2.21 to 2.23 Å which are well within the expected range.[46,58,63] Two $bbim^{2-}$ units are arranged side by side i.e, almost in the same plane. The dppz ligand adopts a *syn-anti*-cofacial arrangement i.e., two phenyl units are V-shaped and two pyrazolyl units are arranged anti-cofacially. The N···N distances of dppz in **4a** are 12.550 Å, 12.665 Å and 12.616 Å, 12.479 Å (N3···N5/N7···N2). The pyrazolyl unit is co-ordinated to rhenium *trans* to carbonyl unit and is oriented along the Re-CO axis. The plane of the pyrazolyl ring is not overlying on the plane of the bbim unit. The biphenyl spacer is arranged as V-shape with the dihedral angle of 97/91°. Among the two phenyl units, one adjacent to coordinated pyrazolyl unit overlie the bbim unit in a face tilted manner. The two pyrazolyl units of the bidentate ligand is coordinated to two rhenium atoms, each coordinated to one bischelating motifs. This type of arrangement leads to metallocycle of longer length. The crystal structure of **4a** showed various types of intermolecular interactions including weak H-bonding interactions (H···O≡C–Re) that play a profound role in the supramolecular network structure.[62] Along the '*c*' axis, molecules pack in "abab" pattern, forming supramolecular helical superstructure via C–H···π (C20-H···C45 = 2.959 Å and 175°) and C–H···O≡C–Re (C21–H···O2 = 2.505 Å and 145°). Three adjacent molecules along the *c*-axis interact non-covalently resulting in one dimensional helical twist with distance of 59 Å. Along the *b*-axis, columnar pattern was found and intermolecular C–H···O≡C–Re (C59–H···O12 = 2.65 Å and 151°; C54–H···O5 = 2.658 Å and 148°), and Re–C≡O(5)···O(10)≡C–Re (2.916 Å and 109°/98°) contacts hold the two adjacent molecules.

3.3.3. Solution Dynamics and Structural Transformation.

It is well-known that metal-N(pyrazolate/pyrazolyl/pyrazole)-based complexes undergo various structural transformation in the solution due to the dynamic nature of the metal-pyrazolyl bond.[24,58-59,63-65] The solid-state structures of pyrazolyl-based complexes may differ in the solution state. Therefore, the stability of the metallocycles and the exact nature of the coordination motifs present in the solution state are worth studying due to the fact that the *fac*-[Re(CO)$_3$] core-based acyclic complexes and metallocycles have potential applications in the biomedical fields.[28-30] Metallocycles **1a**–**3a** are sparingly soluble in $CHCl_3$, acetone and DMSO at room temperature and completely soluble in hot DMSO whereas complex **4a** is soluble only in hot DMSO. All the complexes were dissolved in hot d_6–DMSO, allowed to cool down to room temperature and used for further studies. No precipitate was observed from the DMSO–d_6 solution of the metallocycles during the studies and even after a period of two-three days. The ^{1}H NMR spectra of **1a**–**4a** in d_6–DMSO displayed well-separated peaks for both the bis-chelating ligand and dppz motifs (Figure 3.13-3.16).

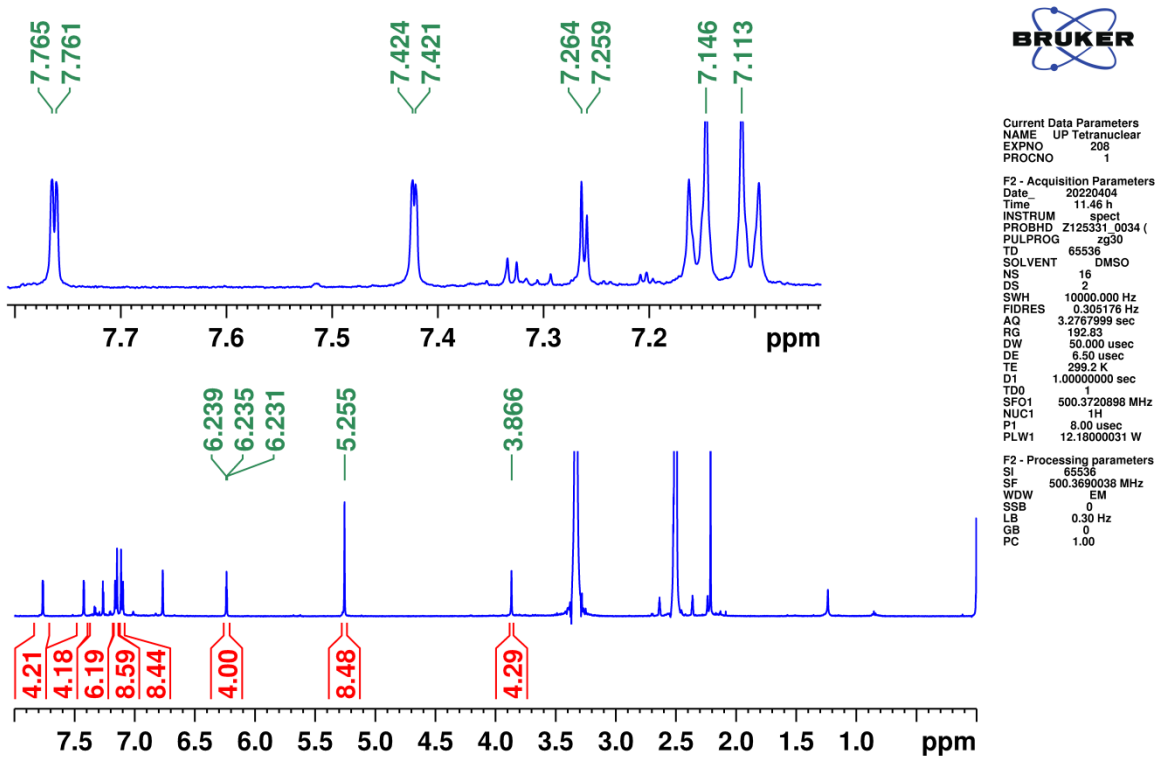

Figure 3.13. ^{1}H NMR spectrum of disassembly products of **1a** in DMSO–d_6.

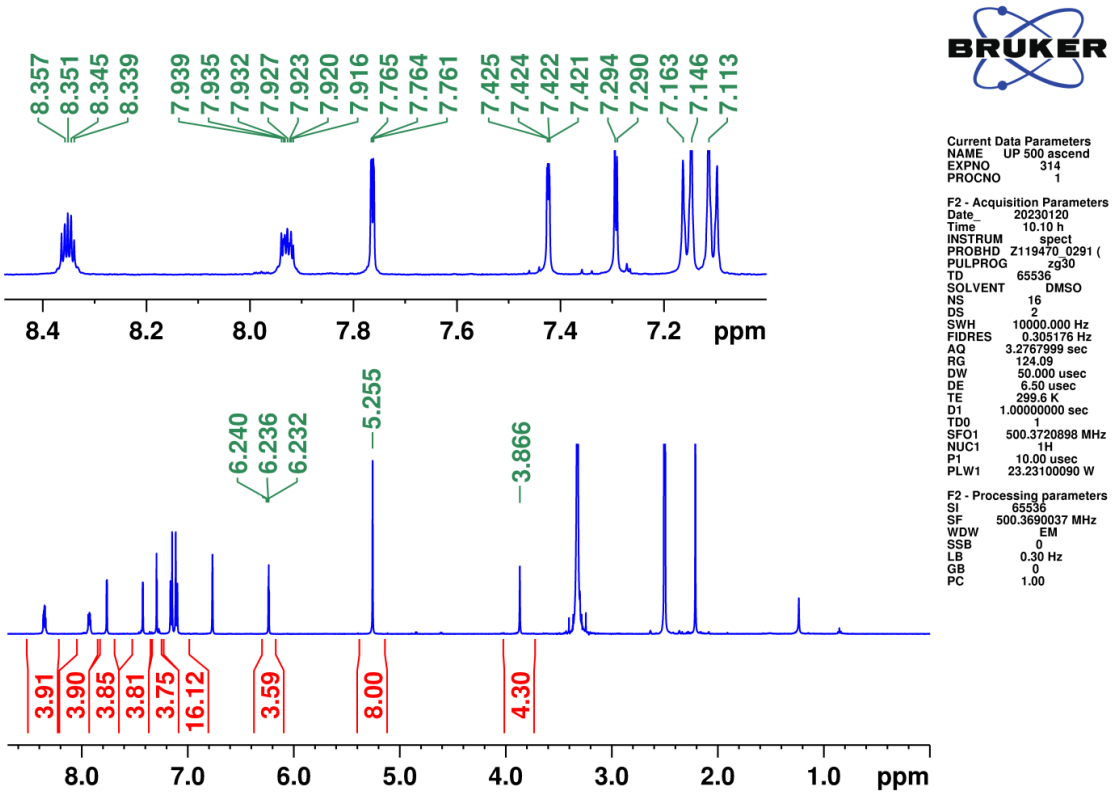

Figure 3.14. ^{1}H NMR spectrum of disassembly products of **2a** in DMSO–d_6 (powder **2a** was dissolved in DMSO–d_6).

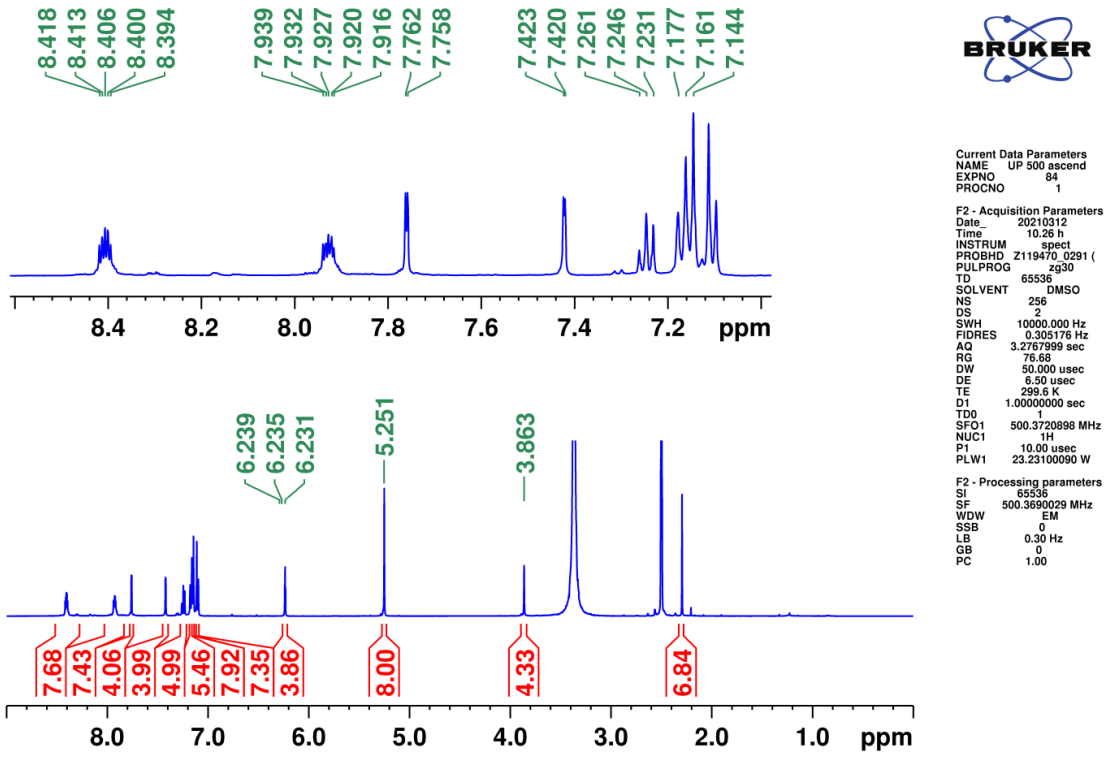

Figure 3.15. ^{1}H NMR spectrum of disassembly products of **3a** in DMSO–d_6 (powder **3a** was dissolved in DMSO–d_6).

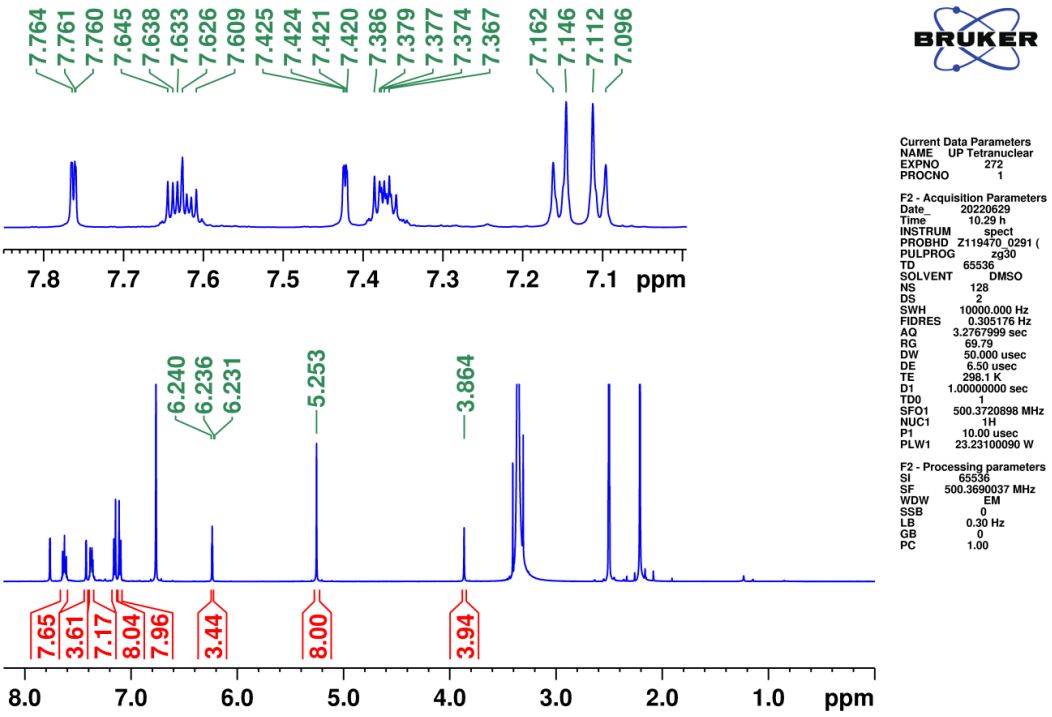

Figure 3.16. ^{1}H NMR spectrum of and disassembly products of **4a** in DMSO–d_6 (crystals **4a** were dissolved in DMSO–d_6).

In all the cases, the protons of the bis-chelating ligand were slightly/significantly downfield/upfield shifted relative to the free bis-chelating ligands, suggesting the coordination of the ligand to the metal cores (Figure 3.17, 3.18, 3.20, 3.22). A doublet peak corresponding to the H^A protons of the dhnq^{2-} motif (δ =7.26 ppm, J = 2.5 Hz) was observed in **1a** and was upfield shifted as compared to that of the proton of free dhnq. The protons of dhaq appeared as two multiplets (H^{B-C}) and one unsymmetrical doublet (H^A) with coupling constant of 2.0 Hz in **2a**. Among these peaks, H^B was shifted downfield, whereas H^C and H^A were shifted upfield relative to that of free H_2-dhaq, suggesting the coordination of dhaq^{2-} motif in **2a**. The protons (H^A and H^B) of dhnd in **3a** appeared as two well-separated multiplets with equal intensity. The H^A peak was shifted slightly downfield compared to that of the free H_2-dhnd. The protons (H^{A-B}) signals of bbim in **4a** appeared as two multiplets and were downfield shifted relative to that of free H_2-bbim. The data indicate that the bis-chelating ligand symmetrically coordinated to two rhenium cores.

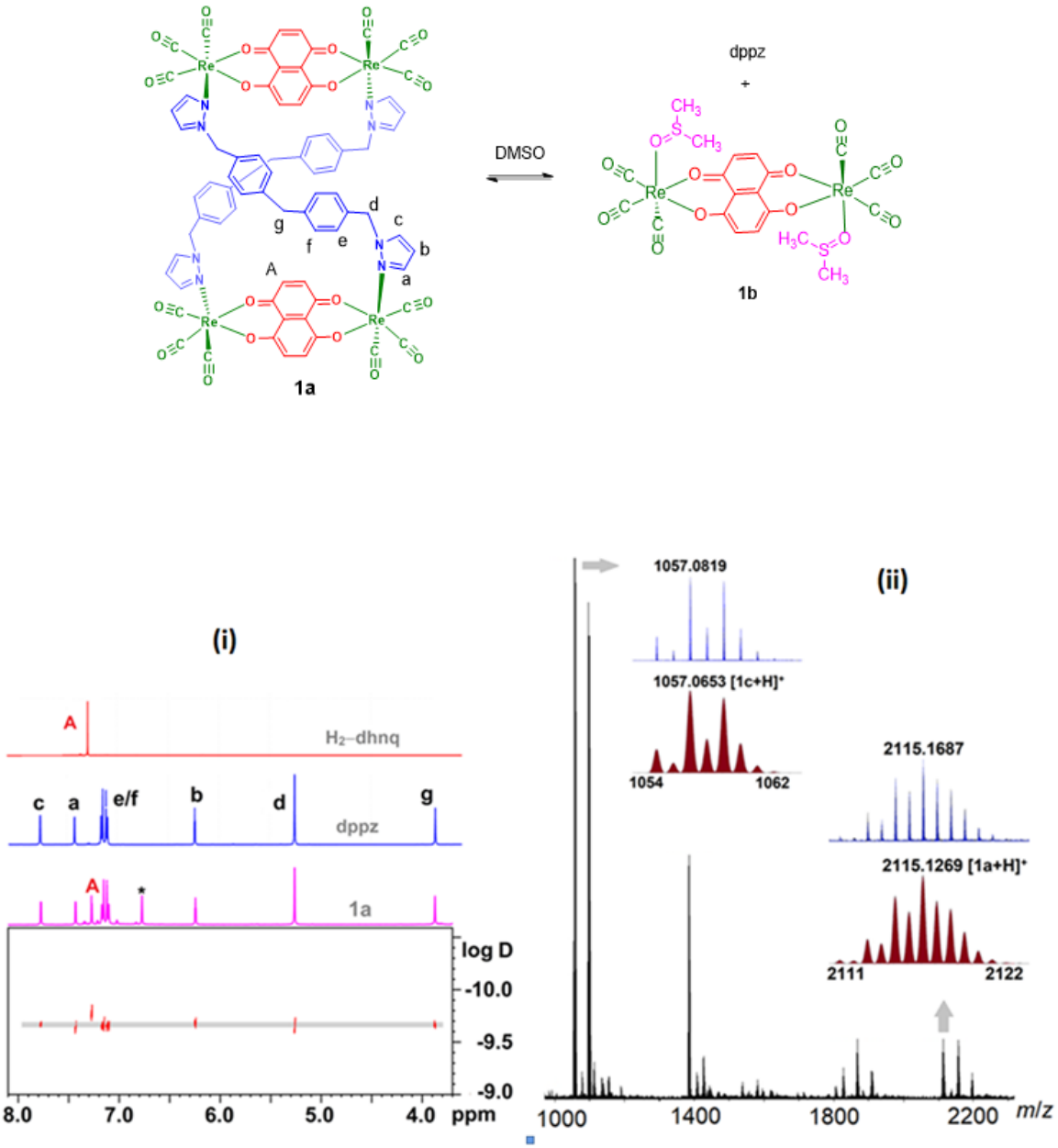

Figure 3.17. (i) NMR spectra of H_2-dhnq, dppz and ^{1}H DOSY spectrum of disassembly products of **1a** in d_6-DMSO. (ii) HR-ESI-MS spectrum of **1a** (inset shows experimental and calculated isotopic distribution for peaks corresponding to figure-eight tetranuclear [**1a** + H]$^+$ and dinuclear [**1c** + H]$^+$ in solvent.

On the other hand, the signals of the protons of the dppz in **1a**-**4a** remain similar to that of the free dppz. It is well-known that the proton adjacent to coordinated nitrogen atom generally shifts to downfield region due to the loss of electron density. Further, the C-H proton directing toward the π-electron cloud undergoes upfield shift due to the ring current effect. Based on the X-ray structures, the protons of the dppz motif are expected to appear in the downfield and upfield regions. However, the protons of the dppz did not show any shift in

comparison to the free dppz. Therefore, this can be explained if metallocycles **1a**-**4a** in d_6-DMSO after heating disassembled into acyclic dinuclear DMSO adduct of the general formula *fac*-[{$(CO)_3$Re(μ-L)Re$(CO)_3$}$(DMSO)_2$] (**1b**, L = dhnq; **2b**, L = dhaq; **3b**, L = dhnd; **4b**, L = bbim) and dppz which are in dynamic equilibrium (Schemes 2-3). The disassembled reaction process may go through via the dinuclear acyclic complexes *fac*-[{$(CO)_3$Re(μ-L)Re$(CO)_3$}(L)] (**1c**, L = dhnq; **2c**, L = dhaq; **3c**, L = dhnd; **4c**, L = bbim). This is probable because of the labile nature of metal-pyrazolyl bonds observed in many systems and non-labile nature of bis-chelating dinuclear complex.[24,31] Further to attain stable electronic configuration around rhenium metal center, each metal can receive one DMSO molecule. To understand further about the species present in the solution, 2D diffusion-ordered ^{1}H DOSY NMR spectroscopy was carried out (Figure 3.17, 3.19, 3.21, 3.23). Metallomacrocycle **1a** displays two sets of peaks which are very close to each other, indicating the presence of two units possibly **1c** and dppz. The ^{1}H DOSY spectra of other metallomacrocycles **2a**-**4a** showed two types of peaks which are well-separated, suggesting the presence of two motifs in the solution. The value of one-set of the peaks corresponding to the protons of the dppz in all the complexes is similar to that of the value found for the free dppz.

The above result suggested that one of the disassembly products is free dppz and the other should be the dinuclear DMSO adduct complexes **1c**-**4c**. To gain insight about the structure of the molecular species, the solutions were analyzed by ESI mass spectrometry. All the metallomacrocycles displayed relatively less intense peaks corresponding to tetranuclear motifs and strong peaks corresponding to the dinuclear complexes (**1c**-**4c**) (*m/z*: 1057.0819 for [**1c**+ H]$^+$; *m/z*: 1107.0808 for [**2c**+ H]$^+$; *m/z*: 1157.0852 for [**3c**+ H]$^+$; *m/z*: 1101.1126 for [**4c**+ H]$^+$). The experimental isotopic distribution peaks for both the tetranuclear metallocycles and dinuclear complexes match with the theoretical values. No peaks corresponding to the DMSO adduct of dinuclear complexes **1b**-**4b** were found in the ESI-MS spectra. The ^{1}H-NMR and ESI-MS analysis of **1a**-**4a** in DMSO solution indicates the dynamic nature of the metallocycles.

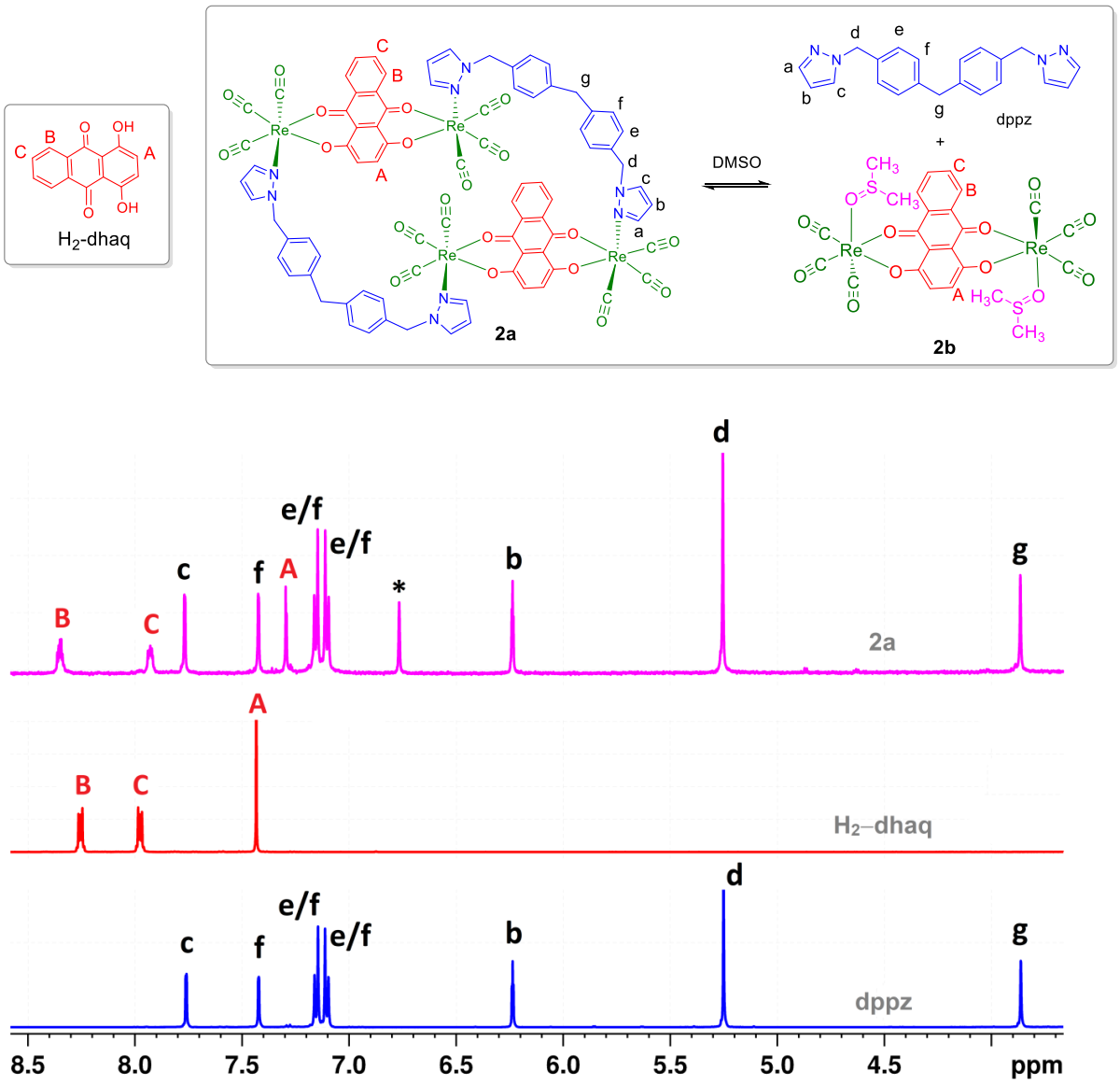

Figure 3.18. Partial ^{1}H NMR spectra of dppz, H_2-dhaq and disassembly products of **2a** in DMSO–d_6 (powder **2a** was dissolved in DMSO–d_6) (* = mesitylene).

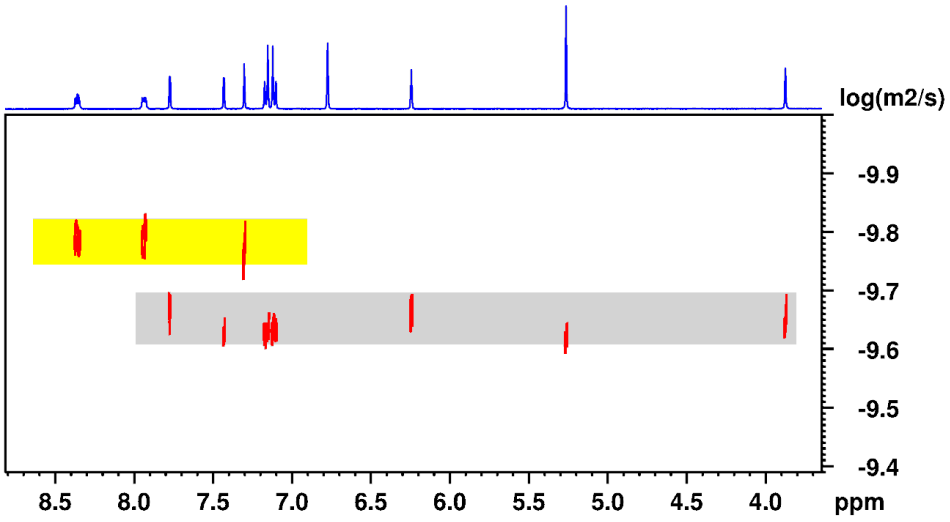

Figure 3.19. DOSY spectrum of disassembly products of **2a** in DMSO–d_6 (powder **2a** was dissolved in DMSO–d_6).

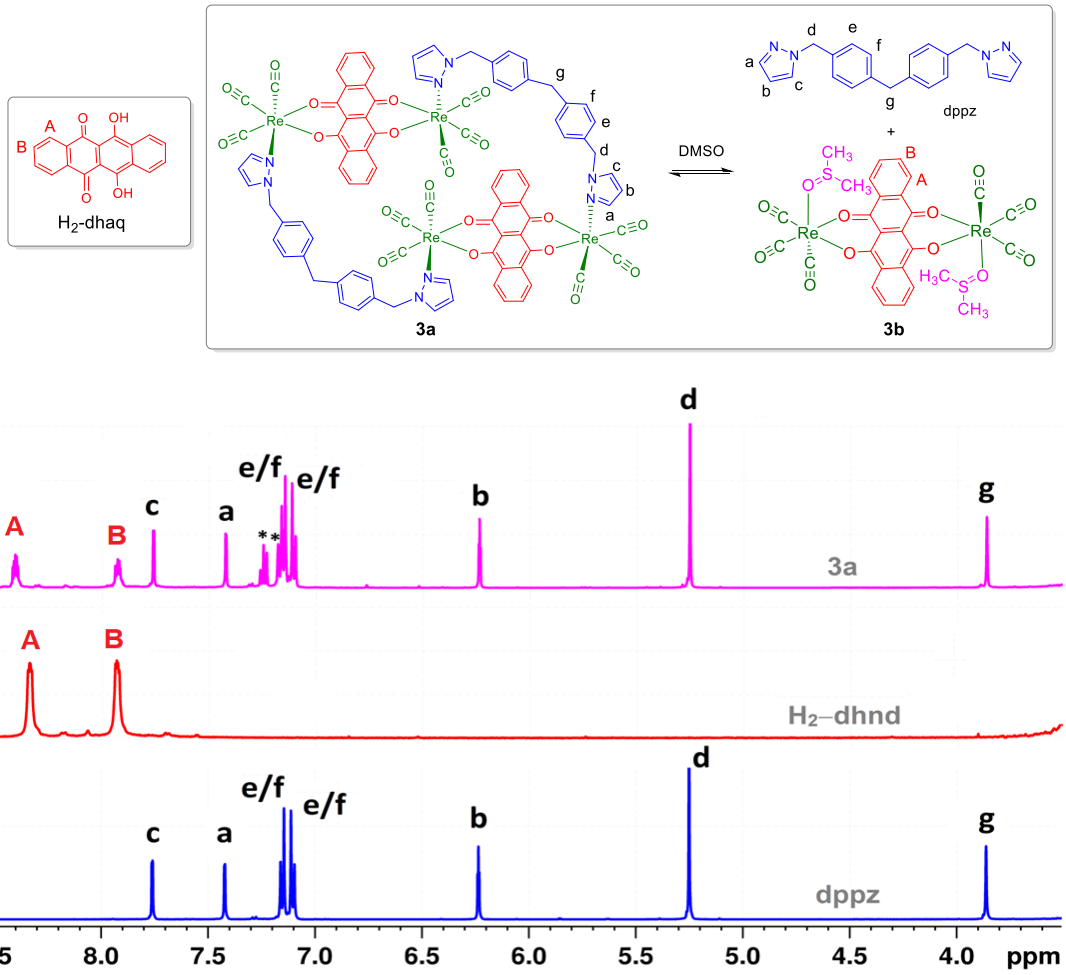

Figure 3.20. Partial ^{1}H NMR spectra of dppz, H_2-dhnd and disassembly products of **3a** in DMSO–d_6 (powder **3a** was dissolved in DMSO–d_6) (* = toluene).

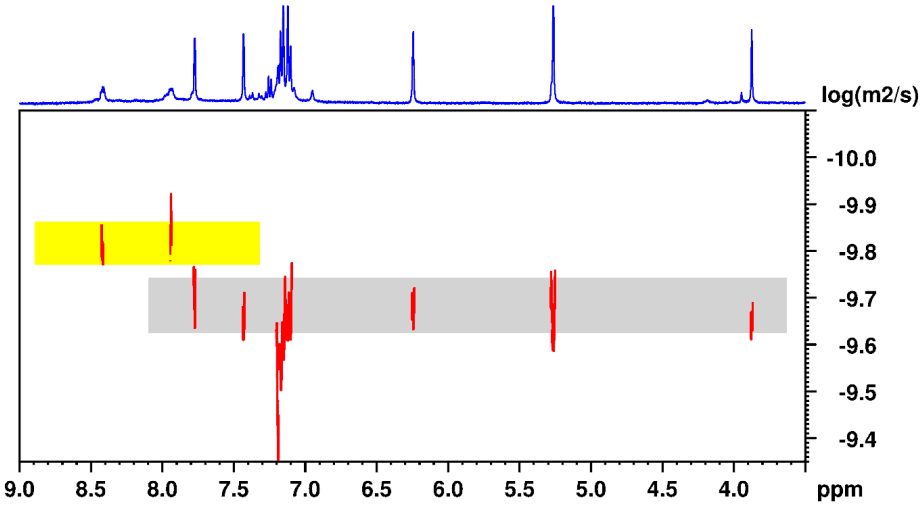

Figure 3.21. DOSY spectrum of disassembly products of **3a** in DMSO–d_6 (powder **3a** was dissolved in DMSO–d_6).

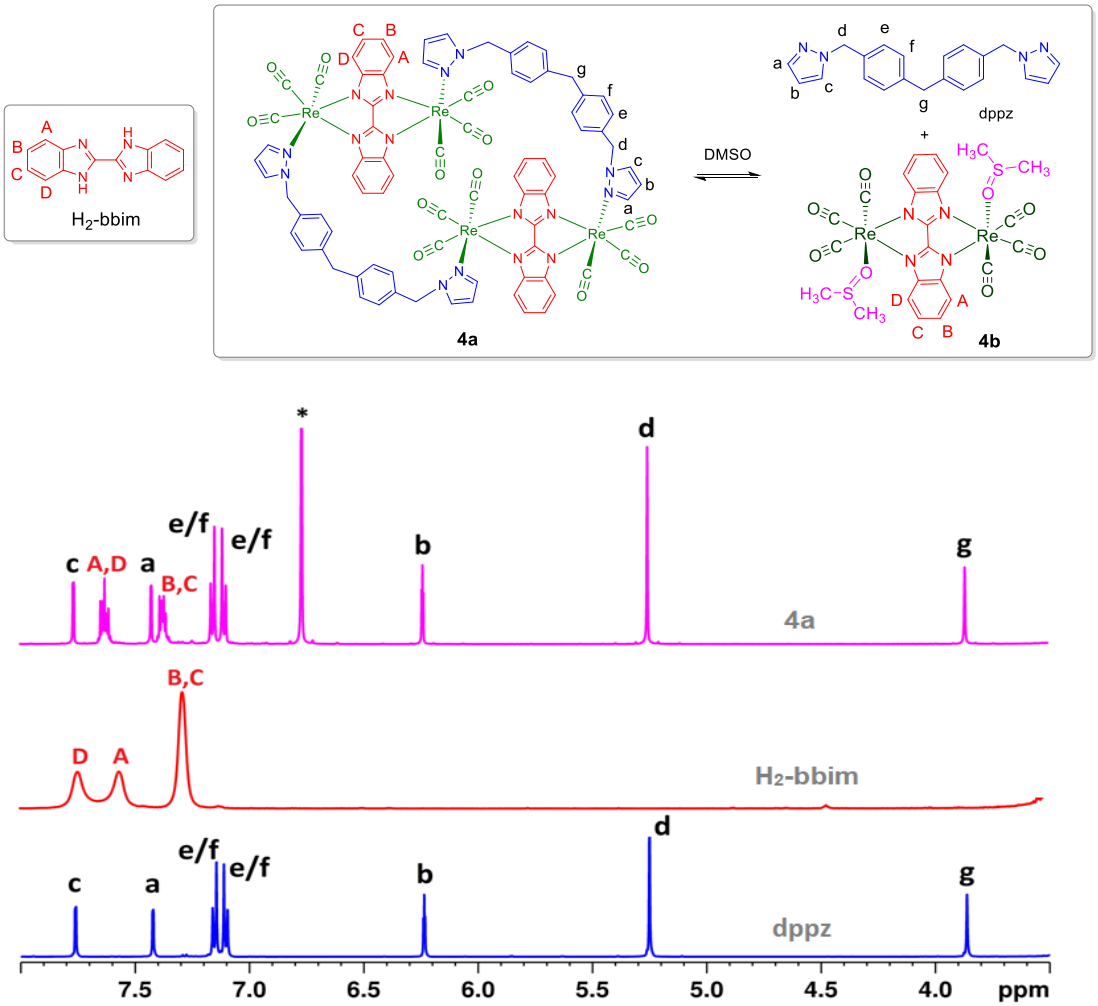

Figure 3.22. Partial ^{1}H NMR spectra of dppz, H_2-bbim and disassembly products of **4a** in DMSO–d_6 (crystals **4a** were dissolved in DMSO–d_6) (* = mesitylene).

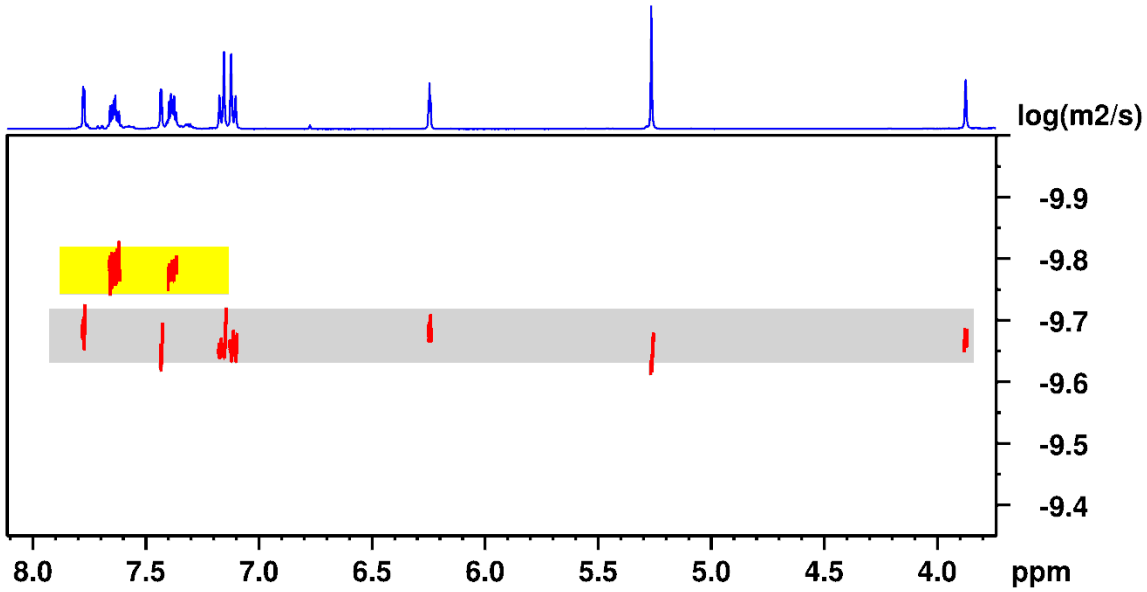

Figure 3.23. DOSY spectrum of and disassembly products of **4a** in DMSO–d_6 (crystals **4a** were dissolved in DMSO–d_6).

Component induced supramolecular transformations in metallocycles occur because of rearrangement or partial or complete disassembly of the structural framework units on addition of another competitive building block, which leading to the formation of more stable- or new discrete supramolecular structures.[66-70] To utilize the dynamic nature of M–N (rhenium-pyrazolyl) bond and the dynamic nature of metallocycles **1a**-**4a** in DMSO solution (Schemes 2-3), competitive selectivity studies were carried out using different donor ligands such as 4,4′-bipyridine (4,4′-bpy), 4,7-phenanthroline (4,7-Phen), bis(4-((1H-benzoimidazole-1-yl)methyl)phenyl)methane (dpbim) (dpbim) and 1,3,5-triaza-7-phosphaadamantane (PTA). The supramolecular reactions of the metallocycles with the chosen ligands were carried out by adding equivalent or excess amount of the donor to DMSO-d_6 solution of the metallocycles, heated and are analyzed using ^{1}H NMR and ESI-Mass analysis (Scheme 3.2, 3.3, Figure 3.24).

When 4,4′-bpy was subjected to a DMSO-d_6 solution of **1a**-**4a**, changes were observed in the ^{1}H NMR spectra for complexes **2a** and **4a**, in particular appearance of new proton peaks that correspond to coordination of 4,4′-bpy to the rhenium core as found in **4** and **11** (Figures 3.24-3.27).[56-57] This indicates that structural transformation takes place by ligand exchange process. Supramolecular structural transformation occurring in the present case was further confirmed by X-ray analysis of single crystals formed in the NMR tube containing **4a** and

4,4′-bpy in DMSO-d_6. The solid state structure unambiguously confirmed the formation of the molecular rectangle *fac*-[({Re(CO)$_3$}$_4$(bbim)$_2$(4,4′-bpy)$_2$] (**11**).

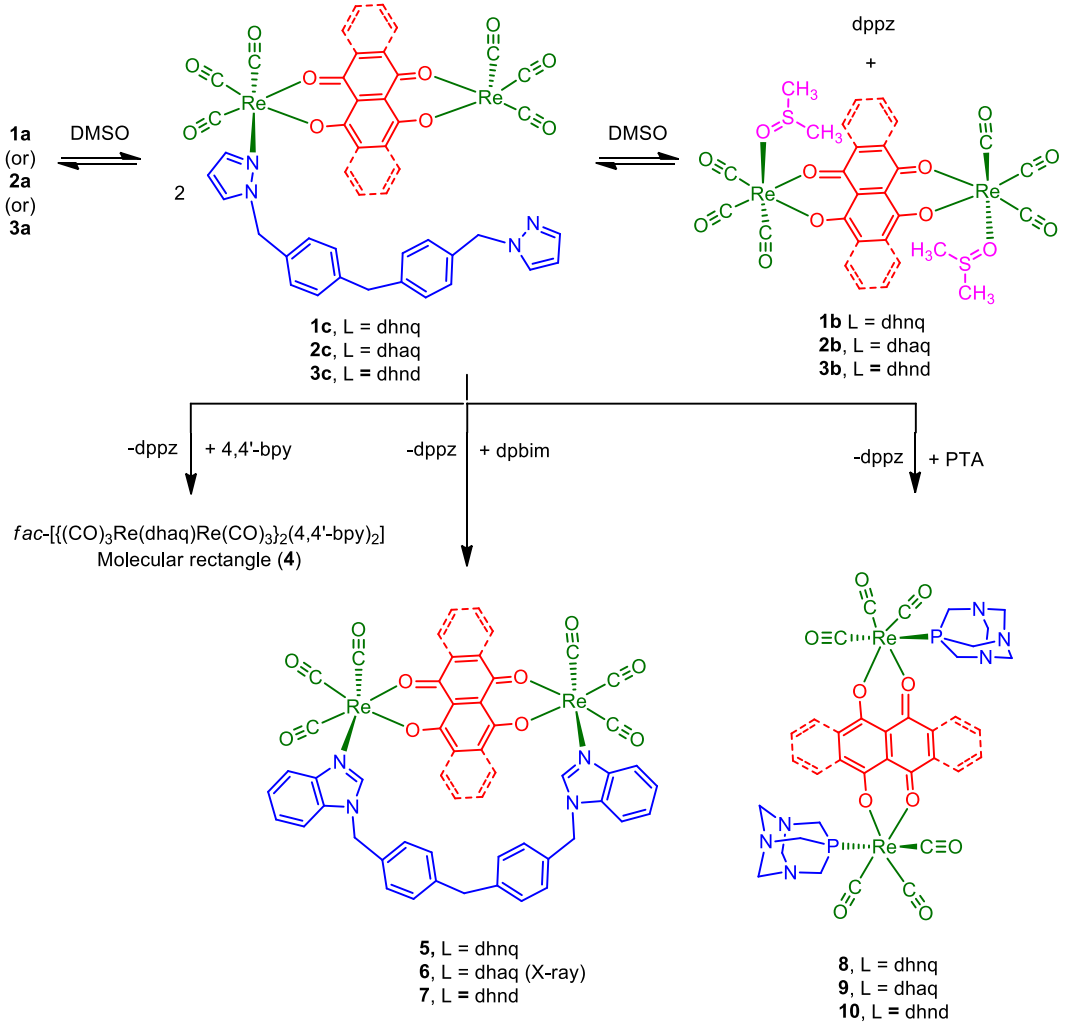

Scheme 3.2. Proposed dynamic nature of **1a** (or) **2a** (or) **3a** and component-induced supramolecular transformations into tetranuclear rectangle (**4**), dinuclear metallocycles (**5- 7**) and dinuclear acyclic complexes (**8-10**) in DMSO.

However, tetranuclear heteroleptic molecular rectangles consisting of *fac*-[Re(CO)$_3$] cores, two bbim^{2-} and two 4,4′-bpy units are known.[56] Hence, no detailed discussion of molecular structure of molecular rectangle **11** is included. Surprisingly, no proton peak shifts of 4,4′-bpy were observed in the ^{1}H NMR spectrum of **1a** + 4,4′-bpy and **3a** + 4,4′-bpy in DMSO-d_6 indicating that ligand exchange did not occur in these cases.

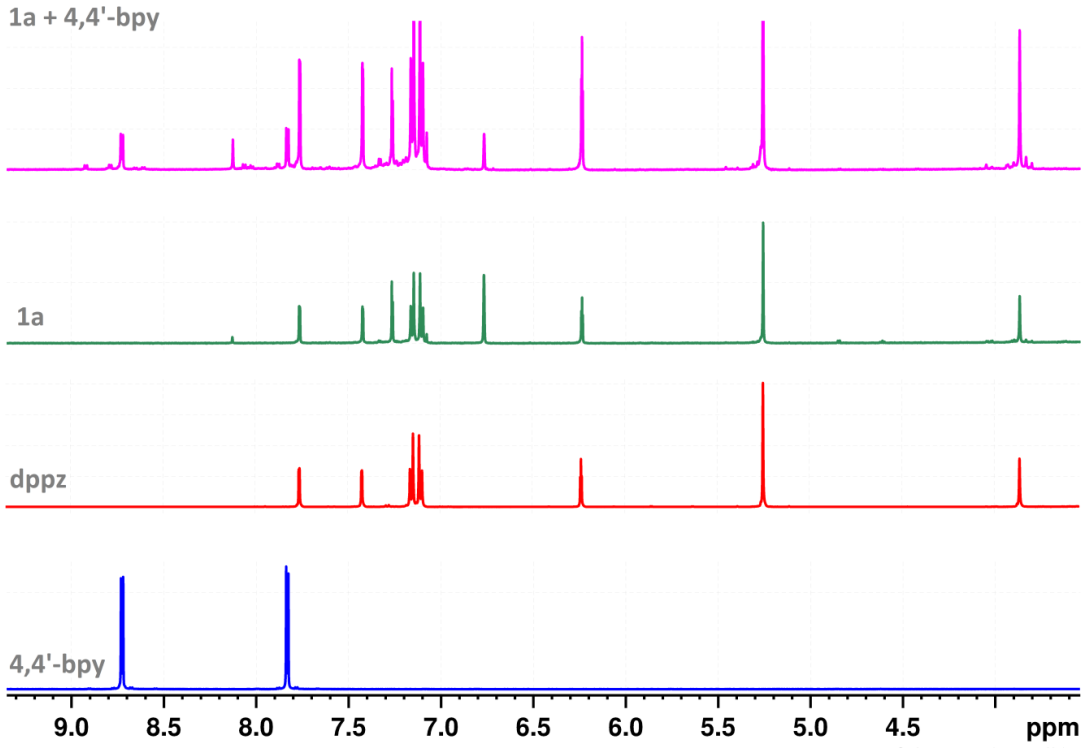

Figure 3.24. Partial ^{1}H NMR spectra of 4,4′-bpy, dppz, **1a** and **1a** + 4,4′-bpy in DMSO–d_6 (where **1a** = crystals **1a** were dissolved in DMSO–d_6).

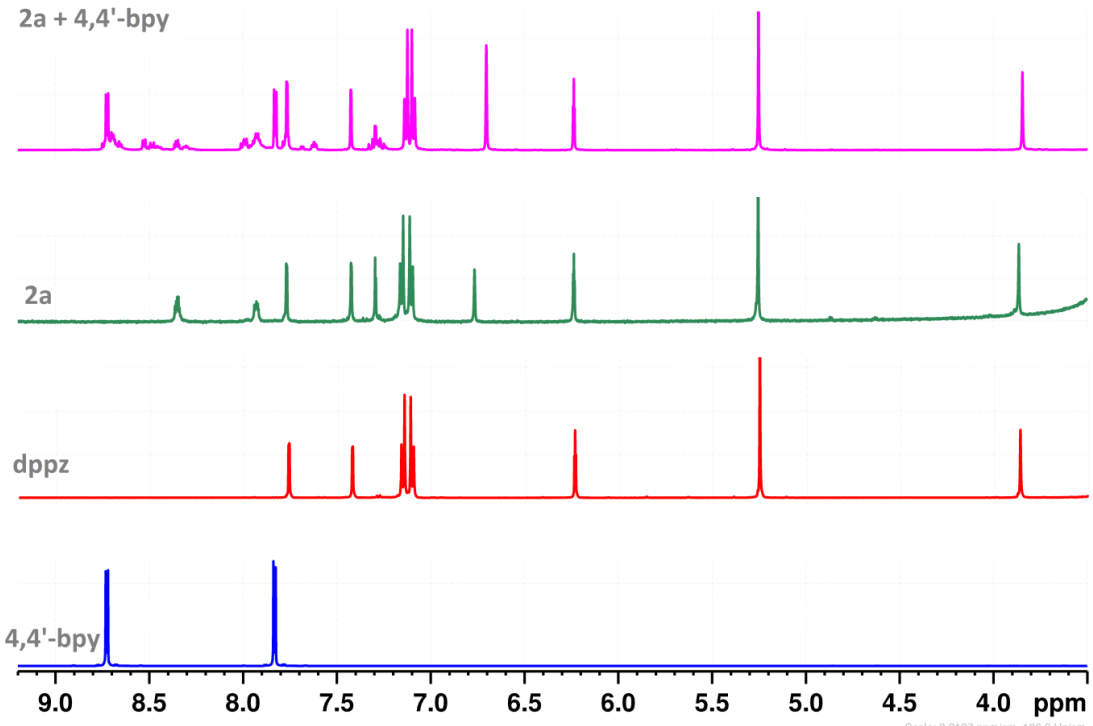

Figure 3.25. Partial ^{1}H NMR spectra of 4,4′-bpy, dppz, **2a** and **2a** + 4,4′-bpy in DMSO–d_6 (where **2a** = powder **2a** was dissolved in DMSO–d_6).

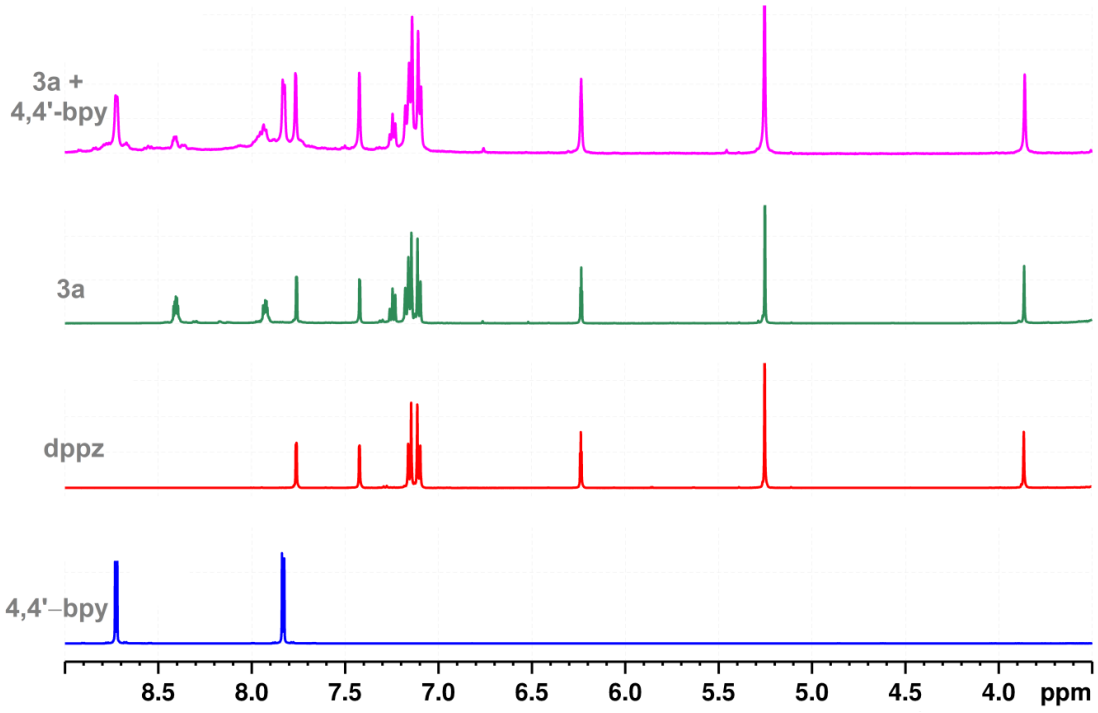

Figure 3.26. Partial ^{1}H NMR spectra of 4,4′-bpy, dppz, **3a** and **3a** + 4,4′-bpy in DMSO–d_6 (where **3a** = powder **3a** was dissolved in DMSO–d_6).

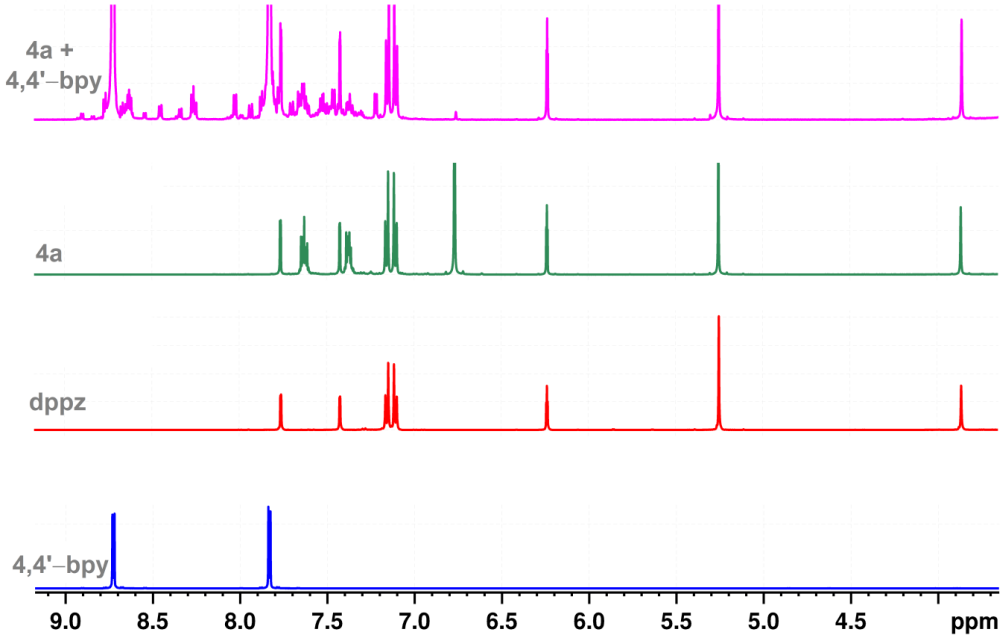

Figure 3.27. Partial ^{1}H NMR spectra of 4,4′-bpy, dppz, **4a** and **4a** + 4,4′-bpy in DMSO–d_6 (where **4a** = crystals **4a** were dissolved in DMSO–d_6).

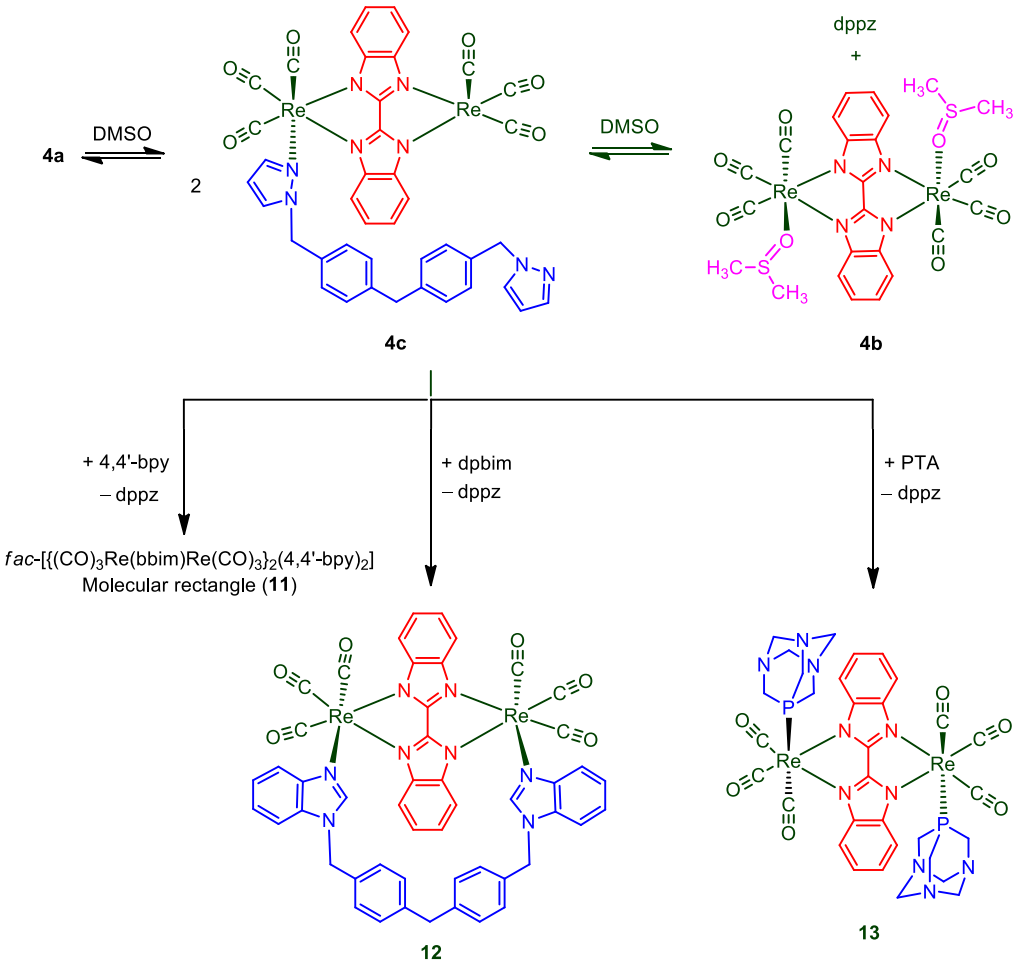

Scheme 3.3. Proposed dynamic nature of 4a in the solution and component-induced supramolecular transformations into tetranuclear rectangle (**11**), dinuclear metallocycle (**12**) and dinuclear acyclic complex (**13**) in DMSO.

The ligand 4,7-Phen is rarely used in the construction of *fac*-[$Re(CO)_3$] core-based metallocycles. The known four 4,7-Phen-based rhenium metallocycles contain either dhnq or dhaq motif.[35] Therefore, supramolecular transformation reactions of metallocycles **1a**-**4a** with 4,7-Phen were attempted. Upon addition of 4,7-Phen to DMSO-d_6 solution of **1a**-**4a**, no changes were observed in the ^{1}H NMR spectra of the complexes (Figure 3.28-3.31). The ESI-Mass spectra of the above mixture did not show any peaks corresponding to the expected new/known tetranuclear metallocycles. The data indicates that dppz is the preferred ligand over 4,7-Phen in the current self-assembly combinations.

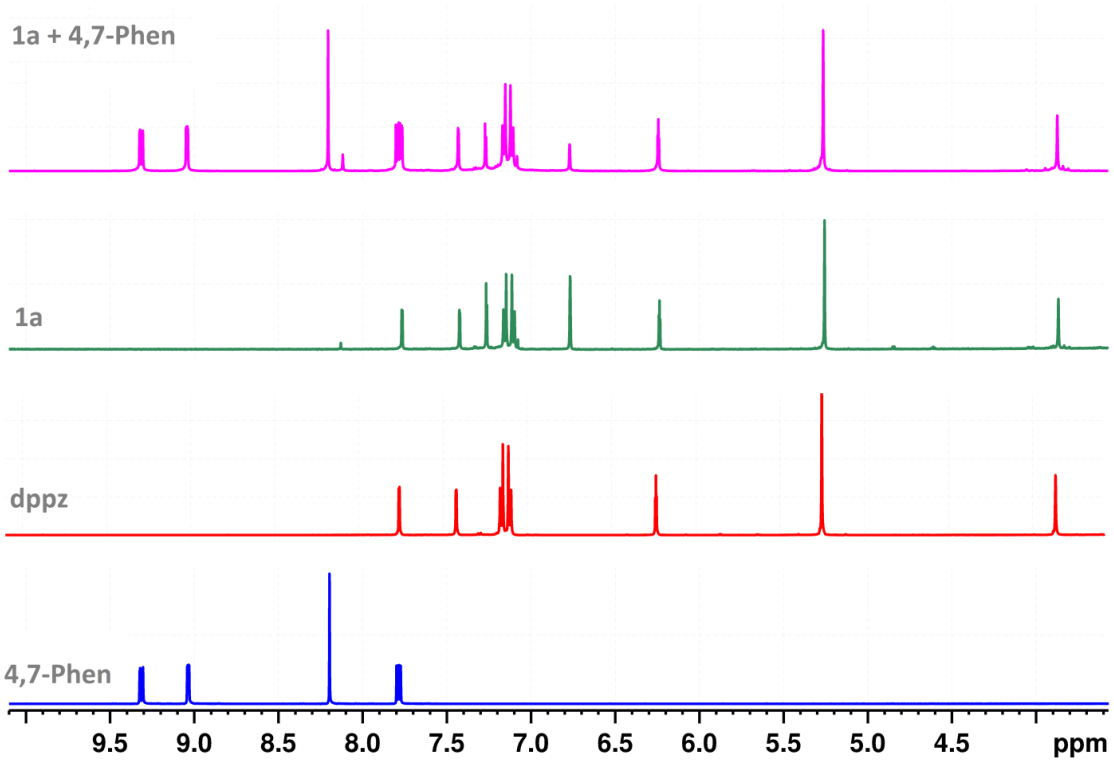

Figure 3.28. Partial ^{1}H NMR spectra of 4,7-Phen, dppz, **1a** and **1a** + 4,7-Phen in DMSO–d_6 (where **1a** = crystals **1a** were dissolved in DMSO–d_6).

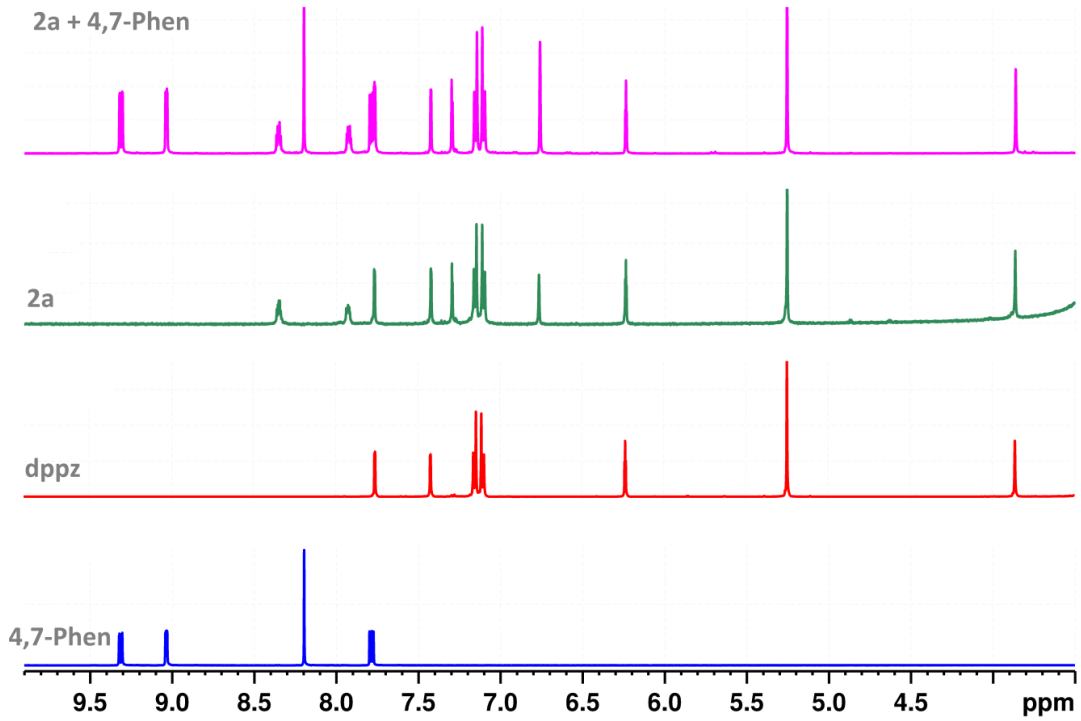

Figure 3.29. Partial ^{1}H NMR spectra of 4,7-Phen, dppz, **2a** and **2a** + 4,7-Phen in DMSO–d_6 (where **2a** = powder **2a** was dissolved in DMSO–d_6).

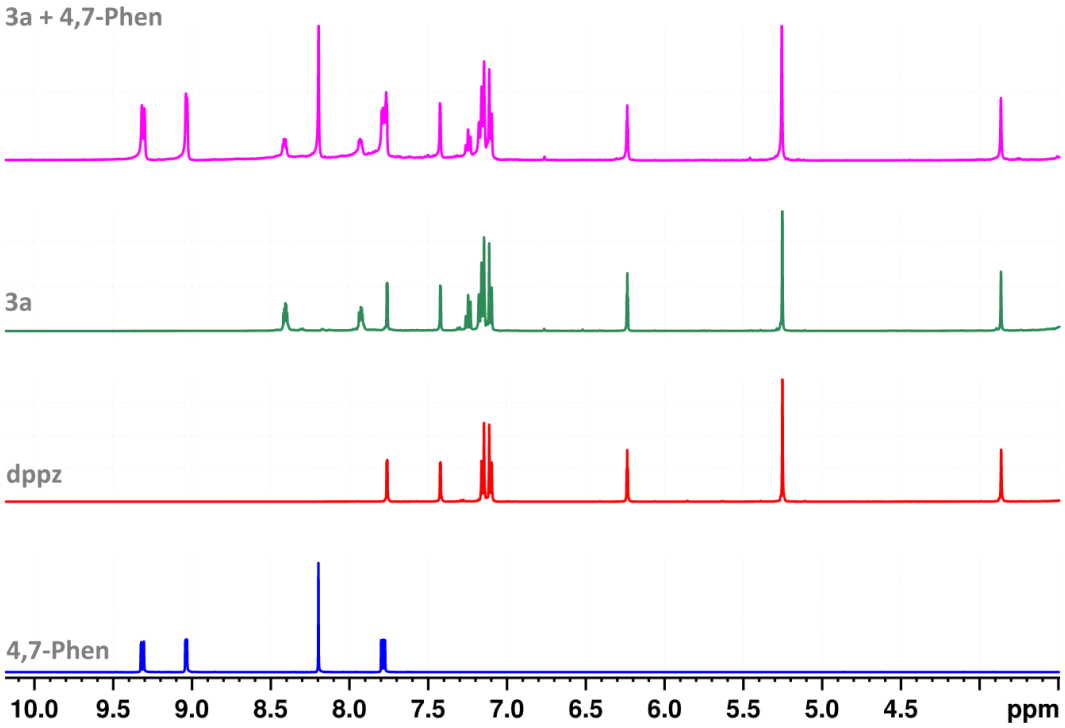

Figure 3.30. Partial ^{1}H NMR spectra of 4,7-Phen, dppz, **3a** and **3a** + 4,7-Phen in DMSO–d_6 (where **3a** = powder **3a** was dissolved in DMSO–d_6).

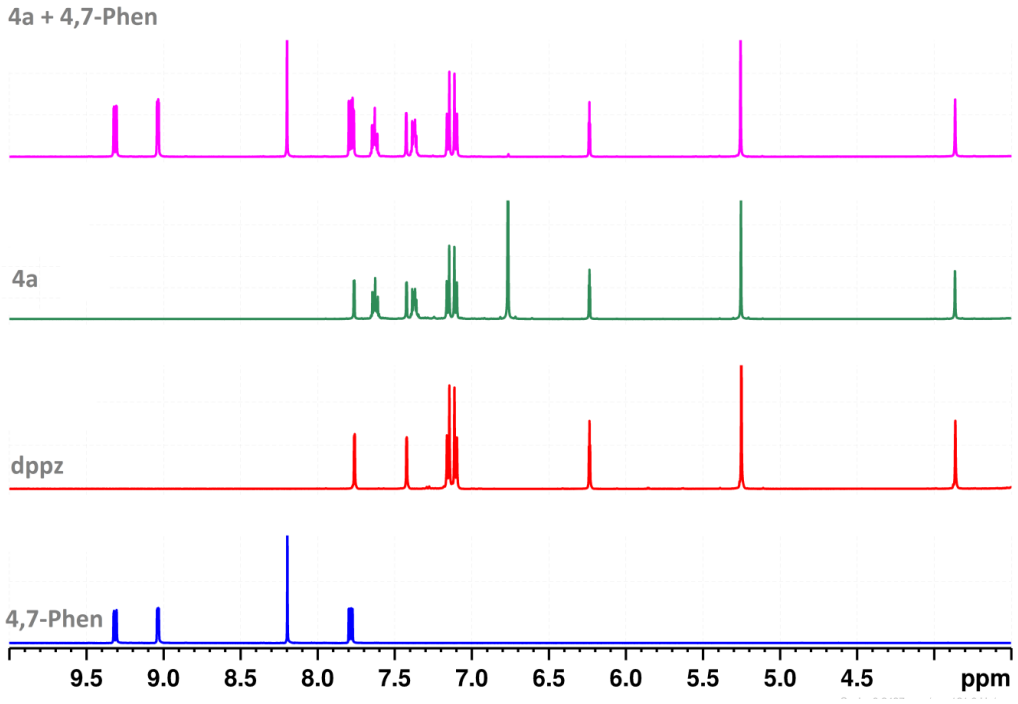

Figure 3.31. Partial ^{1}H NMR spectra of 4,7-Phen, dppz, **4a** and **4a** + 4,7-Phen in DMSO–d_6 (where **4a** = crystals **4a** were dissolved in DMSO–d_6).

Further when competitive experiment was performed with benzimidazolyl-based ditopic donor dpbim in the solution of complexes **1a**-**4a**, the ^{1}H NMR spectra showed the binding of dpbim ligand over dppz ligand with the appearance of new sets of peaks which were shifted relative to the free dpbim ligand (Figure 3.32-3.3.33, 3.5, 3.40). The ESI-mass spectra of the mixture displayed molecular ions peaks (*m/z*: 1259.1300 for [**7**+ H]$^{+}$ and 1203.1549 for [**12**+ H]$^{+}$), confirming the formation of dinuclear complexes *fac*-[{Re(CO)$_3$}$_2$(L)(dpbim)] (where L = dhnd for **7**; bbim for **12**) (Figure 3.36-3.37, 3.38-3.39). Our group previously reported the formation of dinuclear metallocycle by the reaction of H_2-dhnd/ H_2-dhaq, $Re_2(CO)_{10}$ and dpbim. Among the metallacycles, the complexes comprising dhnd was unambiguously proved by SC-XRD analysis. Ligand exchange phenomenon was further confirmed by the solid state structure of **6** which adopts dinuclear M_2LL'-type metallocyclic structure (Figure 3.34).

The rhenium tricarbonyl cores are chelated by rigid dianionic bis-chelating dhaq and clipped by neutral dpbim nitrogen donor. The dhaq motif is significantly above the Re•••Re plane and bent towards the center of the metallocycle. The distance between two Re atoms is found to be 8.41 Å and the N2•••N3 distance is 9.16 Å. The benzimidazolyl motifs of dpbim ligand are arranged with dihedral angle of 76°. The orientations of both the ligand frames create an internal cavity which perfectly accommodates solvent DMSO. The DMSO molecule is stabilized in the cavity via cumulative hydrogen bonding (d = C21–H···O=S(CH$_3$)$_2$ = 2.25 Å, 141°; d = C49–H···O=S(CH3)2 = 2.43 Å, 127°) contacts and CH···π interactions occurs between the methyl units of DMSO and π surface of both the benzimidazolyl motif and dhaq unit. The guest molecule dictates the unusual arrangement of the metallocycle which is facilitated by the flexible nature of the neutral ditopic ligand. One molecule of **6** interacts with an adjacent molecule via Re–C≡O(6)···O(19)≡C–Re (2.97 Å), Re–C≡O(5)···O(18)≡C–Re (2.92 Å) interactions to form a non-covalent dimer. This dimer further interacts with another adjacent dimer via CH···π contacts between the benzimidazolyl motif of one with the phenyl spacer unit of another.

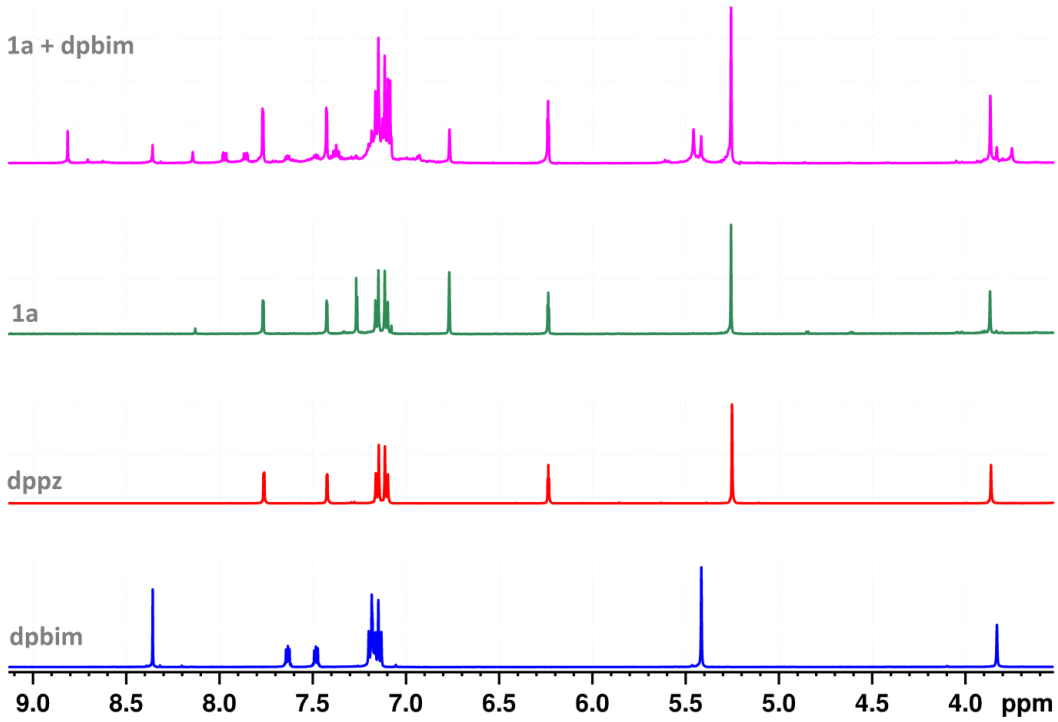

Figure 3.32. Partial ^{1}H NMR spectra of dpbim, dppz, **1a** and **1a** + dpbim in DMSO–d_6 (where **1a** = crystals **1a** were dissolved in DMSO–d_6) (where **1a** = crystals **1a** were dissolved in DMSO–d_6).

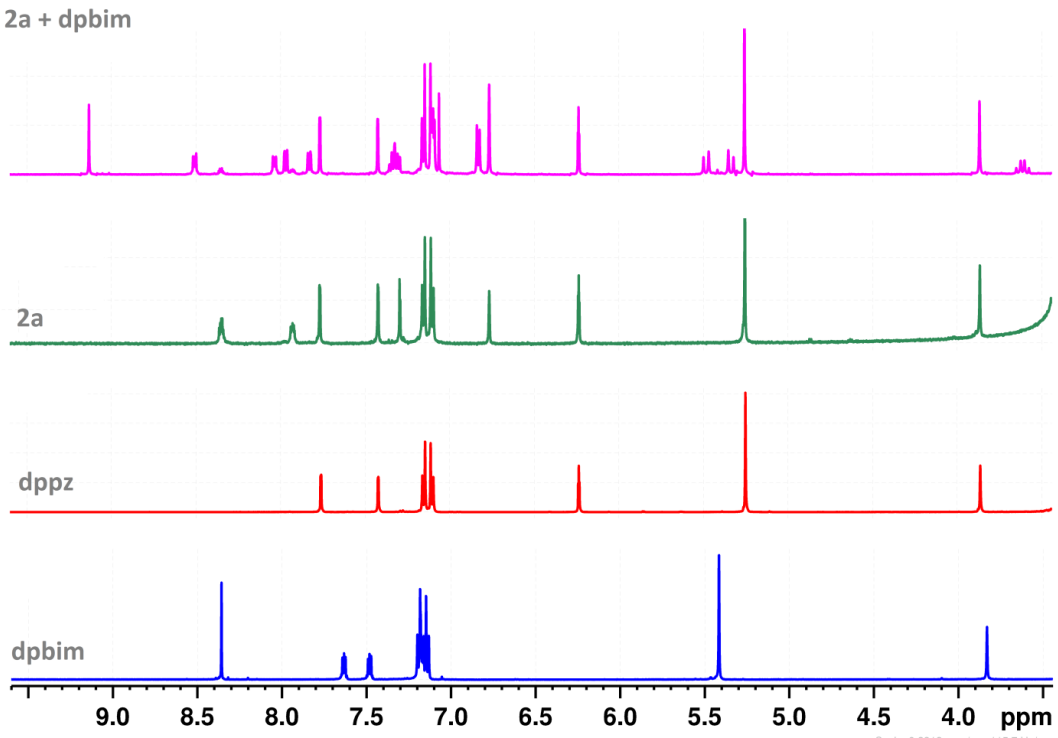

Figure 3.33. Partial ^{1}H NMR spectra of dpbim, dppz, **2a** and **2a** + dpbim in DMSO–d_6 (where **2a** = powder **2a** was dissolved in DMSO–d_6).

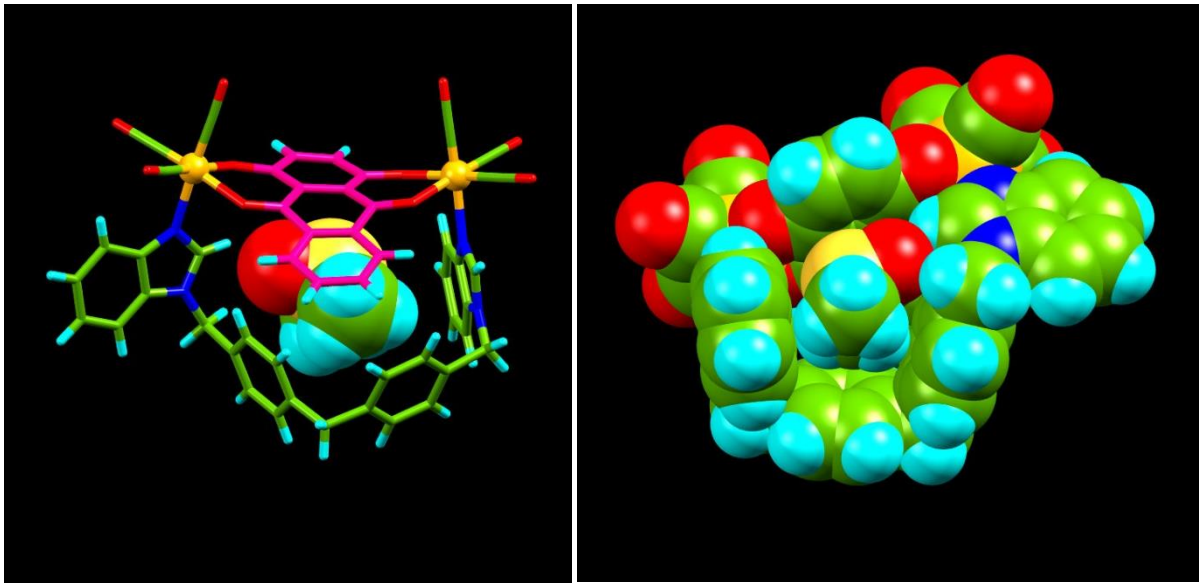

Figure 3.34. Stick (back view) and space-filling (front view) representations of metallocycle **6** with DMSO guest molecule. Color code: C = Green/purple, H = Aqua, N = Blue, O = Red, S = Yellow, and Re = Orange.

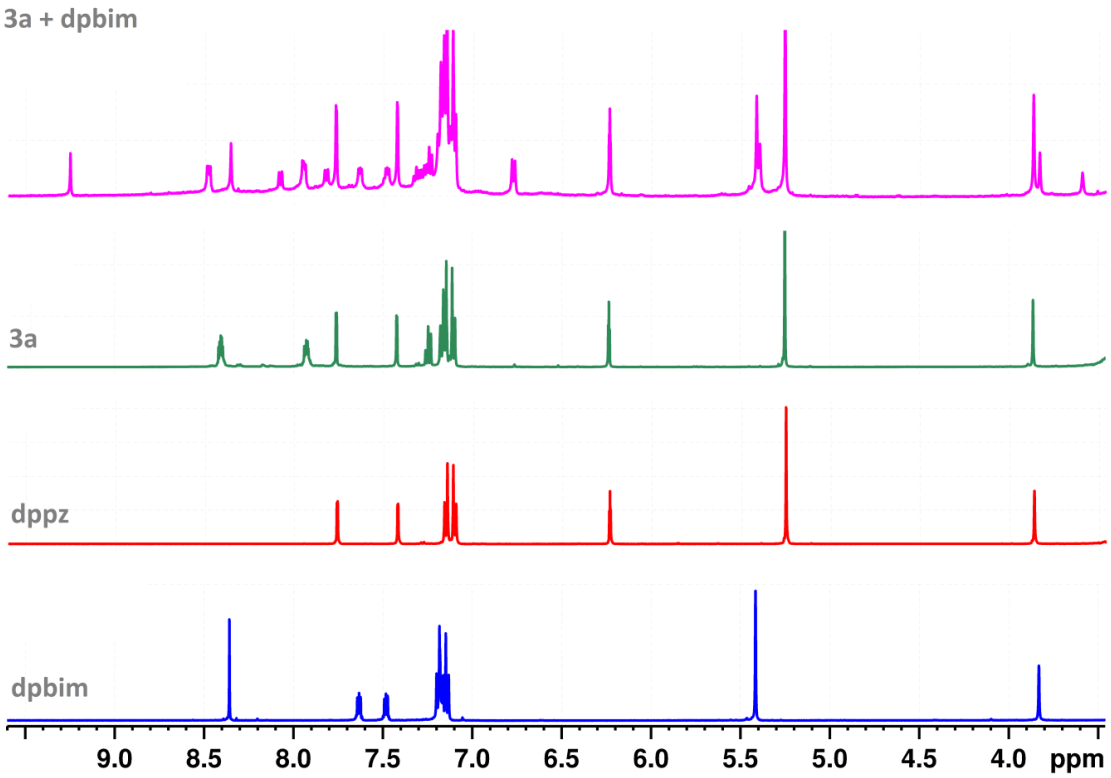

Figure 3.35. Partial ^{1}H NMR spectra of dpbim, dppz, **3a** and **3a** + dpbim in DMSO–d_6 (where **3a** = powder **3a** was dissolved in DMSO–d_6).

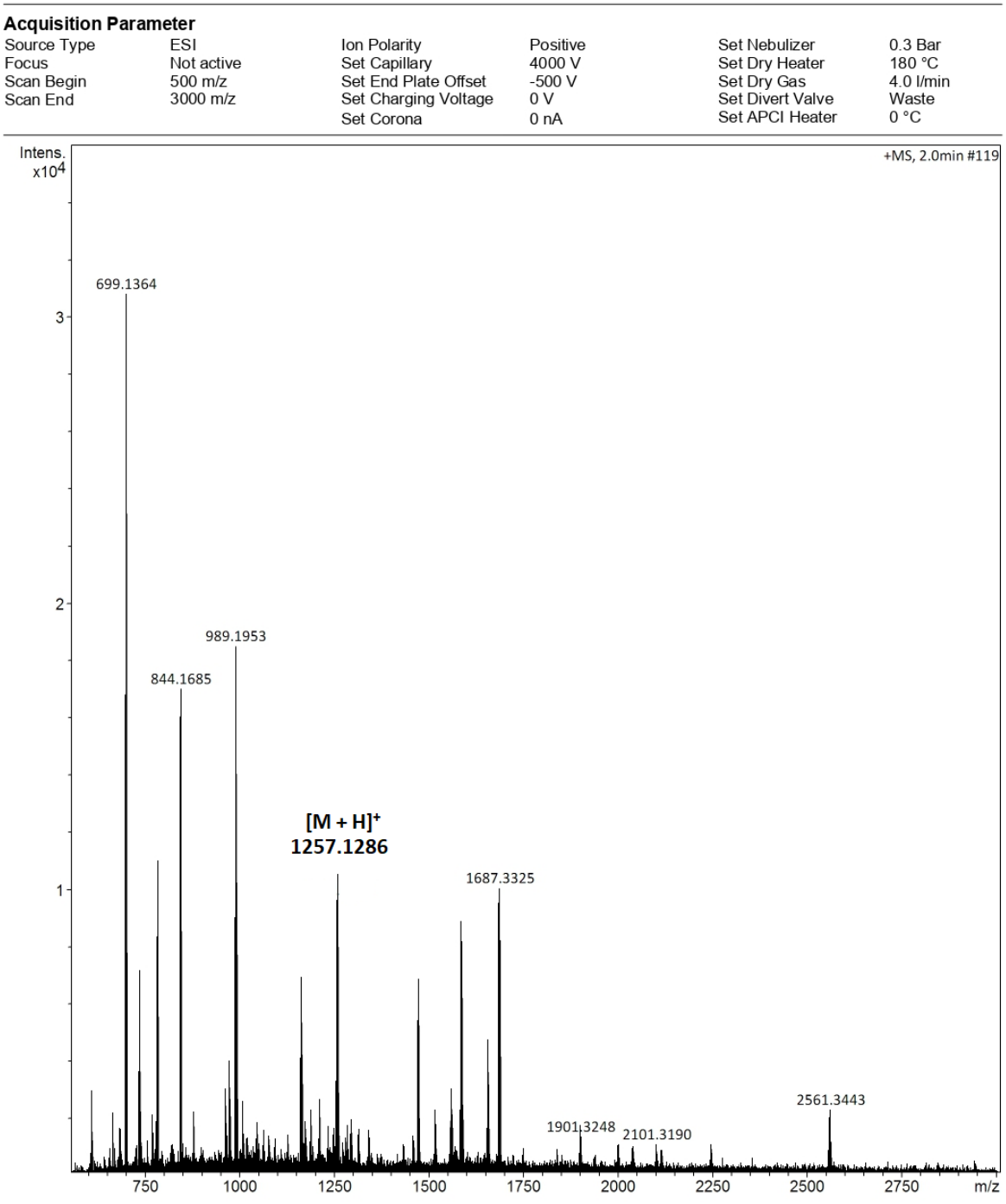

Figure 3.36. ESI mass spectrum of **3a +** dpbim in positive ion mode.

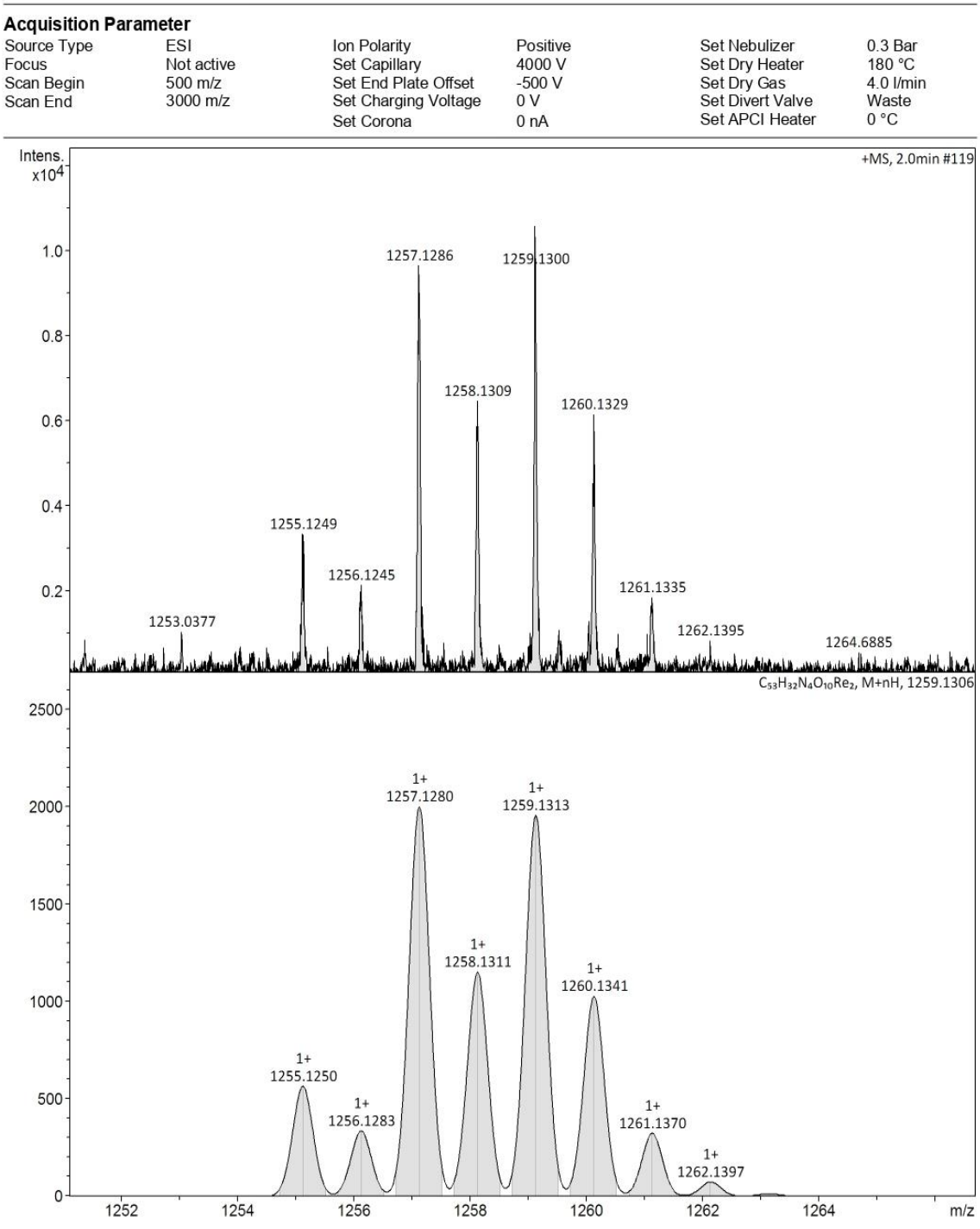

Figure 3.37. Experimental and calculated ESI mass spectra of **7** in positive ion mode.

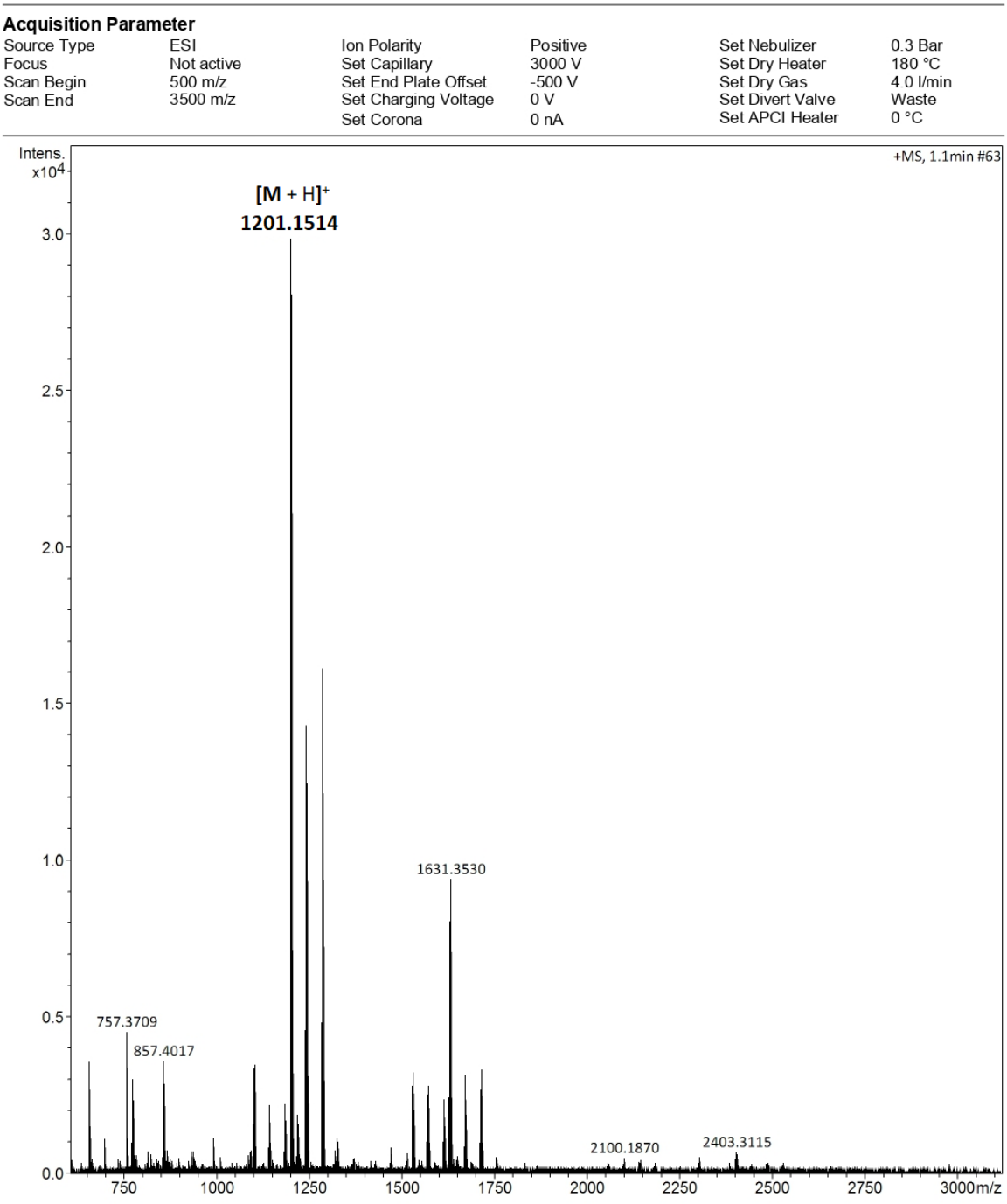

Figure 3.38. ESI mass spectrum of **4a +** dpbim in positive ion mode.

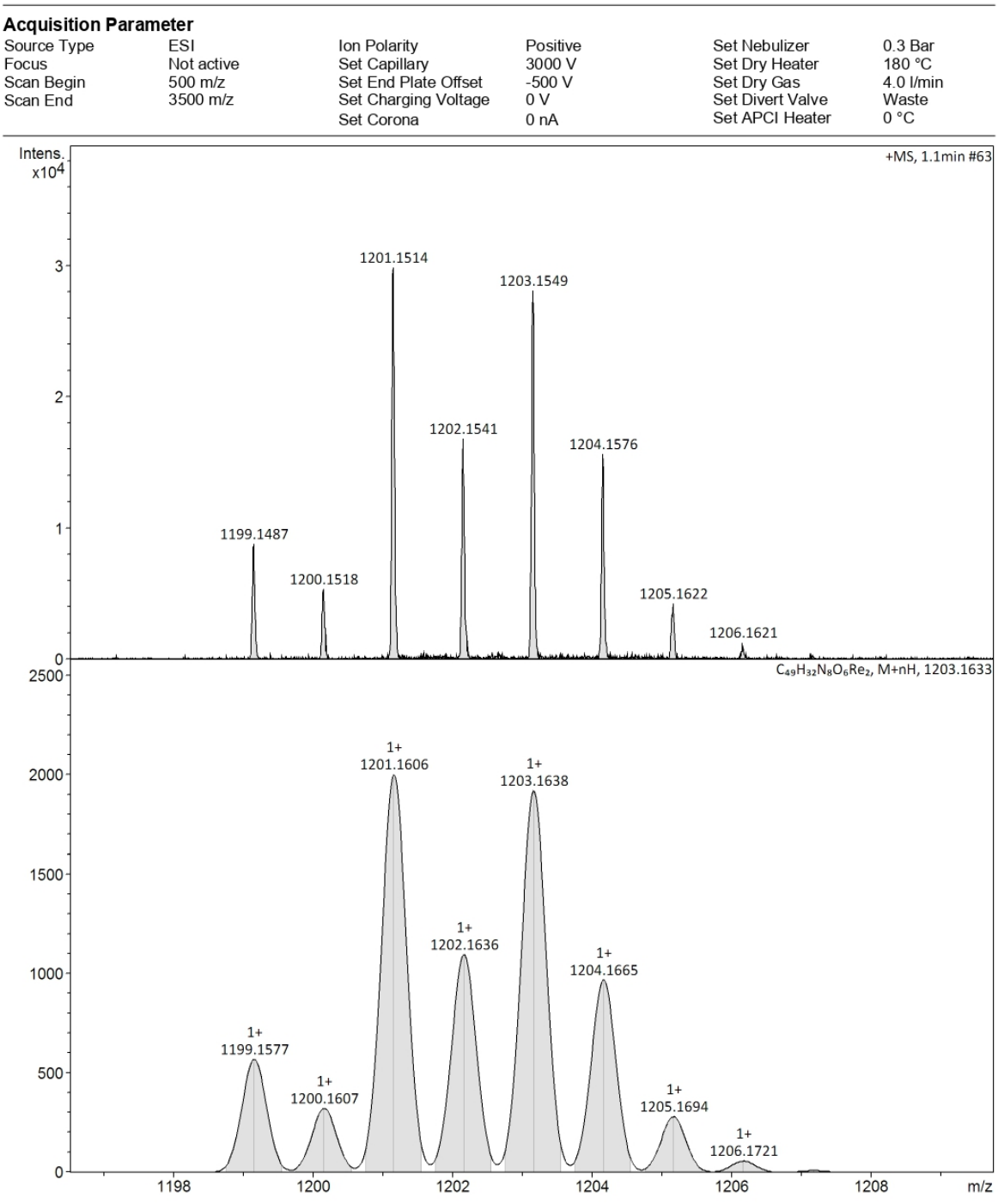

Figure 3.39. Experimental and calculated ESI mass spectra of **12** in positive ion mode.

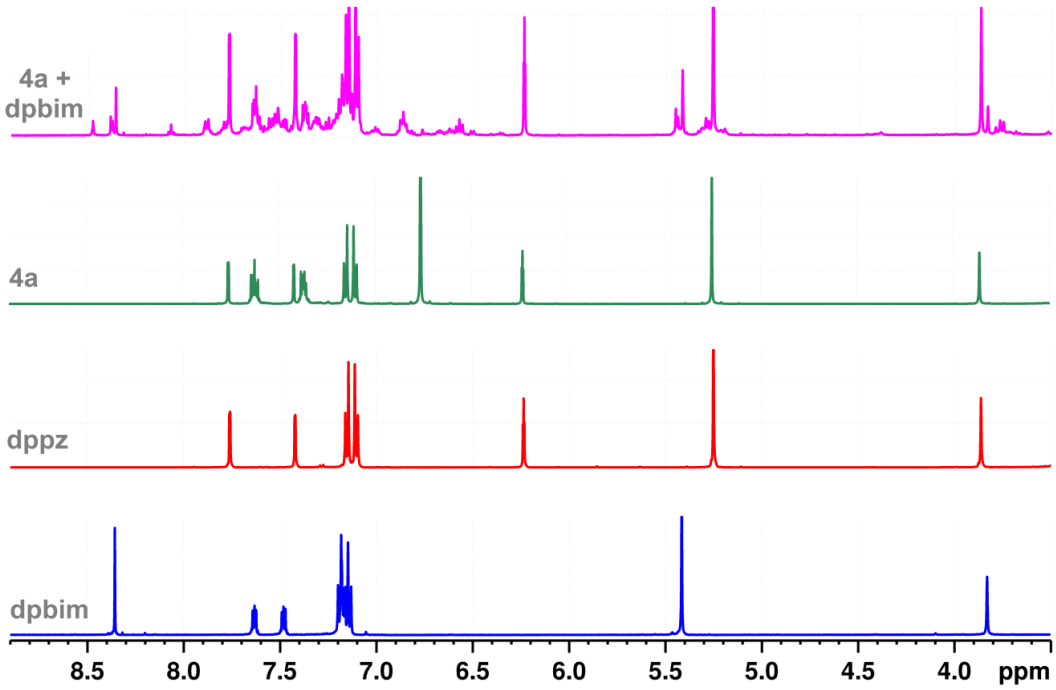

Figure 3.40. Partial ^{1}H NMR spectra of dpbim, dppz, **4a** and **4a** + dpbim in DMSO–d_6 (where **4a** = powder **4a** were dissolved in DMSO–d_6).

Similarly, 1,3,5-triaza-7-phosphaadamantane (PTA) was added to the d_6-DMSO solution of complexes **1a**–**4a**. Changes in both the ^{1}H and ^{31}P NMR spectra were observed, indicating that the ligand exchange takes place with PTA, resulting in acyclic dinuclear complexes *fac*-[{Re(CO)$_3$(PTA)}$_2$(L)] (where L = dhnq for **8**; dhaq for **9**; dhnd for **10**; bbim for **13**) (Figure 3.41-3.44). Among these complexes, complexes **9** and **10** exist as single isomer in the solution due to the appearance of single peak (δ = –56.99 ppm for **9** and δ = –56.56 ppm for **10**) in ^{31}P NMR which are downfield shifted relative to the free PTA ligand (δ = –104.25 ppm). On the other hand, ^{31}P NMR spectra of complex **10** displayed four peaks (δ = –11.978, –57.2397, –77.6733, and –85.4257 ppm) with different intensity which are downfield shifted as compared to free PTA ligand possibly because of presence of isomers in the solution. ^{31}P NMR spectra of complex **13** displayed four peaks (δ = –71.21, –71.43, –72.44, and –72.69 ppm) with different intensity which are significantly downfield shifted in compared to the free PTA ligand. The data proves that phosphorus ligand coordinated to the rhenium center. The ESI-MS spectra of the mixture of metallomacrocycle and PTA displayed peaks (*m/z* = 1092.1028 for [**9** + H]$^+$, *m/z* = 1087.1148 for [**13**+H]$^+$), corresponding to the acyclic dinuclear complexes (Figure 3.45-3.46, 3.51-3.52).

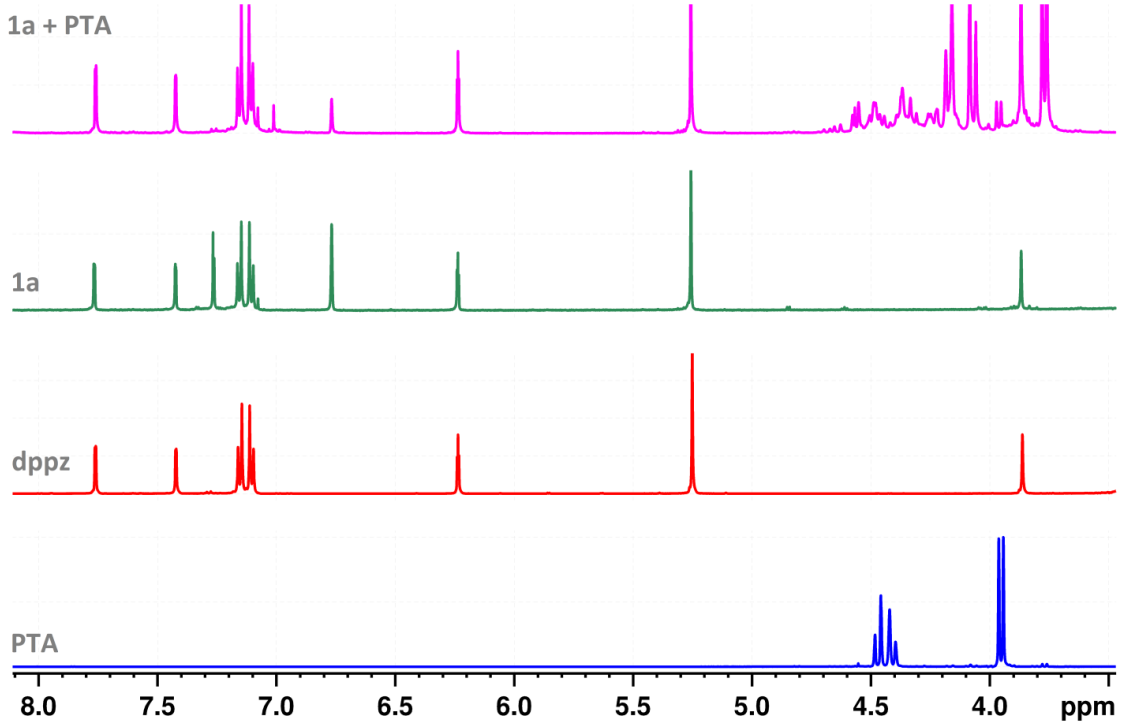

Figure 3.41. Partial ^{1}H NMR spectra of PTA, dppz, **1a** and **1a** + PTA in DMSO–d_6 (where **1a** = crystals **1a** were dissolved in DMSO–d_6) (where **1a** = crystals **1a** were dissolved in DMSO–d_6).

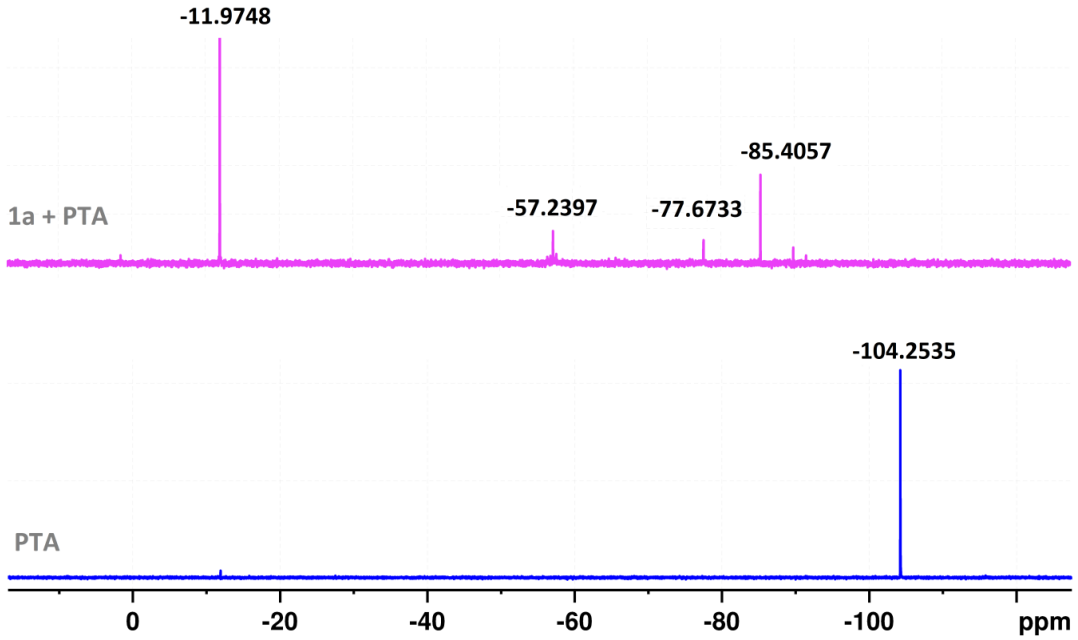

Figure 3.42. ^{31}P NMR spectra of PTA and **1a** + PTA in DMSO–d_6 (where **1a** = crystals **1a** were dissolved in DMSO–d_6).

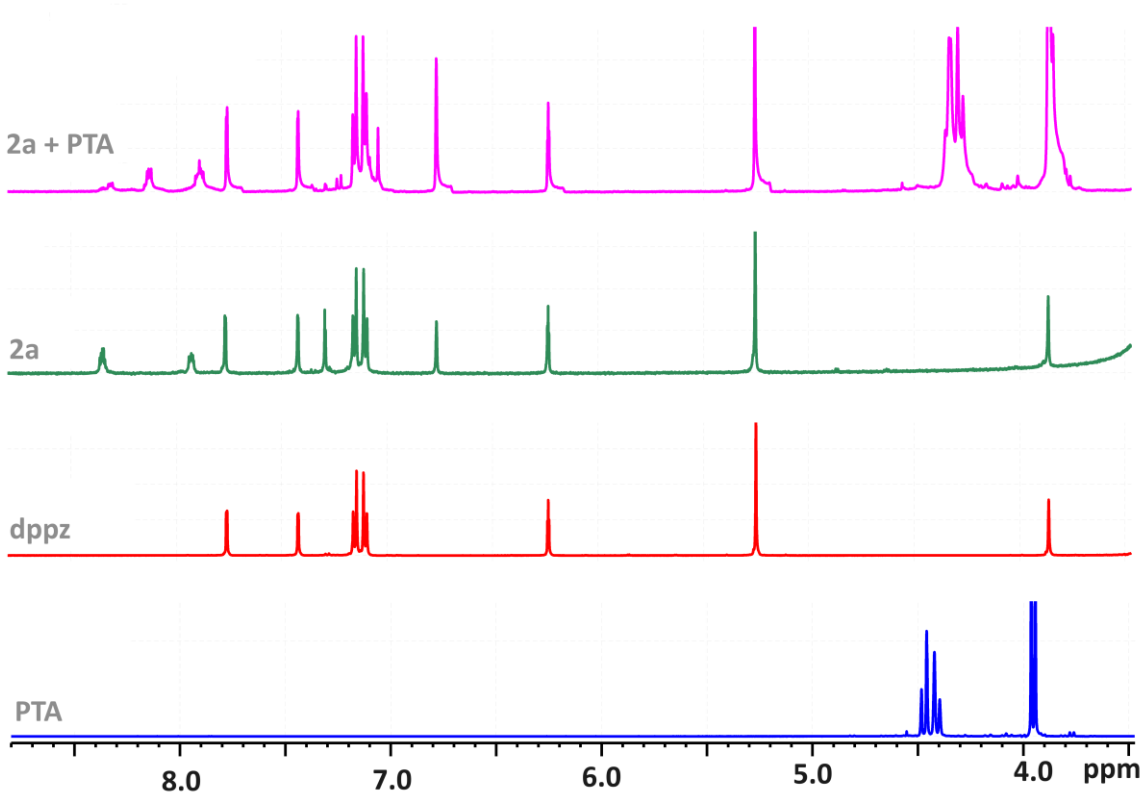

Figure 3.43. Partial ^{1}H NMR spectra of PTA, dppz, **2a** and **2a** + PTA in d_6-DMSO.

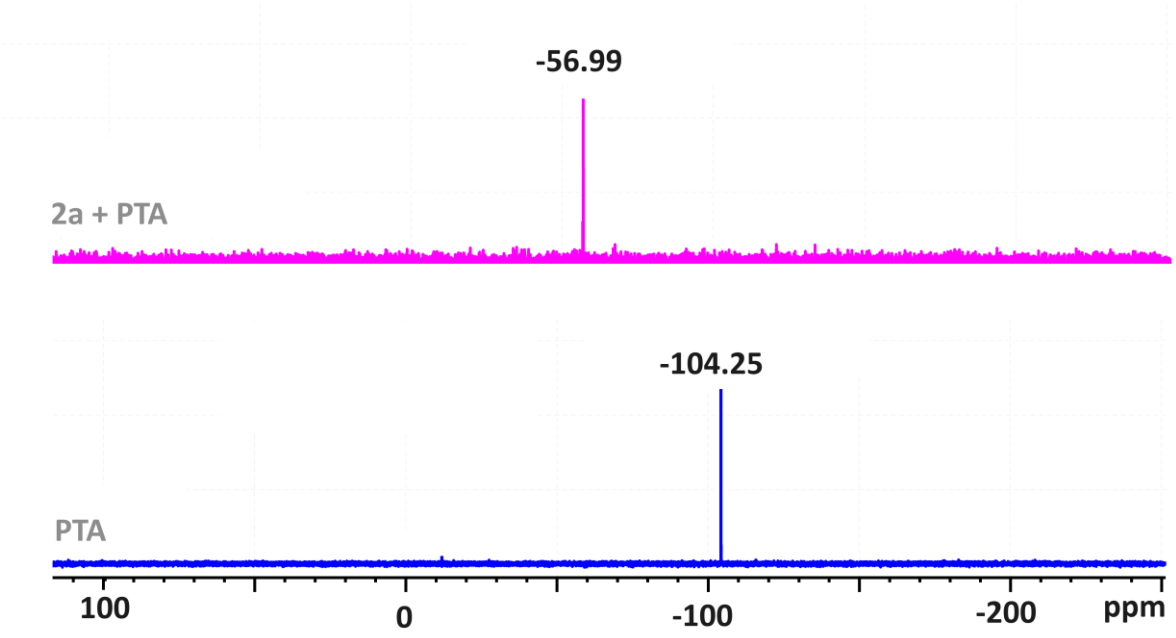

Figure 3.44. ^{31}P NMR spectra of PTA and **2a** + PTA in d_6-DMSO (**2a** = powder **2a** was dissolved in d_6-DMSO).

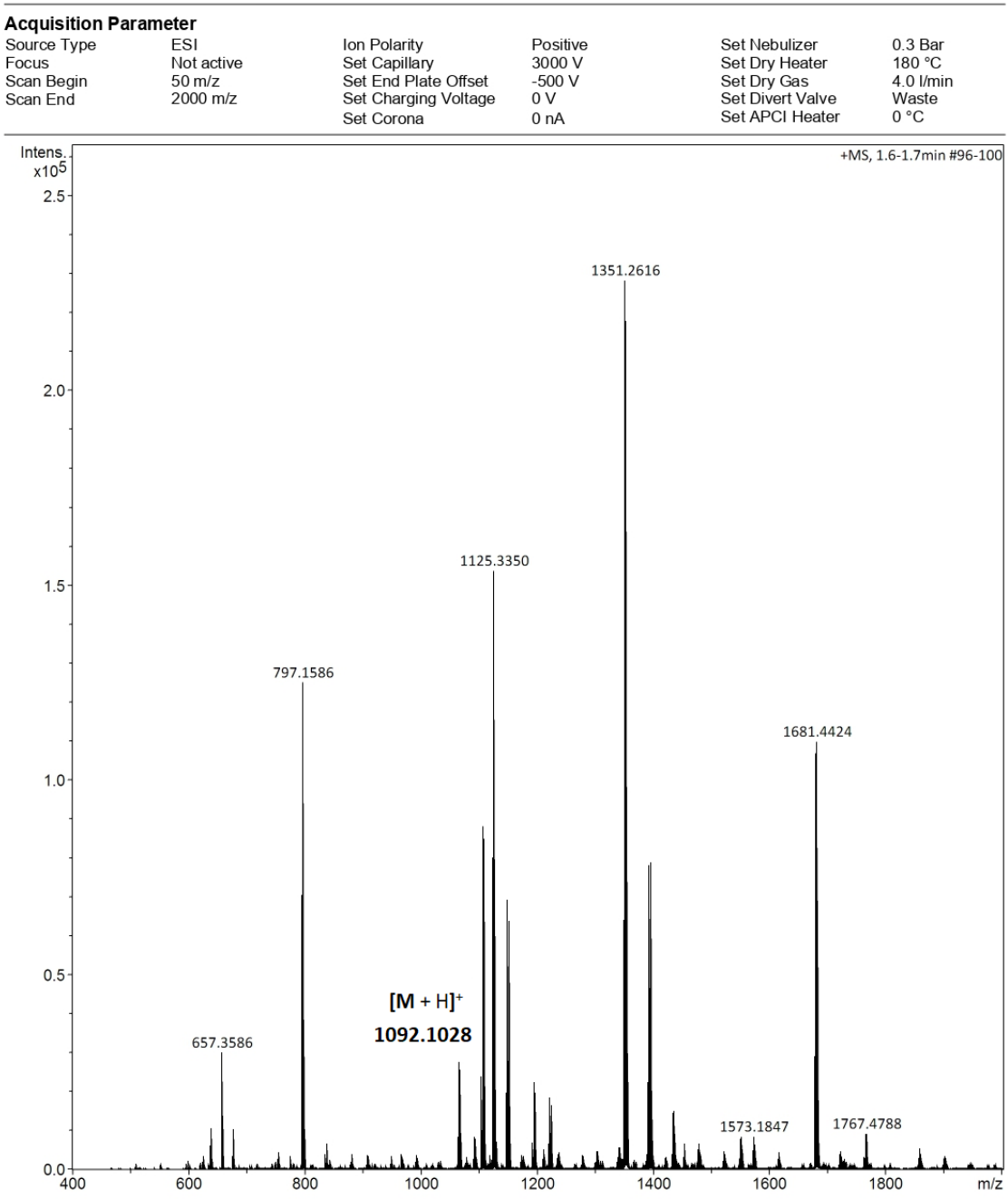

Figure 3.45. ESI mass spectrum of **2a +** PTA in positive ion mode.

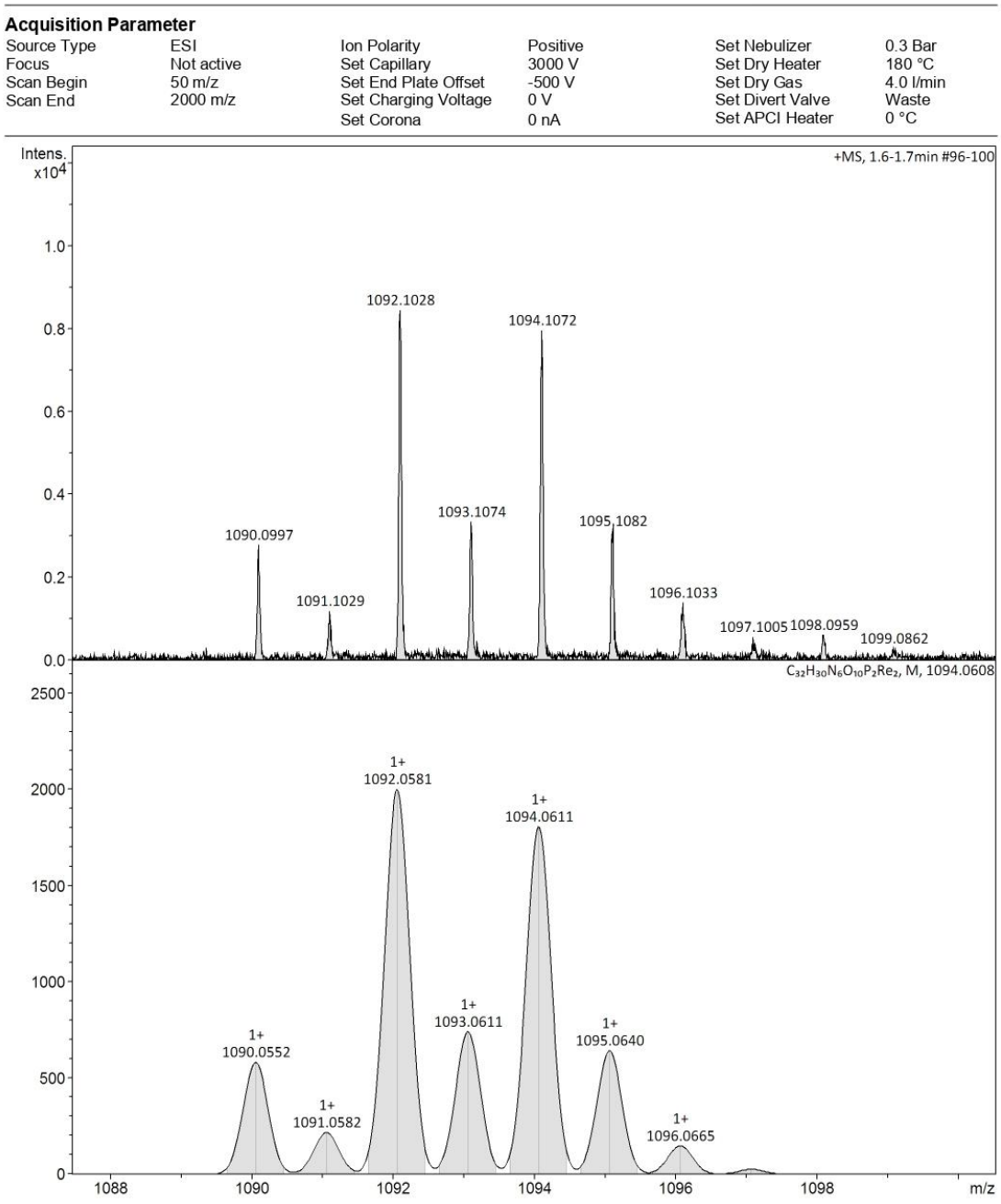

Figure 3.46. Experimental and calculated ESI mass spectra of **9** in positive ion mode.

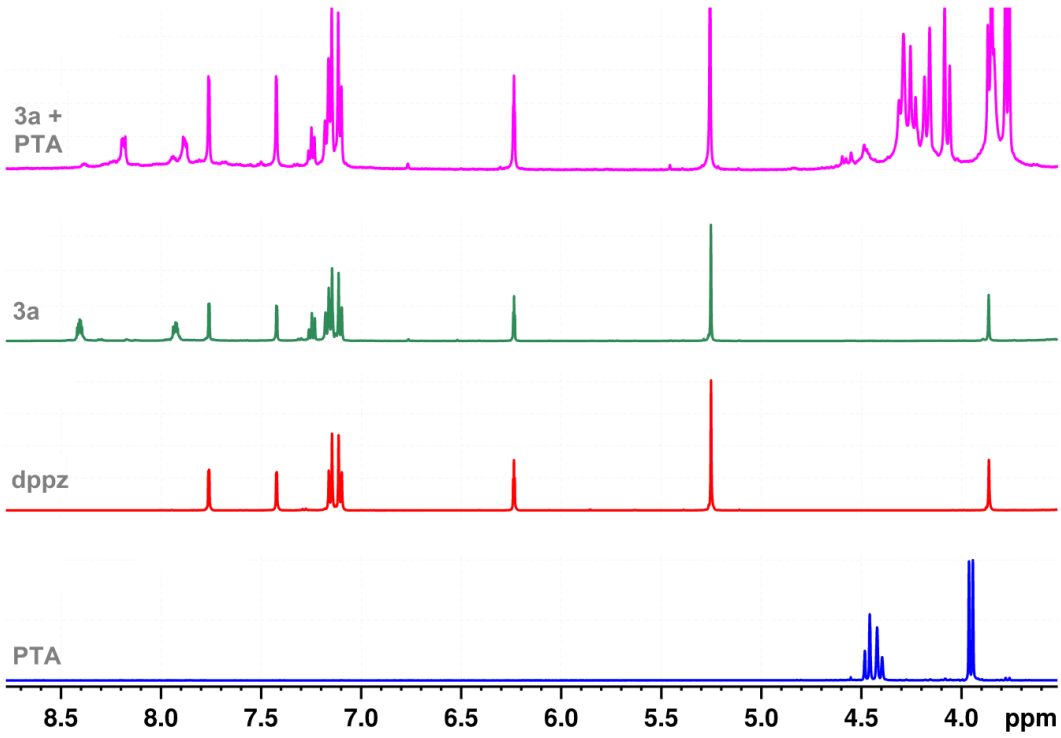

Figure 3.47. Partial ^{1}H NMR spectra of PTA, dppz, **3a** and **3a** + PTA in DMSO–d_6 (where **3a** = powder **3a** was dissolved in DMSO–d_6).

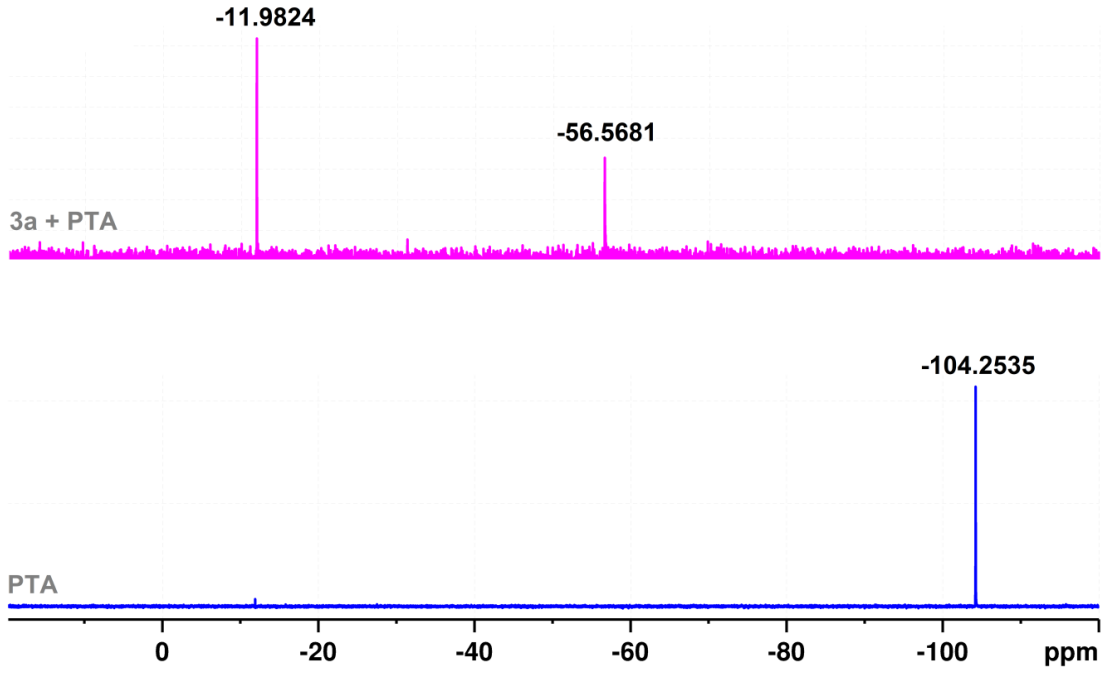

Figure 3.48. ^{31}P NMR spectra of PTA and **3a** + PTA in DMSO–d_6 (where **3a** = powder **3a** was dissolved in DMSO–d_6).

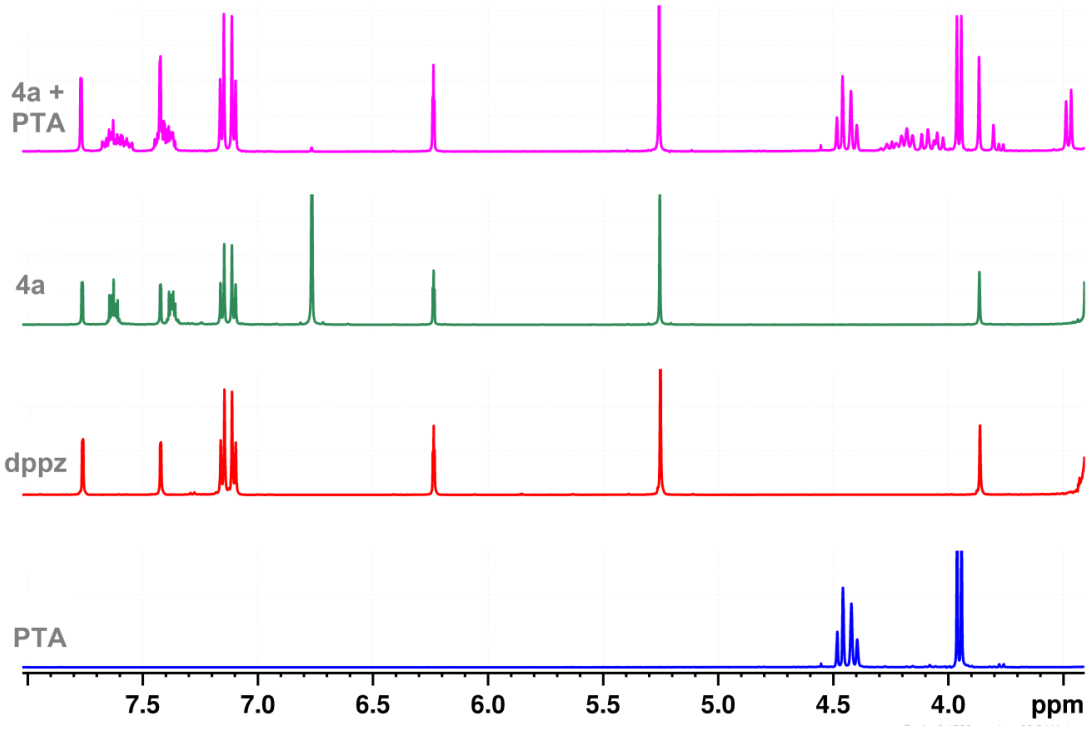

Figure 3.49. Partial ^{1}H NMR spectra of PTA, dppz, **4** and **4** + PTA in DMSO–d_6 (where **4a** = crystals **4a** were dissolved in DMSO–d_6).

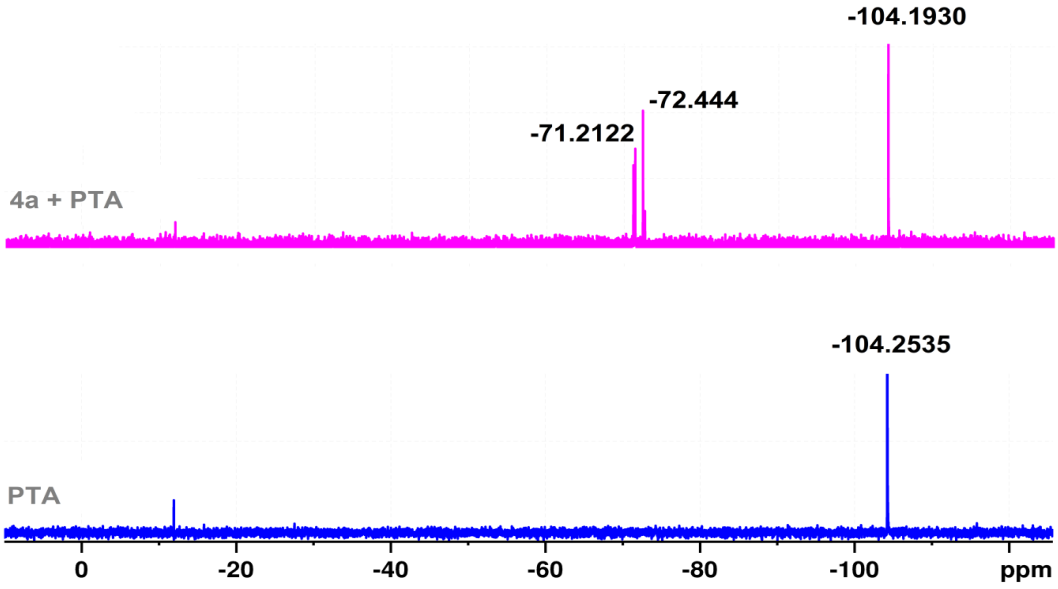

Figure 3.50. ^{31}P NMR spectra of PTA and **4a** + PTA in DMSO–d_6 (where **4a** = crystals **4a** were dissolved in DMSO–d_6).

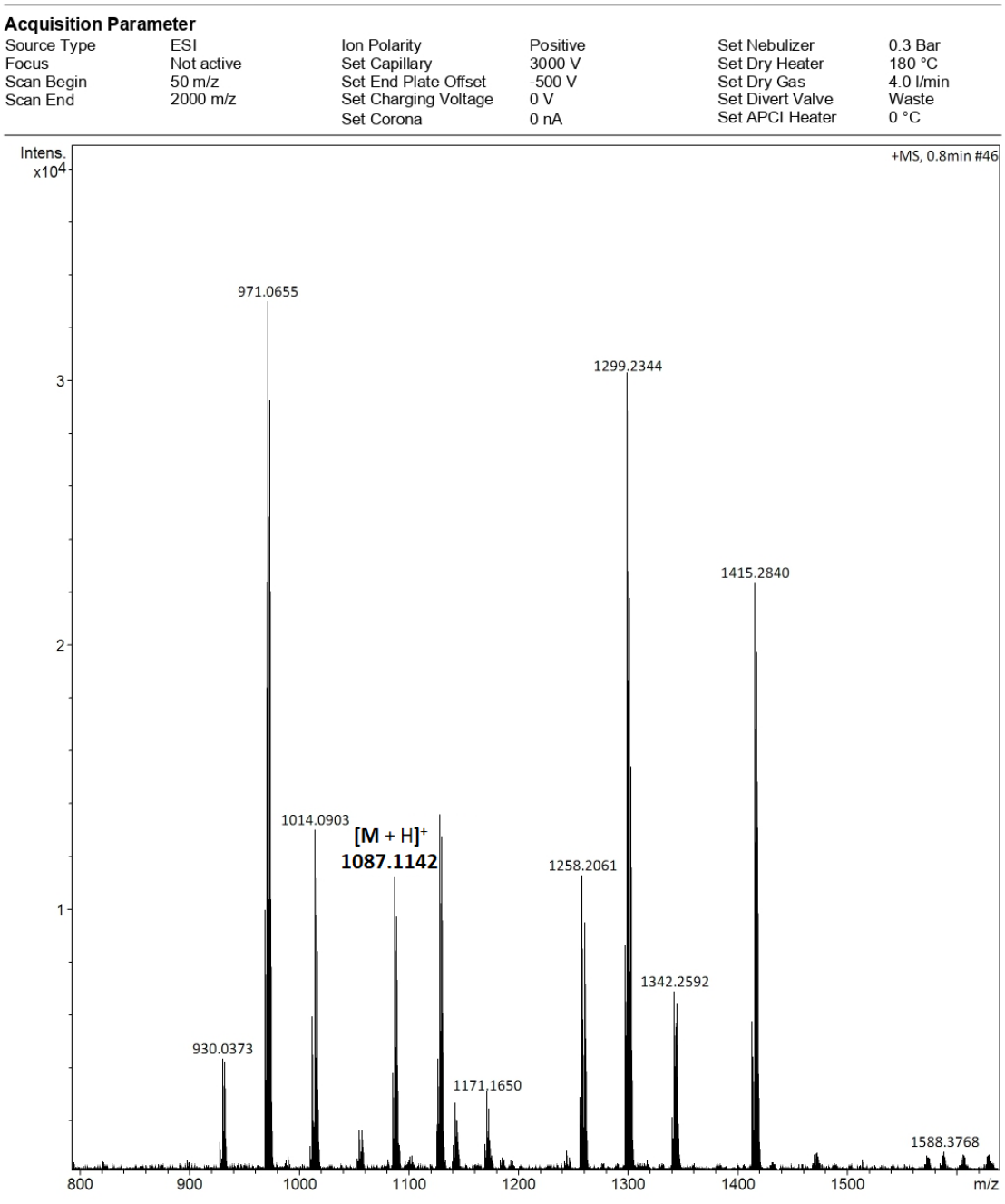

Figure 3.51. ESI mass spectrum of **4a +** PTA in positive ion mode.

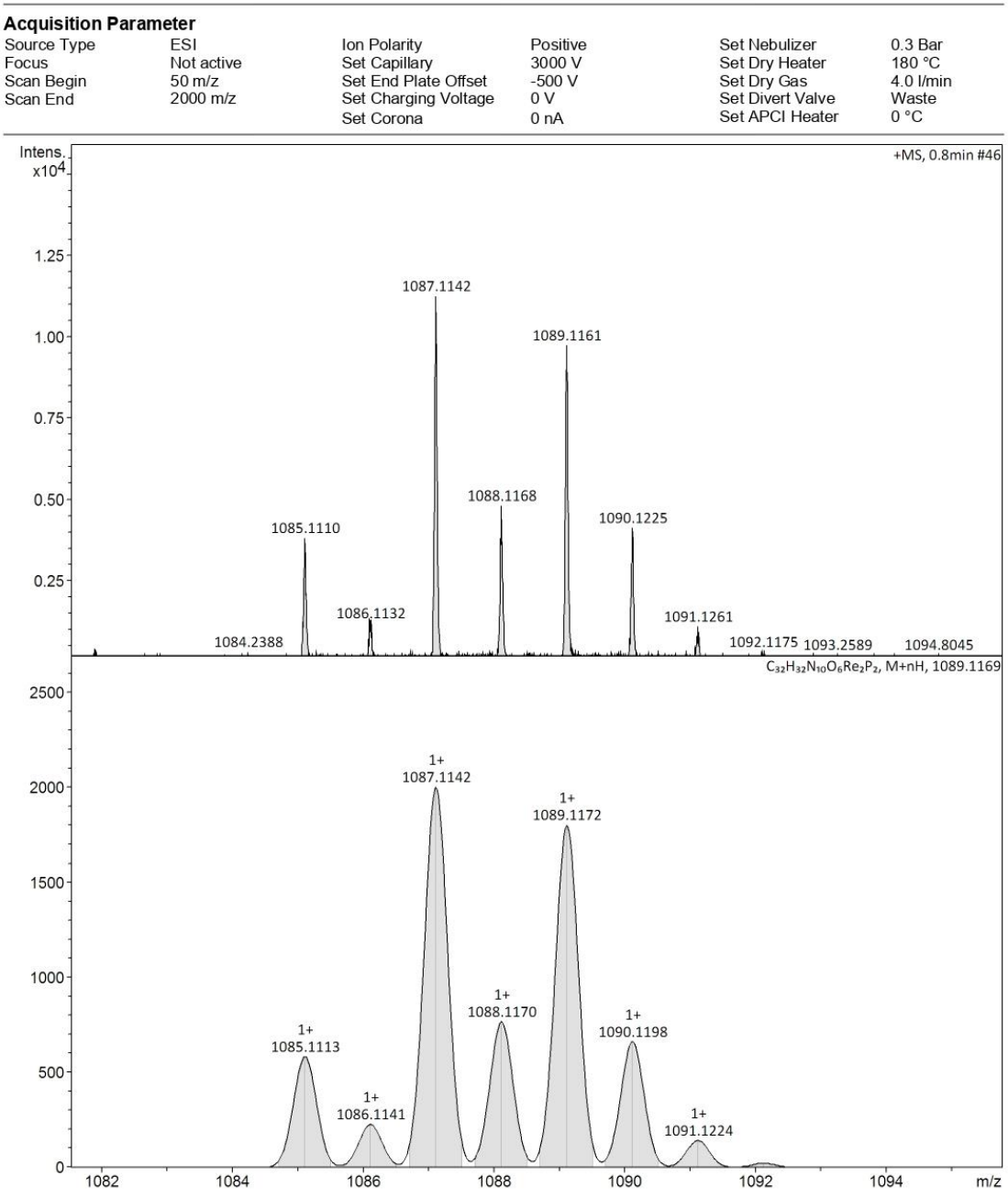

Figure 3.52. Experimental and calculated ESI mass spectra of **13** in positive ion mode.

Further, the formation of complex **13** was also confirmed by SC-XRD analysis. Single crystals suitable for XRD data collection were obtained from the NMR tube after a week. The molecular structure of **13** shows that it is a dinuclear acyclic complex having two *fac*-$Re(CO)_3$ cores, one dianionic bbim motif and two PTA ligands (Figure 3.53). The geometry around the rhenium centers is distorted octahedral with C_3O_2P donors environment. The bbim ligand is almost planar and coordinated two rhenium cores symmetrically. The PTA ligand is coordinated to rhenium center using its phosphorous atom. The two PTA ligands in the complex are arranged in a "Z-type" *trans*-position. The Re–C distances *trans* to the N,N(bbim) atoms are 1.922 Å (Re1–C8), and 1.914 Å (Re1–C10), whereas Re–C distance *trans* to the P(PTA) atom is 1.931 Å (Re1–C9). The longer Re–C distance *trans* to PTA can be ascribed to the *trans* effect of PTA due to stronger π-acceptor ability of PTA.[71-73] The Re•••Re distance is 5.753 Å which is in the expected range. Each molecule interacts with the neighboring molecule through various intermolecular supramolecular interactions. Two neighboring molecules are arranged in such way that PTA of one molecule faces the PTA of another molecule which contact each other through C–H•••N hydrogen bonding interactions (d = C15-H•••N8 = 2.705 Å; C14-H•••N8 = 2.672 Å) and C–H•••H–C dispersion contacts (d = C13-H••• H-C14 = 2.340 Å).

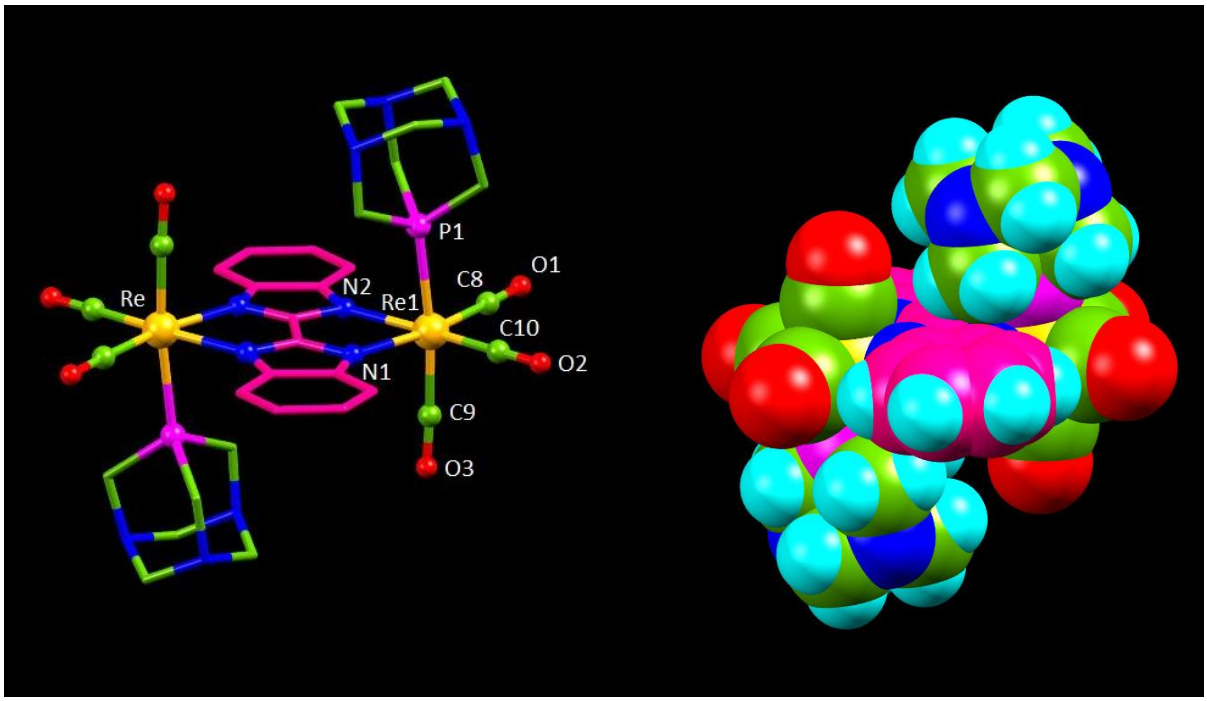

Figure 3.53.. Ball & stick and space-filling representations of molecular structure of **13**. Color code: C = Green/purple, H = Aqua, N = Blue, O = Red, S = Yellow, and Re = Orange.

3.4 Conclusion

In conclusion, neutral heteropetic metallacycles having figure-eight-shaped architecture and "*Z*'-type" structure (**1a**–**4a**) were obtained from $Re_2(CO)_{10}$, rigid bischelating ligands and flexible ditopic pyrazolyl donor dppz. To the best of our knowledge, this is the first synthetic report on heteroleptic *fac*-[$Re(CO)_3$] core-based coordination-driven self-assembly approach for figure-eight shaped metallocycle. The metallacycles were found to be in dynamic equilibrium with disassembly products in the solution state. The dynamic nature of rhenium-pyrazolyl coordination bond in the metallacycles was further utilized in transforming the metallocycles into pyridyl/benzimidazolyl nitrogen donor-based metallocycles such as molecular rectangles (**4**, **11**), dinuclear metallocycles (**5-7**, and **12**) and phosphine donor-based acyclic complexes (**8-10** and **13**) via component induced supramolecular transformation reactions with the addition of various types of competing ligands. The results reveal that modulation of the size of the rigid bis-chelating ligand and the coordination angle of pyrazolyl donor directs the final shape of the metallocyclic architecture during the self-assembly process thereby providing insights for design of hitherto unknown *fac*-[$Re(CO)_3$] core-based intricate topological architectures including figure-eight supramolecules. Further, rhenium metallocycle coordinated with pyrazolyl ligand is attractive because of the easily breakable rhenium-pyrazolyl bond in a DMSO solution. The pyridyl/imidazolyl ligands have the ability to substitute the pyrazolyl donors through supramolecular transformation. The results may pave the way to the development of less explored competitive ligand-induced supramolecular transformations in rhenium carbonyl-based metallocycles.

3.5 References

1. R. Saha, B. Mondal and P. S. Mukherjee, *Chem. Rev*. 2022, **122**, 12244–12307.
2. S. Samantray, S. Krishnaswamy and D. K. Chand, *Nat. Commun*. 2020, **11**, 1–8.
3. H. Sepehrpour, W. Fu, Y. Sun and P. J. Stang, *J. Am. Chem. Soc*. 2019, **141**, 14005–14020.
4. A. Pothig and A.Casini, *Theranostics*. 2019, **9**, 3150–3169.
5. G. Yu, M. Jiang, F. Huang and X. Chen, *Curr Opin Chem Biol*. 2021, **61**, 19–31.
6. E. G. Percastegui, T. K. Ronson and J. R. Nitschke, *Chem. Rev.* 2020, **120**, 13480–13544.
7. Z. Huang and J. J. Wilson, *Eur. J. Inorg. Chem*. 2021, **14**, 1312–1324.
8. H. Takesawa and M. Fujita, *Bull. Chem. Soc. Jpn*. 2021, **94**, 2351−2369.
9. I. Mishra, M. Bhol, P. Kalimuthu and M. Sathiyendiran, *Chem. Rec*. 2021, **21**, 594−614.

10. L. L. Dang, H. J. Feng, Y. J. Lin and G. X. Jin, *J. Am. Chem. Soc*. 2020, **142**, 18946–18954.
11. R. S. Forgan, J. P. Sauvage and J. F. Stoddart, *Chem. Rev*. 2011, **111**, 5434–5464.
12. Z. Ashbridge, S. D. P. Fielden, D. A. Leigh, L. Pirvu, F. Schaufelberger and L. Zhang, *Chem. Soc. Rev*. 2022, **51**, 7779–7809.
13. M. Han, D. M. Engelhard and G. H. Clever, *Chem. Soc. Rev*. 2014, **43**, 1848–1860.
14. T. Feng, X. Li, Y. Y. An, S. Bai, L.Y. Sun, Y. Li, Y. Y. Wang and Y. F. Han, *Angew. Chem., Int. Ed*. 2020, **59**, 13516–13520.
15. Y. Inomata, T. Sawada and M. Fujita, *J. Am. Chem. Soc*. 2021, **143**, 16734–16739.
16. Z. Cui, X. Gao, Y. J. Lin and G. X. Jin, *J. Am. Chem. Soc.* 2022, **144**, 2379–2386. And References therein.
17. Z. Cui and G. X. Jin, *Nat. Synth*. 2022, **1**, 635–640.
18. M. C. O'Sullivan, J. K. Sprafke, D. V. Kondratuk, C. Rinfray, T. D. W. Claridge, A. Saywell, M. O. Blunt, J. N. O'Shea, P. H. Beton, M. Malfois and H. L. Anderson, *Nature* 2011, **469**, 72–75.
19. P. Wipf, P. C. Fritch, S. J. Geib and A. M. Sefler, *J. Am. Chem. Soc.* 1998, **120**, 4105–4112.
20. S. C.West, J. K. Countryman and P. Howard-Flanders, *Cell* 1983, **32**, 817–829.
21. J. Huang, D. Liu, S-C.Wang, M. Chen, H. Zhao, K. Li, Y-T. Chan and P. Wang. *Inorg. Chem*. 2019, **58**, 5051−5057.
22. T. R. Schulte, J. J. Holstein, L. Schneider, A. Adam, G. Haberhauer and G. H. Clever, *Angew. Chem. Int. Ed*. 2020, **59**, 22489–22493.
23. T. T. Zhang, T. Chen, L. L. Dang, T. T. Li, K. X. Sun, Y. J. Gao, L. F. Ma and D. S. Li, *J. Solid State Chem*. 2022, **313**, 123320.
24. X. P. Lv, D. H. Wei and G. Y. Yang, *Inorg. Chem*. 2017, **56**, 11310–11316.
25. R. Govindarajan, D. Divya, R. Nagarajaprakash and B. Manimaran, *Chemistry Select* 2018, **3**, 3742–3750.
26. Y. Zhang, M. R. Crawley, C. R. Hauke, A. E. Friedman, T. S. Janik and T. R. Cook, *Eur. J. Inorg. Chem*. 2017, **34**, 4055–4060.
27. J. R. Dilworth, *Coord. Chem. Rev*. 2021, **436**, 213822.
28. E. B. Bauer, A. A. Haase, R. M. Reich, D. C. Crans and F. E. Kuhn, *Coord. Chem. Rev*. 2019, **393**, 79–117.
29. K. Schindler and F. Zobi, *Molecules* 2022, **27**, 539.
30. A. Sharma, N. Vaibhavi, B. Kar, U. Das and P. Paira, *RSC Adv*. 2022, **12**, 20264–20295.

31. P. Thanasekaran, C-C. Lee and K-L. Lu, *Acc. Chem. Res*. 2012, **45**, 1403–1418.
32. B. Tzeng, A. Chao, M. Lin, G. Lee and T. Kuo, *Chem. Eur. J*. 2017, **23**, 18033–18040.
33. E. Q. Procopio, D. Dova, S. Cauteruccio, A. Forni, E. Licandro and M. Panigati, *ACS Omega*. 2018, **3**, 11649–11654.
34. A. Boulay, A. Seridi, C. Zedde, S. Laderia, C. Picard, L. Maron and E. Benoist, *Eur. J. Inorg. Chem*. 2010, 5058–5062.
35. M. Sathiyendiran, C. Tsai, P. Thanasekaran, T. Luo, C. Yang, G. Lee, S. Peng and K. Lu, *Chem. Eur. J*. 2011, **1**, 3343–3346.
36. G. Jin, T. Wang, Y. Sun, Y. Li and J. Ma, *Inorg. Chem*. 2020, **59**, 15019–15027.
37. C. Y. Chan, P. A. Pellegrini, I. Greguric and P. J. Barnard, *Inorg. Chem*. 2014, **53**, 10862–10873.
38. S. Sato and O. Ishitani, *Coord. Chem.Rev*. 2015, **282–283**, 50–59.
39. D. Sinha, S. P. Parua and K. K. Rajak, *J. Organomet. Chem*. 2019, **889**, 62–69.
40. D. Gupta and M. Sathiyendiran, *ChemistrySelect* 2018, **3**, 7439–7458.
41. K. R. Soumya, R. Arumugam, B. Shankar and M. Sathiyendiran, *Inorg. Chem*, 2018, **57**, 10718–10725.
42. R. Arumugam, B. Shankar, K. R. Soumya and M. Sathiyendiran, *Dalton Trans*. 2019, **48**, 7425–7431.
43. B. Shankar, R. Marimuthu, S. D. Sathiyashivan and M. Sathiyendiran, *Inorg. Chem*. 2016, **55**, 4537−4544.
44. R. Govindarajan, R. Nagarajaprakash, V. Veena, N. Sakthivel and B. Manimaran. *Polyhedron*. 2018, **139**, 229–236.
45. G. G. Huang, C. Lee, J. Yang, Z. Lu, M. Sathiyendiran, C. Huang, Y. Kao, G. Lee and K. Lu, *Sens. Actuators B*, 2018, **254**, 424–430.
46. U. Phukon, B. Shankar and M. Sathiyendiran, *Dalton Trans*. 2022, **51**, 16307−16315.
47. M. Bhol, B. Shankar and M. Sathiyendiran, *Dalton Trans*. 2018, **47**, 4494–4500.
48. M. Kedia, B. Shankar and M. Sathiyendiran, *Inorg. Chem*. 2022, **61**, 14506−14510.
49. M. Bhol, B. Shankar and M. Sathiyendiran, *Inorg. Chem*. 2022, **61**, 11497–11508.
50. M. Bhol, C. Guilhem, M. R. Jungfer, M. Roca, U. Abram and M. Sathiyendiran, *Inorg. Chem*. 2022, **61**, 5173–5177.
51. B. Shankar, R. Marimuthu, S. D. Sathiyashivan and M. Sathiyendiran, *Inorg. Chem.* 2016, **55**, 4537–4544.
52. S. M. Lin, M. Velayudham, C. H. Tsai, C. H. Chang, C. C. Lee, T. T. Luo, P. Thanasekaran and K. L. Lu, *Organometallics* 2014, **33**, 40−44.

53. M. Kedia, M. Priyatharsini, S. D. Sathiyashivan, B. Shankar, R. V. Krishnakumar and M. Sathiyendiran, *J. Organomet. Chem*. 2022, **959**, 122123−122129.
54. U. Phukon, M. Priyatharsini and M. Sathiyendiran, *J. Organomet. Chem.* 2020, **923**, 121460.
55. M. Sathiyendiran, C-C. Tsai, P. Thanasekaran, T. T. Luo, C. I.Yang, G. H. Lee, S. M. Peng, K. L. Lu, *Chem. Eur. J*. 2011, **17**, 3343–3346.
56. P. H. Dinolfo, M. E. Williams, C. L. Stern and J. T. Hupp, *J. Am. Chem. Soc*. 2004, **126**, 12989–13001.
57. D. Bhattacharya, M. Sathiyendiran, T. T. Luo, C. H. Chang, Y. H. Cheng, C. Y. Lin, G. H. Lee, S. M. Peng and K. L. Lu, *Inorg. Chem*. 2009, **48**, 3731–3742.
58. J. Xiong, W. Liu, Y. Wang, L. Cui, Y. Z. Li and J. L. Zuo, *Organometallics* 2012, **31**, 3938−3946.
59. G. H. Ning, L. Y. Yao, L. X. Liu, T. Z. Xie, Y. Z. Li, Y. Qin, Y. J. Pan and S. Y. Yu,. *Inorg. Chem*. 2010, **49**, 7783–92.
60. G. M. Sheldrick, Acta Crystallogr., Sect. A: Found. *Crystallogr*. 2008, **64**, 112−122.
61. G.M. Sheldrick, SHELXS-97: Program for Crystal Structure Solution, University of Göttingen, Göttingen, Germany, 1997.
62. G. R. Desiraju, *J. Chem. Soc., Dalton Trans*. 2000, 3745-3751.
63. B. Merillas, E. Cuéllar, A. Diez-Varga, T. Torroba, G. García-Herbosa, S. Fernández, J. Lloret-Fillol, J. M. Martín-Alvarez, D. Miguel and F. Villafañe, *Inorg Chem*. 2020, **59**, 11152–11165.
64. S. Horiuchi and K. Umakoshi, *Coord. Chem. Rev*. 2023, **476**, 214924.
65. M. Guerrero, J. Pons, V. Brabcgadell, T. Parella, X. Solans, M. Font-Bardia and J. Ros, *Inorg. Chem*. 2008, **47**, 11084–11094.
66. D. Samanta and P. S. Mukherjee, *Chem. Eur. J*. 2014, **20**, 12483–12492.
67. S. Ghosh and P. S. Mukherjee, *Organometallics* 2007, **26**, 3362–3367.
68. W. Wang, Y. X. Wang and H. B. Yang, *Chem. Soc. Rev.*, 2016, **45**, 2656–2693.
69. E. Benchimol, B. N. T. Nguyen, T. K. Ronson and J. R. Nitschke, *Chem. Soc. Rev*. 2022, **51**, 5101–5135.
70. A. Garci, S. Marti, S. Schurch and B. Therrien, *RSC Adv*. 2014, **4**, 8597–8604.
71. J. Bravo, S. Bolaño, L. Gonsalvi and M. Peruzzini, *Coord. Chem. Rev*. 2010, **254**, 555–607.

72. I. Chakraborty, S. J. Carrington, G. Roseman and P. K. Mascharak, *Inorg. Chem*. **2017**, *56*, 1534−1545.

73. A. Alguacil, F. Scalambra and A. Romerosa, *Inorg. Chem*. 2022, **61**, 5779–5791.

Chapter 4

Self-assembly of rhenium core-based conjoined bicyclic supramolecule from pyrazole and flexible hexatopic/tetratopic pyrazolyl ligands

Abstract

Bicyclic tetranuclear metallocycles (**1**-**3**) were synthesized using $Re_2(CO)_{10}$ and neutral hexatopic/tetratopic ligands (L^1 and L^2) and pyrazole/Br-pyrazole *via* one pot solvothermal approach. The two rhenium cores in each cycle is bridged by hydroxo and pyrazolate motif. These are the first examples of rhenium(I) based metallocycles with *fac*-[{$Re(CO)_3$}$_2$(μ-OH)(μ-pz)] unit. The complexes were characterized using spectroscopic techniques including X-ray diffraction analysis.

A portion of this work has been published in *J. Organomet. Chem.* **2020**, *8*, 41773–41784.

4.1. Introduction

The coordination driven self-assembly approaches i.e., metal-directed approaches for supramolecular coordination complexes (SCCs), discrete cyclic complexes, are highly successful methods to prepare simple mononuclear SCCs to complex interlocked SCCs.[1-5] Though many metal-directed synthetic rules are now known, continuous use of the known approaches in creating a new design principle to assemble new molecular architectures have been intensely going on due to their intricate architecture and application prospects in materials and medicinal fields. Among the many metal-directed approaches, the partially protected *fac*-$Re(CO)_3$-corner based assembly process using flexible multitopic ligands and neutral bridging ligands recently provided interesting spherical-shaped SCCs with multiple calixarene-shaped solvent accessible cavity on the surface.[4] In particular, tuning the coordinating units of hexatopic ligands remotely by either increasing the fused ring/substituting phenyl rings on imidazolyl yielded overall spheroid SCCs with/without solvent accessible cavity.[4] Tuning the imidazolyl unit by pyrazolyl unit in the hexatopic ligand may provide two kinds of SCCs. Spheroid shaped SCC with interconnecting calixarene cavities because of the adjacent arrangement of two heteroatoms in pyrazolyl. In the case of hexatopic imidazolyl/benzimidazolyl-based SCCs, the C-H unit (N-C_2H-N) of imidazolyl, which is directed into the spheroid, acts as a steric unit blocking the channel of the cavities.[4] The second option is hitherto unexplored SCC because the small change in the binding angle of the donor units in the ligand i.e., from imidazolyl to pyrazolyl, may direct different coordination angle to adjust octahedral geometry around the *fac*-$Re(CO)_3$ core. Herein a new serendipitously formed conjoined bicyclic complex with a new type of bonding combination with a flexible hexatopic ligand, pyrazole and *fac*-$Re(CO)_3$ from $Re_2(CO)_{10}$ is presented. Two new similar conjoined bicyclic complexes were also synthesized using tetratopic pyrazolyl based ligand, Br-pyrazole/pyrazole and $Re_2(CO)_{10}$ in a one-pot solvothermal process using toluene as solvent.

4.2. Experimental

4.2.1. Materials and Methods

$Re_2(CO)_{10}$, toluene, pyrazole, DMF, and NaOH were purchased from commercial sources and used as received. Hexakis(bromomethyl)benzene, and 1,2,3,4,5,6-hexakis((pyrazol-1-yl)methyl) benzene (L^1), 1,2,4,5-tetrakis((pyrazol-1-yl)methyl) benzene (L^2) were synthesized following literatures.[4,6] ATR-IR spectra were recorded on Nicolet iS5 IR spectrophotometer. ^{1}H-NMR spectra were recorded on a Bruker Avance III 500 MHz spectrometer. High resolution mass spectra (HR-MS) for ligand L^1, L^2 and complex **1**-**3** were measured on a Bruker maXis mass spectrophotometer.

4.2.2. Crystallography

Single crystal X-ray data of crystal of **1**-**3** were collected on a Bruker D8 QUEST diffractometer [λ(Mo Kα) = 0.71073 Å]. The structures were solved by direct methods using SHELXS-2014/5 (Sheldrick 2014) and refined using the SHELXL-2018/3 (Sheldrick, 2018) program (within the WinGX program package).[7] Non-H atoms were refined anisotropically.

4.2.3. Synthesis of Complexes

Synthesis of 1

A mixture of $Re_2(CO)_{10}$ (100.1 mg, 0.153 mmol), H-pyz (21.8 mg, 3.26 mmol) and L^1 (29 mg, 0.051 mmol), and undistilled toluene (15 mL) was taken in a Teflon flask that was placed in a steel bomb. The bomb was kept in an oven maintained at 160 °C for 48 h and then cooled to 25 °C. Good quality flower like uniform pale yellow single crystals of **1** (52.5 mg, 56%) were obtained. The crystals were separated by filtration and washed with toluene. ATR-IR (cm^{-1}) 2007, 1927 and 1865 (CO).

Synthesis of 2

A mixture of $Re_2(CO)_{10}$ (50 mg, 0.076 mmol), H-pz-Br (12.60 mg, 0.039 mmol), L^2 (15.50 mg, 0.085 mmol), and undistilled toluene (~8 mL) was taken in a Teflon flask that was kept in a steel bomb. The bomb was then kept in an oven maintained at 160° C for 48 hours and subsequently cooled to 30° C. Light yellow good quality crystals were obtained from the

mother liquor after a week. Yield: 34% (48 mg crystals). ATR–IR (cm^{-1}): 3581(s) (OH); 2006 (s) and 1862 (s) (C≡O).

Synthesis of 3

A mixture of $Re_2(CO)_{10}$ (100.9 mg, 0.015 mmol), H-pz (10.40 mg, 0.15 mmol), L^2 (30.50 mg, 0.076 mmol), and undistilled toluene (~12 mL) was taken in a Teflon flask that was kept in a steel bomb. The bomb was then kept in an oven maintained at 160° C for 48 hours and subsequently cooled to 30° C. Light yellow good quality crystals were obtained from the mother liquor after a week. Yield: 39% (50 mg crystals). ATR-IR (cm^{-1}): 3571(s) (OH); 2005 (s) and 1855 (s) (C≡O). HRMS-ESI (*m/z*): $[M + H]^+$ calcd for $C_{23}H_{19}N_6O_7Re_2$, 863.0397; found, 863.0405. ^{1}H NMR (500 MHz, $CDCl_3$): 8.18 (d, *J* = 2.1 Hz,4, H^A), 7.88 (s, 4H, H^e), 6.95 (d, *J* = 2.4 Hz, 4H, H^a), 6.92 (d, *J* = 13.3 Hz, 4H, H^d (-CH_2-)), 6.64 (d, *J* = 2.5 Hz, 4H, H^c), 6.42 (t, *J* = 2.18 Hz, 2H, H^B), 5.79 (t, *J* = 2.5 Hz, 4H, H^b), 5.2 (d, *J* = 13.5 Hz, 4H, H^d (-CH_2-)).

4.3. Results and discussion

4.3.1. Synthesis and characterization of metallocycle 1.

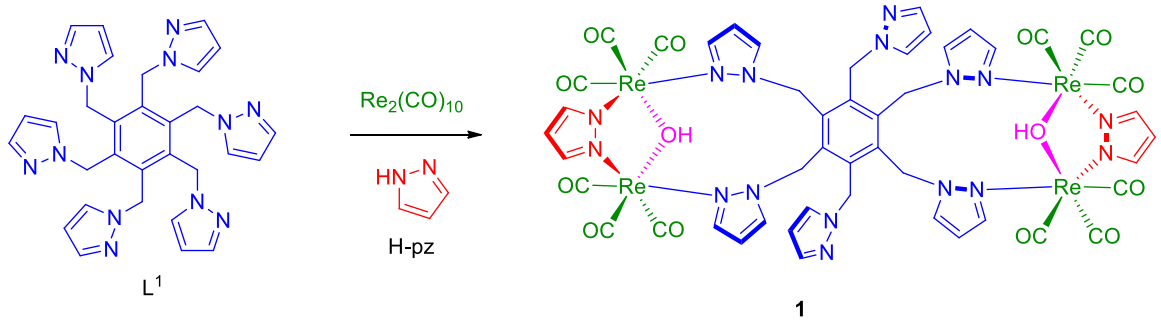

Scheme 4.1. Synthesis of metallocycle **1.**

Self-assembly of $Re_2(CO)_{10}$, L^1 and pyrazole (H-pz), in toluene by solvothermal approach resulted in complexes **1.** (Scheme 4.1) The product is air and moisture-stable and soluble in DMSO. The ATR-IR spectrum of the complex displayed three strong bands (1865, 1927, and 2007 cm^{-1}), which are the characteristic peaks for the *fac*-$Re(CO)_3$ core in the complex.

Further, the IR spectrum of crystal of **1** shows a sharp band at 3556 cm^{-1}, indicating the presence of hydroxyl group (Figure 4.1). The ^{1}H NMR spectrum of crystals of **1** in d_6-DMSO showed mutiple signals in the region of 8.1 to 5.0 ppm in contrary to simple pattern expected for a symmetrical arrangement of pyrazolyl and pyrazolate motifs (Figure 4.2). Though the complex contains three kinds of pyrazole motifs in the form of coordinated anionic pyrazolate, coordinated neutral pyrazolyl and uncoordinate pyrazolyl motifs, eight kinds of chemically different protons are expected. Though attempts were made to assign the protons singnals of these three motifs in **1**, it become fruitless. However, the ^{1}H NMR spectrum of **1** in d_6-DMSO at 60 °C displayed less signals compared to that of the spectrum of **1** at 25 °C (Figure 4.3). It is possible that the complex exists in various conformers in the solution which do not interchange fast-enough in the NMR time scale at 25 °C. However, few conformers of **1** may interchange in the solution at 60 °C.

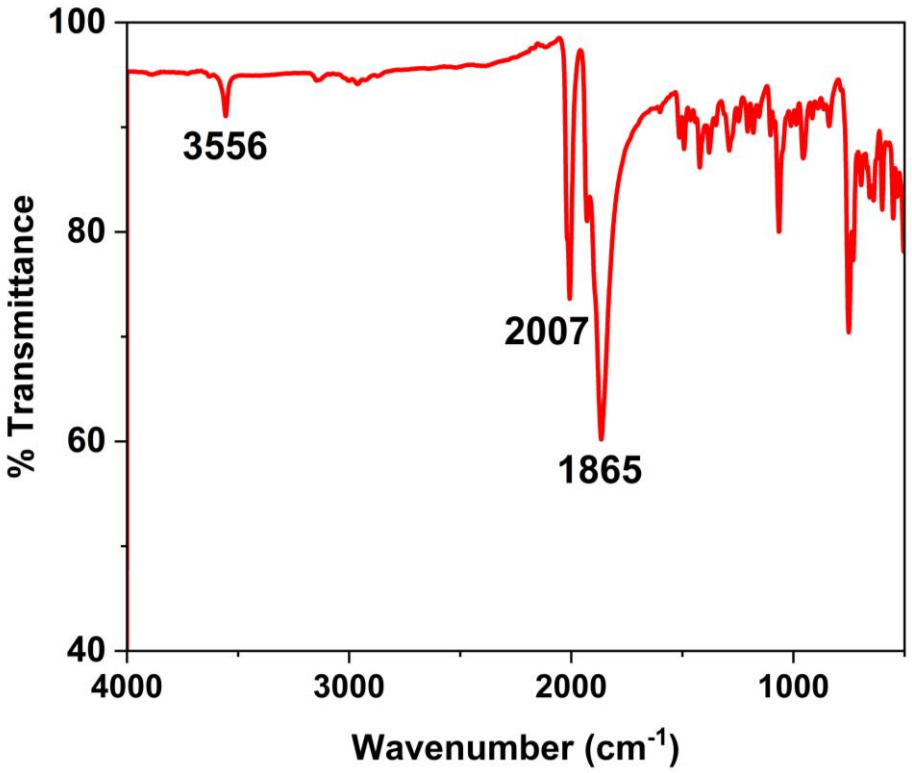

Figure 4.1. ATR-IR spectrum of **1.**

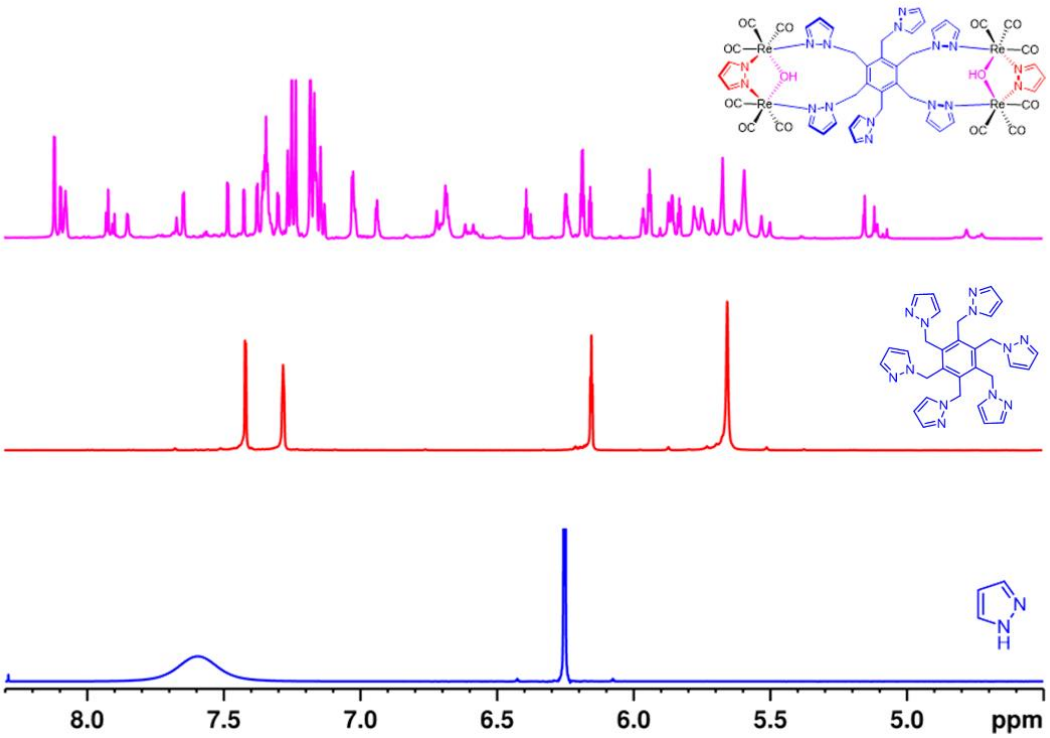

Figure 4.2. Partial ^{1}H NMR spectra of **1,** L^{1} and pyrazole in DMSO–d_6.

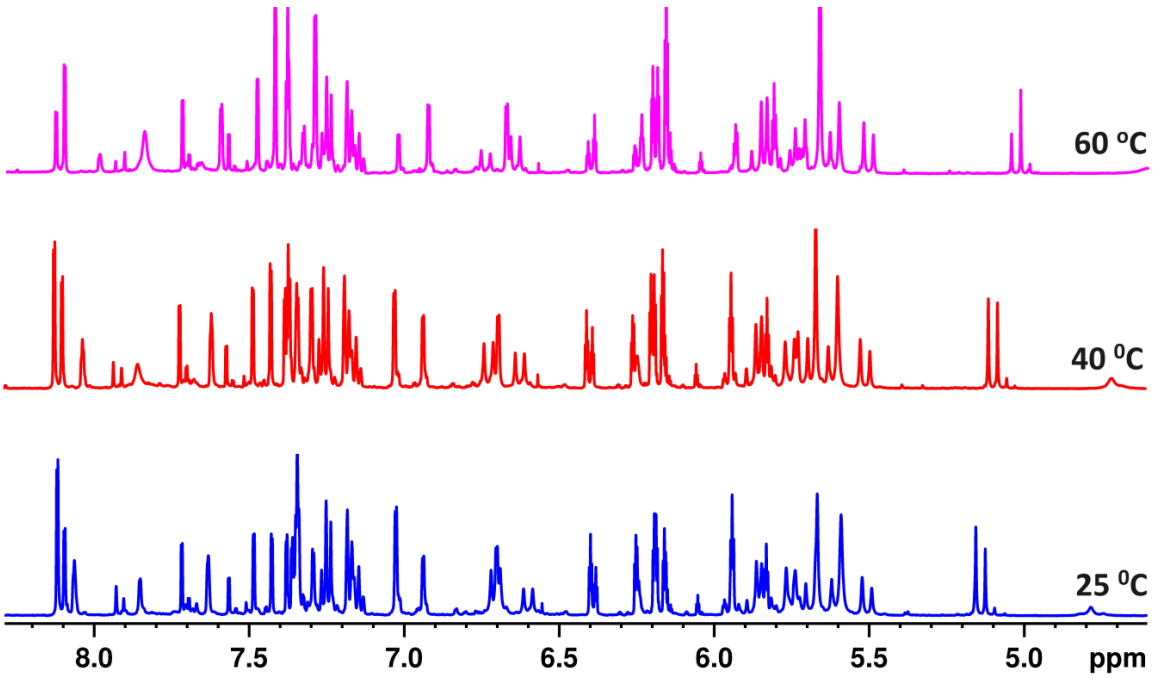

Figure 4.3. Partial ^{1}H NMR spectra of **1** at variable temperature in DMSO–d_6.

4.3.2. Molecular structure of metallocycle 1.

A single crystal X-ray diffraction analysis of **1** reveals that it consists of four *fac*-$Re(CO)_3$ cores, two anionic pyrazolate units, two hydroxyl ions, and one hexatopic pyrazolyl ligand. The complex **1** contains two metallacyclic units that have one common phenylene framework and can be regarded as conjoined bicyclic supramolecular coordination complex (Figure 4.4).[4-5,2f] Each cyclic motif of **1** contain two *fac*-$Re(CO)_3$ motifs which are bridged by both a pyrazolate (k^1:k^1-μ-pz) and a hydroxyl ion (μ^2-OH). Two *ortho* pyrazolyl units of the hexatopic ligand coordinated to the dimeric unit, *fac*-[{$(Re(CO)_3)_2(\mu^2$-OH)(k^1:k^1-μ-pz)}$_2$], resulting the cyclic structure. Both the cyclic motifs take "Z"–type *trans* arrangement in **1**. The two bond distances of $Re–N_{(pyrazolate)}$ (2.154(10) and 2.148(9) Å) indicates that the pyrazolate coordinated to two rhenium atoms symmetrically. Similarly, the hydroxyl ion is coordinated the two Re atoms symmetrically ($Re–O_{(OH)}$ = 2.146(7) and 2.150(7) Å).[6] The bond distances observed in **1** is similar to the previously known $Re(CO)_3$-core based complexes/SCCs.[9] The $Re–N_{(pyrazolyl)}$ distances (2.219(8) and 2.230(8) Å) are slightly larger than that of the $Re–N_{(pyrazolate)}$ but within the range normally found in $Re–N_{(neutral)}$ coordination mode. The distance between the two rhenium atoms in the cyclic motif is 3.790 Å. The two pyrazolyl units are parallel to each other with the centroid to the centroid distance of 3.513 Å (dihedral angle = 14°), suggesting the presence of the intramolecular π···π stacking interactions. Two pyrazolyl, a pyrazolate and the central benzene ring of hexatopic ligand provide partial cone-shaped calix[4]arene structure i.e., metallacalix[4]arene to the cyclic motif of **1**.[4] The cavity of cyclic unit is reduced due to the intramolecular π···π interactions between the pyrazolyl motifs. The hexatopic ligand used its four pyrazolyl units for making two cyclic motifs. The remaining two uncoordinated pyrazolyl units of the hexatopic ligand are arranged in the *para* position (1,4-position) in phenylene unit of **1**. The uncoordinated pyrazolyl units are away from the centre of the molecule. Overall, the six pyrazolyl motifs in the hexapodal ligand are arranged *syn*,*syn*,*syn*, *anti*,*anti*,*anti*-orientation in **1**. It is well known that neutral poly-pyrazolyl donors/pyrazoly/pyrazolate based *fac*-$Re(CO)_3$ complexes are well known.[9] The interactions of solvent toluene molecules with the pseudo-calixarene structure are shown in the (Figure 4.4d) The methyl group of the toluene contacts with the basal benzene of **1** via the C–H···π contacts (C28···C14, d = 3.450 Å; C28–H···C14, d = 2.736 Å, and C28–H···C14 = 131°). In addition, the toluene has contacts with carbonyl oxygen atoms (C28(H)···O3, d = 3.594 Å and C28(H) ···O4, d = 3.168 Å). To the best of our

knowledge, the dinuclear cyclic unit, *fac*-[{Re(CO)$_3$}$_2$(μ-OH)(μ-pz)] for making any kind of Re(CO)$_3$-core based supramolecular coordination complexes are scarce.[3-5] Up to now, the *fac*-Re(CO)$_3$-core based SCCs use either an organic bis-chelating ligands including symmetrical (N∩N-N∩N/ N∩O-N∩O/O∩O-O∩O) and asymmetrical motif (N∩N-N∩C) or symmetrical "μ^2-XR (X = O/S/Se and R = H/alkyl/CH$_2$Ar; Ar = aryl/heteroaryl) motifs for making the *fac*-Re(CO)$_3$-core based SCCs.[3-5] However, the SCCs based on rigid ditopic/tritopic ligands having pyrazole donor units have been emerging with other metal ions recently.[2e]

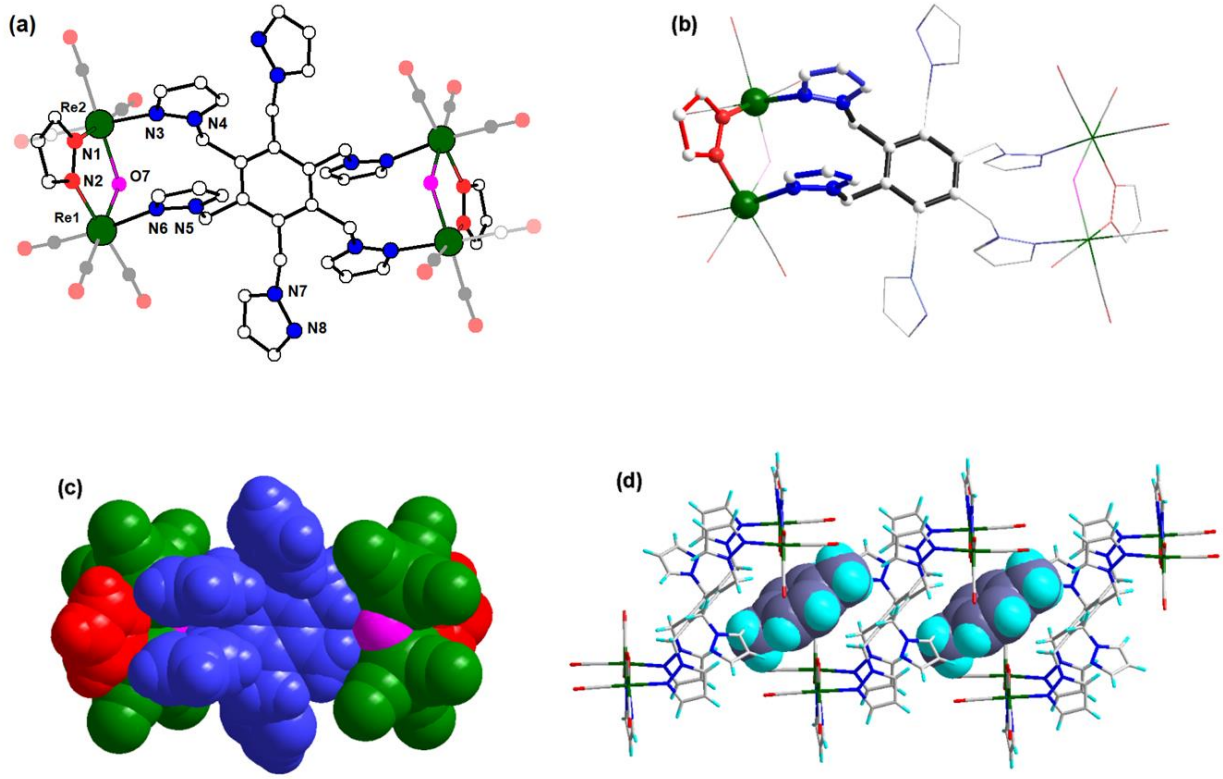

Figure 4.4. Molecular structure of **1.** (H atoms are omitted for clarity (a-b); six CO units are shown in dull color (a); one of the partial cone-shaped calix[4]arene unit, metallacycles, is shown in ball and thick stick model (b); space-filling view of **1** showing Re(CO)$_3$ in green, pyrazolate in red, oxygen of OH in rose, and hexatopic N donor in blue (c); three adjacent SCCs of **1** with two lattice toluene molecules (space-filling view) and toluene appears as *p*-xylene due to symmetry operation).

It is worth to mention that the core [(Re(CO)$_3$)$_2$(μ-OH)(μ-pz)] in **1** is structurally similar to a well-studied complexes, *cis*-[{Pt(NH$_3$)$_2$}$_2$(μ-OH)(μ-pz′)](NO$_3$)$_2$ (**I-II**, where pz = pyrazolate for **I**, and pz = 1,2,3-triazolate for **II**). The complexes **I-II** are well studied and are known to display cytotoxicity on numerous human tumor cell lines. The coordinated hydroxo anion of

I-II is believed to be a leaving motif thus creating two vacant sites in **I-II** for coordination on DNA.[10] The *fac*-$Re(CO)_3$-core based complexes have been emerging the potential molecules for a various medicinal fields.[11] Therefore, we believe that complexes like **1-3** may be biologically active due to the structural similarities to complexes **I-II**.

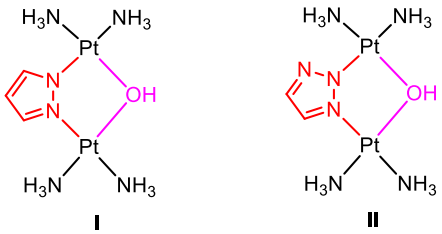

4.3.3. Synthesis and characterization of metallocycle 2-3.

In order to check if the multiple ^1H NMR peaks in complex **1** is due to presence of isomers in solution owing to two uncoordinated pyrazolyl motifs or due to dynamic nature of metal-pyrazolyl bonds, a tetratopic pyrazolyl based ligand (L^2) was synthesized. Self-assembly of $Re_2(CO)_{10}$, L^2 and pyrazole (H-pz)/Br-pyrazole(Br-pz) in toluene by solvothermal approach resulted in complexes **2** and **3** respectively. The FT-IR spectrum of the complexes displayed two strong bands in the region (1855and 2007 cm^{-1}), which are the characteristic peaks for the *fac*-$Re(CO)_3$ core in the complexes. Further, the IR spectrum shows a sharp band at 3581 cm^{-1} for crystal of **2** and 3571 cm^{-1} for **3** indicating the presence of hydroxyl group (Figure 4.5-4.6).

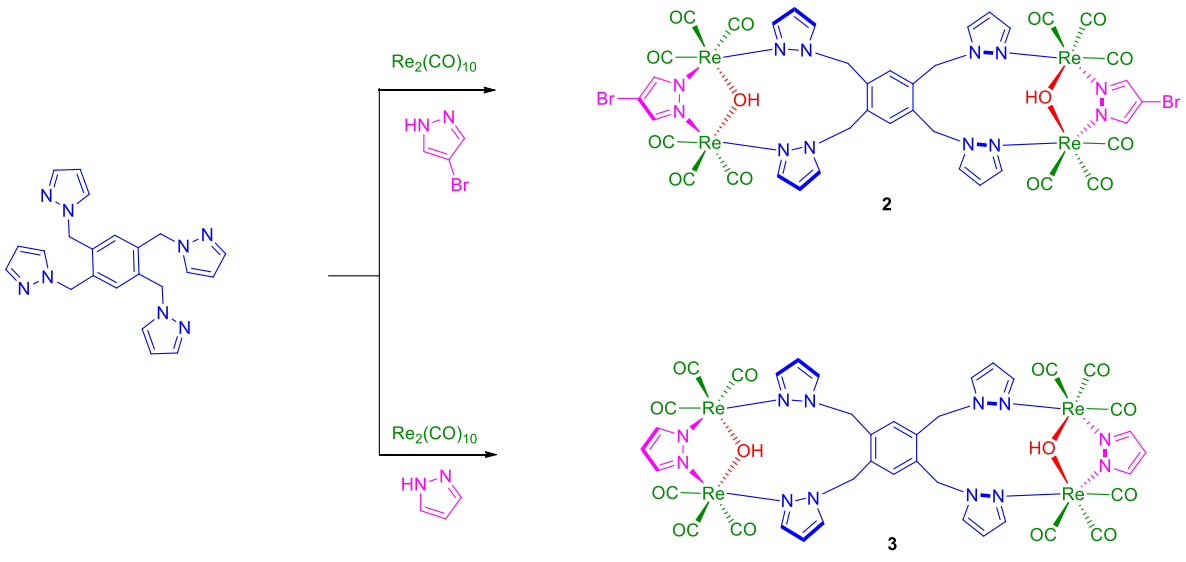

Scheme 4.2. Synthesis of metallocycles **2** and **3**.

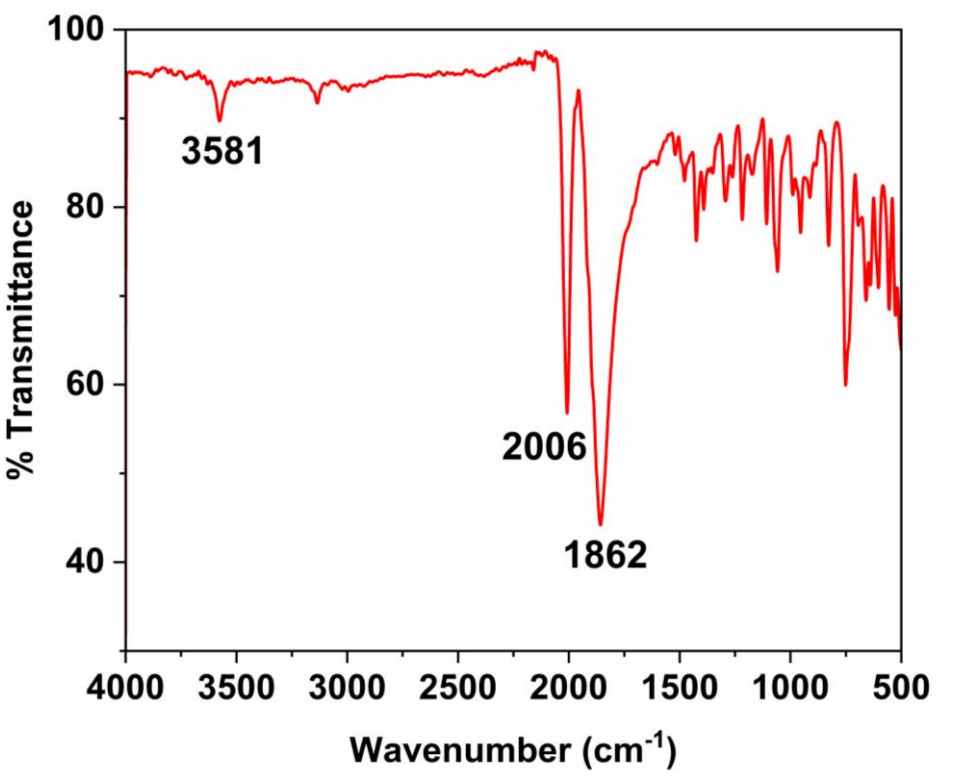

Figure 4.5. ATR-IR spectrum of **2**.

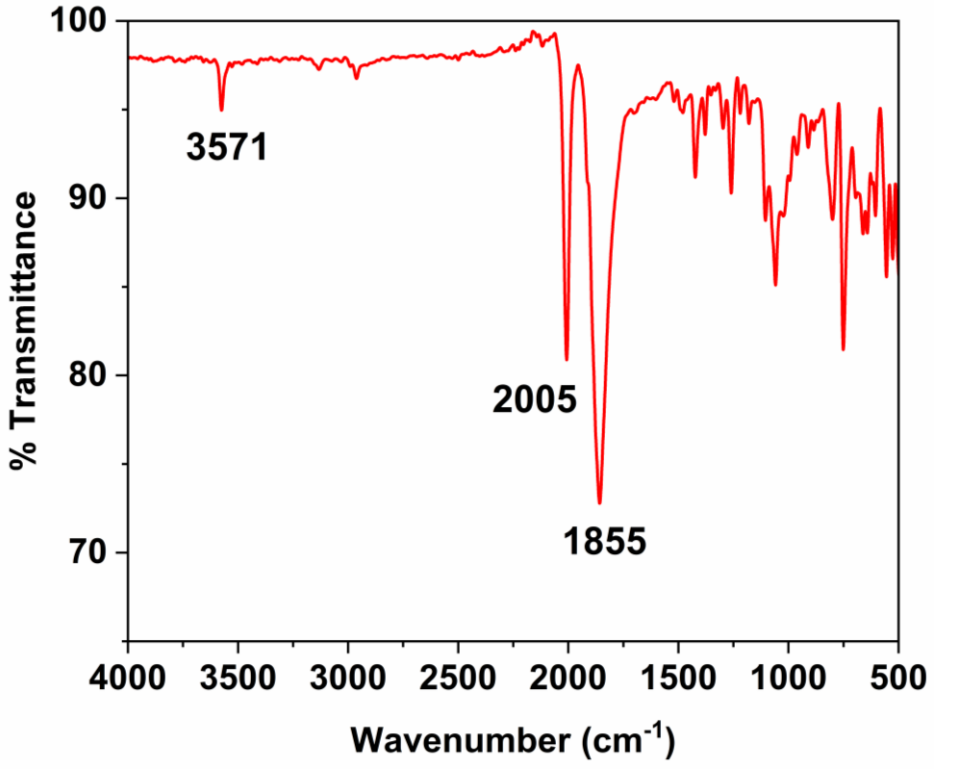

Figure 4.6. ATR- IR spectrum of **3**.

4.3.4. Molecular structure of metallocycle 2 and 3.

Suitable crystals for SC-XRD analysis was obtained from the bomb itself. The XRD data reveals the molecular structure of **2** and **3** consist of four *fac*-$Re(CO)_3$ cores, two anionic Br-pyrazolate units for **2**/pyrazolate units for **3**, two hydroxyl ions, and one tetratopic pyrazolyl ligand (Figure 4.7-4.8). In each case two metallacyclic cores are present which are connected through one common phenylene framework leading to the formation of a conjoined bicyclic architecture. Each cyclic motif contains two *fac*-$Re(CO)_3$ motifs which are bridged by both Br-pyrazolate for **2**/pyrazolate for **3** and a hydroxyl ion. The two cyclic motifs are arranged in *trans* arrangement leading to a "Z"–type arrangement in complexes **2** and **3**. The two bond distances of $Re–N_{(pyrazolate)}$ (2.130 Å for **2** and 2.164 Å for **3**) indicates that the azolate coordinated to two rhenium atoms symmetrically. Similarly, the hydroxyl ion is coordinated to the two Re atoms symmetrically ($Re–O_{(OH)}$ = 2.157 Å for **2** and 2.159 Å for **3**). The $Re–N_{(pyrazolyl)}$ distances (2.230 Å for **2** and 2.227 Å for **3**) are slightly larger than that of the $Re–N_{(pyrazolate)}$ but within the range normally found in $Re–N_{(neutral)}$ coordination mode. In each cycle the two pyrazolyl motifs are parallel to each other and stabilized via intramolecular π···π stacking interactions with centroid to the centroid distance of 3.274 Å for **2** and 3.408 Å for **3** respectively. The two rhenium atoms in each cycle are separated by a distance of 3.843 Å in both the complexes. Similar to complex **1** the cavity of cyclic unit in **2-3** is reduced due to the intramolecular π···π interactions between the pyrazolyl motifs.

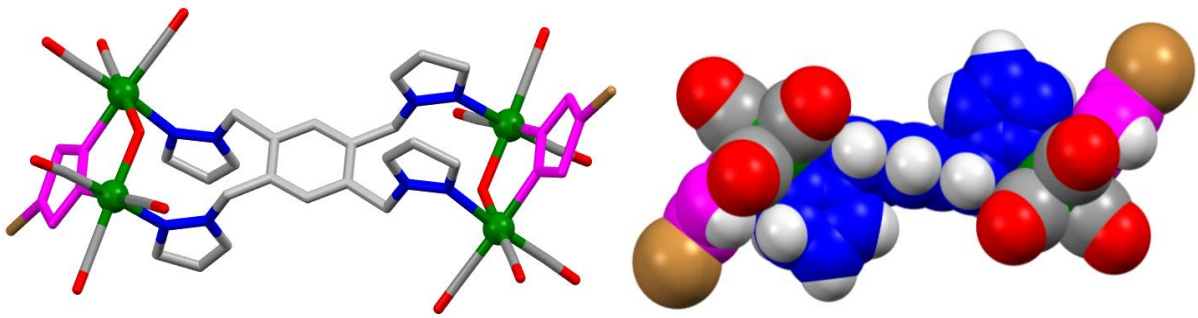

Figure 4.7. Molecular structure of **2** in capped stick (H atoms are removed for clarity) and spacefill model**.** Color code: C = grey for L^2 & pink for Br-pz and CO; Re = green; H = white; N = blue for L^2 & pink for Br-pz; O = red & Br = golden.

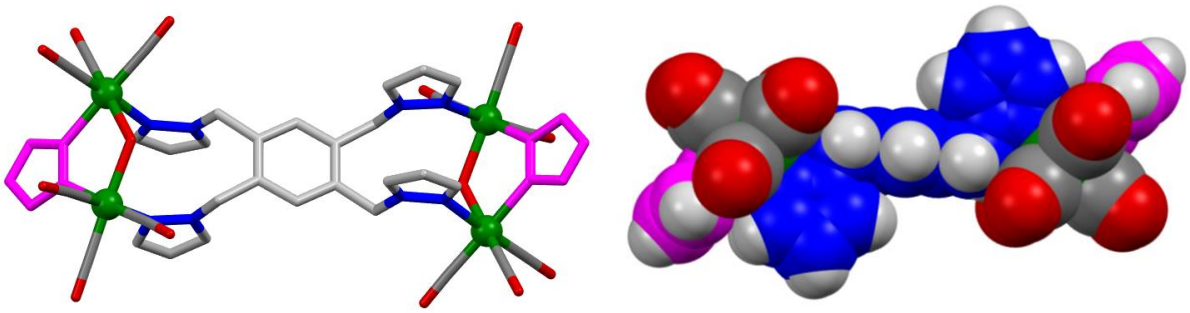

Figure 4.8. Molecular structure of **3** in capped stick (H atoms are removed for clarity) and spacefill model**.** Color code: C = grey for L^2 & pink for pz and CO; Re = green; H = white; N = blue for L^2 & pink for pz & O = red.

4.3.5. ^{1}H NMR spectra of metallocycles 2 and 3.

The ^{1}H NMR spectrum of crystals of **2** in d_6-DMSO showed mutiple signals in the region of 8.1 to 4.8 ppm in contrary to simple pattern expected for a symmetrical arrangement of pyrazolyl and pyrazolate motifs (Figure 4.9). In an ideal situation the complex NMR patterns should contain coordinated anionic pyrazolate and coordinated neutral pyrazolyl ligand peaks. More number of proton peaks were observed, which upon closer look revealed that free pyrazolyl ligand peaks are also present in the solution. Similar kind of peaks were also observed for complex **3** with presence of free tetratopic ligand peaks in d_6-DMSO (Figure 4.10). However complex **3** is also found to be soluble in $CDCl_3$, and the ^{1}H NMR spectrum recorded in $CDCl_3$ showed the presence of only complex peaks with no free ligand peaks (Figure 4.11-4.12). So, the protons associated with free ligand peaks in d_6-DMSO solution is may be because of decomposition of a certain amount of the complexes in d_6-DMSO solution.

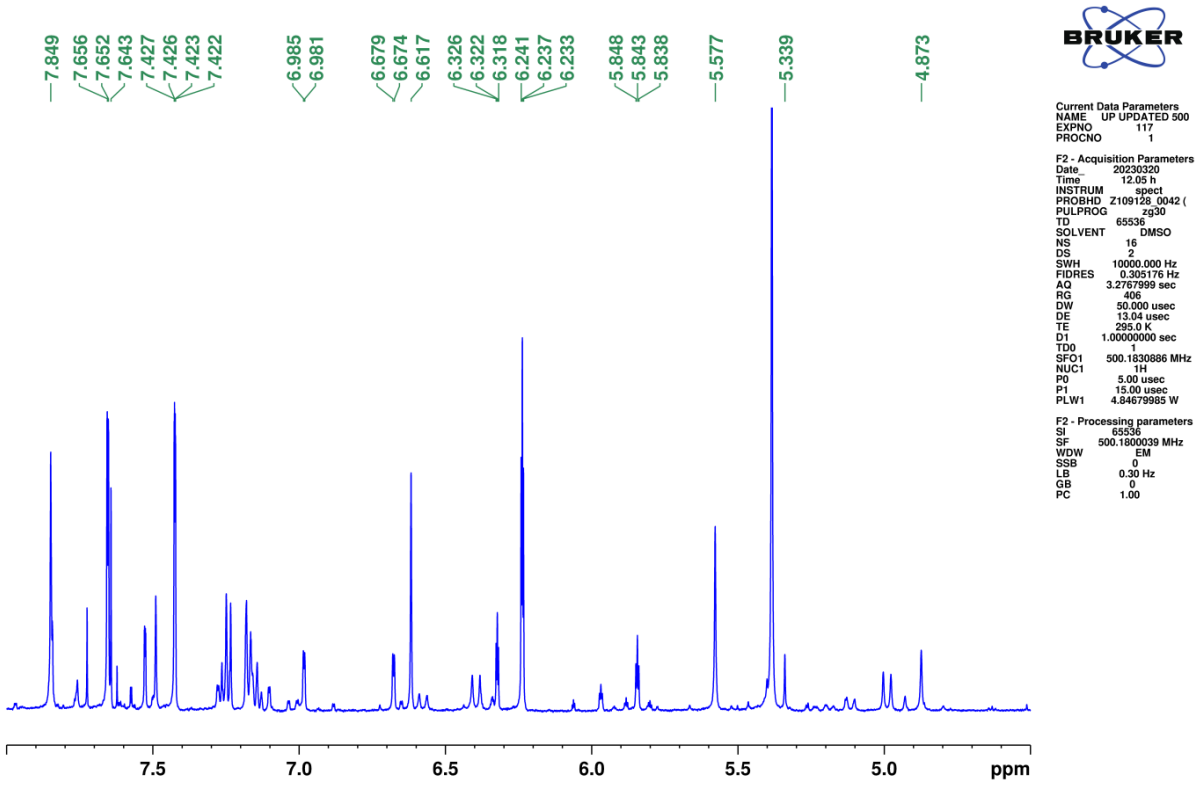

Figure 4.9. Partial ^{1}H NMR spectrum of **2** in DMSO–d_6.

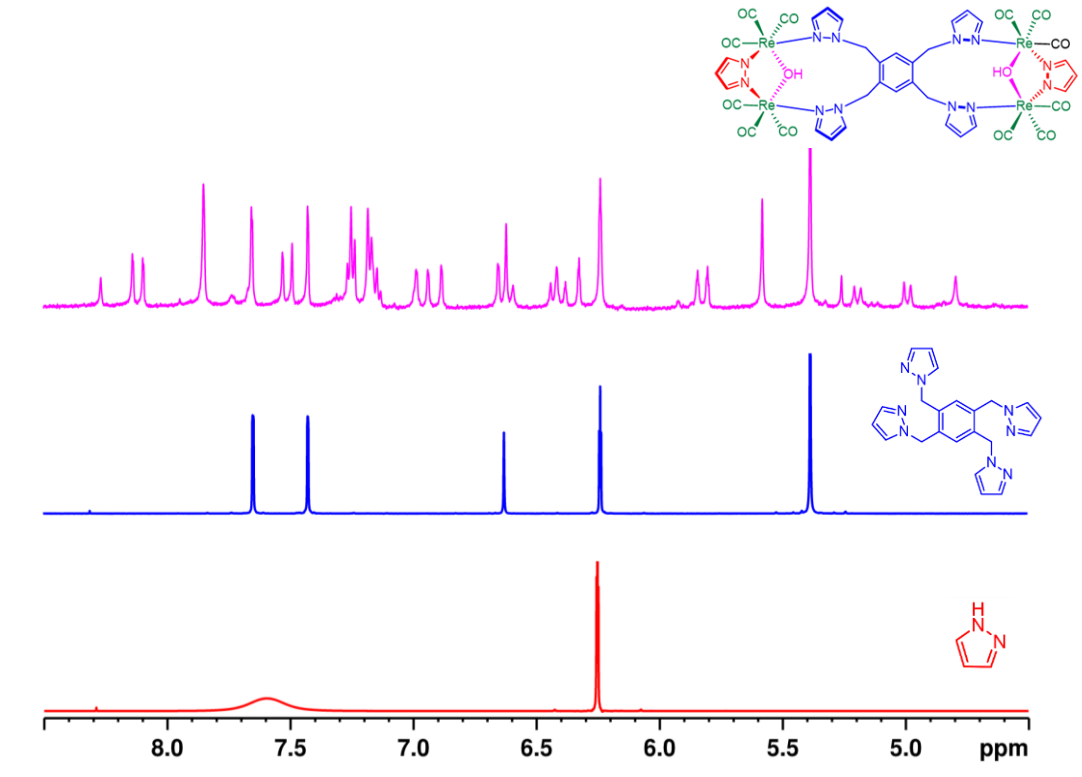

Figure 4.10. Partial ^{1}H NMR spectra of **3**, L^2 and pyrazole in DMSO–d_6.

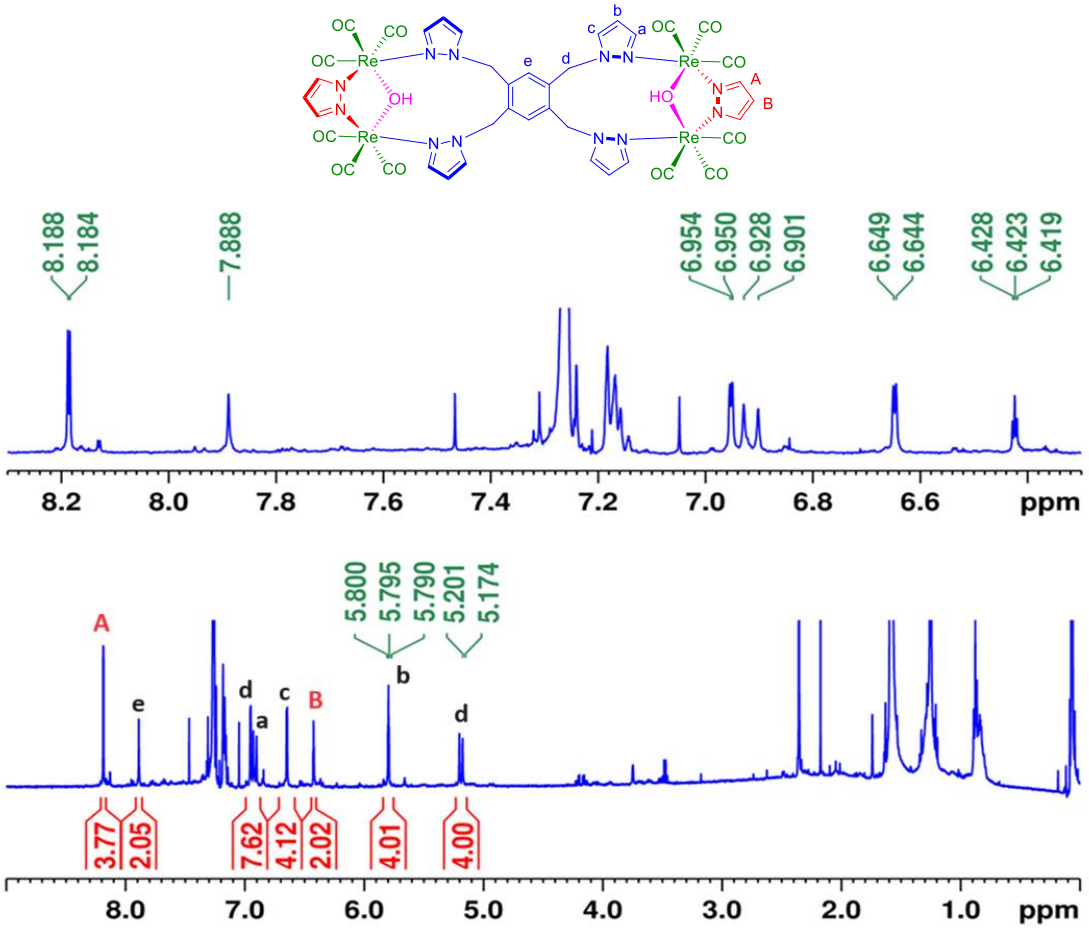

Figure 4.11. Partial ^{1}H NMR spectra of **3** in $CDCl_3$.

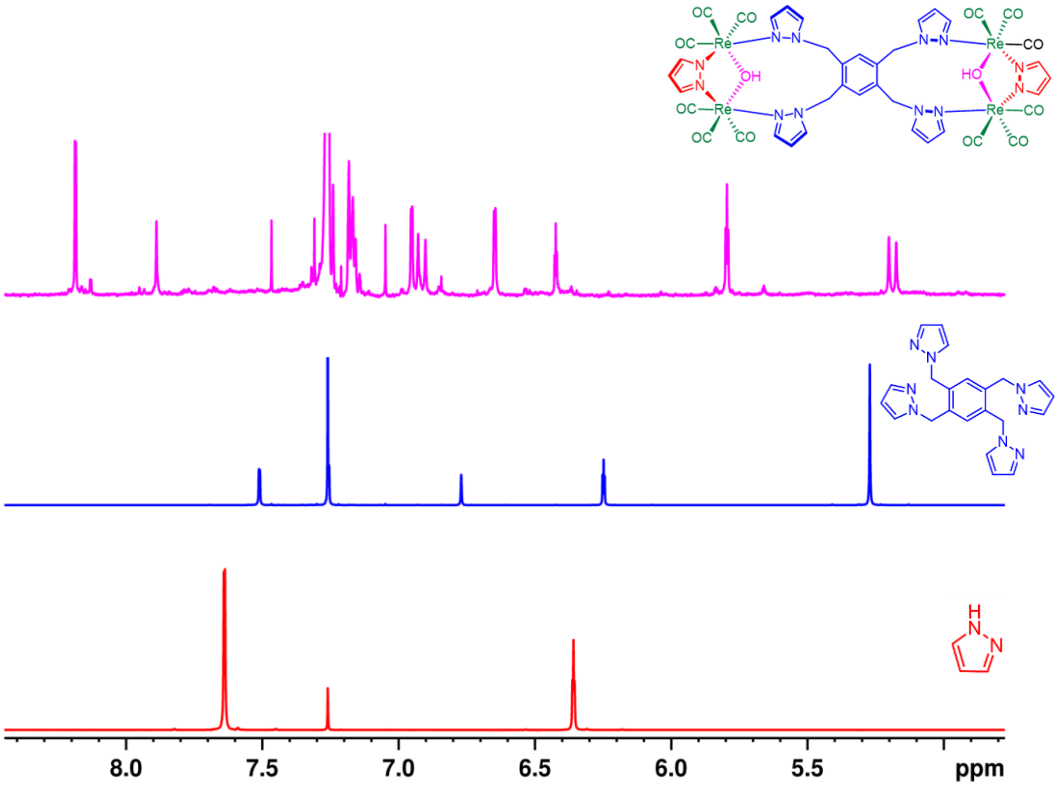

Figure 4.12. Partial ^{1}H NMR spectra of **3**, L^2 and pyrazole in $CDCl_3$.

4.4 Conclusion

In conclusion, neutral conjoined bicyclic supramolecular coordination complexes were assembled using the new type of metal-ligand bonding combinations, partially protected tritopic metal acceptor *fac*-$Re(CO)_3$-core, pyrazolate rigid bridging N-donor, hydroxyl (OH) bridging motif, and neutral flexible hexatopic/tetratopic pyrazolyl ligand. The bridging between two *fac*-$Re(CO)_3$ core is through azolato and hydroxo motif leading to the $[Re(CO)_3(\mu^2\text{-}OH)(\mu\text{-}pz)Re(CO)_3]$ core.

4.5 References

1) J. M. Lehn, Supramolecular Chemistry, Concepts and Perspectives, VCH, Newyork, 1995; (b) J. F. Stoddart, *Angew. Chem., Int. Ed*. 2017, **56** , 11094; (c) J. P. Sauvage, *Angew. Chem., Int. Ed*. 2017, **56,** 11080; (d) B. L. Ferringa, *Angew. Chem., Int. Ed.* **2017**, **56,** 11060; (e) R. Chakrabarty, P. S. Mukherjee and P. J. Stang, *Chem. Rev*. 2011, **111**, 6810 and references therein; (f) D. Fujita, Y. Ueda, S. Sato, N. Mizuno, T. Kumasaka and M. Fujita, *Nature*, 2016, **540,** 563 and references therein; (g) B. J. Holliday and C. A. Mirkin, *Angew. Chem. Int. Ed*. 2001, **40,** 2022.

2) (a) Y. Lu, H. N. Zhang and G. X. Jin, *Acc. Chem. Res*. 2018, **51**, 2148; (b) C. J. Brown, F. D. Toste, R. G. Bergman and K. N. Raymond, *Chem. Rev.* 2015, **115,** 3012; (c) Z. He, W. Jiang and C.A. Scalley, *Chem. Soc. Rev*., 2015, **44,** 779; (d) N. J. Young and B. P. Hay, *Chem. Commun*., 2013, **49,** 1354; (e) Y. Cui, Z. M. Chen, X. F. Jiang, J. Tong and S. Y. Yu, *Dalton Trans.*, 2017, **46,** 5801; (f) S. Samantray, S. Krishnaswamy and D. K. Chand, *Nat. Commun*. 2020, **11,** art. no. 880.

3) (a) P. H. Dinolfo and J. T. Hupp, *Chem. Mater*. 2001, **13,** 3113; (b) P. Thanasekaran, R. T. Liao, Y. H. Liu, T. Rajendran, S. Rajagopal and K. L. Lu, *Coord. Chem. Rev*. 2005, **249,** 1085; (c) P. Thanasekaran, C. C. Lee and K. L. Lu, *Acc. Chem. Res.* 2012, **45,** 1403; (d) A. Kumar, S. S. Sun and A. J. Lees, *Coord. Chem. Rev*. 2008, **252,** 922; (e) D. Gupta and M. Sathiyendiran, *ChemistrySelect*, 2018, **3**, 7439; (f) S. Sato and O. Ishitani, *Coord. Chem. Rev*. 2015, **282,** 50.

4) (a) B. Shankar, R. Marimuthu, S. D. Sathiyashivan and M. Sathiyendiran, *Inorg. Chem.* 2016, **55**, 4537; (b) B. Shankar, P. Elumalai, S. D. Sathiyashivan and M. Sathiyendiran, *Inorg. Chem*. 2014, **53,** 10018; (c) P. Elumalai, R. Kanagaraj, R. Marimuthu, B. Shankar, A. C. Kalita and M. Sathiyendiran, *Dalton Trans.*, 2015, **44**, 11274.

5) (a) B. Shankar, P. Elumalai, R. Shanmugam, V. Singh, D. T. Masram and M. Sathiyendiran, *Inorg. Chem*. 2013, **52,** 10217; (b) B. Shankar, R. Arumugam, P. Elumalai and M. Sathiyendiran, *ACS Omega*, 2016, **1**, 507; (c) P. Rajakannu, P. Elumali, F. Hussain and M. Sathiyendiran, *J. Orgomet. Chem.* 2013, **725,** 1.

6) N. Koch and M. Mazik, *Synthesis* 2013,**45,** 3341.

7) (a) G.M. Sheldrick, A short history of SHELX, ActaCrystallogr. A64 (2008) 112-122; (b) L.J. Spek, Single-crystal structure validation with the program PLATON, Appl. Crystallogr. 2003, **36,** 7-13.

8) (a) B. L. Murphy, S. C. Marker, V. J. Lambert, J. J. Woods, S. N. MacMillan and J. J. Wilson, *J. Orgomet. Chem*. 2020, **907**, 121064.

9) (a) M. A. Halcrow, *Dalton Trans*., 2009, 2059; (b) Y. Cui, Z. M. Chen, X. F. Jiang, J. Tong and S. Y. Yu, *Dalton Trans.*, 2017, **46,** 5801; (c) J. Pérez and L. Riera, *Eur. J. Inorg. Chem*. 2009, 4913; (d) R. F. Semeniuc and D. L. Reger, *Eur. J. Inorg. Chem*. 2016, 2253 and references therein; (e) G. A. Ardizzoi, G. LaMonica, A. Maspero, M. Moret and N. Masciocchi, *Eur. J. Inorg. Chem*. 1998, 1503.

10) (a) S. Kishimoto, M. Yasuda, R. Suzuki, S. Fukushima, *Biometals*, 2016, **29,** 1075; (b) S. Komeda, M. Lutz, A. L. Spek, Y. Yamanaka, T. Sato, M. Chikuma and J. Reedijk, *J. Am. Chem. Soc*. 2002, **124,** 4738; (c) S. Komeda, M. Lutz, A. L. Spek, A. V. Vargiu, A. Magistrato, *ChemMedChem*. 2014, **19**, 1966.

11) (a) E. B.Bauer, A. A. Haase, R. M. Reich, D. C. Crans and F. E. Kühn, *Coord. Chem. Rev.* 2019, **393,** 79; (b) A. A. Haase, E. B. Bauer, F. E. Kühn and D. C. Crans, *Coord. Chem. Rev.* 2019, **394,** 135; (c) F. L. Thorp-Greenwood, V. Fernandez-Moreira, C.O. Millet, C. F. Williams, J. Cable, J. B. Court, A. J. Hayes, D. Lloyd and M. P. Coogan, *Chem. Commun.* 2011, **47,** 3096; (d) M.P. Coogan, V. Fernandez-Moreira, B. M. Kariuki, S. J. A. Pope and F. L. Thorp-Greenwood, *Angew. Chem. Int. Ed.* 2009, **48,** 4965; (e) D. Gupta, V. Singh, S. Hohloch, M. Sathiyendiran, K. Tedin and B. Sarkar, *Polyhedron*, 2015,**100,** 243. (f) B. Ramakrishna, R. Nagarajaprakash, V. Veena, N. Sakthivel and B. Manimaran, *Dalton Trans*. 2015, **44,** 17629.

Chapter 5

Self-assembly of a new class of azolato bridged rhenium(I) metallocycles as anticancer agents

Abstract

The design, synthesis and biological studies of complexes that display anticancer activities are necessary to provide lead synthetic pathway to prepare drugs to reduce/completely avoid the serious side effects of Pt(II)-based drugs. A new type azolato and hydroxo bridged multicomponent rhenium metallocycles **1-4** were synthesized via self-assembly approach and characterized using analytical and spectroscopic techniques. The cytotoxity of these complexes against triple negative breast cancer cells (4T1) were studied. The complexes were found to display higher cytotoxicity against 4T1 cells than cisplatin.

5.1. Introduction

Small inorganic complexes such as cisplatin, carboplatin, and oxaliplatin are well-known frontline chemotherapeutic drugs used against various types of cancer cells. Because of the poor selectivity and severe side effects linked to these compounds, intense research has been going on for the design and synthesis of alternative metallodrugs.[1] Diverse metal ions including gallium, titanium, rhenium, ruthenium, palladium, platinum, silver, and gold have been used in the preparation of potential anticancer agents.[2-3] Among the metal complexes, rhenium complexes, particularly *fac*-[$Re(CO)_3$-based complexes are emerging as one of the promising class of anticancer agents with the potential to overcome the drawbacks of the Pt-based drugs.[4-7] Considerable research on acyclic *fac*-[$Re(CO)_3$ core-based complexes as anticancer agents have been explored, leading to initiation of clinical trials for fourteen Re complexes.[4d,5,6] Therefore, the design and synthesis of new cyclic rhenium complexes and their biological studies are of utmost importance in search of new class of anticancer metallodrugs.

Cancer is one of the most invasive diseases with the highest mortality rate. In particular, breast cancer is the leading cause of cancer death in women. New type of complexes as drugs are needed to treat the triple-negative breast cancer (TNBC) due to its exceptional aggressiveness, high metastatic potential, tendency for recurrence, poor prognosis and low survival rates.[8a] 4T1 cell line is genetically similar to human metastatic triple negative breast cancer cell which leads to over 17 % breast cancer cases annually.[8b] We rationalized that designing small 2D/3D metallocycle with properly positioned hydrogen bonding donors/acceptors would yield a molecule capable of fitting into DNA grooves and achieving stabilization through a cumulative network of non-covalent interactions, thus resulting in cancer cell death. Further, when designing new metallocycle as anticancer agent, it is important to take into consideration the cost-effectiveness of the starting materials and ease of synthesis. Till date, most of the *fac*-[$Re(CO)_3$-based acyclic and cyclic complexes studied for anticancer properties are assembled using 2,2′-bipyridine/1,10-phenonthroline/pyridyl as one of the main organic building units.[4,7a-c]

This study presents new type of small multi-component rhenium metallocycles which consists of azolate, hydroxyl, α,α′-bis(pyrazol-1-yl)-o-xylene (bpz)/1,2,-bis(benzimidazol-1-ylmethyl)benzene (XyBim) nitrogen donor, and two rheniumtricarbonyl groups. The metallocycle is self-assembled via multi-component coordination-driven self-assembly approach. The metallocycles **1-4** were found to show effective anticancer property against

triple negative breast cancer (TNBC) cells in vitro, exceeding that of cisplatin. Molecular docking studies of **1** with BDNA provided insights into the binding posture and nature of interactions with DNA.

5.2. Experimental

5.2.1. Materials and Methods

$Re_2(CO)_{10}$, pyrazole (H-pz), indazole (H-ind), 1,2-bis(bromomethyl)benzene, NaOH, tetrabutylammonium bromide (TBAB) and toluene were purchased and used as received. α,α'-Bis(pyrazol-1-yl)-*o*-xylene (bpz), 1,2-bis((benzo[d]imidazol-1-yl)methyl)benzene (XyBim) were prepared using a known procedure.[9] ATR-IR spectra were recorded on a Nicolet iS5 IR spectrophotometer. NMR spectra were recorded on a BrukerAvance III 500 MHz spectrometer. ESI-MS spectra were recorded on Bruker-maXis, mass spectrometer.

5.2.2 Crystallography

Single crystal X-ray data of **1** was collected on a Rigaku Oxford Diffractometer (λ(Mo Kα) = 0.71073 Å) and **2-3** were recorded on Bruker D8 QUEST diffractometer with Mo-Kα radiation (λ = 0.71073 Å). The molecular structures were solved by direct methods using SHELXS–97 (Sheldrick 2008) and refined using the SHELXL–2018/3 program (within the WinGX program package).[10-11] Non-H atoms were refined anisotropically.

5.2.3. Synthesis of Complexes

Synthesis of 1

A mixture of $Re_2(CO)_{10}$ (50 mg, 0.076 mmol), pyrazole (5.20 mg, 0.076 mmol), bpz (18.30 mg, 0.076 mmol), and undistilled toluene (~7 mL) was taken in a Teflon flask that was kept in a steel bomb. The bomb was then kept in an oven maintained at 160 °C for 48 hours and subsequently cooled to 30°C. Light yellow good quality crystals were obtained from the mother liquor after a week. Yield: 53% (35 mg crystals). ATR–IR (cm^{-1}): 3566(s) (OH), 2012 (s) (C≡O) and 1860 (s) (C≡O). HRMS-ESI (*m*/*z*): $[M + H]^+$ calcd for $C_{23}H_{19}N_6O_7Re_2$, 863.0397; found, 863.0405. ^{1}H NMR (500 MHz, $CDCl_3$): 8.16 (d, *J* = 2.1 Hz, 2H, H^A), 7.64 (m, 4H, H^{e-f}), 6.89 (d, *J* = 2.2 Hz, 2H, H^a), 6.74 (d, *J* = 13.45 Hz, 2H, H^d -CH_2-), 6.57 (d, *J* =

2.5 Hz, 2H, H^c), 6.38 (t, *J* = 2.05 Hz, 1H, H^B), 5.68 (t, *J* = 2.5 Hz, 2H, H^b), and 5.06 (d, *J* = 13.45 Hz, 2H, H^d -CH_2-).

Synthesis of 2

Brown crystals of **2** were obtained by following a similar synthetic approach to that for metallocycle **1**, using $Re_2(CO)_{10}$ (50 mg, 0.076 mmol), indazole (9.0 mg, 0.076 mmol), bpz (18.2 mg, 0.076 mmol), and undistilled toluene (~7 mL). Yield: 64% (45 mg crystals). ATR-IR (cm^{-1}): 3548(s) (OH), 2001 (s)(C≡O) and 1857 (s) (C≡O). HRMS-ESI (*m*/*z*): $[M + H]^+$ calcd for $C_{27}H_{21}N_6O_7Re_2$, 913.0559; found, 913.0542. ^{1}H NMR (500 MHz, $CDCl_3$): 8.85 (d, *J* = 2.1 Hz, 1H, H^A), 8.18 (d, *J* = 8.18 Hz, 1H, H^E), 7.81 (d, *J* = 8.15 Hz, 1H, H^B), 7.46 (merged, 4H, $H^{e,e',f,f'}$), 7.43 (merged, 2H, $H^{C,D}$), 6.81 (d, *J* = 2.15 Hz, 1H, H^a), 6.76 (dd, *J* = 2.9, 2H, H^d), 6.71 (d, *J* = 2.2 Hz, 1H, Ha'), 6.54 (t, *J* = 2.6 Hz, 2H, $H^{b,b'}$), 5.58 (t, *J* = 2.5 Hz, 1H, H^c), 5.55 (t, *J* = 2.5 Hz, 1H, $H^{c'}$), and 5.09 (dd, *J* = 2.9 Hz, 2H, $H^{d'}$).

Synthesis of 3

Yellow crystals of **3** were obtained by following a similar synthetic approach to that for metallocycle **1**, using $Re_2(CO)_{10}$ (50 mg, 0.076 mmol), pyrazole (5.20 mg, 0.076 mmol), XyBim (25.9 mg, 0.076 mmol), and undistilled toluene (~6 mL). Yield: 52% (38 mg crystals). ATR-IR (cm^{-1}): 3650(s) (OH), 2001 (s)(C≡O) and 1852 (s) (C≡O). HRMS-ESI (*m*/*z*): $[M + H]^+$ calcd for $C_{31}H_{23}N_6O_7Re_2$, 963.0715; found, 963.0698. ^{1}H NMR (500 MHz, DMSO-d_6): 7.73 (d, *J* = 2.1 Hz, 2H, H^A), 7.71-7.69 (m, 2H, H^{g-d}), 7.62-7.60 (m, 2H, H^h), 7.5-7.4 (m, 2H, H^{b-e}), 7.0 (t, 2H, H^c), 6.9 (t, 2H, H^d), 6.41 (s, 2H, H^a), 6.0 (t, 1H, H^B), 5.59 (d, 2H, H^f) and 5.22 (d, 2H, H^f).

Synthesis of 4

Golden yellow crystals of **4** were got by following a similar synthetic approach to that for metallocycle **1**, using $Re_2(CO)_{10}$ (50 mg, 0.076 mmol), indazole (9.00 mg, 0.076 mmol), XyBim (25.9 mg, 0.076 mmol), and undistilled toluene (~6 mL). Yield: 60% (47 mg crystals). ATR-IR (cm^{-1}): 3650 (s) (OH), 2003 (s)(C≡O), 1884 (s) (C≡O), and 1840 (s) (C≡O). HRMS-ESI (*m*/*z*): $[M + H]^+$ calcd for $C_{35}H_{25}N_6O_7Re_2$, 1013.0872; found, 1013.0891.

5.2.4. Biological Studies

Materials and Methods

Roswell Park Memorial Institute (RPMI) media, trypsin−EDTA, Dimethyl sulfoxide (DMSO), Phosphate buffer (pH 7.0), Tris-HCl buffer (pH 7.4), and US origin fetal bovine serum (FBS) were purchased from HiMedia Chemicals, Mumbai, India. Syringe filters (0.2 μm) were acquired from Sartorius (Carrigtwohill, Ireland). Milli-Q water was used from the Millipore, Billerica, MA system.

Cell lines and Maintenance

Murine mammary carcinoma cell line (4T1) was acquired from the National Center for Cell Science (NCCS), Pune, India. The cell lines were cultured and maintained in high glucose DMEM/RPMI media supplemented with 10% (v/v) FBS, 1% L-glutamine, and 100 U/streptomycin/penicillin at 37 °C in a humidified atmosphere with 5% CO_2. The final concentration of DMSO for the biological experiments is 0.1%.

Cell Viability on Tested Cancer Cells

The MTT assay was performed to determine the cell viability of **Re1** and ligand bpz in 4T1 cell lines. 96-well plates were seeded with 4T1 (7×10^3 cells/well), each with suitable growth media for the ambient environment. Fresh media containing various concentrations of **Re1**, bpz, and cisplatin were added to the well plates and maintained for 24 hours of incubation. Then, MTT reagent (5 mg/mL) was added and incubated for 3 hours. Then the MTT reagent supernatant was carefully removed, and the developed formazan crystals were neutralized by adding 1% DMSO to the wells. Using the microplate reader (BIORAD Microplate Reader), the absorbance of the dissolved formazan crystals was measured at 570 nm.

Circular dichroism

Solutions of metallocycle **1(**5 μM**)**, bpz (40 μM) and cisplatin (50 μM) with CT-DNA (100 μM of base pair equivalent to 0.064 mg/ml) was prepared. The CT-DNA stock solution was prepared in Tris-HCl (5 mM) buffer solution. A JASCO J-810 spectropolarimeter in a 0.2 cm cuvette, scanning from 210 to 300 nm, was used for recording the measurements. Baseline line corrections were done using the buffer solution and for each reading three cycles were performed.

Molecular docking and interaction analysis

Using the PDB ID:1BNA, the B-DNA dodecamer was retrieved from RCSB (https://www.rcsb.org/).[12] All the unwanted water and other molecules were removed. Then, using AutoDock Vina we docked the inhibitor metal complex with DNA. [13-14] The metal complex was docked considering a grid box with a dimension of X = 15.2 Å, Y = 19.9 Å, and Z = 8.9 Å created around the DNA. Based on the binding affinity, the best binding pose was determined by analyzing the top ten poses. Afterward, the DNA-inhibitor complex was subjected to interaction analysis using Discovery Studio Visualizer 4.5 (https://discover.3ds.com/discovery-studio-visualizer-download).

5.3. Results and discussion

5.3.1. Synthesis and characterization of metallocycle 1.

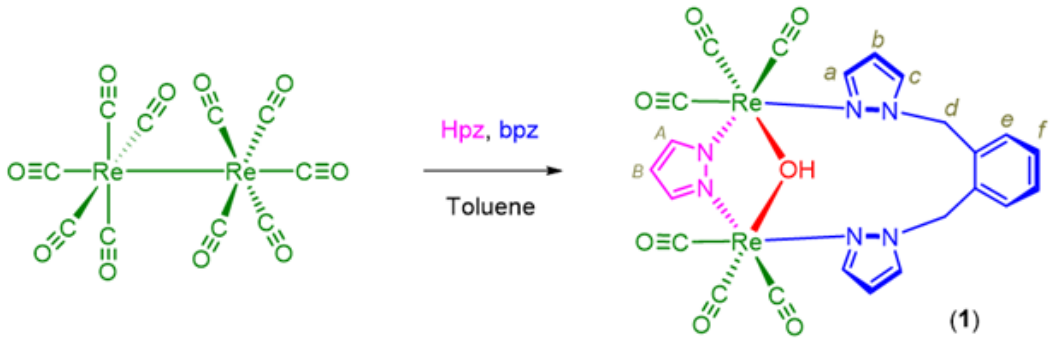

Scheme 5.1. Synthesis of metallocycle **1**

Metallocycle *fac*-[{Re(CO)$_3$}$_2$(μ_2-OH)(μ-pz)(bpz)] (**1**) was synthesized by treating $Re_2(CO)_{10}$, pyrazole (Hpz), bpz and undistilled toluene under solvothermal approach (Scheme 5.1). The complex is air and moisture stable. The IR spectrum of **1** displayed two strong bands at 2009 and 1862 cm^{-1} and a sharp single peak at 3560 cm^{-1}, characteristic of *fac*-Re(CO)$_3$ core and coordinated hydroxyl group, respectively (Figure 5.1). The ESI mass analysis of **1** displayed molecular ion peak (*m/z* = 863.0405 for [**1** + H]$^+$) that matches with the theoretical value (Figure 5.2-5.3). In ^{1}H NMR spectrum of **1** ($CDCl_3$) proton peaks are well resolved for both pyrazolate and bpz. The protons of the pyrazolate pyrazolate in **1** appeared as one sharp doublet and one triplet with 2:1 ratio, corresponding to H^A and H^B

protons. The H^A is significantly downfield shifted, whereas H^B is downfield shifted slightly relative to that of starting compound pyrazole (Hpz), suggesting the symmetric coordination of the pyrazolate to rhenium cores. Protons H^{a-c} of the pyrazolyl motifs were significantly upfield shifted, whereas H^{e-f} of phenyl spacer were merged and downfield shifted. The upfield shift for H^{a-c} indicated that the two pyrazolyl motifs in **1** are arranged in face-to-face manner closely having π···π contacts, thus these protons experience ring current effect. Two well-separated doublets (J = ~17 Hz) were observed for the methylene protons in **1**, suggesting that the protons are present in two different chemical environments. The above ^1H NMR results suggest that the cyclic structure of the compound remains intact in $CDCl_3$ solution (Figure 5.4-5.6).

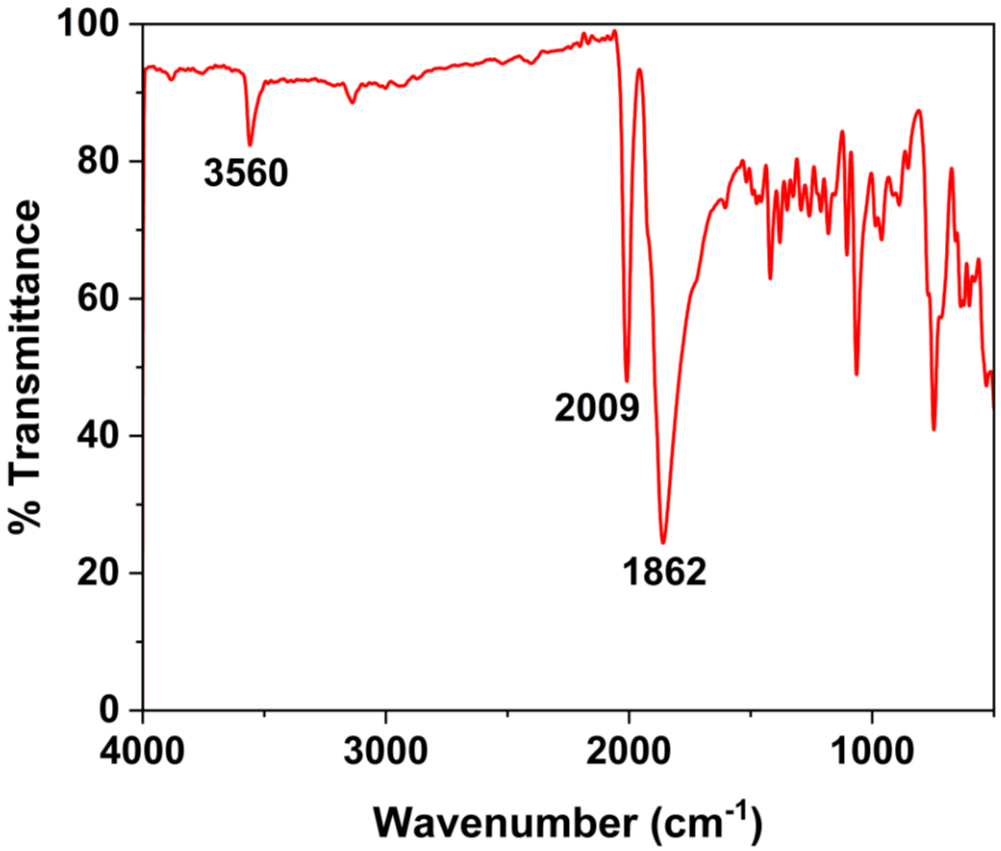

Figure 5.1. ATR-IR spectrum of **1**.

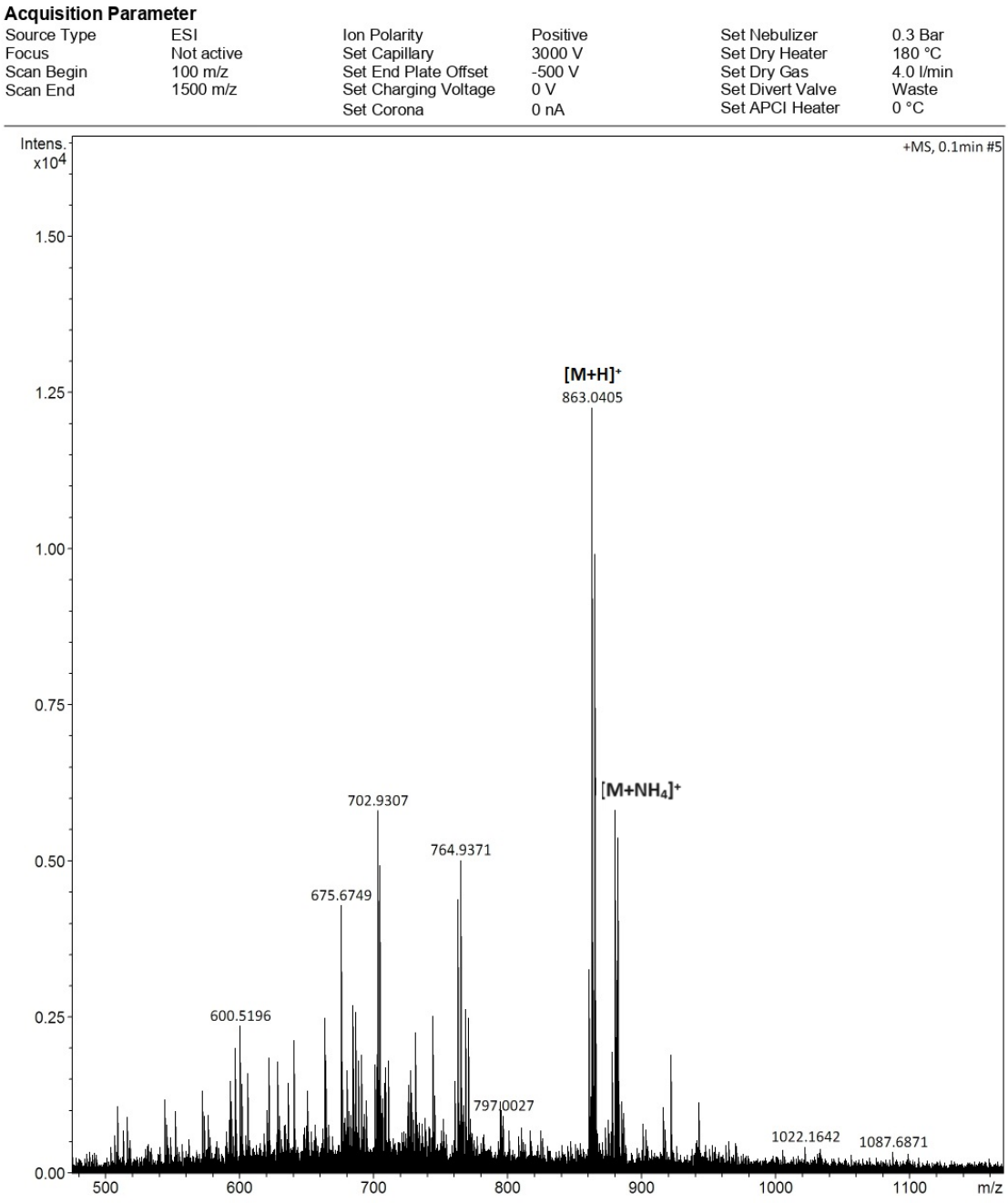

Figure 5.2. ESI mass spectrum of **1** in positive ion mode in $CDCl_3$.

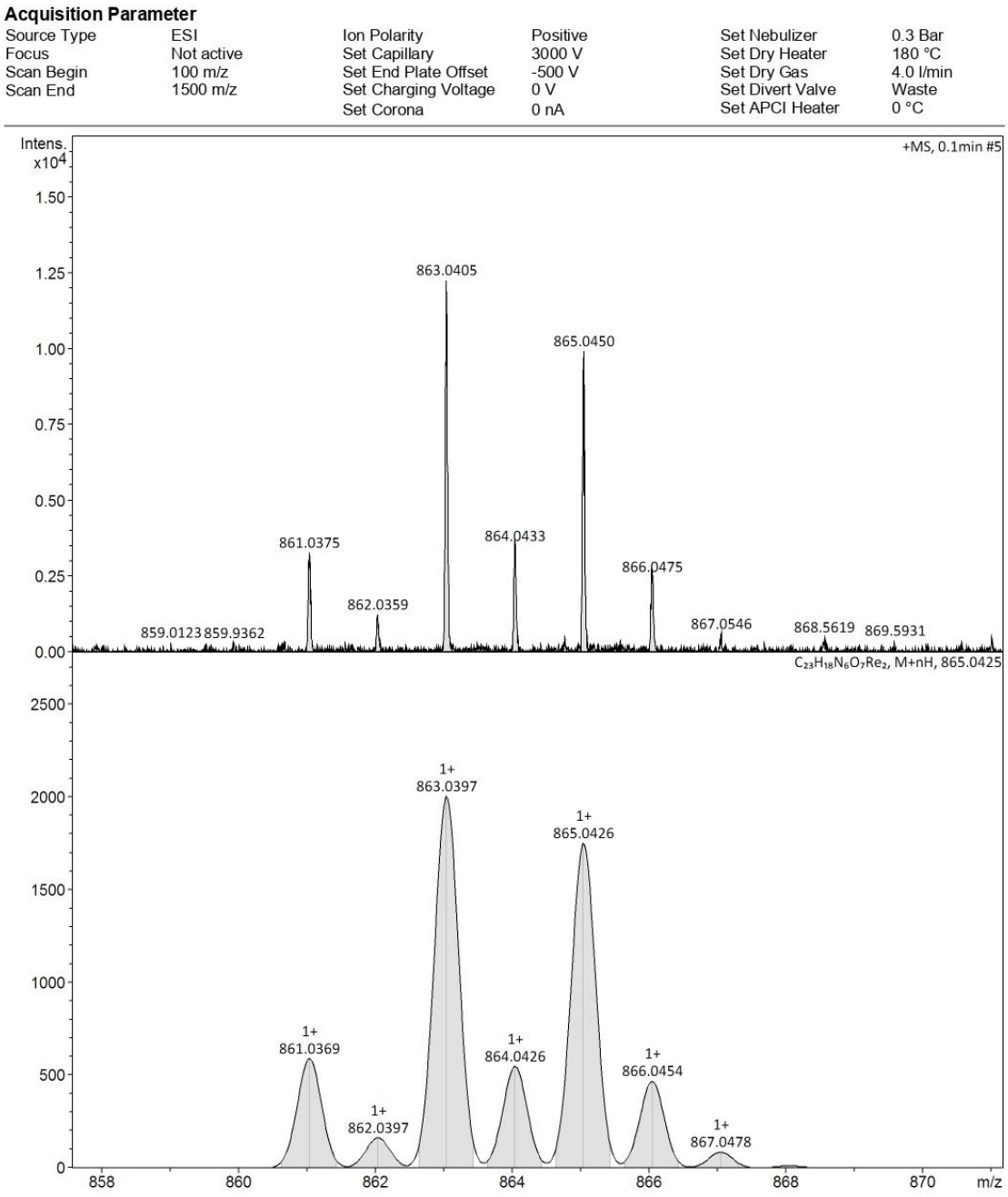

Figure 5.3. Experimental and calculated ESI mass spectra of **1** in positive ion mode ($CDCl_3$).

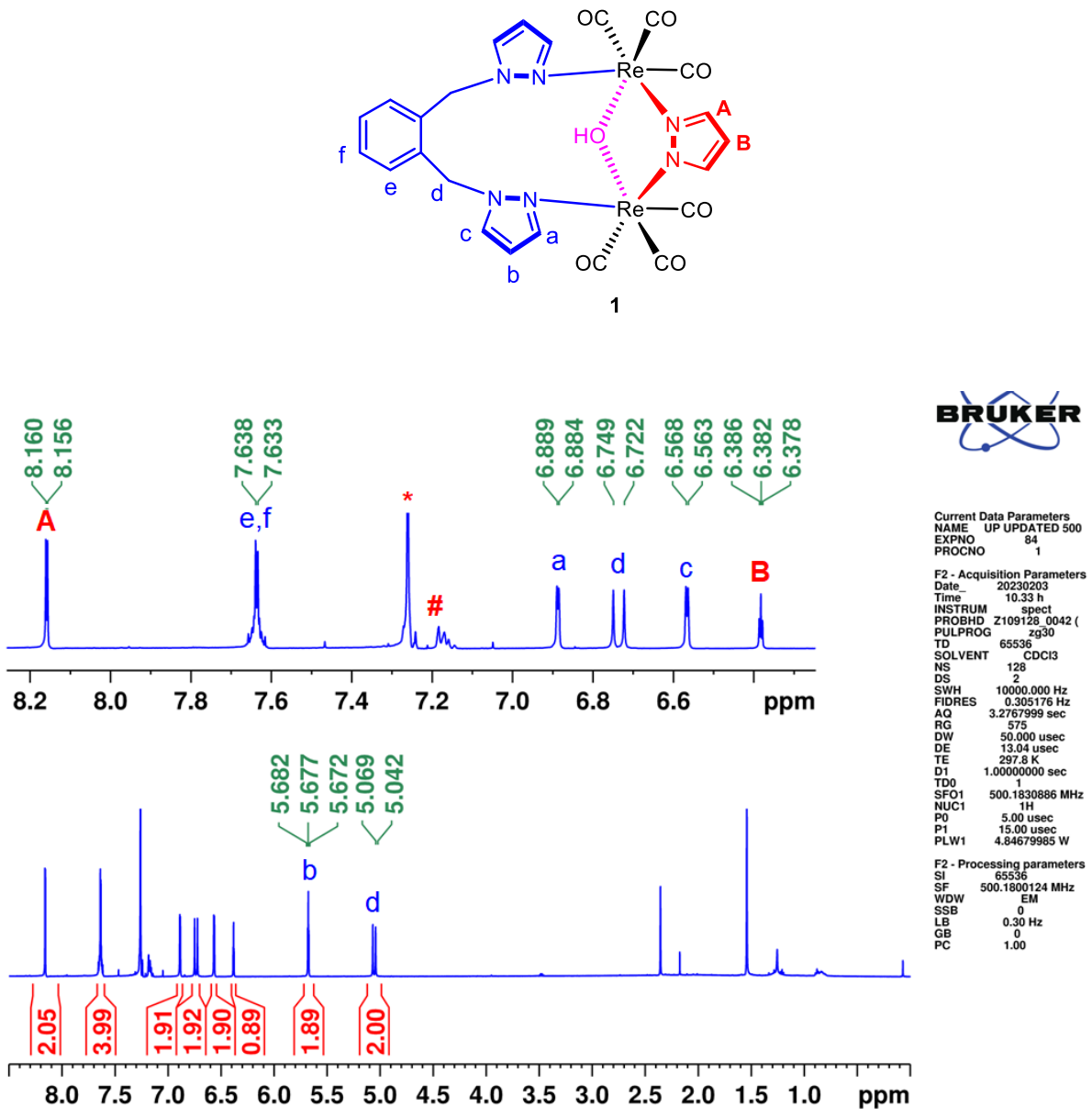

Figure 5.4. ^{1}H NMR spectrum of **1** in $CDCl_3$.

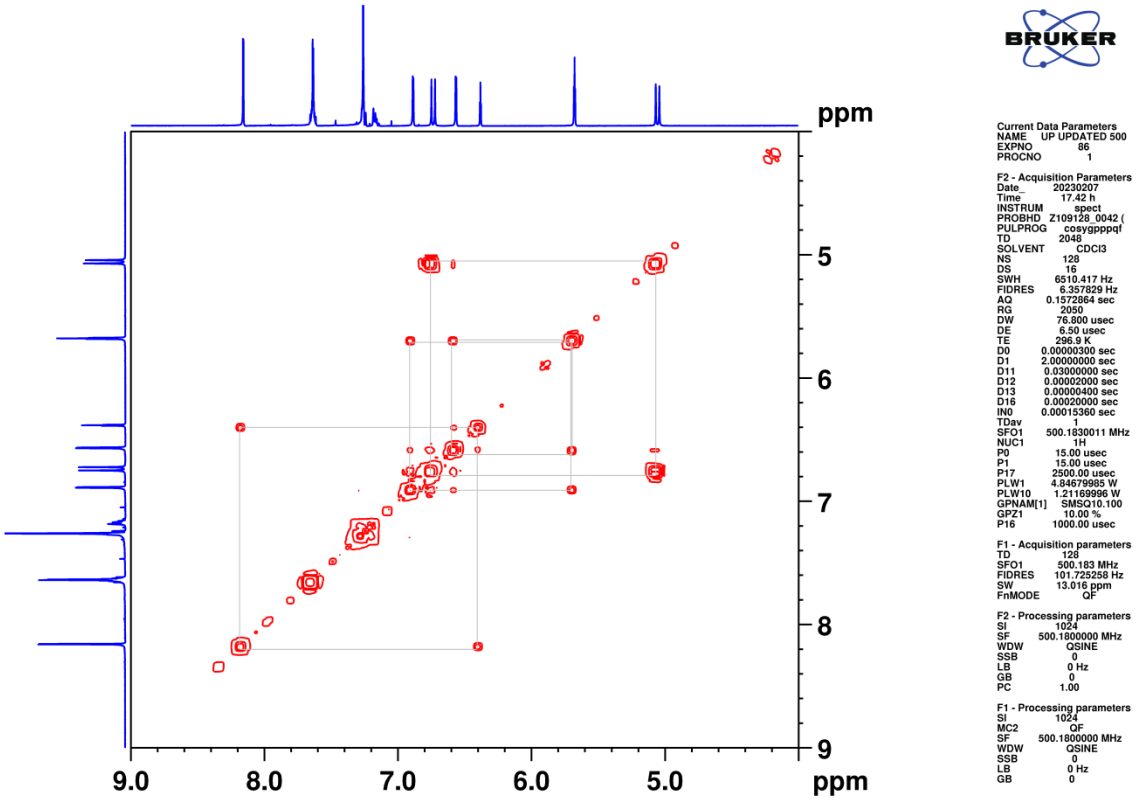

Figure 5.5. ^{1}H–^{1}H COSY NMR spectrum of **1** in $CDCl_3$.

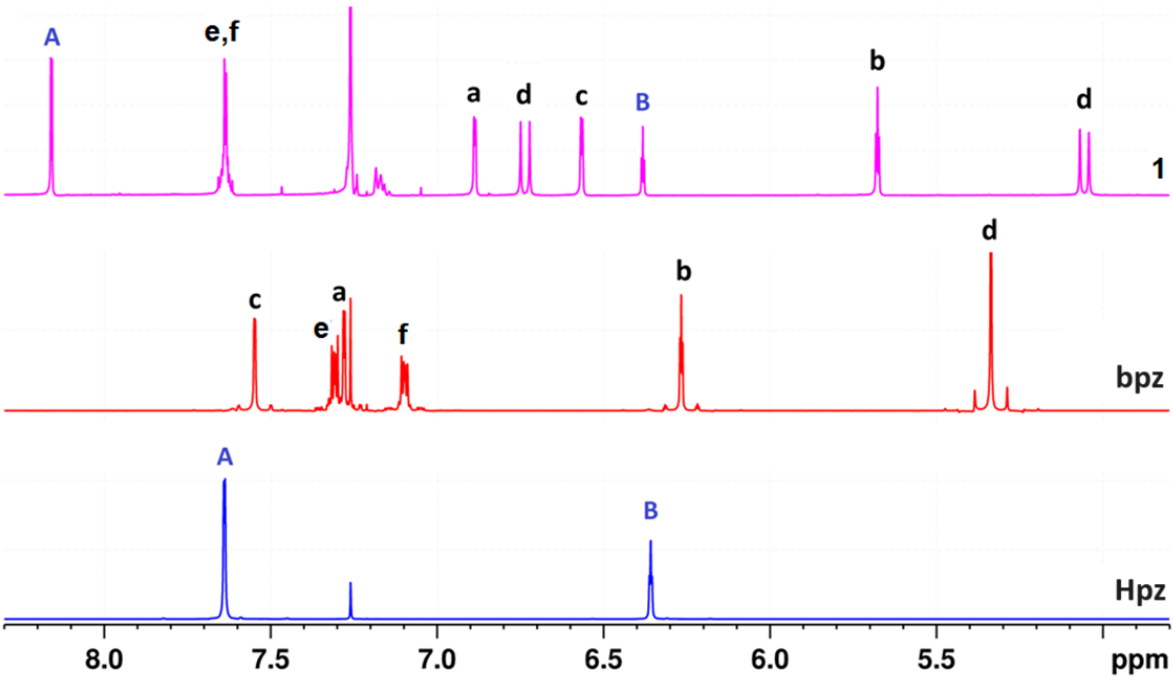

Figure 5.6. Partial ^{1}H NMR spectra of ligands and metallocycle **1** in $CDCl_3$.

5.3.2. Molecular Structure of Metallocycle 1

The X-ray study reveals that **1** adopts cyclic structure which consists of pyrazolate-hydroxo-bridged dinuclear motif *fac*-[{$(CO)_3$Re}(μ_2-OH)(μ-pz){Re$(CO)_3$}] and one bpz ligand. Pyrazolate and hydroxo unit are in the same plane, whereas the two pyrazolyl units are orthogonal to these anionic units and phenyl unit (Figure 5.7). All four aromatic units are directed towards one direction and contact each other via very weak C–H•••π contacts. The rhenium ion adopts an octahedral geometry. Both the *fac*-[Re$(CO)_3$] units are at one edge of the metallocycle with all six carbonyl groups pointed outward. The overall size of metallocycle is 11.82 Å (H18···H20) × 8.18 Å (H20···O7) × 8.17 (H13···O8) Å. Each metallocycle interacts with six neighboring molecules via intermolecular C–H•••O(Re–CO) interactions which occur between the hydrogen atom of pyrazolate/pyrazolyl/methylene to the oxygen of the metal coordinated carbonyl group. Solvent toluene molecules in the crystal lattice contact with coordinated carbonyl oxygen atoms of the metallocycle.

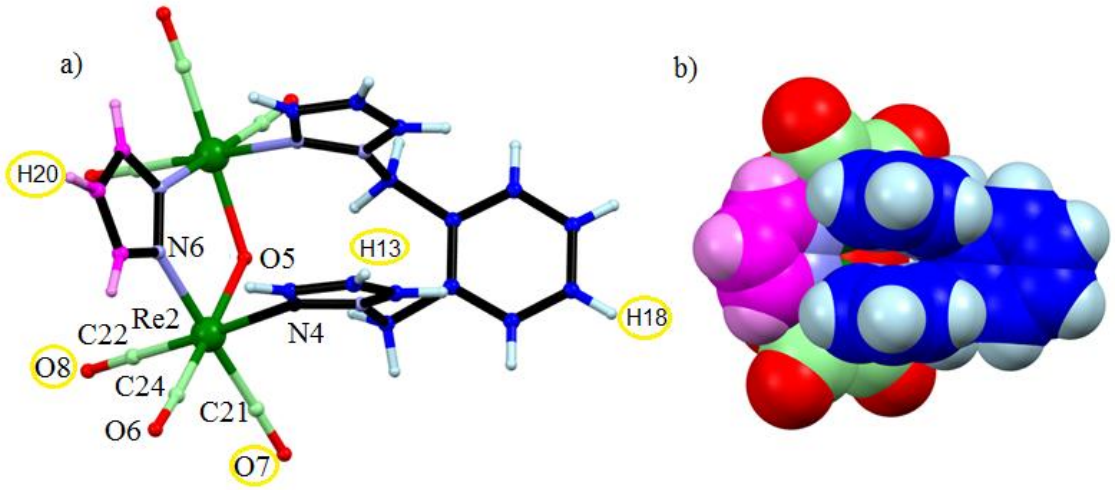

Figure 5.7. Ball & stick (a) and space-filling (b) views of molecular structure of **1**. Selected bond distances, Å: Re2–N6 = 2.149(6), Re2–N4 = 2.227(5), Re2–O5 = 2.164(3), Re2–C22 = 1.904(8), C22–O8 = 1.152(8), Re2–C24 = 1.885(8), C24–O6 = 1.159(8), Re2–C21 = 1.922(7), C21–O7 = 1.138(7).

5.3.2. Stability studies of 1 in DMSO

Neutral metal complexes consisting of *fac*-[$Re(CO)_3$] core and heteroarene-based ligand framework without polar substituent group(s) are generally soluble in DMSO and insoluble in H_2O. The complexes were dissolved in DMSO and diluted with buffer solutions for the biological studies. It is important to mention here that few complexes are stable in the solid state and dissociate into new complexes and free ligands in DMSO. Therefore, the solution studies such as NMR and ESI-MS analysis of the complexes in DMSO is very important for assessing the stability as the biological activity depends upon the molecular species present in the solution. Hence, an investigation of metallocycle **1** in d_6-DMSO was carried out. The ^{1}H NMR spectrum of **1** exhibited three distinct sets of patterns, affirming the existence of three molecular species within the solution, a finding corroborated by the DOSY spectrum. One group of chemical resonances corresponds to the metallocycle **1**, while the other groups of peak correspond to unbound bpz ligand and protons of the pyrazole/pyrazolate (downfield shifted slightly in comparison to ligand Hpz). (Figure 5.8-5.9) The result revealed that a major amount of **1** retains its cyclic structure in DMSO, whereas the remaining metallocycle disassembled into free bpz and a disintegrated *fac*-$Re(CO)_3$ complex (Figure 2) at room temperature. This was further supported by ESI-MS spectra, which revealed peaks corresponding to both the metallocycle and the free bpz for the sample of the metallocycle **1** as such. (Figure 5.10) Further, to assess the stability of the metallocycle over time, a series of ^{1}H NMR experiments were conducted at various time intervals. Changes in the peak intensities without any additional peak for **1** in d_6-DMSO were observed at intervals of 0, 1, 2 and 4 hours (Figure 5.12). The patterns remained consistent from 6, 8 and up to 48 hours. In contrast, upon subjecting **1** to heating, the intensities of the protons of the free bpz increased, while those of the metallocycle decreased. With further strong heating, the solution exclusively displayed peaks corresponding to the free ligand bpz and pz. The data suggest that at room temperature the metallocycle experienced partial disassembly and a small portion of it disassembles into bpz and a disintegrated *fac*-$Re(CO)_3$ complex (X) during the initial stage, reached an equilibrium state at 5 hours, and maintained this equilibrium even after 48 hours at room temperature.

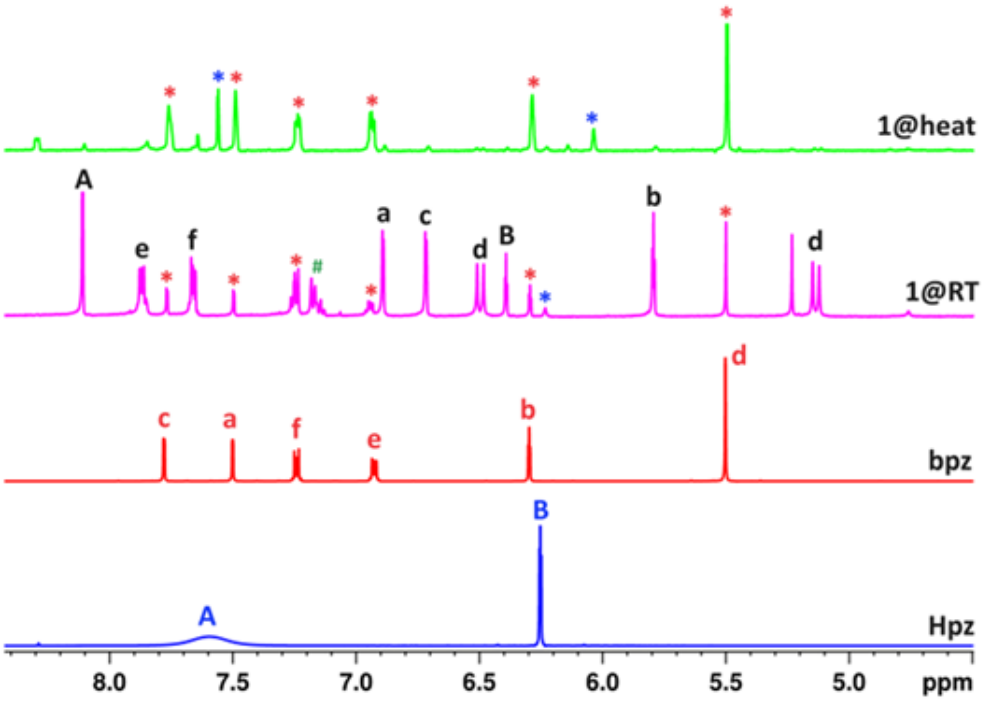

Figure 5.8. ^{1}H NMR spectra of Hpz, bpz, **1**@RT (without heat) and **1**@heat (with heat) in d_6-DMSO, * indicate peaks belong to diassembled bpz and Hpz;

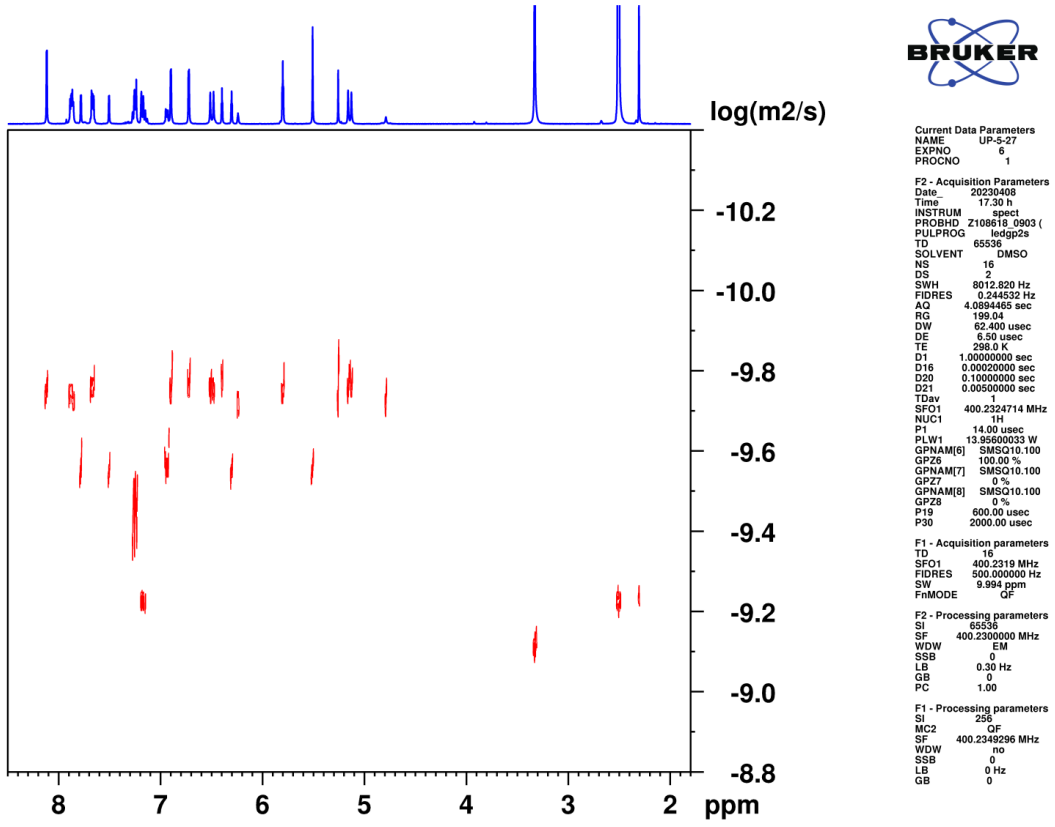

Figure 5.9. Partial DOSY spectrum of **1** in DMSO-d_6.

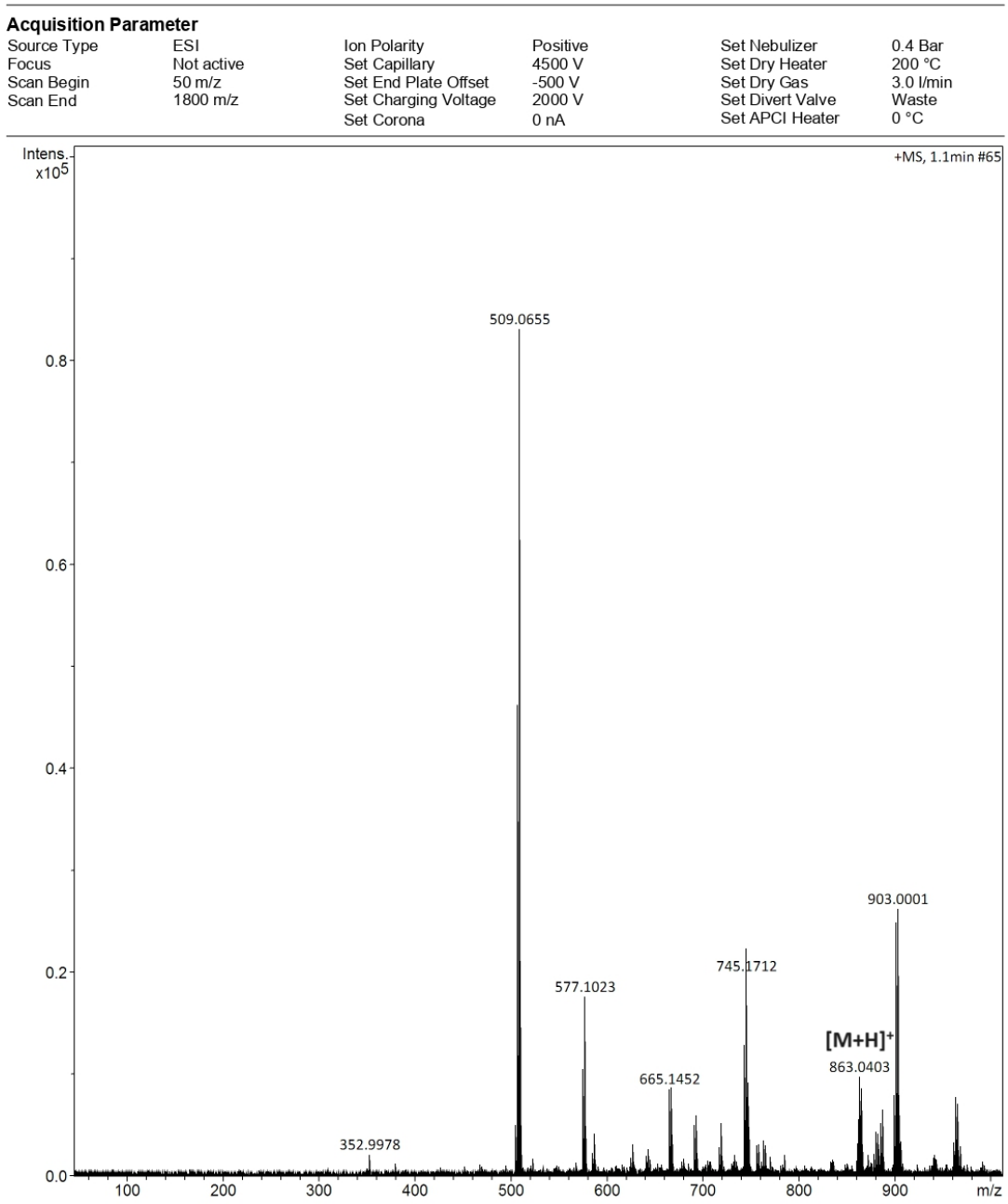

Figure 5.10. ESI mass spectrum of disassembly products of **1** (crystals of **1** were dissolved in DMSO-d_6) in DMSO diluted with ACN.

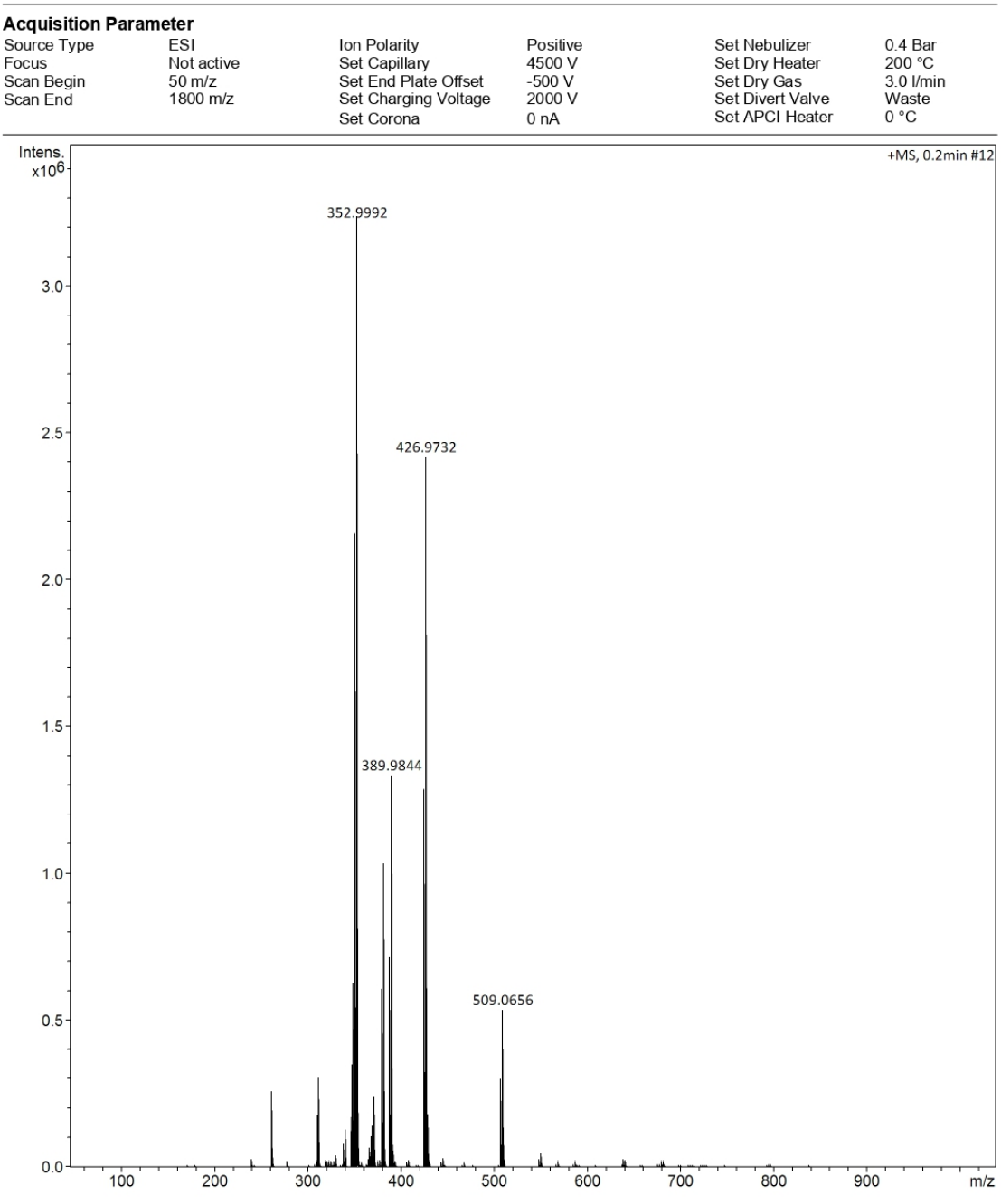

Figure 5.11. ESI mass spectrum of disassembly products of **1** (crystals of **1** were dissolved in DMSO-d_6 and heated at boiling temperature for 1 min) in DMSO diluted with ACN.

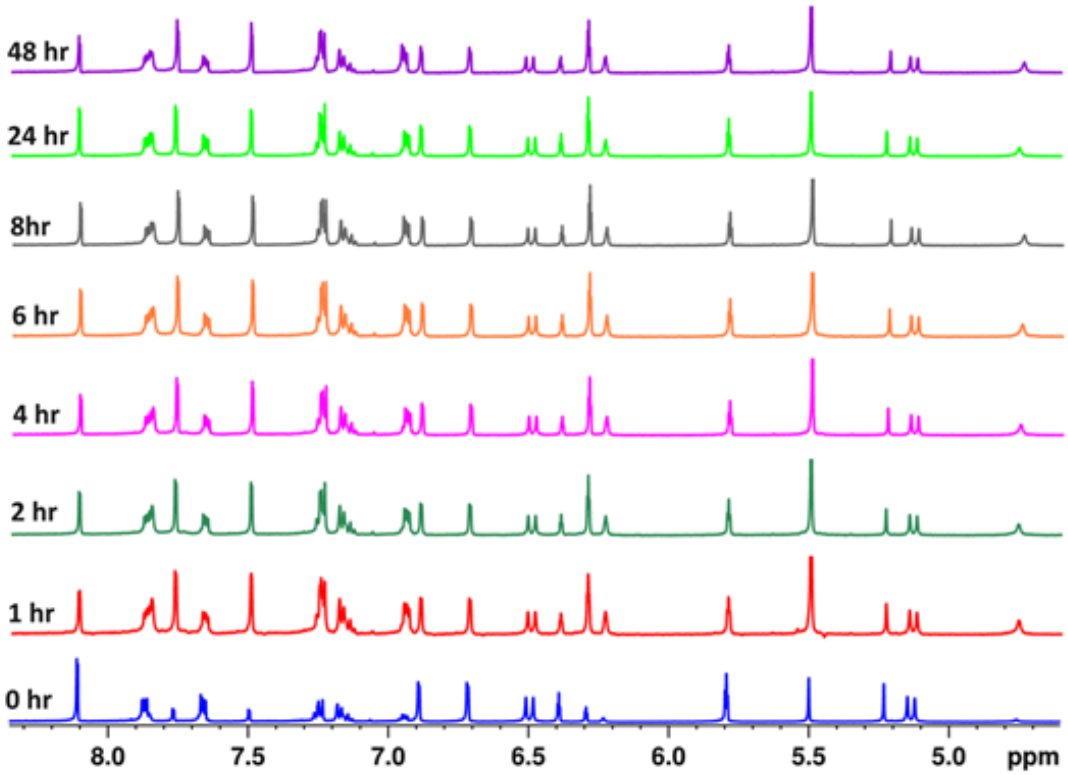

Figure 5.12. Partial ^{1}H NMR spectra of **1** in DMSO-d_6 recorded at various time intervals

Conversely, strongly heated solution of **1** contains free bpz and disintegrated *fac*-Re(CO)$_3$ complex. The solution exposed to intense heating showed no peaks beyond ~*m/z* 509 in ESI-MS spectra, signifying the complete absence of the metallocycle **1** in the solution (Figure 5.11). The stability studies reveal that the metallocycle, a disintegrated *fac*-Re(CO)$_3$ complex and free bpz are present in DMSO solution of **1** at room temperature. In contrast, free bpz, disintegrated *fac*-Re(CO)$_3$ complex are present in the strongly heated solution. Though metallocycle **1** in DMSO exists as a mixture of molecules (**Re1** = **1** + bpz + X) at RT and (**ML** = bpz + X) after heat; the metallocycle is expected to show biological activity due to its compact structure and the presence of metal carbonyl units.

5.3.3. Biological studies of 1

Hence, the anticancer properties of **Re1** and **ML** are investigated along with control molecules (free ligand bpz, and cisplatin, and untreated cells (referred as control in the figures) towards 4T1 cancer cells. Cell viability study of **Re1**, **ML**, bpz, and cisplatin toward triple negative breast cancer cells (4T1) were studied using MTT assay (Figure 5.13-5.15). The study reveals that **Re1** displayed 10 times higher cytotoxicity towards 4T1 cells than cisplatin. Free ligand bpz did not result in notable cell death in 4T1 cell lines. The IC_{50} (μM) values, 50±2.9 for bpz; 40±3.5 for cisplatin, 50 for ML, and 5±4.2 for **Re1**, strongly imply that metallocycle **1** plays a prominent role in killing the cancer cells. Hence, further biological studies were conducted only on **Re1**, bpz and cisplatin. The cytotoxicity of **Re1** against 4T1 cancer cells may be due to the intact metallocycle or the cumulative effect of all the components present in the solution along with the metallocycle.

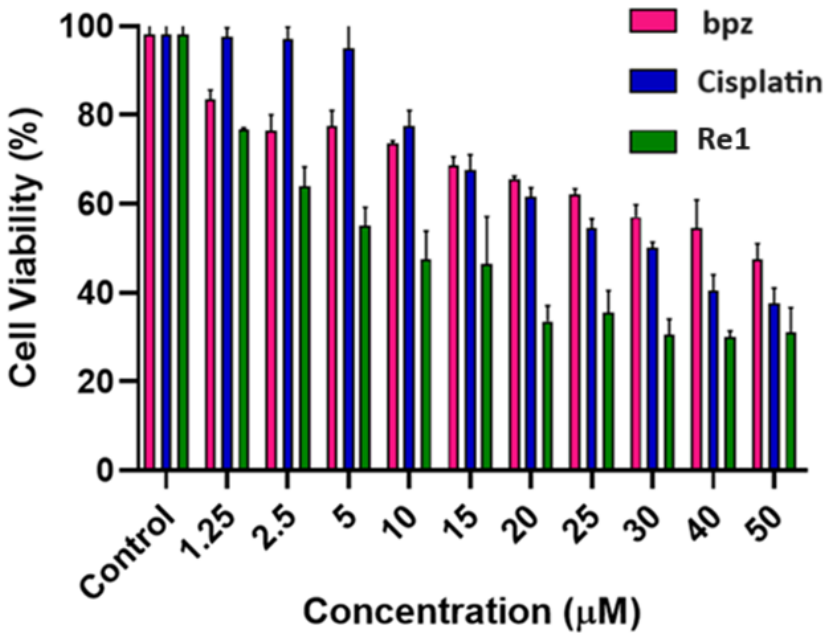

Figure 5.13. Determination of IC_{50} values of **1**@RT i.e **Re1** and bpz using MTT assay on murine breast cancer cell line 4T1. Untreated cells are used as a negative control, and Cisplatin is used as a positive control.

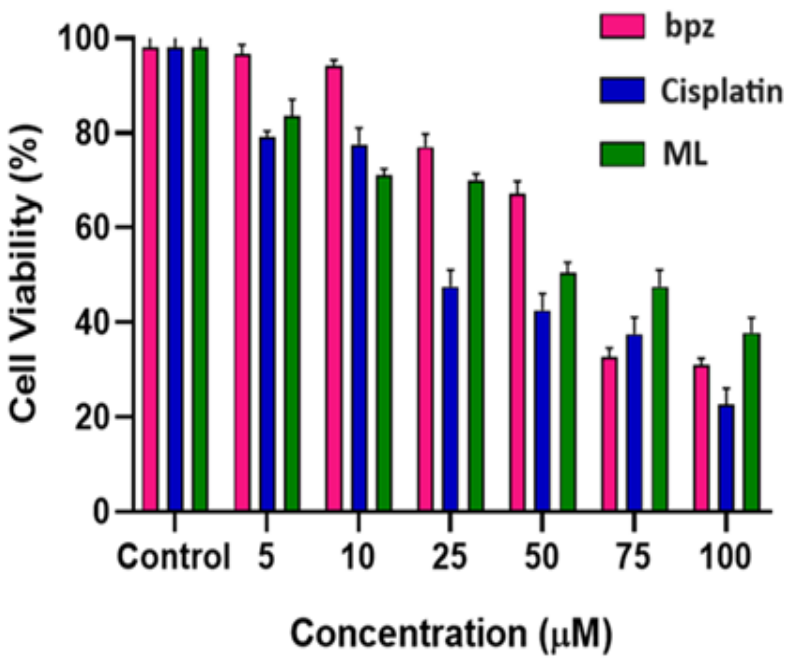

Figure 5.14. Determination of IC_{50} values of **1**@heat i.e **ML** and bpz using MTT assay on murine breast cancer cell line 4T1. Untreated cells are used as a negative control, and cisplatin is used as a positive control.

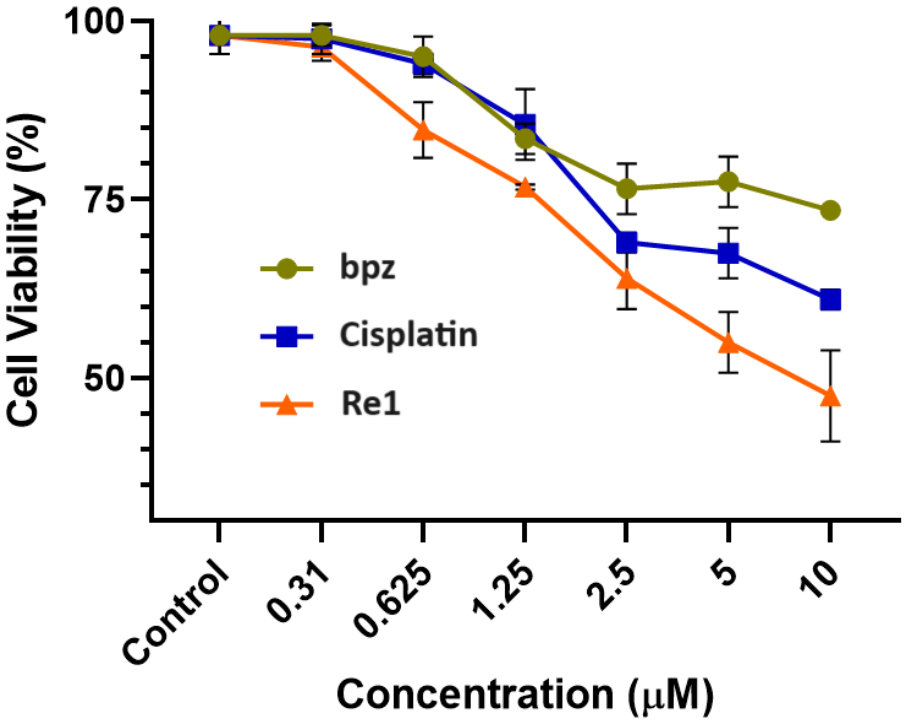

Figure 5.15. Dose-responsive curves of free ligand bpz, cisplatin and **Re1** against triple negative breast cancer cells (4T1) after 24h incubation.

To gain insights into the interactions between metallocycle with DNA, circular dichroism (CD) studies were carried out. Circular Dichroism (CD) studies were conducted at room temperature examining the conformational changes induced in CT-DNA by the metallocycle. The CD spectrum of CT-DNA exhibits two bands: a negative peak at 245 nm, attributed to polynucleotide helicity, and a positive peak at 275 nm, indicative of base pair stacking. The CD spectrum of the metallocycle treated with CT-DNA displayed a reduction in the intensity of both the positive and negative bands (Figure 5.16) Particularly, the negative bands intensity experienced a substantial decrease in comparison to only CT-DNA, signifying that the binding of the metallocycle has an impact on CT-DNA's helical structure. A similar trend is observed for CT-DNA treated with cisplatin. These three experiments collectively provide strong evidence of an interaction between metallocycle **1** and DNA, thus resulting in cell death.

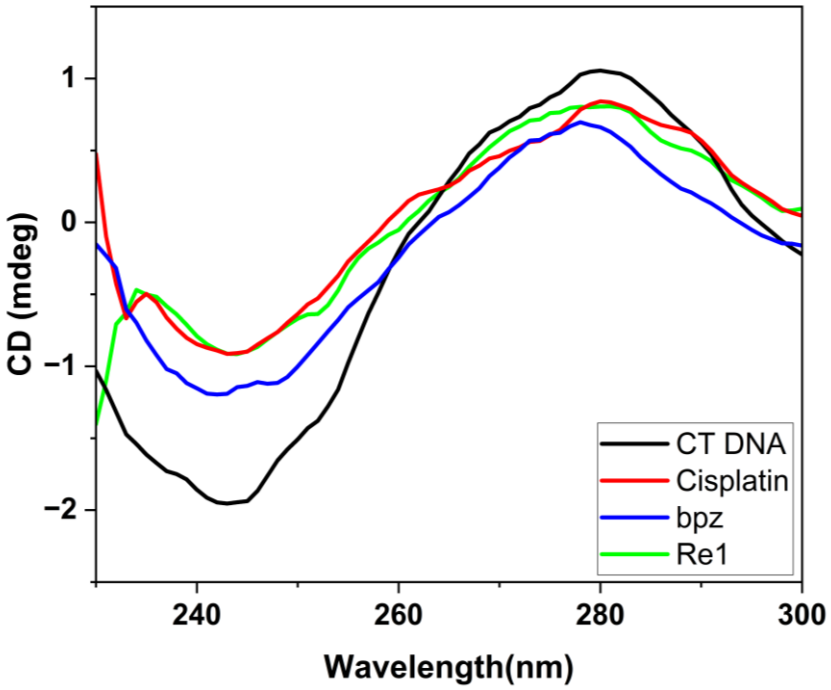

Figure 5.16. Circular Dichroism spectra displaying effect of **Re1**, bpz and cisplatin on DNA structure.

5.3.4. Molecular docking

Molecular docking studies were performed to elucidate the binding posture and the nature of the noncovalent interactions between metallocycle **1** and B-DNA dodecamer. The studies revealed that the metallocycle fits well in both the major and minor grooves of DNA which is stabilized through various noncovalent contacts. Metallocycle **1** exhibits binding affinities of

–8.3 kcal/mol and –8.5 kcal/mol in the major and minor grooves of DNA, respectively. Specifically, the metallocycle shows a multimodal binding affinity with DNA, with a stronger preference for the minor groove (Figure 5.17A-5.17C). The metallocycle is stabilized with DNA through intermolecular hydrogen bonds, involving guanine and cytosine with the oxygen atom of the rhenium-coordinated carbonyl unit, and π-π stacking interaction, involving guanine and pyrazolyl motif. Similarly, the docking position, 3D depiction, and 2D interaction diagrams of **1** within the major groove of DNA are shown (Figure 5.16D-5.16F). These figures revealed the presence of multiple noncovalent interactions between **1** and DNA including hydrogen bonds between adenine and the coordinated carbonyl unit and π···π stacking contacts between adenine and the phenyl group of bpz of metallocycle.

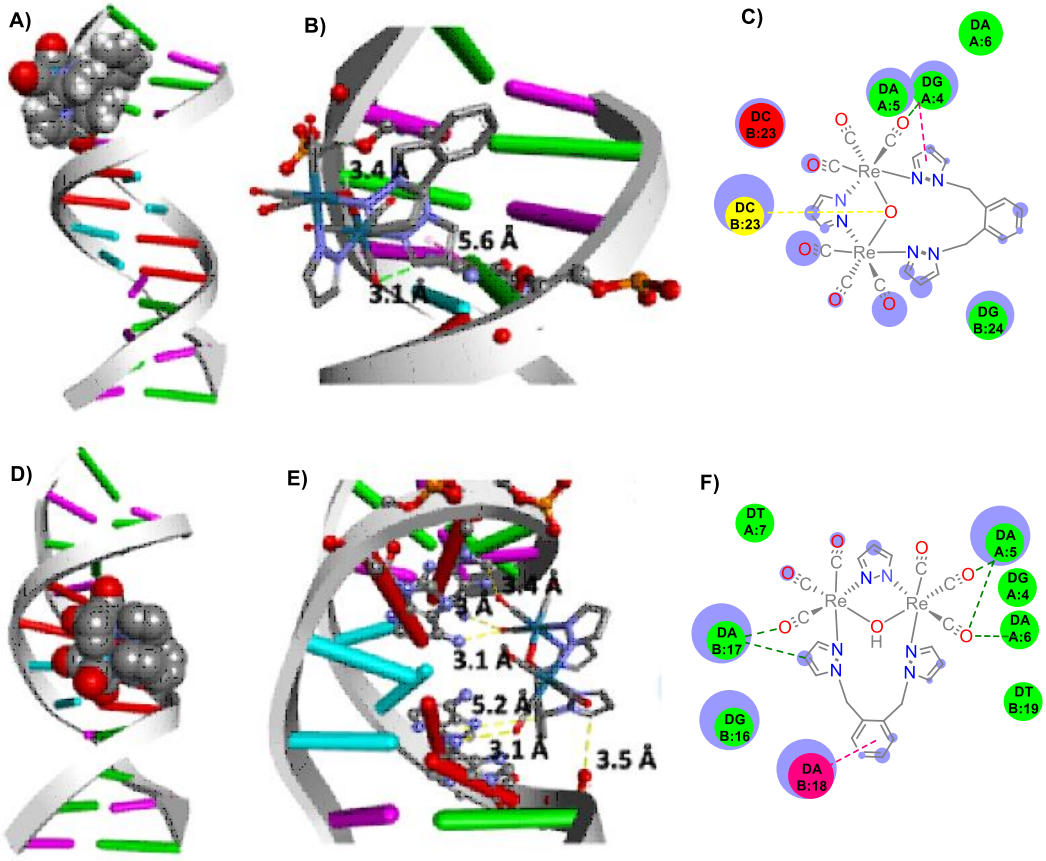

Figure 5.17. Docked conformations of metallocycle **1** with the minor and major grooves of B-DNA.

5.3.5. Synthesis and characterization of metallocycles 2-4.

Since the metallocycle **1** shows good cytotoxicity against 4T1 cells so efforts were made for synthesizing azolato bridged complexes which are stable in DMSO-d_6 solution. Metallocycle **2-4** were synthesized by treating $Re_2(CO)_{10}$, pyrazole (Hpz for **3**)/indazole(HIn for **2** and **4**), bpz(for **2**)/Xybim(for **3** and **4**) and undistilled toluene using solvothermal approach (Scheme 5.2). The complexes were air and moisture stable. Complexes **2**–**4** display two strong C≡O stretching bands in 2000–1860 cm^{-1} region, characteristic of *fac*-[$Re(CO)_3$] motif (Figure 5.18-5.20). ESI–MS spectra of the metallocycles show molecular ion peaks (*m*/*z* 913.0542 for $[\mathbf{2}+H]^+$, *m*/*z* 96.0698 for $[\mathbf{3}+H]^+$ and *m*/*z* 1013.0891 for $[\mathbf{4}+H]^+$), that matches with the theoretical values (Figure 5.21-5.26). Complex **2** is soluble both in chloroform and DMSO. The ^{1}H NMR spectrum of **2** in $CDCl_3$ display well resolved peaks corresponding to proton peaks of both indazolate and bpz ligands (Figure 5.27-5.28). The H^A and H^E protons of indazolate in **2** are significantly upfield shifted, H^B is slightly upfield shifted, H^C is significantly downfield shifted whereas H^D is slightly downfield shifted relative to that of H-In indicating the binding of H-In to rhenium cores. Protons $H^{a,a'-c,c'}$ of the pyrazolyl motifs were significantly upfield shifted whereas H^{e-f} of phenyl spacer were merged and significantly downfield shifted. However ^{1}H NMR spectrum of **2** in DMSO-d_6 shows similar pattern as **1** with presence of free bpz proton peaks in the spectrum indicating dissociation of a portion of the metallocycle in DMSO-d_6 solution (Figure 5.29-5.30). Complexes **3** and **4** are only soluble in DMSO. The ^{1}H NMR spectrum of **3** and **4** in DMSO-d_6 display well resolved peaks corresponding to proton peaks of both Hpz for **3**/H-In for **4** and XyBim ligands. The H^A and H^B protons of pyrazolate in **3** are slightly/significantly upfield/downfield shifted respectively. A similar pattern was seen for complex **4.** The ^{1}H NMR spectrum recorded after 72 hrs shows no change in spectrum indicating the stability of the complexes **3** and **4** in DMSO solution even after many days (Figure 5.31-5.36).

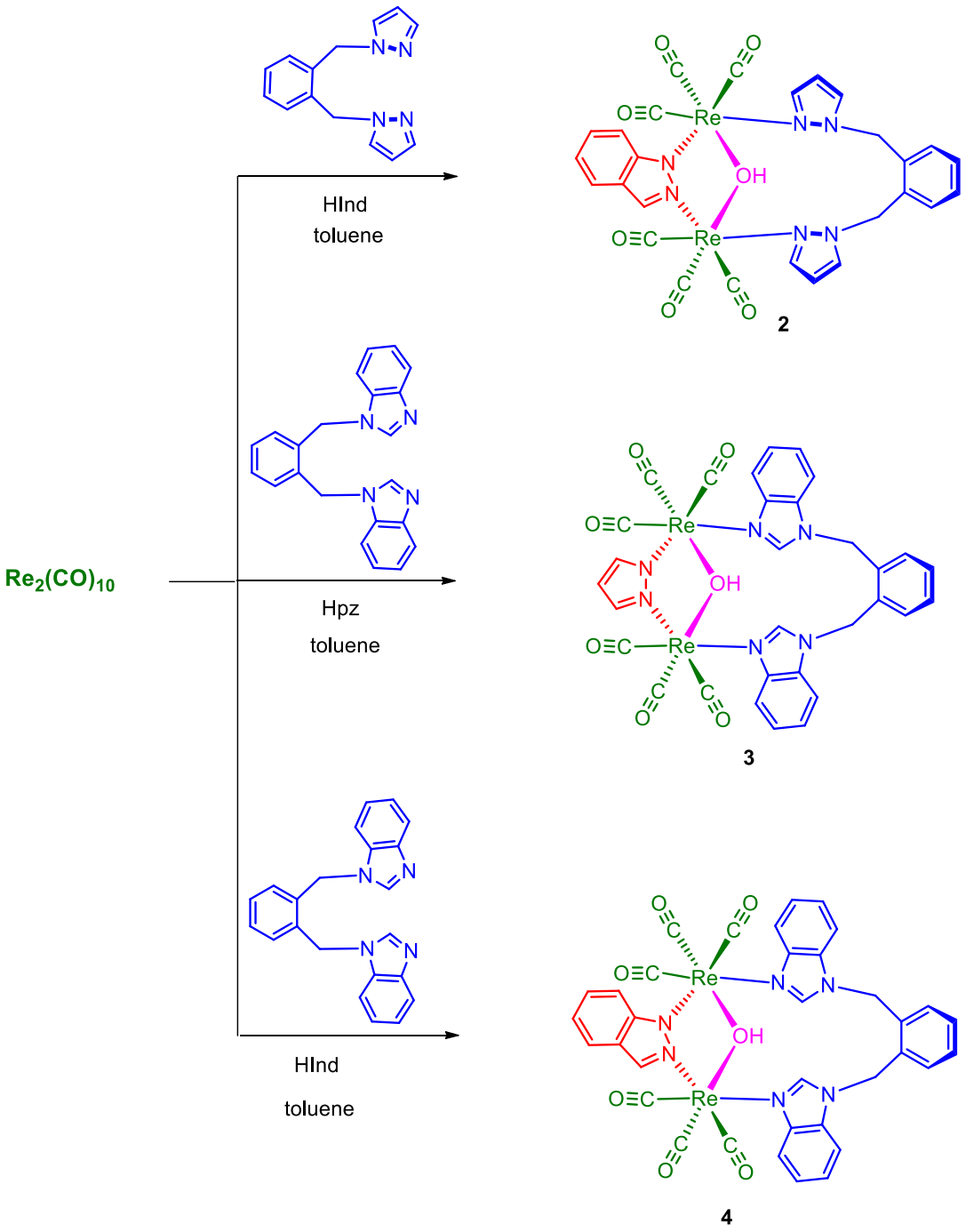

Scheme 5.2. Synthesis of metallocycles **2-4.**

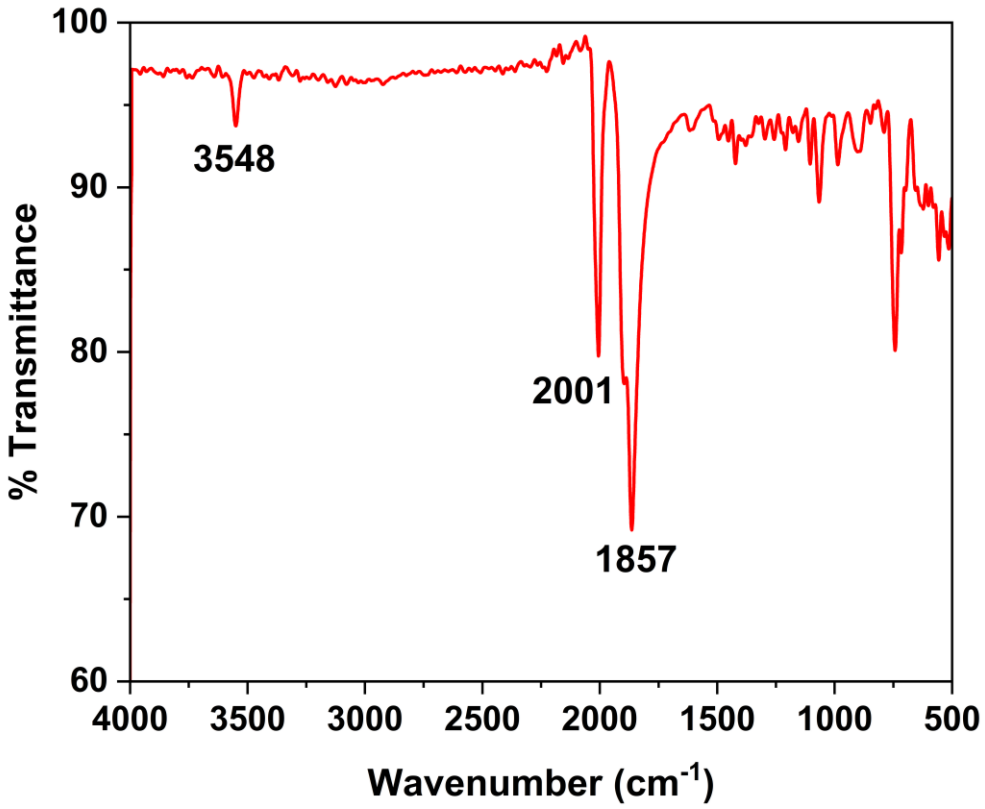

Figure 5.18. ATR-IR spectrum of **2**.

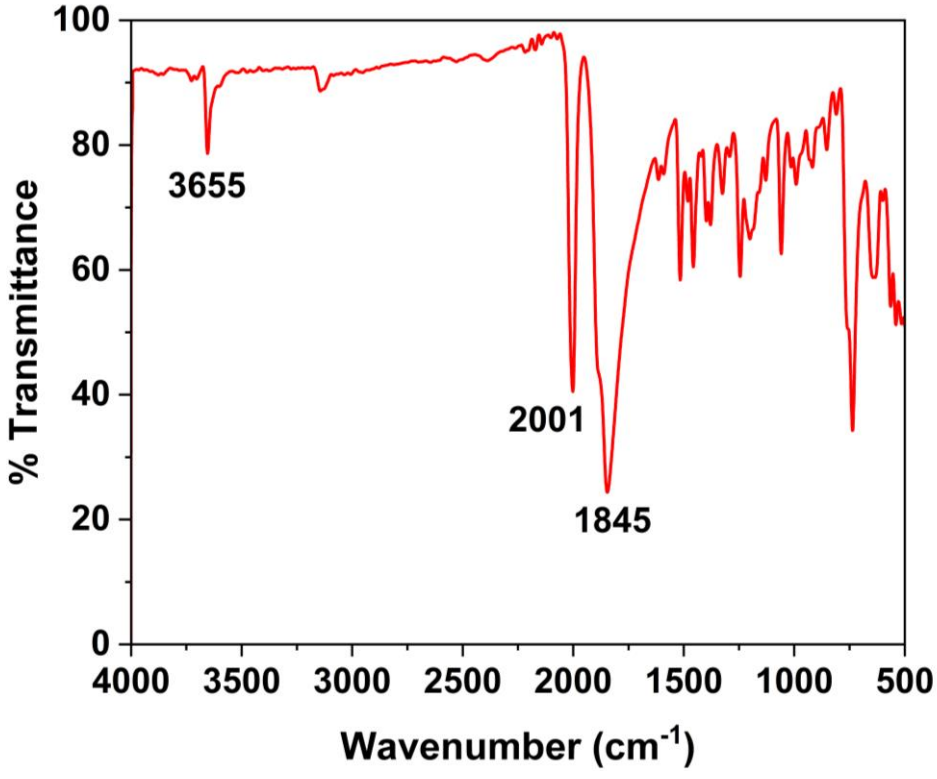

Figure 5.19. ATR-IR spectrum of **3**.

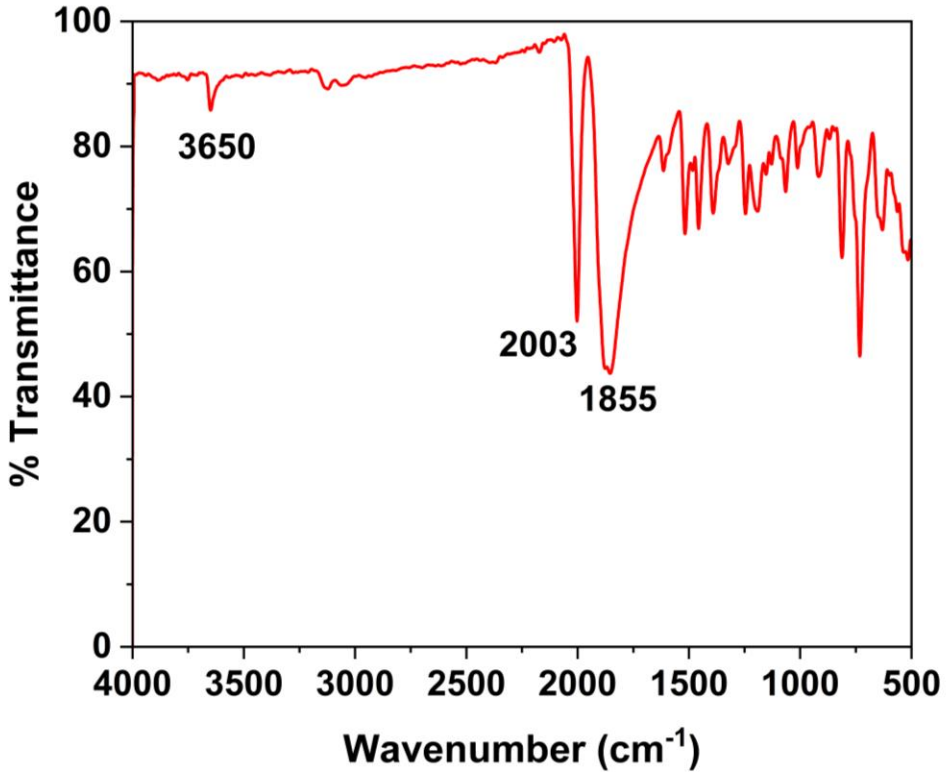

Figure 5.20. ATR-IR spectrum of **4**.

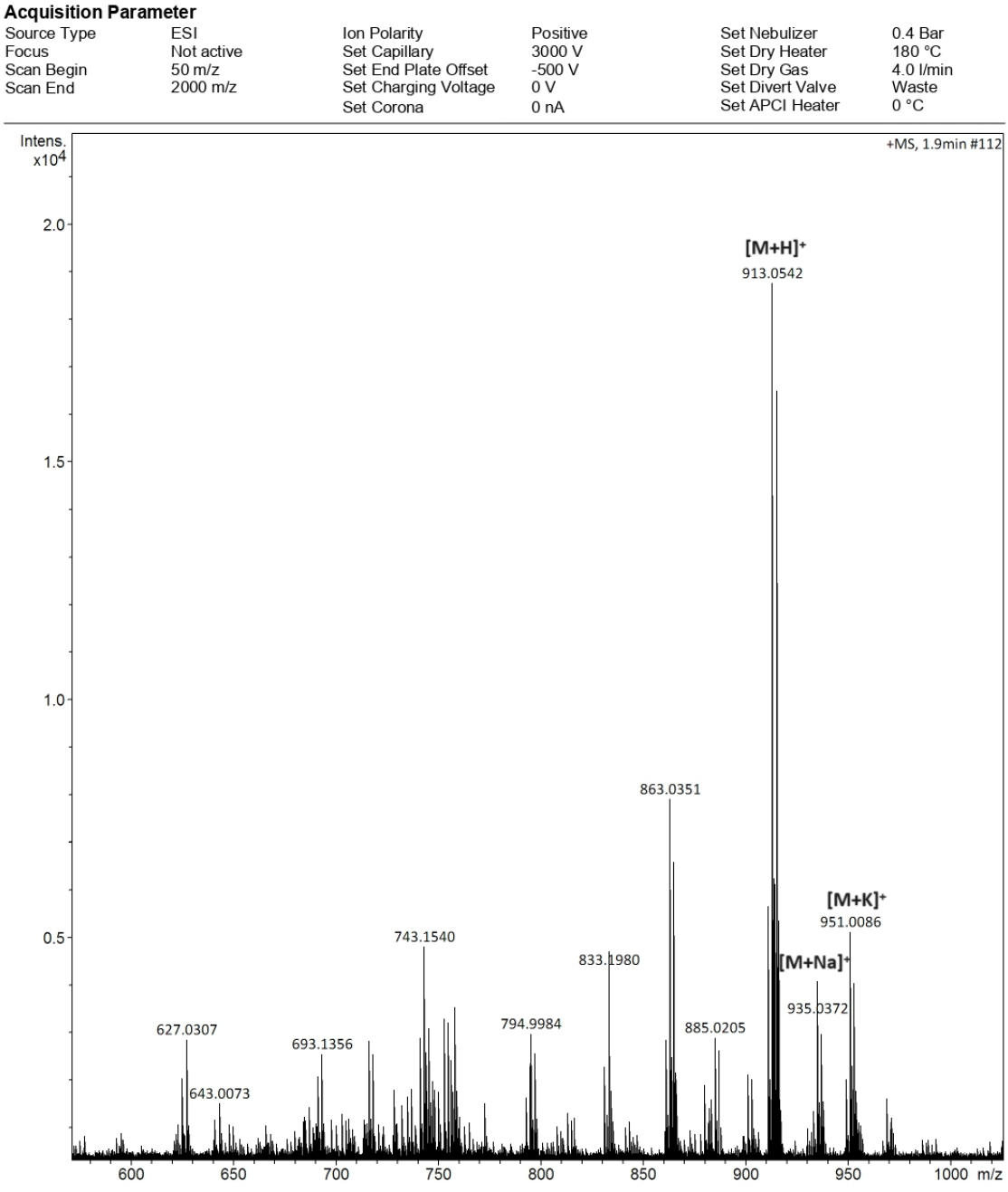

Figure 5.21. ESI mass spectrum of **2** in positive ion mode in DMSO-d_6.

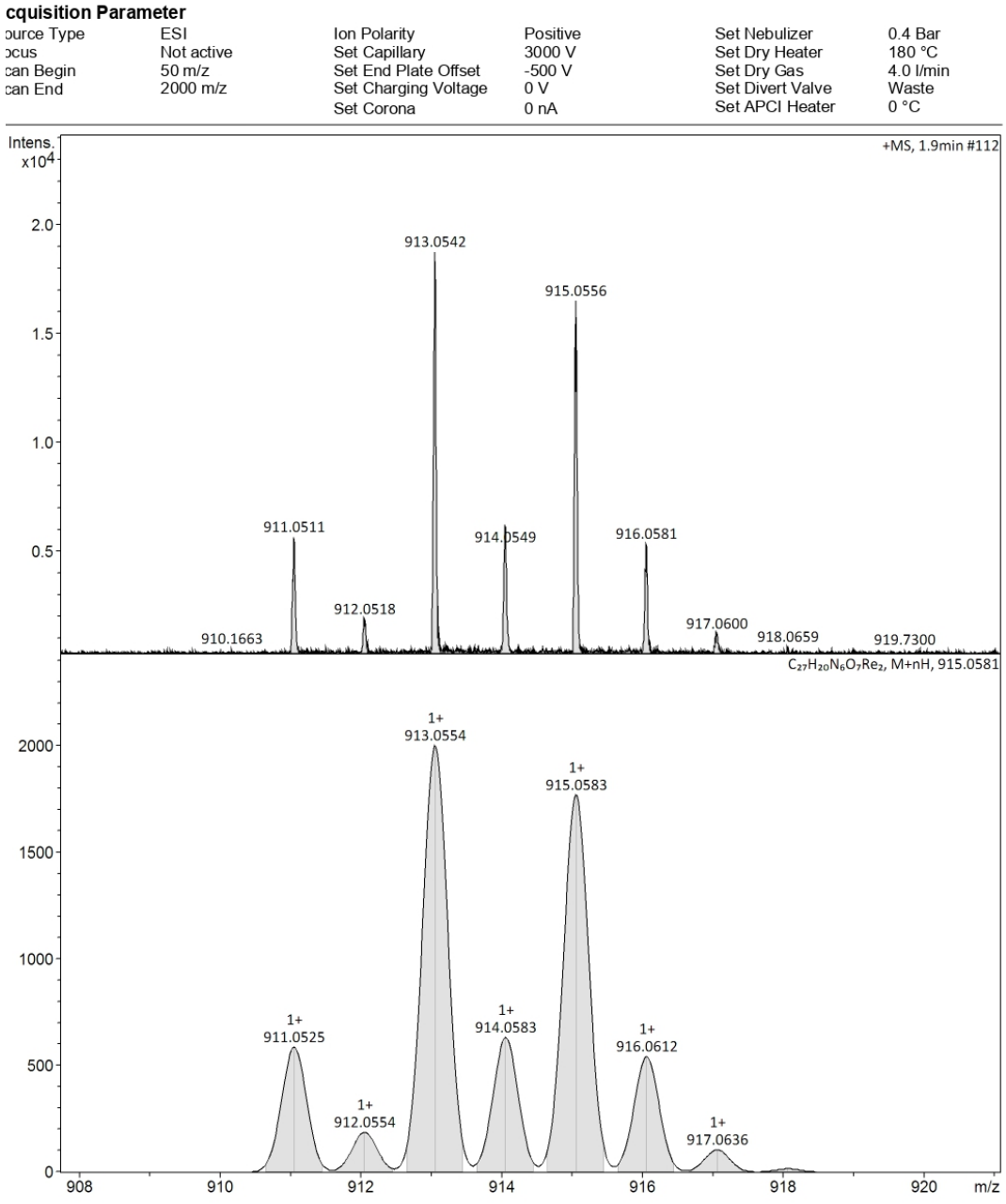

Figure 5.22. Experimental and calculated ESI mass spectra of **2** in positive ion mode in DMSO-d_6.

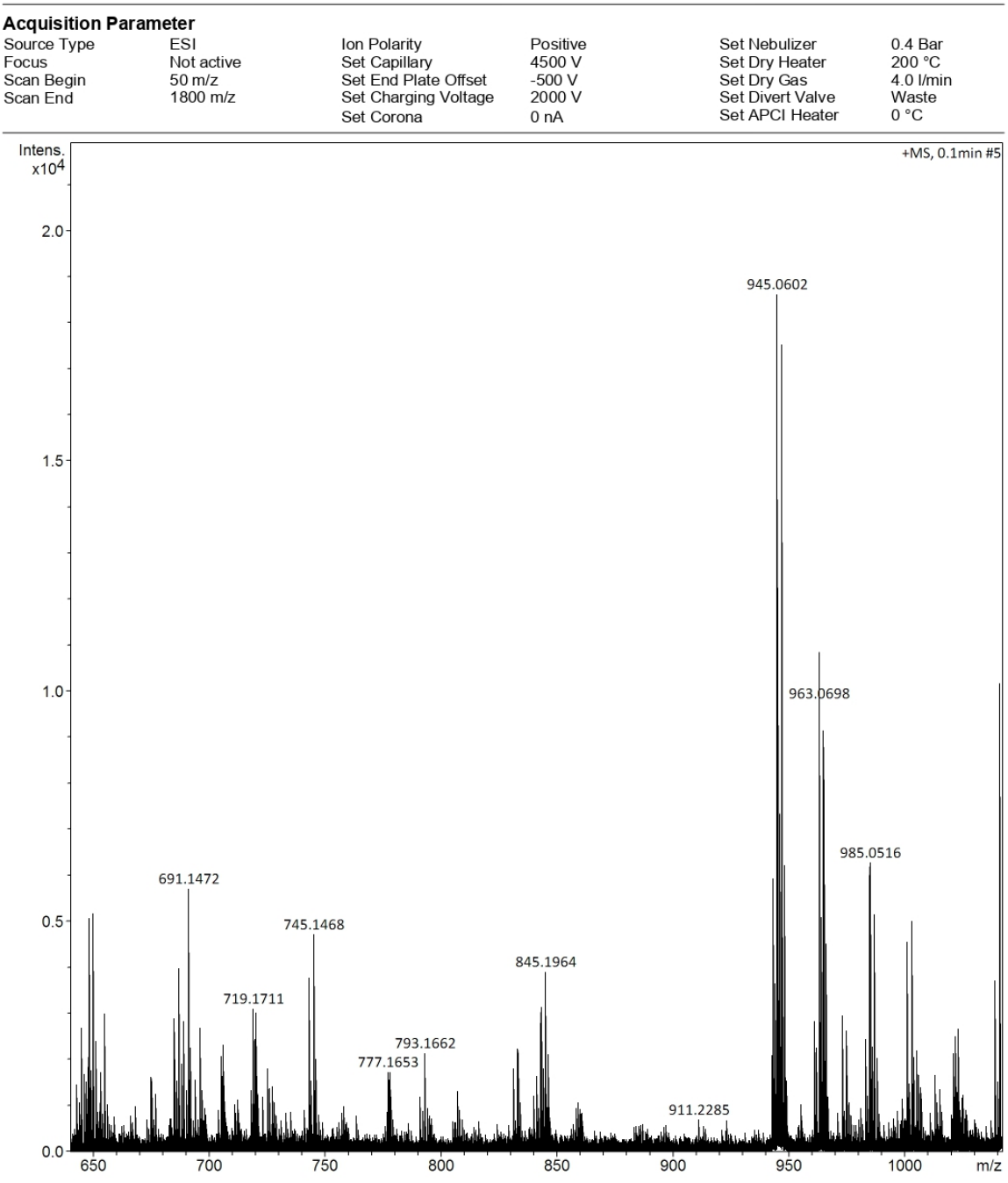

Figure 5.23. ESI mass spectrum of **3** in positive ion mode in DMSO-d_6.

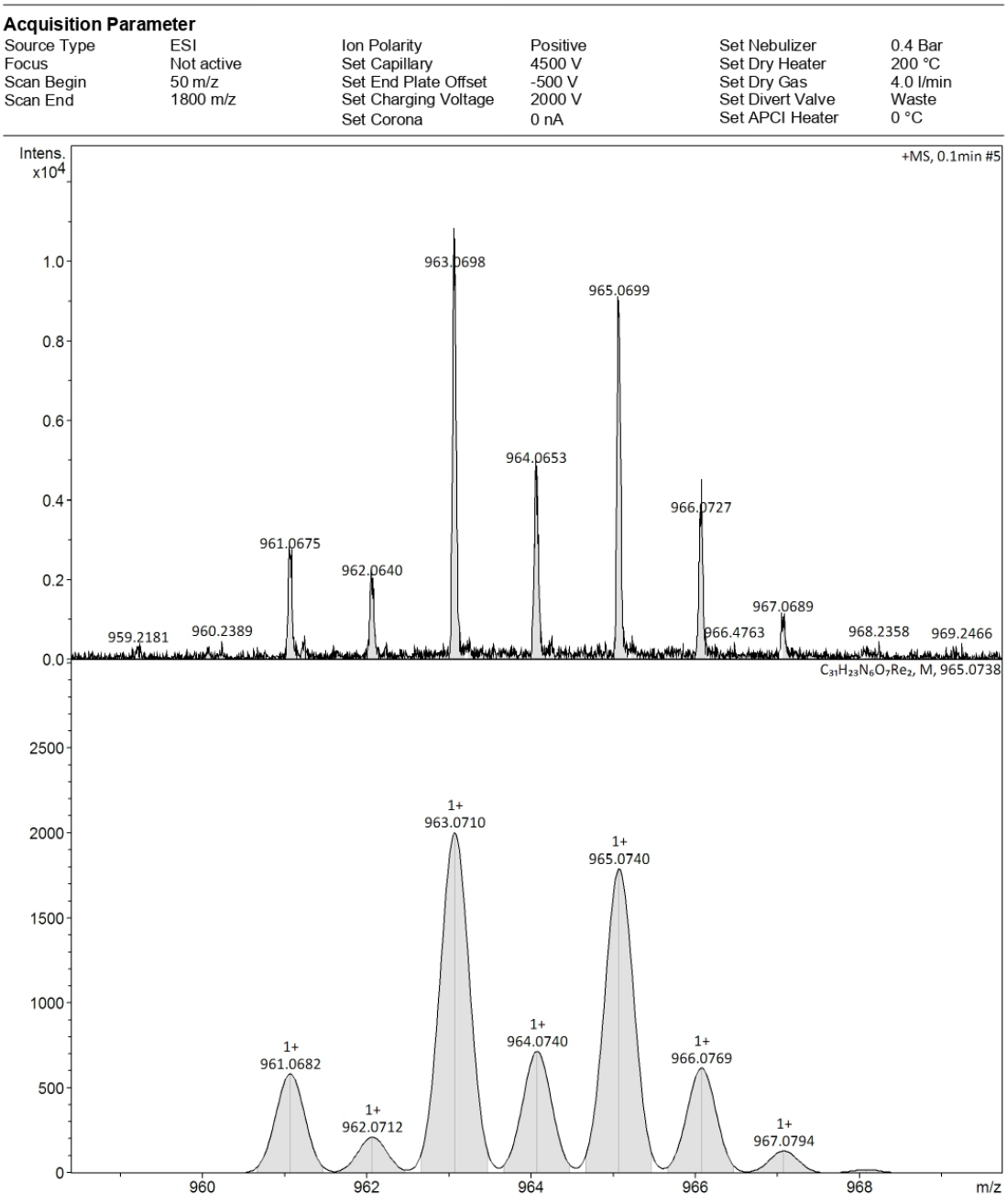

Figure 5.24. Experimental and calculated ESI mass spectra of **3** in positive ion mode in DMSO-d_6.

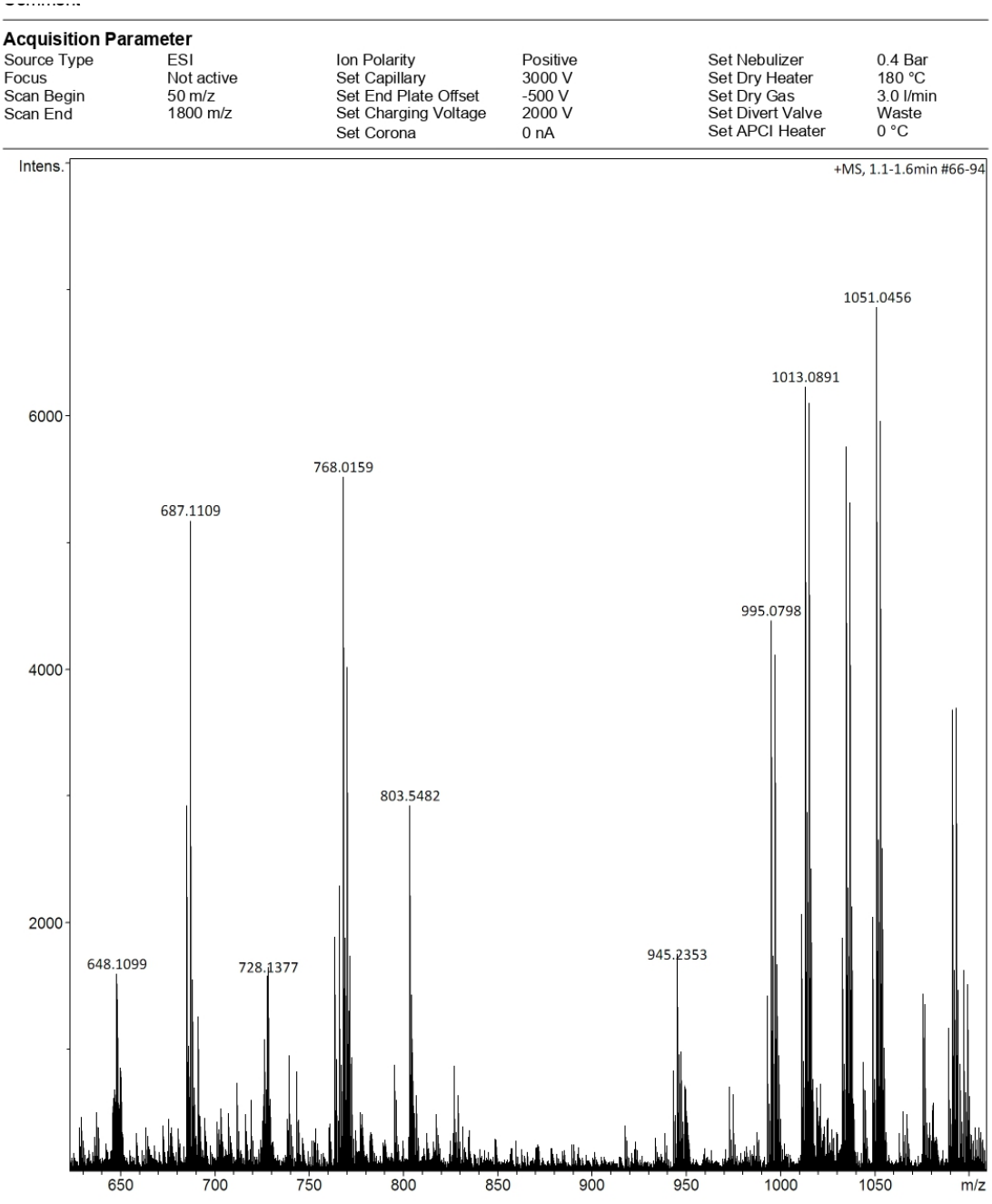

Figure 5.25. ESI mass spectrum of **4** in positive ion mode in DMSO-d_6.

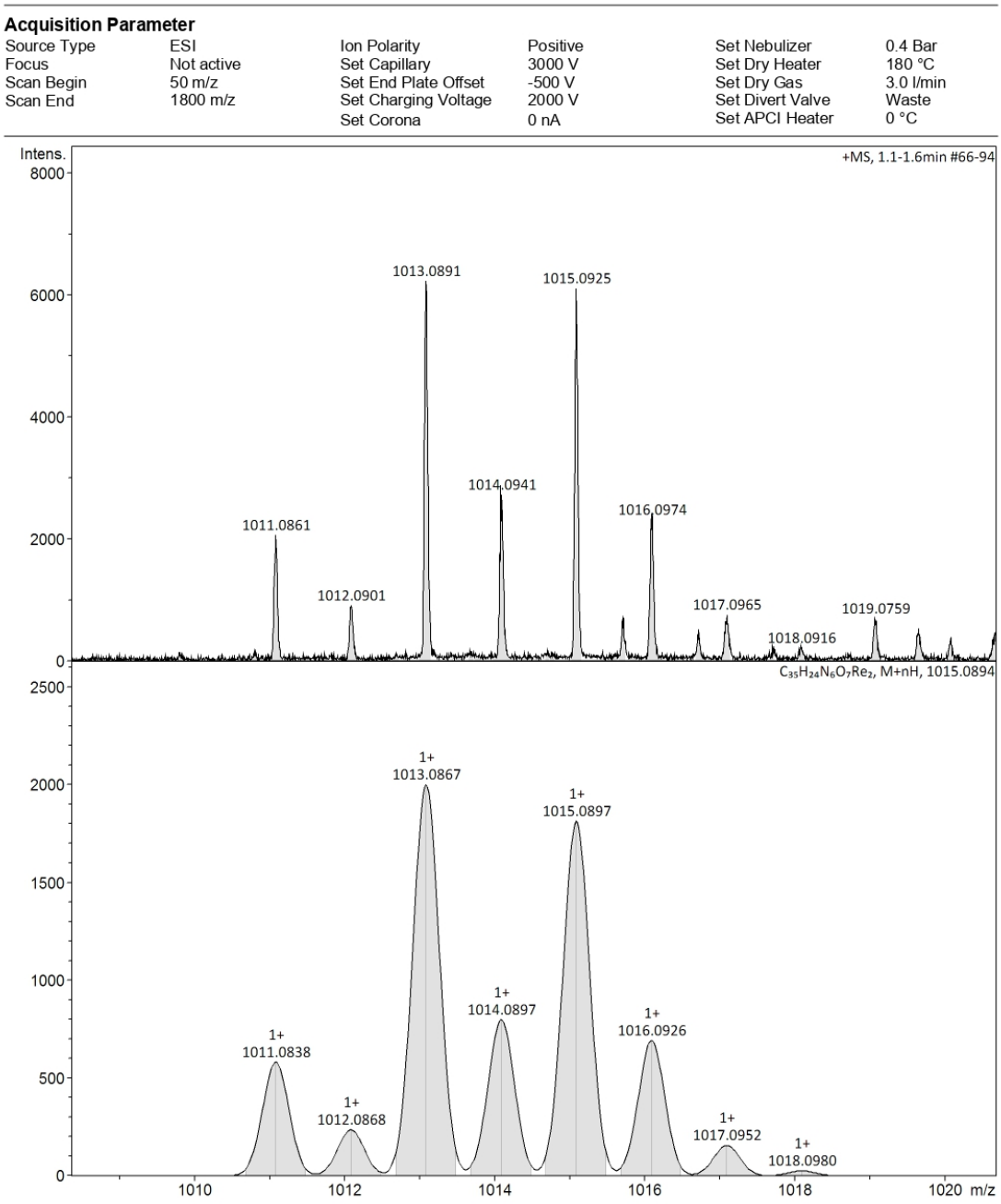

Figure 5.26. Experimental and calculated ESI mass spectra of **4** in positive ion mode in DMSO-d_6.

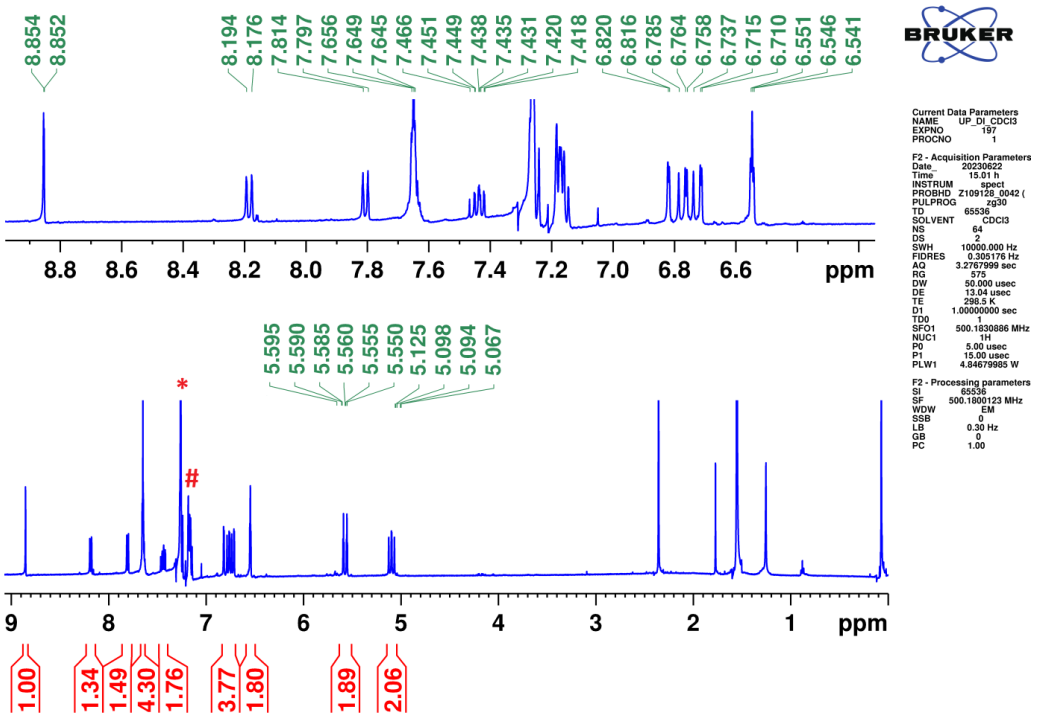

Figure 5.27. ^{1}H NMR spectrum of **2** in $CDCl_3$.

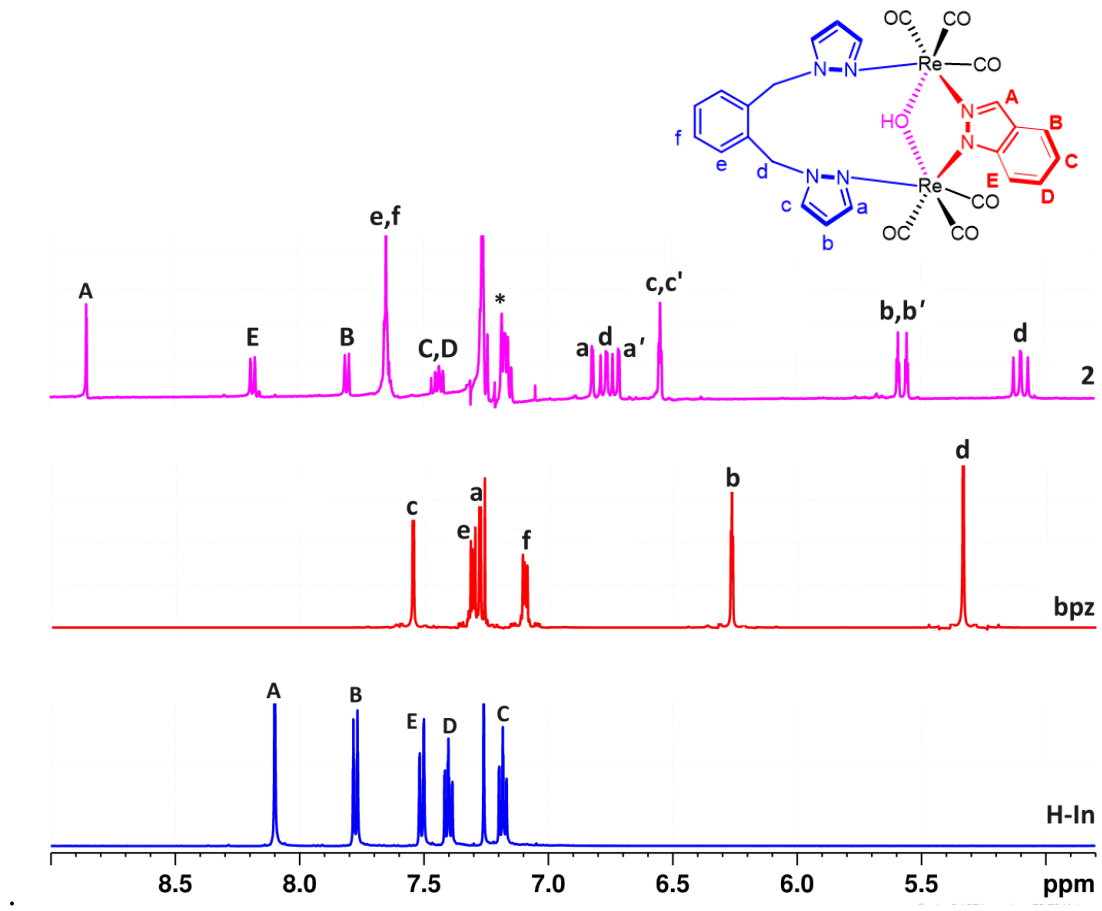

Figure 5.28. Partial ^{1}H NMR spectra of ligands and metallocycle **2** in $CDCl_3$.

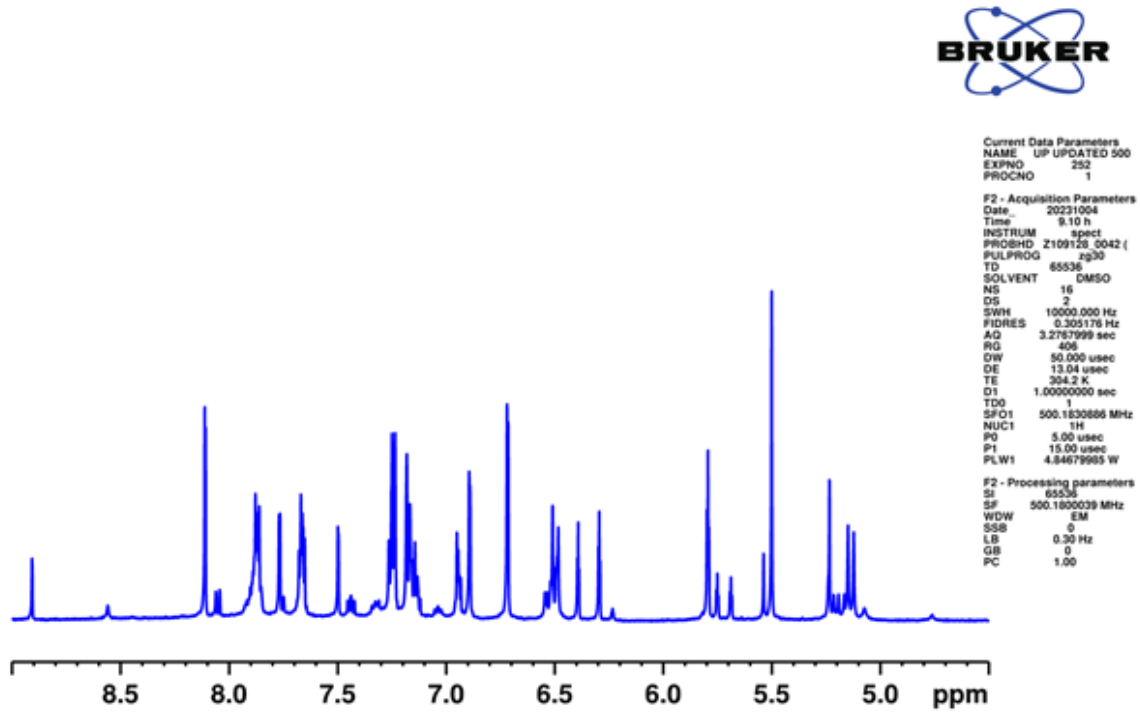

Figure 5.29. Partial ^{1}H NMR spectrum of **2** in DMSO-d_6.

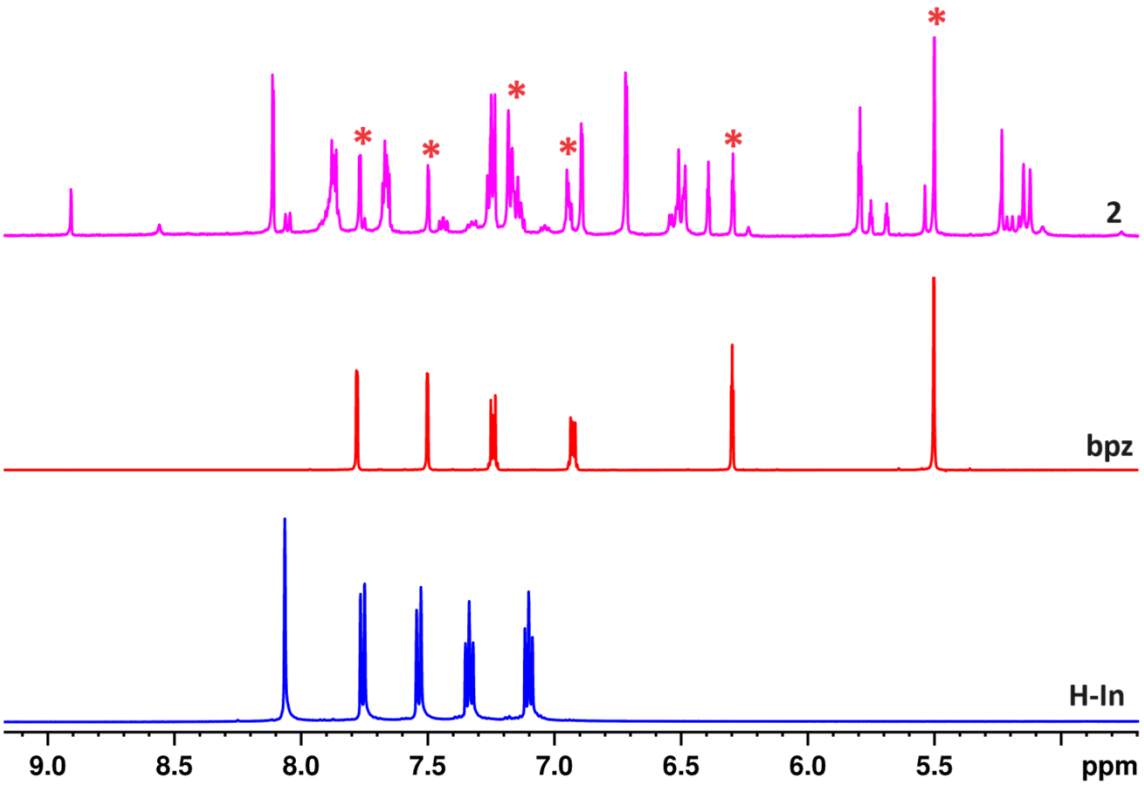

Figure 5.30. NMR spectra of **2**, bpz and H-In in DMSO-d_6.

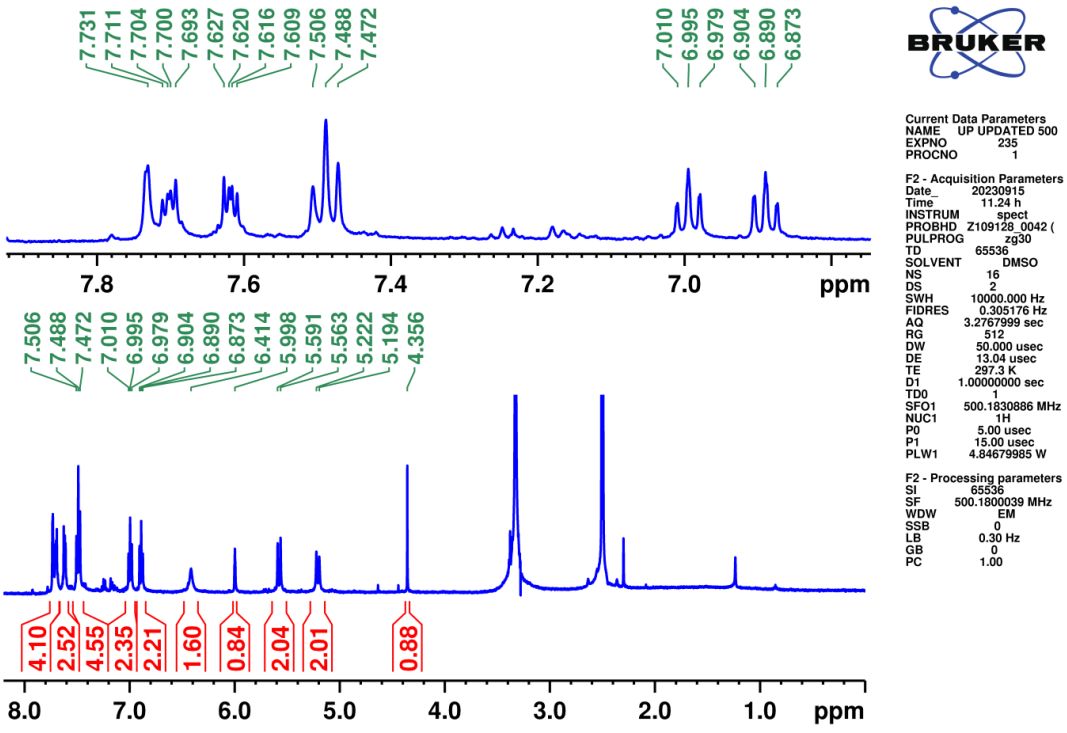

Figure 5.31. ^{1}H NMR spectrum of **3** in DMSO-d_6.

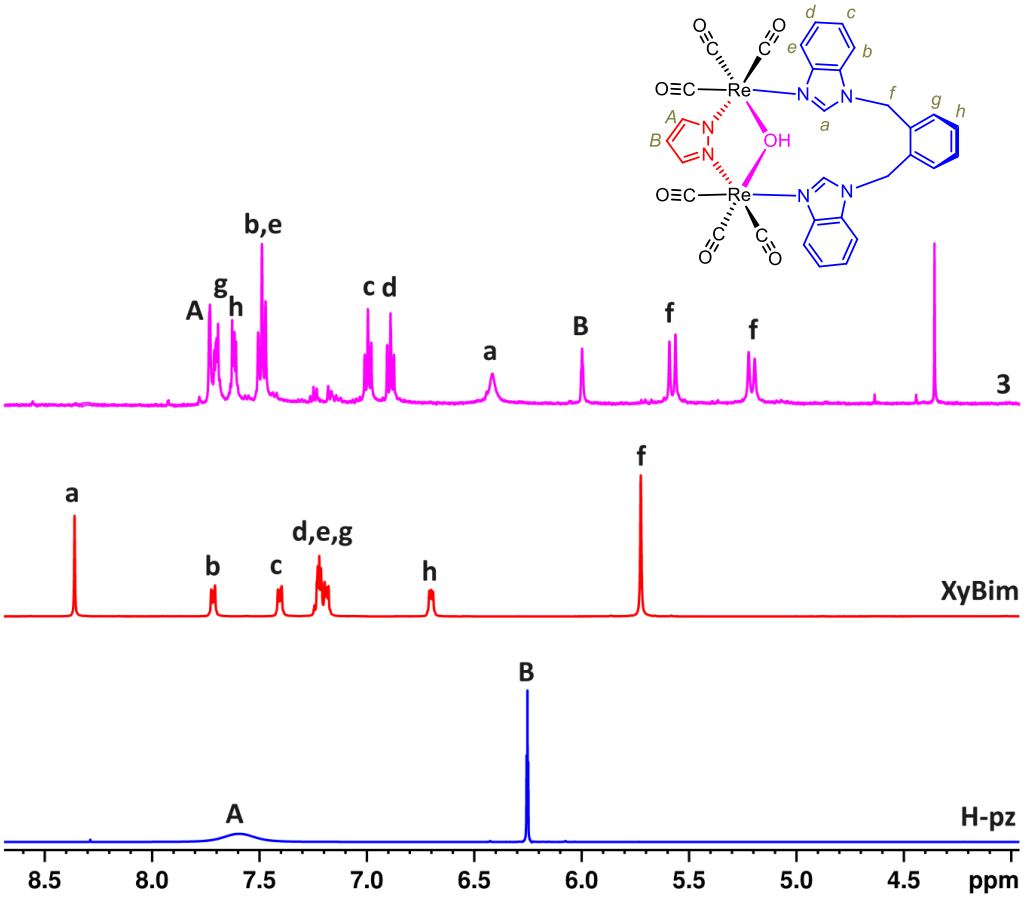

Figure 5.32. Partial ^{1}H NMR spectra of ligands and metallocycle **3** in DMSO-d_6.

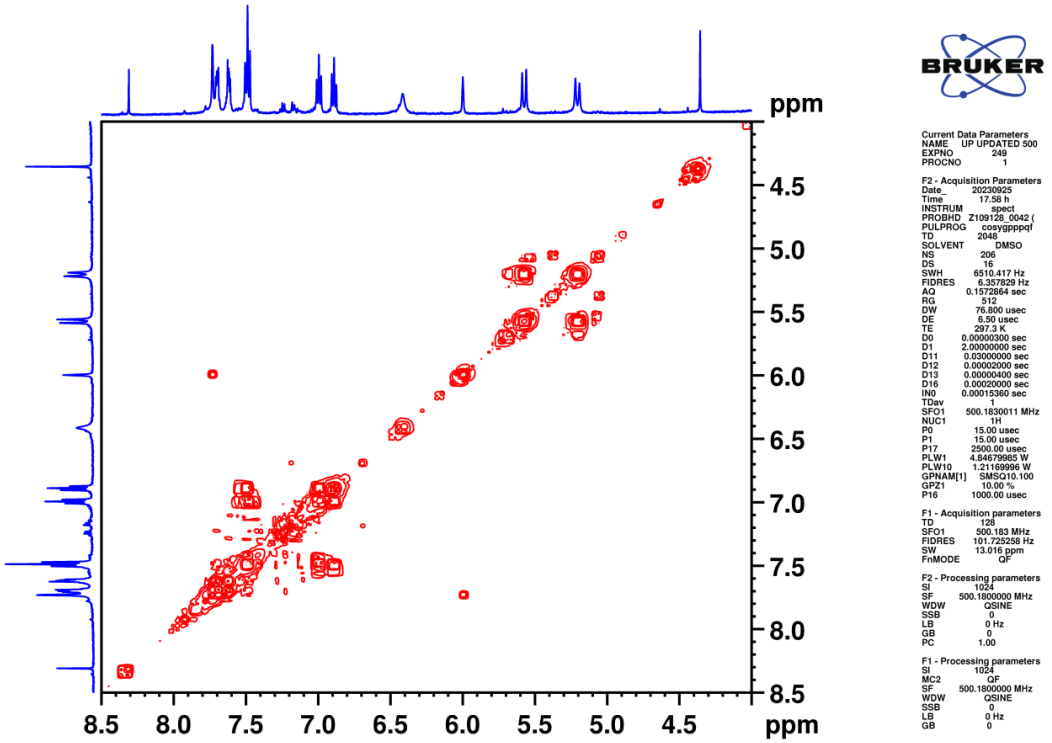

Figure 5.33. COSY NMR spectra of metallocycle **3** in DMSO-d_6.

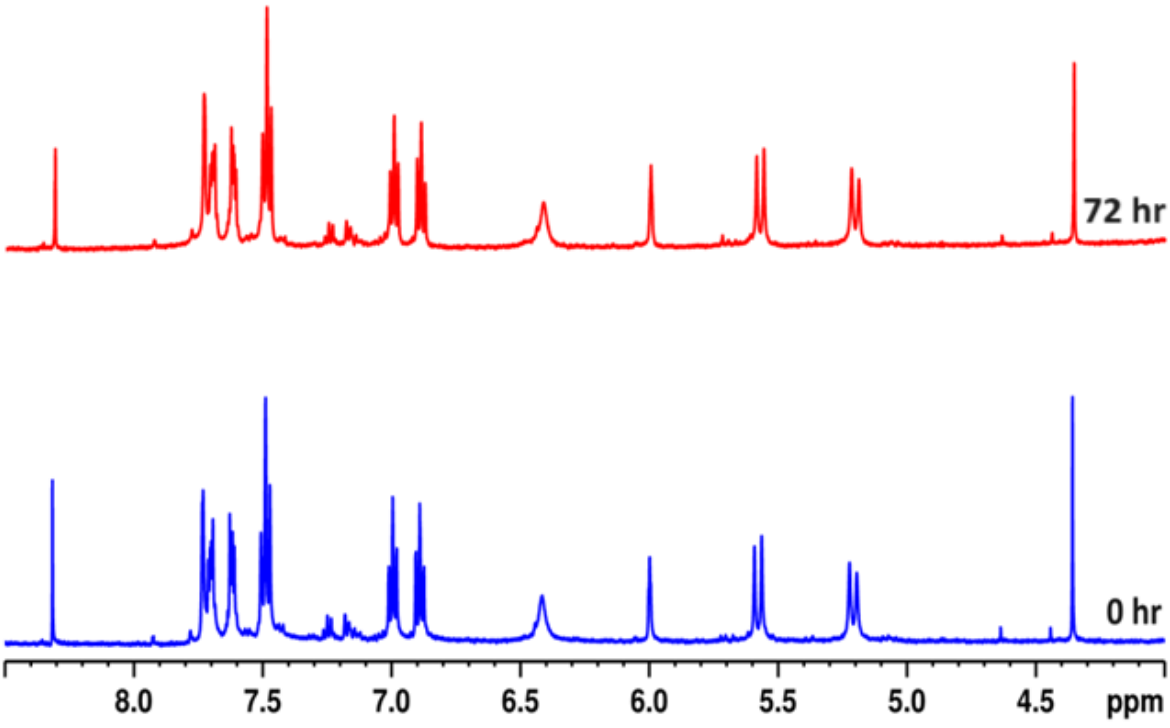

Figure 5.34. Partial ^{1}H NMR spectra of metallocycle **3** in DMSO-d_6 at 0 hr and 72 hr.

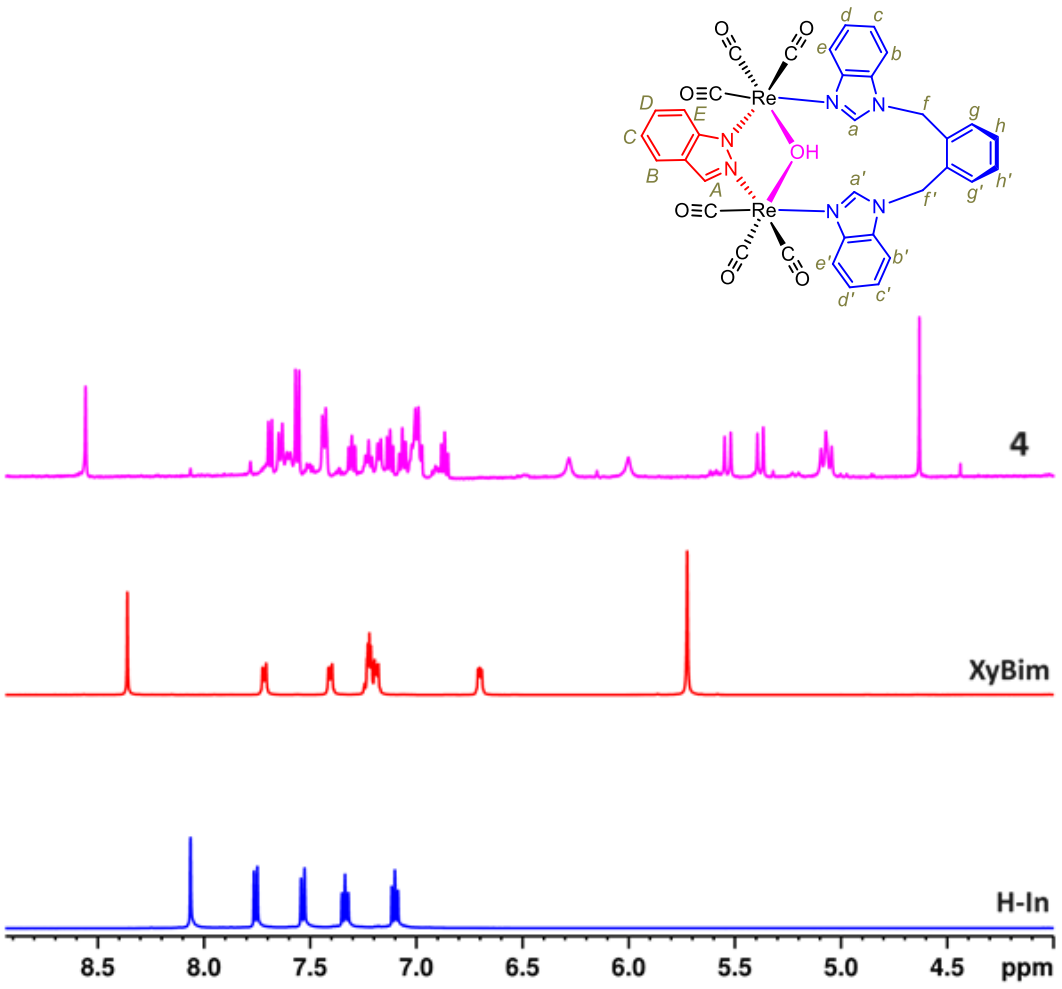

Figure 5.35. Partial ^{1}H NMR spectra of ligands and metallocycle **4** in DMSO-d_6.

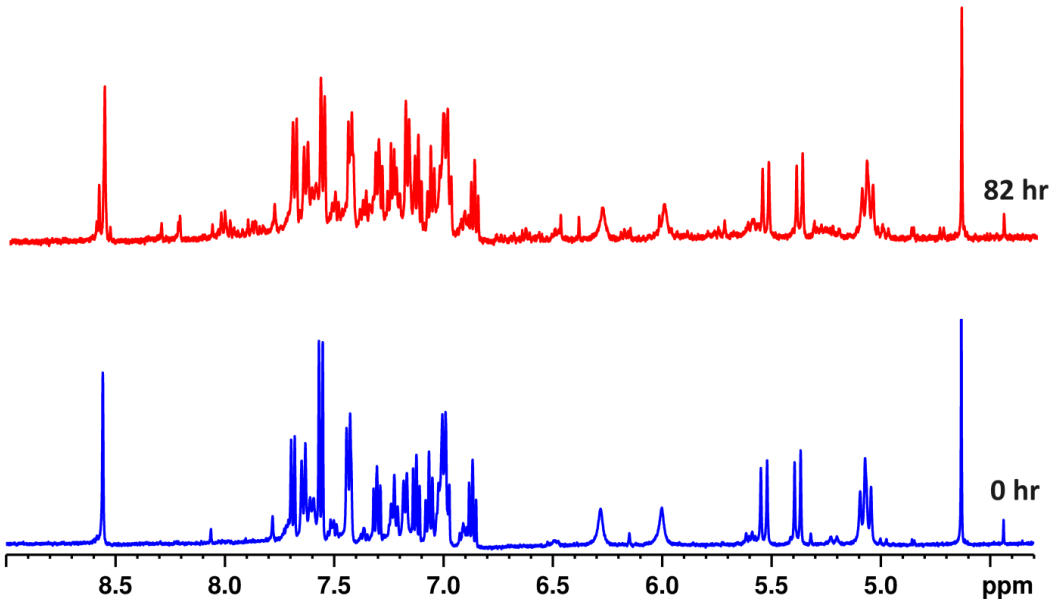

Figure 5.36. Partial ^{1}H NMR spectra of metallocycle **4** in DMSO-d_6 at 0 hr and 82 hr.

5.3.6. Molecular Structures of Metallocycles 2-3

The SC-XRD data reveals that **2** adopts dinuclear cyclic structure consisting of indazolate-hydroxo-bridged dinuclear motif *fac*-[{$(CO)_3$Re}(μ_2-OH)(μ-Ind){Re$(CO)_3$}] and one bpz ligand (Figure 5.37). Indazolate and hydroxo unit are in the same plane, whereas the two pyrazolyl units are orthogonal to these anionic units and phenyl unit. All four aromatic units are directed towards one direction. Both the *fac*-[Re$(CO)_3$] motifs are at one edge of the metallocycle with all six carbonyl groups pointed outward.

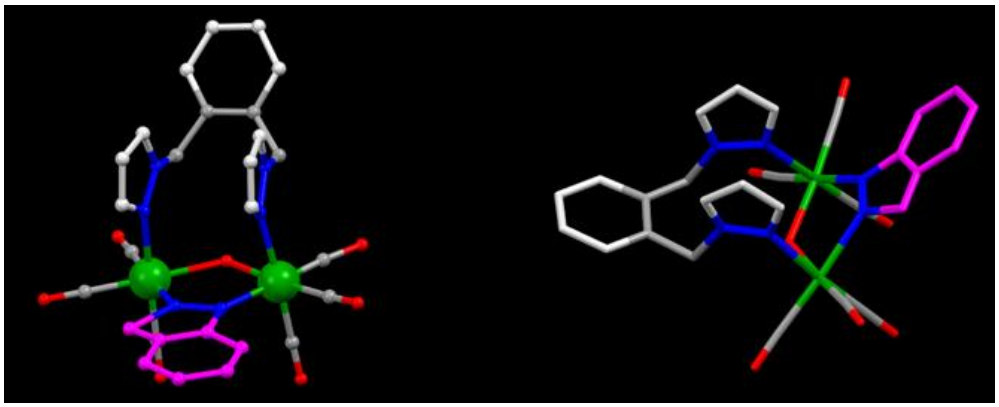

Figure 5.37. Various views of molecular structure of **2** in capped stick model (H atoms are removed for clarity). Color code: C = grey for XyBim and CO & pink for pz; O = red, N = blue, Re = green.

Molecular structure of **3** consist of two *facial*-Rheniumtricarbonyl cores, one pyrazolate unit, one hydroxyl motif and one XyBim motif (Figure 5.38). Two *fac*-[Re$(CO)_3$ cores are bridged by pyrazolate-hydroxo- motifs resulting in the dinuclear metallocycle. Pyrazolate and hydroxo unit are in the same plane, which are orthogonal to the benzimidazolyl motifs. The two benzimidazolyl motifs are parallel to each other and stabilized via $\pi\cdots\pi$ interactions. The pyrazolate motif and the phenyl ring of the XyBim are directed towards each other.

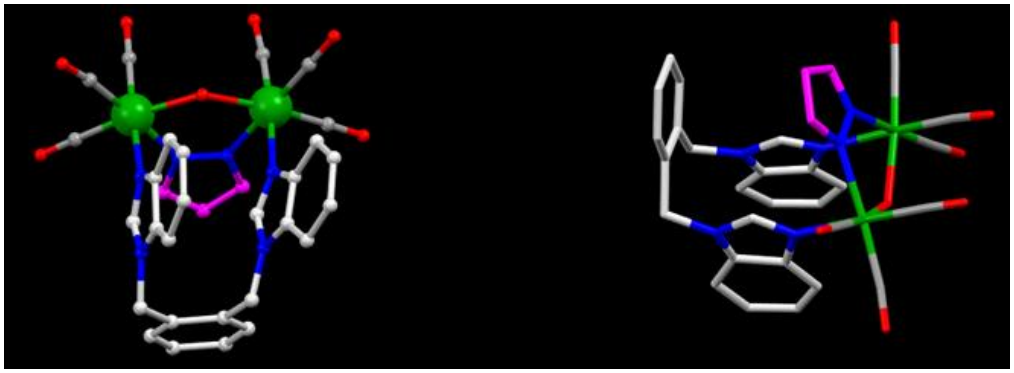

Figure 5.38. Various views of molecular structure of **3** in capped stick model (H atoms are removed for clarity). Color code: C = grey for XyBim and CO & pink for pz; O = red, N = blue, Re = green.

5.3.7. Biological studies of 2-4

MTT assay was carried out to find out the cytotoxicity effect of the complexes **2-4**, XyBim and cisplatin towards 4T1 cells. The study reveals that among the complexes **2-4**, complex **4** shows maximum cytotoxicity towards 4T1 cells (Figure 5.39). The IC_{50} (μM) values are found to be 5 for **2**; 2.5 for **3**, 1.25 for **4**. As compared to cisplatin complex **4** is 40 times more cytotoxic towards 4T1 cancer cells. This may to due to the presence of benzimidazolyl and indazolate motifs in the complex which provides a greater surface for non-covalent interactions with DNA leading to cell death.

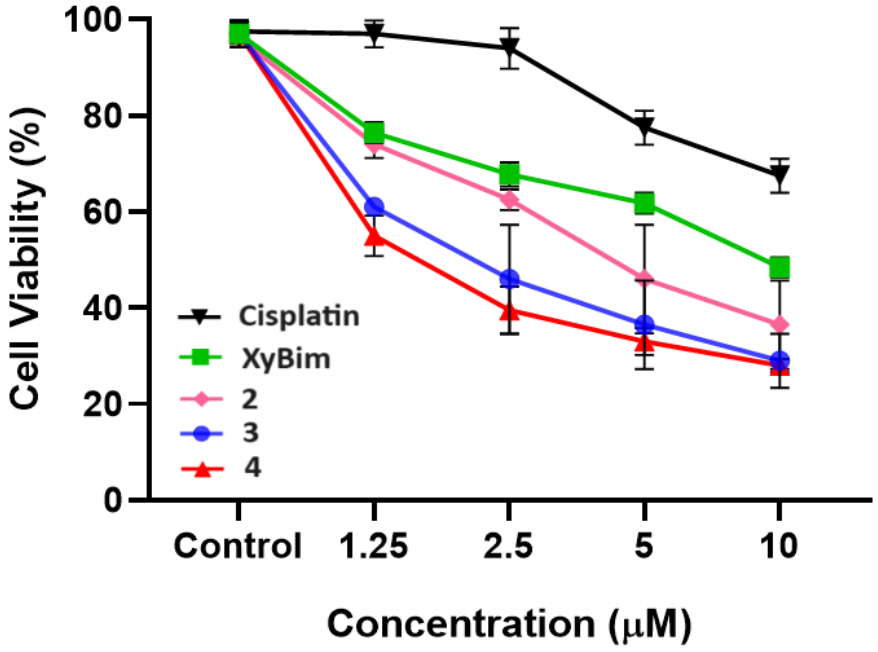

Figure 5.39. Dose-responsive curves of free ligand bpz, cisplatin and **Re1** against triple negative breast cancer cells (4T1) after 24 h incubation.

5.4 Conclusion

In conclusion, a new type of neutral, stable, small dirhenium metallocycle consisting of pyrazolate, hydroxyl, bidentate pyrazolyl clip and two rheniumtricarbonyl cores, was synthesized. The pyrazolate and hydroxyl motifs are necessary to hold two dirhenium tricarbonyl cores close to each other to provide compact metallocyclic structure. At room temperature, the metallocycle **1** in DMSO undergoes partial disassembly into the free bpz, H-pz and a disintegrated *fac*-[$Re(CO)_3$] complex. The metallocycle exhibits superior anticancer activity compared to cisplatin against the triple negative breast cancer cell line (4T1). Controlled experiment clearly demonstrated that the free ligands and the disassembled

complex are not responsible for the anticancer properties. It is the metallocycle that plays a crucial role in anticancer activity. The molecular docking studies revealed that the metallocycle preferentially binds strongly with the minor groove of DNA through various non-covalent interactions. This was further proved from the synthesis of stable azolato-hydroxo bridged complexes using benzimidazolyl ligand which when performed MTT assay reveals that complex **4** with benzimidazolyl and indazolate ligands shows maximum cytotoxicity than cisplatin against 4T1 cells. These findings suggest that the metallocycle's compact size, strategically positioned hydrogen bonding donor groups in the form of coordinated carbonyl units, and aromatic surface are well-suited to fit within DNA grooves, thereby triggering cell death.

5.5. References

1) (a) S. Dilruba and G. V. Kalayda, *Cancer Chemother. Pharmacol.* 2016, **77**, 1103−1124. (b) N. Devarajan, R. Manjunathan and S. K. Ganesan, *Crit. Rev. Oncol. Hematol.* 2021, **162**, 103327. (c) S. P. Vaidya, S. Gadre, R. T. Kami-setti and M. Patra, *Biosci Rep.* 2022, **42** (5): BSR20212160.
2) (a) X. Li, Z. Shi, J. Wu, J. Wu, C. He, X. Hao and C. Duan, *Chem. Commun.* 2020, **56**, 7537. (b) A. Pöthig and A. Casini, *Theranostics* 2019, **9**, 3150-3169. (c) A. K. Singh, A. Kumar, H. Singh, P. Sonawane, P. Pathak, M. Grishina, J. P. Yadav, A. Verma and P. Kumar, *Chem. Biodiversity* 2023, **20**, e20230006. (d) R. Paprocka, M. Wiese-Szadkowska, S. Janciauskiene, T. Kosmalski, M. Kulik and A. Helmin-Basa, *Coord. Chem. Rev.* 2022, **452**, 214307. (e) H. Sepehpour, W. Fu, Y. Sun and P. J. Stang, *J. Am. Chem. Soc.* 2019, **141**, 14005-14020. (f) G. Yu, M. Jiang, F. Huang and X. Chen, *Curr. Opin. Chem. Biol.* 2021, **61**, 19-31. (g) J. Karges, *Angew. Chem. Int. Ed.* 2022, **61**, e202112236.
3) (a) S. Pete, N. Roy, B. Kar and P.Paira, *Coord. Chem. Rev.* 2022, **460**, 214462. (b) P. Nicholas, N. P. Bigham and J. J. Wilson, *J. Am. Chem. Soc.* 2023, **145**, 9389–9409. (c) K. Kirakci, M.A. Shestopalov and K. Lang, Coord. Chem. Rev. 2023, 481, 215048.
4) (a) A. Sharma, N. Vaibhavi, B. Kar, U. Das and P. Paira, *RSC Adv*., 2022, **12**, 20264. (b) K. Schindler and F. Zobi, *Molecules* 2022, **27**, 539. (c) A. Leonidova and G. Gasser, *ACS Chem. Biol.* 2014, **9**, 2180–2193. (d) E. B. Bauer, A. A. Haase, R. M. Reich, D. C. Crans and F. E. Kühn, *Coord. Chem. Rev.* 2019, **393**, 79–117. (e) H. S. Liew, C-W. Mai, M.

Zulkefeli, T. Madheswaran, L. V. Kiew, N. Delsuc and M. L. Low, *Molecules* 2020, **25**, 4176. (f) Z. Huang and J.J. Wilson, *Eur. J. Inorg. Chem*. 2021, 1312-1324. (g) J. R. Dilworth, Coord. Chem. Rev. 2021, 4356, 213822. (i) D. Gupta and M. Sathiyendiran, *ChemistrySelec*t 2018, **3**, 7439-7458.

5) (a) S. C. Marker, A. P. King, R. V. Swanda, B. Vaughn, E. Boros, S. B. Qian and J. J. Wilson, *Angew. Chem. Int. Ed.* 2020, **59**, 13391-13400. (b) E. Lucy, L. E. Enslin, K. Purkait, M. D. Pozza, B. Saubamea, P. Mesdom, H. G. Visser, G. Gasser and M. Schutte-Smith, *Inorg. Chem.* 2023, **62**, 12237–12251. (c) X. Su, W. J. Wang, Q. Cao, H. Zhang, B. Liu, Y. Ling, X. Zhou and Z. W. Mao, *Angew. Chem. Int. Ed.* 2022, **61**, e202115800. (d) P. Collery, V. Veena, A. Harikrishnan and D. Desmaele, *Invest New Drugs* 2019, **37**, 973-983.
6) (a) A. Kastl, S. Dieckmann, K. Whler, T. Vçlker, L. Kastl, A. L. Merkel, A. Vultur, B. Shannan, K. Harms, M. Ocker, W. J. Parak, M. Herlyn and E. Meggers, *Chem Med Chem* 2013, **8**, 924-927. (b) B. Mavroidi, A. Kaminari, K. Makrypidi, A. Shegani, P. Bouziotis, I. Pirmettis, M. Papadopoulos, M. Sagnou and M. Pelecanou, *Invest New Drugs* 2022, **40**, 497-505. (c) Z. Y. Pan, C. P. Tan, L. S. Rao, H. Zhang, Y. Zheng, L. Hao, L. N. Ji and Z. W. Mao, *Angew. Chem. Int. Ed.* 2020, **59**, 18755-18762. (d) P. V. Simpson, I. Casari, S. Paternoster, B. W. Skelton, M. Falasca and M. Massi, *Chem. Eur. J.* 2017, **23**, 6518-6521. (e) Z-Y. Pan, D-H. Cai and L. He, *Dalton Trans.*, 2020, **49**, 11583. (f) J. Delasoie, A. Pavic, N. Voutier, S. Vojnovic, A. Crochet, J. Nikodinovic-Runic and F. Zobi, *Eur. J. Med. Chem.* 2020, **204**, 112583.
7) (a) B. Ramakrishna, R. Nagarajaprakash, V. Veena, N. Sakthivel and B. Manimaran, *Dalton Trans.* 2015, **44**, 17629-17638. (b) M. Karthikeyan, R. Govindarajan, E. Duraisamy, V. Veena, N. Sakthivel and B. Manimaran, *ChemistrySelect* 2017, **2**, 3362-3368. (c) R. Govindarajan, R. Nagarajaprakash, V. Veena, N. Sakthivel and B. Manimaran, *Polyhedron* 2018, **139**, 229-236.
8) (a) L. C. Bailey-Downs, J. E. Thorpe , B. C. Disch, A. Bastian, P. J. Hauser, T. Farasyn, W. L. Berry, R. E. Hurst, M. A. Ihnat, PLoS ONE. 2014, **9**, e98624. (b) C. K. Anders and L. A. Carey, *Clinical Breast Cancer* 2009, **9**, S73–S81.
9) M. Charbonneau, G. Addoumieh, P. Oguadinma and A. R. Schmitzer, *Organometallics* 2014, **33**, 6544–6549.
10) Sheldrick, G. M. A short history of SHELX. Acta Crystallogr., Sect. A: Found. Crystallogr. 2008, **64**, 112−122.

11) Sheldrick, G.M. SHELXS-97: Program for Crystal Structure Solution, University of Göttingen, Göttingen, Germany, 1997.

12) Drew, H. R., Wing, R. M., Takano, T., Broka, C., Tanaka, S., Itakura, K., & Dickerson, R. E. (1981). Structure of a B-DNA dodecamer: conformation and dynamics. Proceedings of the National Academy of Sciences 78(4), 2179-2183.

13) Eberhardt, J., Santos-Martins, D., Tillack, A.F., Forli, S. AutoDock Vina 1.2.0: New Docking Methods, Expanded Force Field, and Python Bindings. Journal of Chemical Information and Modeling. 2021

14) Trott, O., & Olson, A. J. AutoDock Vina: improving the speed and accuracy of docking with a new scoring function, efficient optimization, and multithreading. Journal of computational chemistry 2010, **31**, 455-461.

Chapter 6

Conclusion and Future Prospects

Abstract

The thesis entitled "Self-assembly of Rhenium(I) Metallocycles Using Pyrazole Based Ligands" discusses the design and synthesis of *facial*-rheniumtricarbonyl based metallocycles of various architectures by using ligands containing pyrazole as the coordinating motifs with ancilliary ligands. Several architectures such as monohelicates, "*figure-eight"*, "*Z*" shaped molecules, conjoined bicyclic metallocycles and compact dinucler metallocyles were synthesized. This chapter summarizes the thesis work and gives a brief perspective of future direction of the research work.

6.1. Overview of the present work

The facial rheniumtricarbonyl core provides a platform for synthesizing a variety of 2D and 3D architectures that are known to be robust, inert and can be functionalized for potential application prospects. These complexes are potential candidates in the field of molecular recognition, sensing, bioimaging and as anticancer agents.[1-4] With the choice of predesigned ligands in presence of ancilliary ligands and $Re_2(CO)_{10}$ metallocycles of diverse shapes and sizes can be synthesized.[2] The use of flexible ligands in the synthesis of metallocycles is less explored as compared to their rigid counterparts because of the lack of predictability of its conformation in the final structure.[3] The use of imidazolyl, benzimidazolyl or napthanoimidazolyl as the coordinating motifs in the synthesis of flexible ligands is well explored. However the use of pyrazole based ligands in the synthesis of rhenium based metallocycles are not much explored. Pyrazole like imidazole is a 5-membered heterocycle with two N atoms in the adjacent positions and is known as a potent medical scaffold with wide range of biological activities. This research focuses on introducing pyrazolyl motif as the coordinating motif in the synthesis of rhenium based metallocycles and study how the change in coordinating motif dictates the final architecture.

Two pyrazolyl based neutral ditopic ligands were synthesized and characterized. Using the synthesized pyrazolyl based ligand, rigid bischelating donor and $Re_2(CO)_{10}$ under solvothermal conditions neutral rhenium(I) based dinuclear helicates were synthesized. The complexes were found to be helical in nature with only the neutral ditopic ligand wrapping around in a helical arrangement leading to the formation of dinuclear double stranded monohelicates. This type of helical arrangement is new in the rhenium based helicate architecture. This study provides a design strategy for synthesis of dinuclear monohelicates.

The change in length and breadth of the rigid ancilliary ligands also may affect the final architecture of the complexes. So keeping the neutral pyrazolyl based donor intact, bischelating anionic donors of longer width and breadth were used which lead to the synthesis of tetranuclear metallocycles. A "*figure-eight*" and "*Z*" shaped metallocycles were synthesized and characterized. The complexes were found to be in dynamic equilibrium in DMSO with continuous disassembly and reassembly of the components owing to the dynamic nature of the metal-pyrazolyl bond. This dynamic nature of the complexes was further utilized to transform these metallocycles into other known/unkown metallocycles and acyclic complexes using suitable competing ligands via ligand-induced supramolecular

transformations. The results may pave the way to the development of less explored competitive ligand-induced supramolecular transformations in rhenium carbonyl-based metallocycles.

This research work also provides a new synthetic principle for synthesis of conjoined bicyclic complexes. Hexatopic/tetratopic pyrazolyl based donor ligands were used along with pyrazole/Br-pyrazole as anionic donor and $Re_2(CO)_{10}$ using solvothermal approach resulting in the formation of conjoined bicyclic rhenium(I) based metallocycle. The cyclic motif in the metallocycle was connected through the phenylene spacer from the neutral ligand. A new kind of bonding combination was found in which the two rhenium cores were bridged by a azolate motif and hydroxo motif. This bridging combination is not known in the rhenium chemistry.

The pyrazolato and hydroxo bridging between Pt metal cores are well known and these class of complexes were found to be biologically active. In this study we have synthesized four rhenium based dinuclear metallocycles having the azolato and hydroxo bridging. The complexes were synthesized using $Re_2(CO)_{10,}$ pyrazole/indazole as anionic donors and pyrazole/benzimidazole based ditopic donors under solvothermal conditions. Preliminary biological investigations of the complexes shows that these metallocycles exhibits cytotoxicity effects on triple negative breast cancer cells (4T1) with non-covalent interactions with DNA leading to cell death.

Table 6.1. Compounds synthesized in the present study

No.	Discrete supramolecule/acyclic	Type	Shape	Approach
1	*fac*-[{Re(CO)$_3$}$_2$(μ-dhbq)(dppz)]	M_2LL'	Helicate	New
2	*fac*-[{Re(CO)$_3$}$_2$(μ-pydc)(dppz)]	M_2LL'	Helicate	New
3	*fac*-[{Re(CO)$_3$}$_2$(μ-dhbq)(L′)]	M_2LL'	Helicate	New
4	*fac*-[{Re(CO)$_3$}$_2$(μ-pydc)(L′)]	M_2LL'	Helicate	New
5	*fac*-[{Re(CO)$_3$}$_4$(μ-dhnq)$_2$(dppz)$_2$]	$M_4L_2L'_2$	Figure-eight	New
6	*fac*-[{Re(CO)$_3$}$_4$(μ-dhaq)$_2$(dppz)$_2$]	$M_4L_2L'_2$	Z shaped metallocycle	New
7	*fac*-[{Re(CO)$_3$}$_4$(μ-dhnd)$_2$(dppz)$_2$]	$M_4L_2L'_2$	Z shaped metallocycle	New
8	*fac*-[{Re(CO)$_3$}$_4$(μ-bbim)$_2$(dppz)$_2$]	$M_4L_2L'_2$	Z shaped metallocycle	New
9	*fac*-[{Re(CO)$_3$}$_2$(μ-dhnq)(dpbim)]	M_2LL'	Metallocavitand	New
10	*fac*-[{Re(CO)$_3$}$_2$(μ-dhnd)(dpbim)]	M_2LL'	Metallocavitand	New
11	*fac*-[{Re(CO)$_3$}$_2$(μ-bbim)(dpbim)]	M_2LL'	Metallocavitand	New
12	*fac*-[{Re(CO)$_3$}$_2$(μ-dhnq)(PTA)]	M_2LL'	Acyclic	New
13	*fac*-[{Re(CO)$_3$}$_2$(μ-dhaq)(PTA)]	M_2LL'	Acyclic	New
14	*fac*-[{Re(CO)$_3$}$_2$(μ-dhnd)(PTA)]	M_2LL'	Acyclic	New
15	*fac*-[{Re(CO)$_3$}$_2$(μ-bbim)(PTA)]	M_2LL'	Acyclic	New
16	*fac*-[{Re(CO)$_3$}$_4$(μ^2-OH)$_2$(μ-pz)$_2$(L″)]	$M_4L_2L'_2L''$	Bicyclic metallocycle	New
17	*fac*-[{Re(CO)$_3$}$_4$(μ^2-OH)$_2$(μ-Br-pz)$_2$(L″)]	$M_4L_2L'_2L''$	Bicyclic metallocycle	New
18	*fac*-[{Re(CO)$_3$}$_4$(μ^2-OH)$_2$(μ-pz)$_2$(L″)]	$M_4L_2L'_2L''$	Bicyclic metallocycle	New
19	*fac*-[{Re(CO)$_3$}$_2$(μ^2-OH)(μ-pz)(bpz)]	$M_2LL'L''$	Metallocycle	New
20	*fac*-[{Re(CO)$_3$}$_2$(μ^2-OH)(μ-Ind)(bpz)]	$M_2LL'L''$	Metallocycle	New
21	*fac*-[{Re(CO)$_3$}$_2$(μ^2-OH)(μ-pz)(XyBim)]	$M_2LL'L''$	Metallocycle	New
22	*fac*-[{Re(CO)$_3$}$_2$(μ^2-OH)(μ-Ind)(XyBim)]	$M_2LL'L''$	Metallocycle	New

H_2-dhbq = 2,5-dihydroxy-1,4-benzoquinone, H_2-pydc = 2,5-pyrazinedicarboxylic acid, H_2-dhaq = 1,4-dihydroxy-9,10-anthraquinone, H_2-dhnq = 5,8-dihydroxy-1,4-naphthoquinone, H_2-dhnd = 6,11-dihydroxy-5,12-naphthacenedione, H_4-thbq = 2,3,5,6-tetrahydroxy-1,4-benzoquinone, H_2-bbim = Bisbenzimidazole, H_2-RBC = Rigid bischelating ligand, H_2-pBC = 1,4-bis(2-(2-hydroxyphenyl)benzimidazol-1-ylmethyl)benzene, H_2-mBC = 1,3-bis(2-(2-hydroxyphenyl)benzimidazol-1-ylmethyl)2,4,6-trimethylbenzene, dppz = bis(4-((pyrazolyl) methyl)phenyl)methane, dpbim = bis(4-((benzoimidazolyl)methyl)phenyl) methane, bpz = 1,2-bis((pyrazolyl)methyl)benzene, PTA = 1,3,5-Triaza-7-phosphaadamantane, H-pz = Pyrazole, H-Ind = Indazole, H-Br-pz = 4-Bromopyrazole, XyBim = 1,2-bis((benzoimidazolyl)methyl)benzene, L′ (3&4) = bis(4-((pyrazolyl) methyl)phenyl)methanone, L″ = 1,2,3,4,5,6-hexakis((pyrazolyl)methyl)benzene for 16 and 1,2,4,5-tetrakis((pyrazolyl)methyl)benzene for 17&18.

6.2. Future directions

The design and synthesis of metallocycles is an ever evolving process for development of new synthetic metallocycles with functional properties. *fac*-[$Re(CO)_3$] based complexes are known to exhibit interesting properties including kinetic inertness, thermal and photostability.[2] These interesting properties provide various opportunities for development of new supramolecules for application in guest encapsulation or separation, as sensors, light harvesting molecules and anticancer activities. The *fac*-[$Re(CO)_3$] core based complexes can also be used for vibrational bioimaging as strong CO bands are observed in the IR spectra in the region 1800-2000 cm^{-1} which is transparent in the biological systems.[5] Hence the design and synthesis of new rhenium based metallocycles is gaining considerable research interest both as therapeutic and diagnostic agents.

6.3. References

1. (a) P. Thanasekaran, C. C. Lee and K. L. Lu, *Acc. Chem. Res*. 2012, **45**, 1403–1418. (b) P. H. Dinolfo and J. T. Hupp, *Chem. Mater*. 2001, **13**, 3113–3125.
2. D. Gupta and M. Sathiyendiran, *ChemistrySelect*. 2018, **3**, 7439-7458 and references cited there in.
3. (a) T. R. Cook and P. J. Stang, *Chem. Rev*. 2015, **115**, 7001-7045. (b) T. R. Cook, V. Vajpayee, M. H. Lee, P. J. Stang and K. W. Chi, *Acc. Chem. Res.* 2013, **46**, 2464-2474.
4. (a) E. B. Bauer, A. A. Haase, R. M. Reich, D. C. Crans and F. E. Kühn, *Coord. Chem. Rev.* 2019, **393**, 79-117. (b) B. Ramakrishna, R. Nagarajaprakash, V. Veena, N. Sakthivel and B. Manimaran, *Dalton Trans.* 2015, **44**, 17629-17638. (c) R. G. Balasingham, F. L. Thorp-Greenwood, C. F. Williams, M. P. Coogan and S. J. Pope, *Inorg. Chem*. 2012, **51**, 1419−1426. (d) S. Sato and O. Ishitani, *Coord. Chem. Rev*. 2015, **282**–**283**, 50–59.
5. (a) A. Pöthig and A. Casini, *Theranostics* 2019, **9**, 3150-3169. (b) K. Schindler and F. Zobi, *Molecules* 2022, **27**, 539. (c) V. Fernandez-Moreira, F. L. Thorp-Greenwood and M. P. Coogan, *Chem. Commun*. 2010, **46**, 186-202.

Publications

A. Publications from thesis work:

1. **Phukon, U.**; Priyatharsini, M.; Sathiyendiran, M. Self-assembly of rhenium core-based conjoined bicyclic supramolecule from pyrazole and flexible hexatopic pyrazolyl ligands. *J. Organomet. Chem*., **2020**, *923*, 121460.

2. **Phukon**, **U.**; Shankar, B.; Sathiyendiran, M. Self-assembly of a new class of rhenium(I)-based double stranded dinuclear monohelicates with their photophysical and electrochemical studies. *Dalton Trans*., **2022**, *51*, 16307–16315.

3. **Phukon**, **U.**; Kedia, M., Shankar, B.; Sathiyendiran, M. Rhenium-Pyrazolyl based Figure-Eight- and Z Shaped Metallocycles: Self-Assembly, Solid-State Structures, Dynamic Properties in Solution and Competitive Ligand Induced Supramolecular Transformations into Rhenium-Pyridyl/-Benzimidazolyl/-Phosphine based Metallocycles/Acyclic Complexes. *ACS Omega* **2023**, *8*, 41773–41784.

4. **Phukon**, **U.**; Khatun, S.; Kedia, M.; Putta, C. L.; Shankar, B.; Rengan, A. K.; Sathiyendiran, M. Self-assembly of small multicomponent rhenium metallocycle and its effective anticancer activities against triple negative breast cancer cells (C*ommunicated*).

5. **Phukon, U**.; Putta, C. L.; Kedia, M.; Shankar, B.; Rengan, A. K.; Sathiyendiran, M. Effective anticancer activities of azolato and hydroxo bridged rhenium(I) metallocycles against triple negative breast cancer cells (To be communicated).

6. **Phukon, U.**; Shankar, B.; Sathiyendiran, M. Self-assembly and structural characterization of rhenium core-based conjoined bicyclic supramolecule from flexible tetratopic pyrazolyl ligand. (To be communicated).

B. Other Publications:

1. Kedia, M.; Khatun, S.; **Phukon, U.**; Shankar, B.; Rengan, A. K.; Sathiyendiran, M. Trinuclear rhenium(I)-based metallocages as anticancer agents towards human cervical cancer cells. *Dalton Trans.*, **2023**, *52*, 14314-14318.

2. Kedia, M.; Soumya, K. R.; **Phukon, U.**; Mishra, I.; Borkar, R. L.; Vengadeshwaran, P.; Bhol, M.; Sathiyendiran, M. Double ouroboros-shaped noncovalent molecular dimer. *CrystEngComm*, **2023**, *25*, 2518-2522.

3. Soumya, K. R.;[†] Mishra, I.;[†] Kedia, M.,[†] **Phukon, U.**;[†] Borkar, R.;[†] Sathiyendiran, M. in Supramolecular Coordination Complexes: Design, Synthesis and Applications, ed. S. Shanmugaraju, Elsevier, 1st edn, **2022**, 133-153 **([†]Equal Contribution)**.

4. Kanungo, A. D.; Ila; Panda, S.; **Phukon, U.**; Sathiyendran, M.; Krishnamoorthy, G. Excited state dynamics of a double ESIPT unit comprising fluorophore. *J. Photochem. Photobiol. A*, **2024**, *450*, 115412.

Poster and Oral Presentations

1. **Poster:** "Bicyclic supramolecular coordination complex", *CHEMFEST-2020: 17th Annual in- House Symposium,* University of Hyderabad, Telangana, India; 2020 Feb. 27-28.

2. **Oral:** "Self-assembly of Organometallic Helicates", *CHEMFEST-2022: 19th Annual in- House Symposium,* University of Hyderabad, Telangana, India; 2022 Apr. 22-23.

3. **Poster:** "Metallocycles and conjoined bicyclic supramolecules from rhenium(I) core and pyrazolyl donors", *CHEMFEST-2023: 20th Annual in- House Symposium,* University of Hyderabad, Telangana, India; 2023 Mar. 03-04.

4. **Poster**: "Competitive ligand induced supramolecular transformations, solution state dynamics of "*figure-eight*" and "*Z*" shaped rhenium(I) supramolecules", *MTIC 2023: International Conference on Modern Trends In Inorganic Chemistry-XX,* Indian Institute of Science, Bangalore, Karnataka, India; 2023 Dec.14-17 **(Best Poster Award).**

5. **Poster**: "New class of rhenium metallocycles as potential anticancer agents", *MMM III 2023: International Conference on Main group Molecules to Materials,* Indian Institute of Technology Hyderabad & University of Hyderabad, Telangana, India; 2023 Dec. 9-11 **(Best Poster Award by RSC)**.

Self-assembly of Rhenium(I) Metallocycles Using Pyrazole Based Ligands

by UPASANA PHUKON

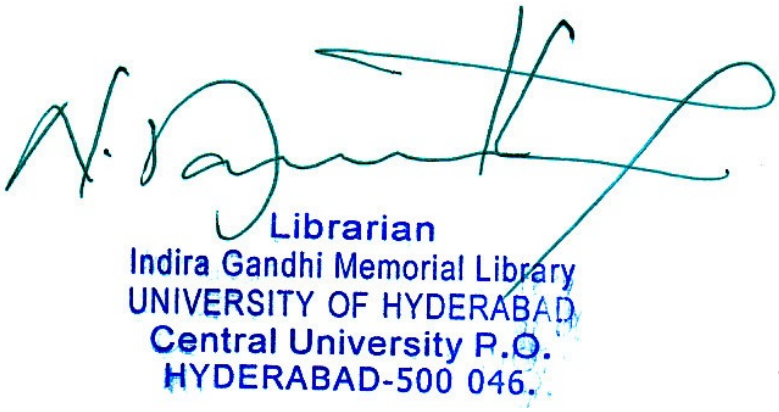

Submission date: 18-Jan-2024 03:30PM (UTC+0530)
Submission ID: 2273120349
File name: Plagarism_5._Final_Thesis_Chapter_1_-_Chapter_6__12-01-24.doc (304.5K)
Word count: 13390
Character count: 79784

Self-assembly of Rhenium(I) Metallocycles Using Pyrazole Based Ligands

ORIGINALITY REPORT

52%	35%	52%	12%
SIMILARITY INDEX	INTERNET SOURCES	PUBLICATIONS	STUDENT PAPERS

PRIMARY SOURCES

1	www.ncbi.nlm.nih.gov Internet Source	27%
2	Submitted to University of Hyderabad, Hyderabad Student Paper	9%
3	Sathiyendiran Malaichamy, Upasana Phukon, Bhaskaran Shankar. "Self-assembly of new class of rhenium(I)-based double stranded dinuclear monohelicates with their photophysical and electrochemical studies", Dalton Transactions, 2022 Publication	6%
4	Upasana Phukon, Moon Kedia, Bhaskaran Shankar, Malaichamy Sathiyendiran. "Rhenium–Pyrazolyl-Based Figure-Eight- and Z-Shaped Metallocycles: Self-Assembly, Solid-State Structures, Dynamic Properties in Solution, and Competitive Ligand-Induced Supramolecular Transformations into Rhenium-Pyridyl/-Benzimidazolyl/-Phosphine-	4%

Based Metallocycles/Acyclic Complexes", ACS Omega, 2023
Publication

5 Upasana Phukon, Bhaskaran Shankar, Malaichamy Sathiyendiran. " Self-assembly of a new class of rhenium( )-based double stranded dinuclear monohelicates with their photophysical and electrochemical studies ", Dalton Transactions, 2022 — 3%
Publication

6 www.researchgate.net — 1%
Internet Source

7 Upasana Phukan, Priya Maruthupandian, Malaichamy Sathiyendiran. "Self-assembly of rhenium core-based conjoined bicyclic supramolecule from pyrazole and flexible hexatopic pyrazolyl ligands", Journal of Organometallic Chemistry, 2020 — 1%
Publication

8 K. R. Soumya, Ramar Arumugam, Bhaskaran Shankar, Malaichamy Sathiyendiran. "Sulfate Donor Based Dinuclear Heteroleptic Triple-Stranded Helicates from Sulfite and Ditopic Nitrogen Donor Ligands and Their Transformation to Dinuclear Homoleptic Double-Stranded Mesocates", Inorganic Chemistry, 2018 — <1%
Publication

9	Upasana Phukon, Maruthupandiyan Priyatharsini, Malaichamy Sathiyendiran. "Self-assembly of rhenium core-based conjoined bicyclic supramolecule from pyrazole and flexible hexatopic pyrazolyl ligands", Journal of Organometallic Chemistry, 2020 Publication	<1 %
10	Isha Mishra, Maruthupandiyan Priyatharsini, Malaichamy Sathiyendiran. "Synthesis and characterization of binuclear manganese carbonyl complex of 1,4-bis(2-(2′-hydroxyphenyl)benzimidazol-1-yl)benzene and dimethylaminopyridine", Journal of Organometallic Chemistry, 2021 Publication	<1 %
11	Ramar Arumugam, Bhaskaran Shankar, K. R. Soumya, Malaichamy Sathiyendiran. " -Re(CO) -based neutral heteroleptic tetrahedrons ", Dalton Transactions, 2019 Publication	<1 %
12	Bhaskaran Shankar, Saugata Sahu, Naina Deibel, David Schweinfurth et al. "Luminescent Dirhenium(I)-Double-Heterostranded Helicate and Mesocate", Inorganic Chemistry, 2014 Publication	<1 %

13	Rajesh Chakrabarty, Partha Sarathi Mukherjee, Peter J. Stang. "Supramolecular Coordination: Self-Assembly of Finite Two- and Three-Dimensional Ensembles", Chemical Reviews, 2011 Publication	<1 %
14	Mamina Bhol, Reema L. Borkar, Bhaskaran Shankar, Saroj Kumar Panda, Mariusz Wolff, Malaichamy Sathiyendiran. "Self-Assembly of Rhenium(I) Double-Stranded Helicate and Mesocate from Flexible Ditopic Benzimidazolyl/Naphthanoimidazolyl N-Donor and Rigid Bis-Chelating Hydroxyphenylbenzimidazolyl N∩OH-Donor Ligands: Synthesis, Characterization, and Photophysical and B-DNA Docking Studies", Inorganic Chemistry, 2023 Publication	<1 %
15	Suram Anitha. "The Complexity of Aluminum-DNA Interactions: Relevance to Alzheimer's and Other Neurological Diseases", Structure and Bonding, 2002 Publication	<1 %
16	vital.seals.ac.za:8080 Internet Source	<1 %

Journal of Organometallic Chemistry 923 (2020) 121460

Contents lists available at ScienceDirect

Journal of Organometallic Chemistry

journal homepage: www.elsevier.com/locate/jorganchem

Communication

Self-assembly of rhenium core-based conjoined bicyclic supramolecule from pyrazole and flexible hexatopic pyrazolyl ligands

Upasana Phukon, Maruthupandiyan Priyatharsini, Malaichamy Sathiyendiran*

School of Chemistry, University of Hyderabad, Hyderabad 500 046, India

ARTICLE INFO

Article history:
Received 13 June 2020
Revised 21 July 2020
Accepted 24 July 2020
Available online 28 July 2020

1. Introduction

The coordination driven self-assembly approaches i.e., metal-directed approaches for supramolecular coordination complexes (SCCs), discrete cyclic complexes, are highly successful methods to prepare simple mononuclear SCCs to complex interlocked SCCs [1–5]. Though many metal-directed synthetic rules are now known, continuous use of the known approaches and create a new design principle i.e., new metal-ligand(s) bonding combinations to assemble new molecular architectures have been intensely going on due to their aesthetical structures and potential future molecules in various areas including materials and medicinal fields. Among the many metal-directed approaches, the partially protected *fac*-$Re(CO)_3$-corner based assembly process using flexible multitopic ligands and neutral bridging ligands recently provided interesting spherical-shaped SCCs with multiple calixarene-shaped solvent-accessible cavity on the surface [4]. In particular, tuning the coordinating units of hexatopic ligands remotely by either increasing the fused ring/docarating phenyl rings on imidazolyl yielded overall spheroid SCCs with/without solvent-accessible cavity [4]. Tuning the imidazolyl unit by pyrazolyl unit in the hexatopic ligand may provide two kinds of SCCs. Spheroid shaped SCC with interconnecting calixarene cavities because of the adjacent arrangement of two heteroatoms in the pyrazolyl motif. In the case of hexatopic imidazolyl/benzimidazolyl-based SCCs, the C-H unit (N-C^2H-N) of imidazolyl, which is directed into the spheroid, acts as a steric unit blocking the channel of the cavities [4]. The second option is hitherto unexplored SCC because the small change in the binding angle of the donor units in the ligand i.e., from imidazolyl to pyrazolyl, may direct different coordination angle to adjust octahedral geometry around the *fac*-$Re(CO)_3$ core. Herein, we report on unexpected conjoined bicyclic supramolecular coordination complex with free two pyrazolyl motifs via a new type of metal-ligand bonding combinations i.e., *fac*-$Re(CO)_3$ from $Re_2(CO)_{10}$, pyrazole, water, and flexible hexatopic pyrazolyl N-donors in a one-pot solvothermal process.

2. Results and discussion

The treatment of $Re_2(CO)_{10}$, pyrazole (H-pz), 1,2,3,4,5,6-hexakis(pyrazol-1-ylmethyl)benzene (L), and toluene under solvothermal closed vessel resulted in pale yellow crystals *fac*-$[\{(Re(CO)_3)_2(\mu^2\text{-}OH)(k^1\text{:}k^1\text{-}\mu\text{-}pz)\}_2L]\cdot C_7H_8$ (**1**$\cdot C_7H_8$) (Scheme 1). The crystals are air and moisture-stable and soluble in DMSO. The FT-IR spectrum of the complex displayed three strong bands (1865, 1927, and 2007 cm^{-1}), which are the characteristic peaks for the *fac*−$Re(CO)_3$ core in the complex [4]. Further, the IR spectrum of crystal of **1** showed a sharp band at 3556 cm^{-1}, indicating the presence of the hydroxyl group (Fig. S1). The ^1H NMR spectrum of crystals of **1** in d_6-DMSO showed multiple signals in the region of 8.1 to 5.0 ppm in contrary to simple pattern expected for a symmetrical arrangement of pyrazolyl and pyrazolate motifs (Fig. S2). Though the complex contains three kinds of pyrazole motifs in the form of coordinated anionic pyrazolate, coordinated neutral pyrazolyl and uncoordinate pyrazolyl motifs, eight kinds of chemically different protons are expected. Though attempts were made to assign the protons signals of these three motifs in **1**, it become fruitless. However, the ^1H NMR spectrum of **1** in d_6-DMSO at 60 °C displayed less signals as well as changing the intensity of few signals compared to that of the spectrum of **1** at 25 °C. The complex may exist in various conformers in the solution which do not interchange each other fast-enough in the proton NMR time scale at 25 °C. However, few conformers of **1** interchange in the solution at 60 °C (Fig. S3).

* Corresponding author.
E-mail address: msathi@uohyd.ac.in (M. Sathiyendiran).

https://doi.org/10.1016/j.jorganchem.2020.121460

Dalton Transactions

ROYAL SOCIETY OF CHEMISTRY

PAPER

View Article Online
View Journal | View Issue

Cite this: *Dalton Trans.*, 2022, **51**, 16307

Self-assembly of a new class of rhenium(I)-based double stranded dinuclear monohelicates with their photophysical and electrochemical studies†

Upasana Phukon,[a] Bhaskaran Shankar [b] and Malaichamy Sathiyendiran *[a]

Received 13th August 2022,
Accepted 18th September 2022

DOI: 10.1039/d2dt02657k

rsc.li/dalton

A new class of double stranded dinuclear monohelicates, *fac*-[{$Re(CO)_3$-(μ-L)-$Re(CO)_3$}L^n] (**1–4**), were self-assembled from $Re_2(CO)_{10}$, a rigid bischelating donor (H_2-L: 1,4-dihydroxybenzoquinone (H_2-dhbq) for **1** and **3**; 2,5-pyrazine dicarboxylic acid (H_2-pydc) for **2** and **4**) and a flexible bis(monodentate) pyrazolyl N donor L^n (L^1 = bis(4-((pyrazolyl)methyl)phenyl)methane for **1** and **2**; L^2 = bis(4-((pyrazolyl)methyl)phenyl)methanone for **3** and **4**) in mesitylene. Metallomacrocycle **1** was confirmed by single crystal X-ray crystallography. Although these helicates contain two organic ligand strands, only one strand is arranged in a helical fashion, which is an unprecedented form in the helicate architecture. The molecular structures of **1–4** as helicates and mesocates were optimized using DFT methods. The dynamic interconversion of the metallomacrocycles in solution was studied by ^{1}H NMR studies. The photophysical properties of **1–4** were studied experimentally and the nature of electronic transitions was determined by TD-DFT analysis. Quinonoid motif-based complexes **1** and **3** displayed strong visible light absorption. The redox properties of **1–4** were studied using cyclic voltammetry.

Introduction

The currently known self-assembly principles using pre-designed organic ligands or naked and partially protected metal ions provide a vast array of 2D- and 3D supramolecular coordination complexes (SCCs = metallomacrocycles) of various sizes and shapes including helicates.[1] Although it appears that limits are reached in the design principle of SCCs, new bonding combinations have been evolving continuously to create simple to complex new supramolecular architectures. Intense research focused on this area is due to the simple synthetic approach *i.e.*, mixing of two/three compounds for the formation of simple and highly complex SCCs and their potential applications in material and biological fields.[2] Among the SCCs, dinuclear double-stranded double helicate is the simplest supramolecule and is known to have potential applications in the field of medicine.[3] In general, dinuclear double helicates can be easily achieved by mixing of naked metal ions and ditopic flexible ligands.[4] However, the use of partially protected metal ions is less common in the self-assembly of dinuclear double-stranded double helicates. In particular, *fac*-[$Re(CO)_3$] core-based complexes as starting materials for assembling dinuclear double helicates are scarce[5a–c] but several dinuclear homotopic- and heterotopic-mesocates are known.[5d–g] It is worth mentioning that the *fac*-[$Re(CO)_3$] core directed self-assembly approach is well-established for making kinetically stable and biologically active SCCs.[6]

Herein, we report a unique self-assembly approach for a new class of dinuclear double-stranded helicates (Fig. 1B). In these dinuclear helicates, only one ligand strand is arranged in a helical fashion. To the best of our knowledge, *fac*-[$Re(CO)_3$] core-based dinuclear heteroleptic monohelicates are unknown. Helicates **1–4** were assembled using $Re_2(CO)_{10}$, a rigid bis-chelating ligand and a flexible ditopic nitrogen donor in a one-pot approach (Scheme 1). The dynamic properties of **1–4** in the solution state were studied by variable temperature NMR spec-

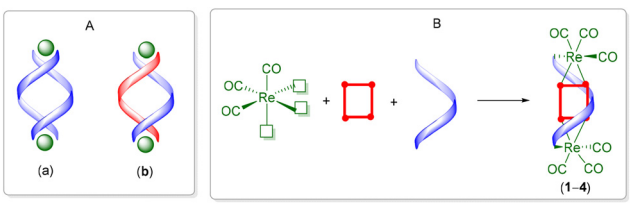

Fig. 1 (A) Commonly observed double-stranded dinuclear (a) homoleptic and (b) heteroleptic double helicates. (B) The design principle of new forms of double-stranded dinuclear monohelicates **1–4**.

[a]*School of Chemistry, University of Hyderabad, Hyderabad-500 046, India. E-mail: msathi@uohyd.ac.in*
[b]*Department of Chemistry, Thiagarajar College of Engineering, Madurai-625015, India*

†Electronic supplementary information (ESI) available: Experimental section and crystallographic data of **1**. CCDC 2110723. For ESI and crystallographic data in CIF or other electronic format see DOI: https://doi.org/10.1039/d2dt02657k

ACS OMEGA

Open Access

http://pubs.acs.org/journal/acsodf

Article

Rhenium−Pyrazolyl-Based Figure-Eight- and Z-Shaped Metallocycles: Self-Assembly, Solid-State Structures, Dynamic Properties in Solution, and Competitive Ligand-Induced Supramolecular Transformations into Rhenium-Pyridyl/-Benzimidazolyl/-Phosphine-Based Metallocycles/Acyclic Complexes

Upasana Phukon, Moon Kedia, Bhaskaran Shankar, and Malaichamy Sathiyendiran*

Cite This: *ACS Omega* 2023, 8, 41773−41784

Read Online

ACCESS | Metrics & More | Article Recommendations | Supporting Information

ABSTRACT: Rhenium(I)tricarbonyl core-based heteroleptic "figure-eight"- and Z-shaped metallocycles (**1a**−**4a**) of the general formula *fac*-[{$(CO)_3Re(\mu$-L)$Re(CO)_3\}_2(dppz)_2$] were self-assembled from $Re_2(CO)_{10}$, H_2-L (H_2-L = 5,8-dihydroxy-1,4-naphthaquinone (H_2-dhnq) for **1a**; 1,4-dihydroxy-9,10-anthraquinone (H_2-dhaq) for **2a**; 6,11-dihydroxy-5,12-naphthacenedione (H_2-dhnd) for **3a**; 2,2′-bisbenzimidazole (H_2-bbim) for **4a**), and bis(4-((pyrazolyl)methyl)phenylmethane) (dppz) via one-pot coordination-driven synthetic approach. The molecular structures of **1a** and **4a** were unambiguously confirmed by single-crystal X-ray diffraction (SC-XRD) methods. The metallocycles in the DMSO solution exist as an acyclic dinuclear−DMSO adduct of the general formula *fac*-[{$(CO)_3Re(\mu$-L)$Re(CO)_3\}(DMSO)_2$] (**1b**, L = dhnq; **2b**, L = dhaq; **3b**, L = dhnd; **4b**, L = bbim) and dppz, which are in dynamic equilibrium. The dynamic behavior of the rhenium−pyrazolyl bond in the solution state was effectively utilized to transform metallocycles **1a**−**4a** into pyridyl/benzimidazolyl/phosphine donor-based heteroleptic metallocycles and acyclic dinuclear complexes (**4**−**13**). These include tetranuclear rectangles *fac*-[{$(CO)_3Re(\mu$-L)$Re(CO)_3\}_2(4,4'$-bpy)$_2$] (**4** and **11**, L = dhaq for **4** and bbim for **11**), dinuclear metallocycles *fac*-[{$(CO)_3Re(\mu$-L)$Re(CO)_3\}$(dpbim)] (**5**−**7** and **12**; L = dhnq for **5**, dhaq for **6**, dhnd for **7**, and bbim for **12**), and dinuclear acyclic complexes *fac*-[{$(CO)_3Re(\mu$-L)$Re(CO)_3\}(PTA)_2$] (**8**−**10** and **13**; L = dhnq for **8**, dhaq for **9**, dhnd for **10**, and bbim for **13**). These transformations were achieved through component-induced supramolecular reactions while treating with competitive ligands 4,4′-bipyridine (4,4′-bpy), bis(4-((1*H*-benzoimidazole-1-yl)methyl)phenyl)methane (dpbim), and 1,3,5-triaza-7-phosphaadamantane (PTA). The reaction mixture in the solution was analyzed using NMR and electrospray ionization mass spectrometry (ESI-MS) analysis. Additionally, crystal structures of **4**, **6**, and **13**, which were obtained in the mixture of the solutions, were determined, providing unequivocal evidence for the occurrence of supramolecular transformation within the system. The results reveal that the size of the chelating ligand and the pyrazolyl donor angle of the ditopic ligand play crucial roles in determining the resulting solid-state metallacyclic architecture in these synthetic combinations. The dynamic behavior of the rhenium−pyrazolyl bond in the metallocycles can be utilized to transform into other metallocycles and acyclic complexes using suitable competing ligands via ligand-induced supramolecular transformations.

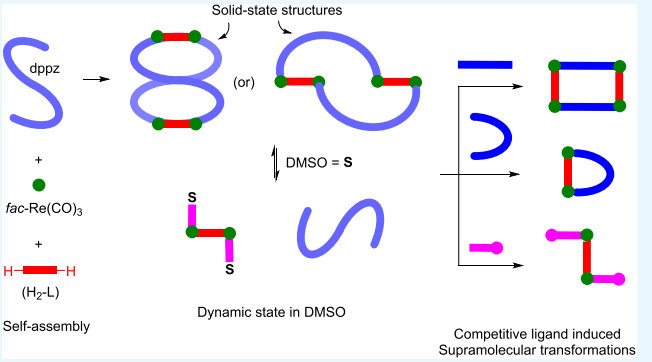

INTRODUCTION

The design and synthesis of metallocycles such as cages, helicates, and simple-to-complex topological architectures via coordination-driven self-assembly have been gaining significant attention owing to their potential applications in materials and medicinal fields.[1−9] Further, new aesthetically appealing molecular architectures including intricate topological metallocyclic architectures such as metallo-links (a series of interlocked metallocyclic rings where at least one ring has to be broken to separate them) and metallo-knots similar to those found in nature can be prepared using the self-assembly.[10−18] Among various topologies, "figure-eight" architecture is one of the elegant self-assembled structures, which is found in natural systems such as Lissoclinamide 7, the recombinant structure of

Received: August 26, 2023
Revised: September 23, 2023
Accepted: October 10, 2023
Published: October 30, 2023

Dalton Transactions

ROYAL SOCIETY OF CHEMISTRY

COMMUNICATION

View Article Online
View Journal | View Issue

Cite this: *Dalton Trans.*, 2023, **52**, 14314

Received 5th August 2023,
Accepted 27th September 2023

DOI: 10.1039/d3dt02535g

rsc.li/dalton

Trinuclear rhenium(I)-based metallocages as anticancer agents towards human cervical cancer cells†

Moon Kedia,[a] Sajmina Khatun,[b] Upasana Phukon,[a] Bhaskaran Shankar,[c] Aravind Kumar Rengan *[b] and Malaichamy Sathiyendiran *[a]

The first examples of spherical-shaped trinuclear rhenium(I) organometallic cages displaying cytotoxic, antimetastatic, antiproliferative and DNA-damaging behavior towards a human cervical (HeLa) cancer cell line are reported. The compact design of the metallocages facilitates their interactions with biosystems leading to comparable efficiency to that of the commonly used anticancer drug cisplatin.

Cancer is one of the deadliest invasive diseases with a high mortality rate worldwide. Although several conventional cancer therapies such as surgery, chemotherapy, and radiation therapy are available, most of the treatments cause severe side effects in cancer patients. Drug resistance is another factor that leads to the therapeutic limitations of conventional Pt-based drugs in cancer treatment. The toxic side effects of these Pt-based drugs such as cisplatin are a consequence of the covalent adducts formed between the complexes and DNA, which can be overcome by the use of supramolecular coordination complexes as anticancer agents that can operate *via* non-covalent contacts. Hence, there is a rising demand for the development of new anticancer drugs with high efficacy. Current research in the field of cancer treatment has led to the discovery of metallodrugs with high therapeutic efficacy and fewer side effects. Various metal ions, such as copper, gallium, palladium, platinum, ruthenium, titanium, gold, silver, and rhenium, have been used to prepare neutral and ionic complexes as potential therapeutic agents.[1–8] Among the metal ions/metal cores used to prepare biologically active acyclic complexes and supramolecular metallocycles/metallocages, *fac*-[Re(CO)$_3$] core-based complexes have emerged as some of the frontrunners in anticancer research due to the intrinsic properties of the *fac*-[Re(CO)$_3$] core such as kinetic inertness, high stability, rich photophysical properties, ease of synthesis and presence of outwardly directed metal-coordinated carbonyl groups.[9–30] A considerable number of acyclic *fac*-[Re(CO)$_3$]-based complexes have been synthesized and studied for their biological properties, in particular, anticancer activity.[10–29,31,32] On the other hand, the application of *fac*-[Re(CO)$_3$]-based 2D metallocycles and 3D metallocages has been explored in various other fields such as molecular recognition, photocatalysis and molecular devices but their anticancer studies are very limited.[30] To date, most of the rhenium-based metallocycles studied for anticancer activities are dinuclear systems, which are usually assembled using a ditopic pyridine donor with an amide spacer as an organic framework and have been found to be effective against various cancer cell lines such as A549, HTB-132, HeLa, NCI-H122 and so on (Table S2†).[27] The increase in the number of *fac*-[Re(CO)$_3$]-cores *i.e.*, from mononuclear to dinuclear, in the metallocycles leads to improved cellular uptake, higher lipophilicity, and better cytotoxicity.[19] *fac*-[Re(CO)$_3$]-core-based metallocycles and metallocages of higher nuclearity as anticancer agents are hitherto unknown. Therefore, we envision that trinuclear or higher nuclearity metallocycles/metallocages made up of biologically relevant organic frameworks such as benzimidazolyl or its derivatives and a kinetically inert biocompatible organometallic *fac*-[Re(CO)$_3$]-core might yield potential anticancer agents. Changes in the organic frameworks, nuclearity, and shape of the metallocycles/metallocages play a significant role in their interactions with biosystems. In particular, spherical-shaped metallocages decorated with multiple metal-coordinated carbonyl groups directed outwards on one side and hydrophobic aromatic motifs on the other side might be good candidates to interact with a biosystem *via* hydrogen bonding C–H···O≡C–M contacts, hydrophobic interactions, C–H···π, π···π contacts, and van der Waals interactions, which play key roles in biological processes. Among the various types of cancers, cervical

[a]*School of Chemistry, University of Hyderabad, Hyderabad-500 046, India. E-mail: msathi@uohyd.ac.in*
[b]*Department of Biomedical Engineering, Indian Institute of Technology, Kandi, Hyderabad-502 284, India. E-mail: aravind@bme.iith.ac.in*
[c]*Department of Chemistry, Thiagarajar College of Engineering, Madurai-625 015, India*

†Electronic supplementary information (ESI) available. CCDC 2265703 and 2265704. For ESI and crystallographic data in CIF or other electronic format see DOI: https://doi.org/10.1039/d3dt02535g

CrystEngComm

ROYAL SOCIETY OF CHEMISTRY

COMMUNICATION

View Article Online
View Journal | View Issue

Cite this: *CrystEngComm*, 2023, **25**, 2518

Received 17th March 2023,
Accepted 5th April 2023

DOI: 10.1039/d3ce00264k

rsc.li/crystengcomm

A double ouroboros-shaped noncovalent molecular dimer†

Moon Kedia, K. R. Soumya, Upasana Phukon, Isha Mishra, Reema L. Borkar, Palanichamy Vengadeshwaran, Mamina Bhol and Malaichamy Sathiyendiran *

A double ouroboros-shaped molecular dimer was crystallized from a tripodal molecule having the ability to adopt conformation similar to molecular tweezers at one end and a lone unit at the other. Two complementary tripodal molecules self-organize into a dimer like two serpents biting each other's tails in a circular fashion.

Mythological symbols, in particular, alchemical symbols have always been inspiring chemists not only for the design and synthesis of artificial molecules (including simple to exotic complex architectures) but also for providing perspective in solving and analysing new structures. One such example is the formulation of the structure of benzene by Kekule, famously known to be inspired by his dream of ouroboros.[1] In Greek mythology, ouroboros implies a snake/serpent eating its own tail in a circular way.[2] The key to make molecular mythological symbols is designing pre-organized organic building units embedded with non-covalent binding motifs.[3–5] Though the symbols painted/carved by alchemists and artists long back look very simple, preparing molecular mimics of them is still quite a challenge. Among many symbols, the double ouroboros is another alchemical symbol mentioned in Greek texts, which portrays two different snakes/serpents eating each other's tails (Fig. 1, right).

From the structural point of view, a simple way for creating molecular double ouroboros is to design bent-shaped molecules or flexible tripodal molecules having the ability to adopt conformation like molecular tweezers at one end and a lone unit at the other end. The tweezers and the lone unit should contain complementary non-covalent binding units to stabilize the self-organized ring dimeric structure. Herein, a tripodal molecule (**TMe**) consisting of three thiabendazolyl terminal units, a mesitylene central spacer, and three methylene connectors was synthesized and characterized (Fig. 2). The X-ray analysis revealed that two adjacent tripodal molecules self-organize to give rise to a dimeric structure $(\mathbf{TMe})_2$ in the solid state like double ouroboros and were stabilized *via* complementary intermolecular C–H···N and H···H contacts. To the best of our knowledge, very few examples of molecular ouroboros have been reported[7] and this dimeric system is the first molecular double ouroboros.

1,3,5-Tri(2-(thiazol-2-yl)benzimidazol-1-ylmethyl)-2,4,6-trimethylbenzene (**TMe**) was synthesized by the reaction of 2-(thiazol-2-yl)-1*H*-benzimidazole (H-Tzbim) and 1,3,5-tri(bromomethyl)-2,4,6-trimethylbenzene in the presence of a strong base. **TMe** is air stable and soluble in CH_2Cl_2, $CHCl_3$, and DMSO. Its formation was confirmed using ESI-Mass analysis and its spectrum displayed molecular ion peak, *m*/*z* $[\mathbf{TMe} + H]^+$ = 760.2099, which matches with the theoretical value (Fig. S5, ESI†). In addition, another significant but relatively weak peak at *m*/*z* 1520.4047 was observed, which corresponds to $[2\ (\mathbf{TMe}) + 2H]^+$. No other prominent peaks were observed at higher mass. The dimer peak may correspond to the dimeric structure found in the solid state or a new form of the dimer.

Fig. 1 Mythological symbol of ouroboros as depicted by Lucas Jennis, in the 1625 alchemical tract De Lapide Philosophico (left) and double ouroboros with two different serpents (right).[2,6]

University of Hyderabad, School of Chemistry, Hyderabad, Telangana, India. E-mail: msathi@uohyd.ac.in

† Electronic supplementary information (ESI) available. CCDC 2131005, 2212948 and 2212949. For ESI and crystallographic data in CIF or other electronic format see DOI: **https://doi.org/10.1039/d3ce00264k**

Journal of Organometallic Chemistry 923 (2020) 121460

Contents lists available at ScienceDirect

Journal of Organometallic Chemistry

journal homepage: www.elsevier.com/locate/jorganchem

Communication

Self-assembly of rhenium core-based conjoined bicyclic supramolecule from pyrazole and flexible hexatopic pyrazolyl ligands

Upasana Phukon, Maruthupandiyan Priyatharsini, Malaichamy Sathiyendiran*

School of Chemistry, University of Hyderabad, Hyderabad 500 046, India

ARTICLE INFO

Article history:
Received 13 June 2020
Revised 21 July 2020
Accepted 24 July 2020
Available online 28 July 2020

1. Introduction

The coordination driven self-assembly approaches i.e., metal-directed approaches for supramolecular coordination complexes (SCCs), discrete cyclic complexes, are highly successful methods to prepare simple mononuclear SCCs to complex interlocked SCCs [1–5]. Though many metal-directed synthetic rules are now known, continuous use of the known approaches and create a new design principle i.e., new metal-ligand(s) bonding combinations to assemble new molecular architectures have been intensely going on due to their aesthetical structures and potential future molecules in various areas including materials and medicinal fields. Among the many metal-directed approaches, the partially protected *fac*-$Re(CO)_3$-corner based assembly process using flexible multitopic ligands and neutral bridging ligands recently provided interesting spherical-shaped SCCs with multiple calixarene-shaped solvent-accessible cavity on the surface [4]. In particular, tuning the coordinating units of hexatopic ligands remotely by either increasing the fused ring/docarating phenyl rings on imidazolyl yielded overall spheroid SCCs with/without solvent-accessible cavity [4]. Tuning the imidazolyl unit by pyrazolyl unit in the hexatopic ligand may provide two kinds of SCCs. Spheroid shaped SCC with interconnecting calixarene cavities because of the adjacent arrangement of two heteroatoms in the pyrazolyl motif. In the case of hexatopic imidazolyl/benzimidazolyl-based SCCs, the C-H unit (N-C^2H-N) of imidazolyl, which is directed into the spheroid, acts as a steric unit blocking the channel of the cavities [4]. The second option is hitherto unexplored SCC because the small change in the binding angle of the donor units in the ligand i.e., from imidazolyl to pyrazolyl, may direct different coordination angle to adjust octahedral geometry around the *fac*-$Re(CO)_3$ core. Herein, we report on unexpected conjoined bicyclic supramolecular coordination complex with free two pyrazolyl motifs via a new type of metal-ligand bonding combinations i.e., *fac*-$Re(CO)_3$ from $Re_2(CO)_{10}$, pyrazole, water, and flexible hexatopic pyrazolyl N-donors in a one-pot solvothermal process.

2. Results and discussion

The treatment of $Re_2(CO)_{10}$, pyrazole (H-pz), 1,2,3,4,5,6-hexakis(pyrazol-1-ylmethyl)benzene (L), and toluene under solvothermal closed vessel resulted in pale yellow crystals *fac*-$[\{(Re(CO)_3)_2(\mu^2\text{-}OH)(k^1\text{:}k^1\text{-}\mu\text{-}pz)\}_2L]\cdot C_7H_8$ (**1**$\cdot C_7H_8$) (Scheme 1). The crystals are air and moisture-stable and soluble in DMSO. The FT-IR spectrum of the complex displayed three strong bands (1865, 1927, and 2007 cm^{-1}), which are the characteristic peaks for the *fac*−$Re(CO)_3$ core in the complex [4]. Further, the IR spectrum of crystal of **1** showed a sharp band at 3556 cm^{-1}, indicating the presence of the hydroxyl group (Fig. S1). The ^1H NMR spectrum of crystals of **1** in d_6-DMSO showed multiple signals in the region of 8.1 to 5.0 ppm in contrary to simple pattern expected for a symmetrical arrangement of pyrazolyl and pyrazolate motifs (Fig. S2). Though the complex contains three kinds of pyrazole motifs in the form of coordinated anionic pyrazolate, coordinated neutral pyrazolyl and uncoordinate pyrazolyl motifs, eight kinds of chemically different protons are expected. Though attempts were made to assign the protons signals of these three motifs in **1**, it become fruitless. However, the ^1H NMR spectrum of **1** in d_6-DMSO at 60 °C displayed less signals as well as changing the intensity of few signals compared to that of the spectrum of **1** at 25 °C. The complex may exist in various conformers in the solution which do not interchange each other fast-enough in the proton NMR time scale at 25 °C. However, few conformers of **1** interchange in the solution at 60 °C (Fig. S3).

* Corresponding author.
E-mail address: msathi@uohyd.ac.in (M. Sathiyendiran).

https://doi.org/10.1016/j.jorganchem.2020.121460

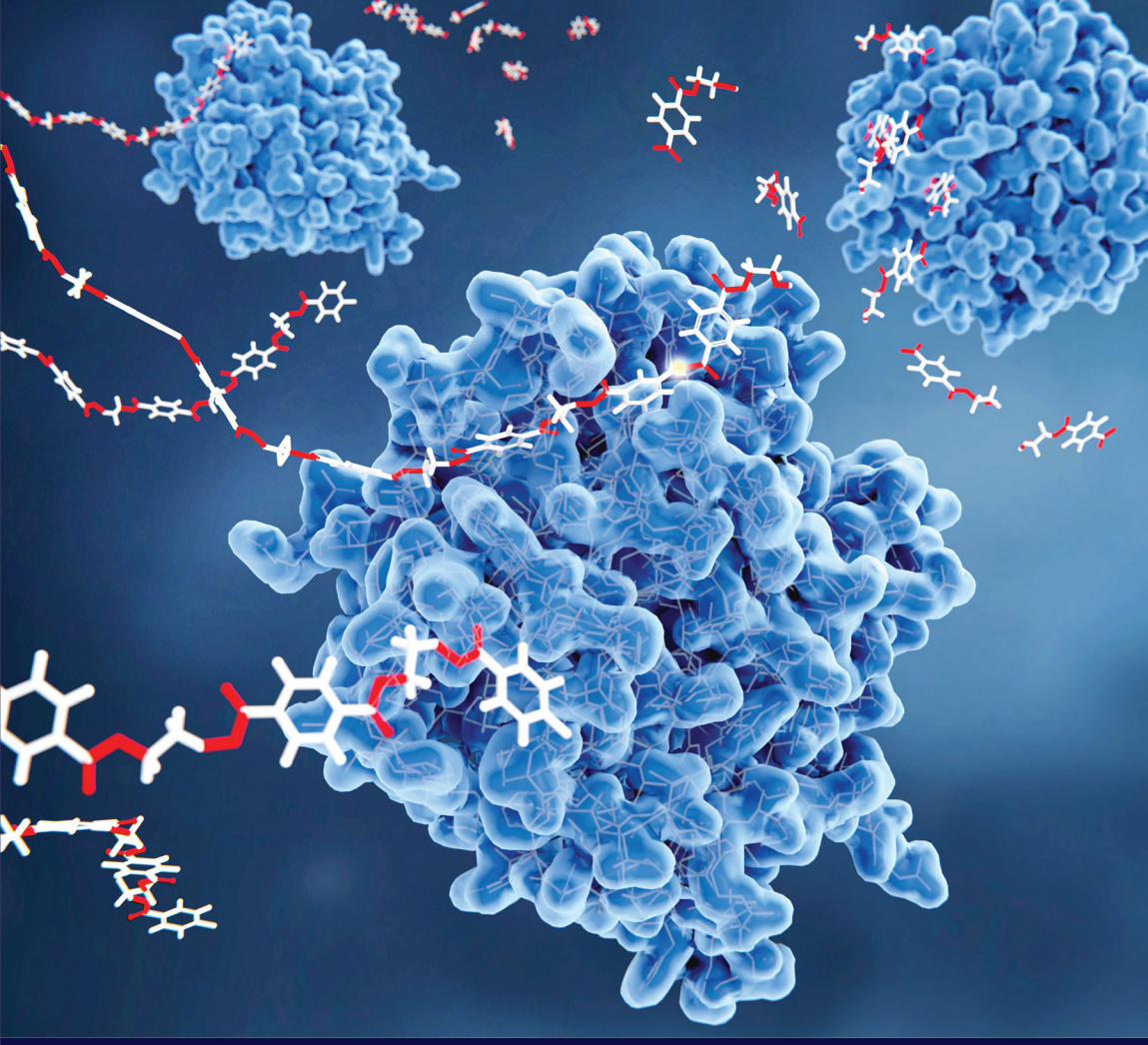

Supramolecular Coordination Complexes

Design, Synthesis, and Applications

Edited by
Sankarasekaran Shanmugaraju

ELSEVIER

Chapter 6

Rhenium (I)-based supramolecular coordination complexes: Synthesis and functional properties

K.R. Soumya*, Isha Mishra*, Moon Kedia*, Upasana Phukon*, Reema Borkar* and Malaichamy Sathiyendiran*
School of Chemistry, University of Hyderabad, Hyderabad, India

6.1 Introduction

Supramolecular coordination complexes (SCCs) assembled using coordination-driven self-assembly approaches are well-defined discrete cyclic 2D and/or 3D architectures that can have widespread applications in various fields of chemistry and biology due to the presence of metal complex unit and the arrangement of organic building frameworks [1–28]. The spontaneous formation of metal–ligand bond between metal acceptors and organic donors provides several synthetic methodologies to develop these SCCs. Until now, a series of rationally designed discrete SCCs with various shapes including polygonal triangle, square, rectangle, higher polygonal 2D architectures and polyhedral 3D architectures via coordination-driven self-assembly are reported by several research groups. The partially protected *fac*-$Re(CO)_3$ core-based SCCs represent a unique class of cyclic assemblies. The key properties associated with these complexes are thermal, kinetic and photo-stability, robustness and metal to ligand charge transfer absorptions and emissions. Re(I)-based cyclic supramolecular architectures with various shapes including dinuclear, trinuclear, tetranuclear squares, rectangles, gondolas, bowls, calixarene, bicycles, hexanuclear prisms, spheroids, wheel, and octanuclear prisms are found in the literature [10–28]. The dimension, flexibility, shape, and intrinsic properties of these SCCs can be easily tuned by modifying the organic ligand framework. The complexes often serve as promising candidates for applications in molecular recognition, catalysis, bioimaging, sensors,

* All authors contributed equally.

Supramolecular Coordination Complexes: Design, Synthesis, and Applications.
DOI: https://doi.org/10.1016/B978-0-323-90582-4.00014-2